UNIVERSITY OF SOUTHAMPTON
DEPARTMENT OF MECHANICAL ENGINEERING

THE INFLUENCE OF VISCOSITY ON TURBINE FLOW METER CALIBRATION CURVES

by

Ali Fakouhi

Presented for the degree of
Doctor of Philosophy
1977

ABSTRACT

Faculty of Engineering and Applied Science

Doctor of Philosophy

The influence of viscosity on turbine flow meter calibration curves

by Ali Fakouhi

The sensitivity of the turbine flow meter to changes in fluid viscosity puts in question claims of accuracy (1%) and repeatability (.2%). The present results show that the output signal is a function of flow-rate and fluid viscosity. A theoretical model applicable to all groups of turbine meter, which explicitly involves fluid viscosity, has been produced, which can be applied to the fluid dynamic characteristics of the turbine flow meter. The Euler turbine equation with modifications to allow for the effect of tip clearance and fluid viscosity has been applied in this work.

Viscosity and flow rate dependence have been considered term by term in the main turbine equation. Experiment leads to a division into two groups, firstly calibration curves produced from helically bladed rotors which have a lower degree of sensitivity with respect to fluid viscosity, and secondly those of constant blade angle rotors which are more sensitive to changes in fluid viscosity.

Fluid dynamic characteristics of the tip clearance flow are discussed as well as the effect of fluid viscosity on the flow pattern in this area. A theoretical model has been made to calculate the tip clearance flow. Also a semi-empirical calculation is shown to predict the calibration curve for a given fluid viscosity according to the design of turbine meter. However, for a particular design and a known calibration curve some suggestions are made of possible improvements in the calibration performance, for instance by optimising tip clearance and bearing friction. The term by term calculation of the main turbine equation allows the prediction of improved insensitivity to the effect of fluid viscosity for certain changes of meter geometry.

ACKNOWLEDGEMENTS

The author wishes to record his indebtedness to his supervisor, Professor S.P. Hutton, for the initiation and guidance he provided, as well as to his parents for practical and theoretical support; also especial thanks to Mr. Thew for his temporary supervision.

The author wishes to express his thanks to Esso Ltd., for the research studentship.

Thanks are also extended to Mr. M.A. Batey, Mr. J.D. Sewill, and the members of the Mechanical and Electrical Workshops of the University of Southampton for their assistance in the change and maintenance of the test rig.

The author acknowledges the assistance of the Computer Centre for their advice, and special thanks to Mrs. W. Rogers for typing this thesis.

LIST OF SYMBOLS

A	=	Term 1 in the main turbine equation
A'_a	=	The total surface area of turbine blades
A_a	=	Cross section area of meter
$A_{F_{blade}}$	=	Axial force action on the turbine blade
A″	=	Prandtl-Schlichting constant for C_{D_o}
B	=	The combined viscosity leakage term in the main turbine equation
Be	=	Laminar constant factor for determining of friction coefficient
B_{trans}	=	Transition constant factor for determining of friction coefficient
B_{turb}	=	Turbulent constant factor for determining of friction coefficient
C	=	The combined torque term in the main turbine equation
c*	=	Radial clearance in the turbine bearing
c	=	Blade chord
$\bar{c}$	=	Absolute velocity in the tip clearance area
C_D	=	Coefficient of drag
C_{D_o}	=	Coefficient of drag for zero angle of attack
C_f	=	Coefficient of skin friction
C_L	=	Coefficient of lift
C_{loss}	=	Coefficient of loss in the turbine cascade
C_s	=	The secondary drag coefficient
D	=	Drag force acting on the turbine blade
dD	=	Elemental drag at radius r
dL	=	Elemental lift at radius r
dr	=	Elemental radius
i	=	Inlet control surface (blade upstream)
id	=	Uniform flow condition
g	=	Leakage ratio empirical function to express leakage flow
k	=	Leakage factor empirical correction function to express the leakage
k_s	=	Roughness size
K	=	The turbine geometry dependent constant factor
D_s	=	Secondary drag force on turbine blade
e	=	Bearing eccentricity

$\bar{K}$	=	Gersten constant factor for displacement thickness
$\bar{\bar{K}}$	=	Gersten constant factor for momentum thickness
L	=	Lift force acting on the turbine blade
L*	=	Bearing axial length
$\bar{L}$	=	Helical pitch
MTE	=	Main turbine equation (eqs. 1.1, 5.15, 5.19, 5.20, 10.1)
m.c.	=	Meter coefficient
N	=	The number of rotor blades
n	=	Speed of the Turbine meter rotation
O	=	Far distance in upstream position of the rotor
o	=	Rotor blades outlet index (outlet control surface)
p_0	=	Pressure in far upstream position
p_{1tip}	=	Pressure in upstream position just before the blade inlet at the blade tip
p_{2tip}	=	Pressure in downstream position just after the blade outlet at the blade tip
p_3	=	Pressure in far downstream position
Q	=	The total volume flow through the turbine meter per second
Q_0	=	Flow rate for fluid velocity U_0 for which the rotors start to rotate
Q_c	=	Tip clearance flow
Q_r	=	The flow rate through the rotor blades
r_h	=	Hub radius
r_m	=	Mean radius = $[(r_t^2 + r_h^2)/2]^{1/2}$
r_t	=	Blade tip radius
r_0	=	Radius of meter casing
$R_{e_{blade}}$	=	Blades Reynolds number
R_e	=	Pipe Reynolds number
$R_{e_{pass}}$	=	Meter annulus Reynolds number
r_p	=	Pipe radius
R	=	Shaft diameter of the Turbine bearing
$r_t \cdot \omega_a$	=	Tip clearance rotational velocity
$A(\nu)$, $B(\nu)$, $C(\nu)$, $D(\nu)$, $E(\nu)$	=	Viscosity dependent parameter defined in App. I. page 110 used to calculate T_1, T_2, T_3
Δg	=	Energy loss

s	=	Blade spacing at radius r
S	=	Axial thrust
t	=	Blade thickness
T_{brake}	=	Brake torque (the sum of all anti-increment torque)
T_{bear}	=	Retarding torque due to the bearing friction
T_d	=	Total driving torque
T_{di}	=	Induced driving torque with zero tip clearance
T_D	=	Retarding fluid drag torque
T_{mech}	=	Torque due to mechanical forces
T_T	=	The movement torque
U	=	Absolute velocity
U_i	=	Reference axial velocity in inlet of the blade
U_o	=	Reference axial velocity in outlet of the blade
U_m	=	Mean axial velocity
u	=	Local axial velocity
$\overline{U}_o$	=	Axial fluid velcotiy for which the rotors start to rotate
v_e	=	Outlet swirl velocity
v_n	=	The normal (perpendicular) component of $\overline{v}$ to the blade area
V_o	=	Outlet relative velocity (relative to the blade)
V_i	=	Inlet relative velocity (relative to the blade)
V_m	=	Mean relative velocity (relative to the blade)
δ_H	=	Displacement thickness
$\overline{v}'$	=	Relative velocity in the tip clearance area produce due to the pressure difference across the turbine blade
V	=	Relative velocity at the blade tip before entering the clearance area
V_{oid}	=	Outlet relative velocity in ideal conditions
$\overline{v}$	=	The resultant component of
W	=	Axial width of the turbine blade
α	=	The angle of attack
$\overline{\alpha}$	=	Angle between Reference beam and Main beam in laser doppler anemometry
T_1, T_2, T_3	=	Different parameter used in MTE (Eqs. 5.11, 5.12, 5.13, 5.14, 5.20, 10.1)

β	=	Blade angle
γ	=	Specific weight of the fluid
δ_H^*	=	Displacement thickness in two dimensional flow observation
δ^*	=	Deviation angle
δ	=	Viscosity coefficient which is zero for high blade Reynolds number at low viscosity
δ_x	=	Displacement thickness in x-direction
δ_y	=	Displacement thickness in y-direction
Γ	=	Circulation in tangential direction with zero tip clearance
Δ^*	=	Displacement thickness for turbine blade
$\overline{\frac{\Delta p^*}{\gamma}}$	=	Kinematic energy in the tip clearance area produced head
Δp_{blade}	=	Pressure difference across the turbine blade
ϵ	=	The value of deviation of meter coefficient from average meter coefficient at high flow rate range
ϵ^*	=	Eccentricity ratio in turbine bearing
$\overline{\epsilon}$	=	The ratio of blade thickness to blade chord
η	=	Dynamic viscosity of the fluid
$\eta_{c\ell}$	=	Tip clearance volumetric (torque) efficiency
η_p	=	Turbine meter pressure efficiency
η_v	=	Turbine meter volumetric efficiency
θ	=	Scattering angle in laser doppler anemometry
θ_i	=	Inlet velocity angle in respect to axis of rotor
θ_o	=	Outlet velocity angle in respect to axis of rotor
θ_m	=	Mean velocity angle in respect to axis of rotor
$\overline{\theta}$	=	Moment of inertia
θ^*	=	Momentum thickness for turbine blade
θ_{oid}	=	Velocity angle for uniform flow condition in respect to axis of rotor
$\aleph$	=	Fi rst term of viscosity dependent parameter in the driving torque
$\overline{\aleph}$	=	Second term of viscosity dependent parameter in the driving torque
Φ	=	Relative meter coefficient
Φ_o	=	Relative meter coefficient in regard to flow rate for which the rotor start to rotate

$\bar{\bar{\aleph}}$	=	Viscosity dependent parameter in the brake torque
λ	=	Wave length
μ	=	Mechanical friction coefficient
$\bar{\mu}$	=	Refractive index of measuring medium
ν	=	Kinematic viscosity of the fluid
ν_0	=	Frequency of pre shift
$\bar{\nu}$	=	Frequency of doppler shift
L.D.A.	=	Laser Doppler Anemometry
B_e^*	=	The constant index for friction coefficient in the laminar zone (Blasius law)
B_{trans}^*	=	The constant index for friction coefficient in the transition zone
B_{turb}^*	=	The constant index for friction coefficient in the turbulent zone (Prandtl-Schlichting)
$\zeta'(Re)$	=	The combined influence of the Reynolds number and friction forces
ω_a	=	Angular rotor velocity
ϕ	=	The turbine flow meter characteristic function which is influenced by turbine flow meter geometry and pipe Reynolds number
X	=	Distance of the pressure tapping from each other
φ'	=	Tip clearance area/Meter annulus area
φ_0	=	The velocity potential
$\Gamma_{tip} = \Gamma_{c\ell}$	=	The tip clearance circulation
τ	=	Shear stress
v_p	=	Axial fluid velocity in the pressure side of the blade
v_s	=	Axial fluid velocity in the sanction side of the blade
η	=	Dynamic viscosity
H	=	Head loss between the pressure tapping points
N_{blade}	=	Hydrodynamic power transferred from fluid to the blades

LIST OF FIGURES

Figure 12 The effect of viscosity on the constant angle blade rotor turbine flow meter, with small bearing friction. (These meters were more affected by viscosity of test fluid).

Figure 13 The comparison between experimental and theoretical results on a commercial turbine flow meter with 6 constant bladed angle rotor

Figure 14 The calculation of the 3 terms of the main turbine equation for a commercial turbine flow meter with a 6 bladed constant angle rotor.

Figure 15 The calculation of the three terms of main turbine equation for a commercial turbine flow meter Type 'C' with 6 bladed constant angle rotor and the first variation in the terms due to the increase in fluid viscosity up to $\nu = 21$ cSt.

Figure 16 The effect of viscosity on the research meter with a 3 bladed constant angle rotor. These are current experimental results and because of the opaqueness of the viscous test fluid some pulses could not be counted. The light beams were too weak to be picked up by photo cells (Fig. 37).

Figure 17 The comparison between experimental and calculation results on a research turbine flow meter with 3 constant bladed angle rotor.

Figure 18 The calculation of the 3 terms of the main turbine equation for a research turbine meter with 3 constant bladed angle rotor.

Figure 19 The effect of viscosity on the research turbine flow meter using magnetic and photocell pickup. There was an overall rise in the calibration curve. (The magnetic pickup detected the lost pulses mentioned in Figs. 16, 20, 27, 37).

Figure 20 The weak pulses reflected on the blade tip, which are lost due to the opaqueness of the viscous test fluid can be found by comparison between the number of pulses detected by magnetic pickup and photo cell pick up.

Figure 21 The effect of viscosity on the research meter with a 3 bladed constant angle rotor. These were Salami's experimental results and because of the opaqueness of the viscous test fluid some pulses could not be counted. (The light beams were too weak to be picked up by the photocells). See Fig. 37.

Figure 22 The effect of viscosity on the turbine flow meter with helical bladed rotor and large bearing friction. (These meters were less sensitive to the change in fluid viscosity).

Figure 23 The comparison between experimental and calculated results for a commercial turbine flow meter with an 8 bladed helical rotor

Figure 24 Calculation of 3 terms of the main turbine equation (59) for a commercial turbine meter with an 8 bladed helical rotor (Water).

Figure 25 The effect of tip clearance on the calibration curves of the helical blade research rotor. These were Tan's experimental results. He proved that an increase in tip clearance causes an overall rise in the calibration curve especially for low flow rates (caused the increase of the hump).

Figure 26 Lee and Karlby's experimental results for the determination of the effect of viscosity on the calibration curve. They connected the linear part and the non-linear part of the calibration curve of two different fluid viscosities. They compensated for the effect of viscosity with an external load, which increases term 3 of MTE and gives a balance between different terms of MTE. This causes the disappearance of the hump created on the calibration curve.

Figure 27 Salami's experimental results for the effect of viscosity on the research turbine flow meter with the constant bladed rotor. Salami missed the beginning and the end of the calibration curve because of the threshold on the counter and excessive pressure in the test length. He also missed a certain number of pulses/lb. because of reasons explained in Figs. 16, 20, 21.

Figure 28 Salami's experimental results for the commercial turbine meter with 3 bladed constant angle rotor. Salami got neither the beginning of the calibration curves (non linear part), because of the threshold of the counter, nor the end of it because of high pressure created in the test line due to an increase in viscosity (pump limit). Dashed lines indicate his expected results in these regions.

Figure 29 The relationship between ϕ and Re for a 6 ins. commercial turbine meter with a 16 bladed helical angle rotor.

Figure 30 The percentage error over the flow rate for the above meter with fluids of different viscosities.

Figure 31 The influence of fluid viscosity on the calibration curve for a commercial 2 ins. turbine meter (linearity ± 0.5% hel. blade).

and the experimental results for a turbine flow meter with a 8 helically bladed rotor. The operational blades Reynolds number for flow rate between 4 to 20 lb/sec. was 1500 to 7500 respectively.

Figure 92 The comparison between the calculated result using the leakage theory and the experimental results for a turbine flow meter with a 6 helically bladed rotor. The operational blades Reynolds number for flow rate between 4 to 20 lb/sec. was 3000 to 15800 respectively.

Figure 93 The comparison between the calculated result using the leakage theory and the experimental results for a turbine flow meter with a 6 helically bladed rotor. The operational blades Reynolds number for flow rate between 4 to 20 lb/sec. was 1400 to 7000 respectively.

Figure 94 The comparison between the calculated value using leakage theory and the experimental value. The operational blade Reynolds number was between 4700 to 938 for the flow rate 20 lb/sec. respectively.

Figure 95 The comparison between the calculated value using leakage theory and the experimental value. The operational blade Reynolds number was between 1956 and 400 for flow rate between 20 to 4 lb/sec. respectively.

Figure 96 The comparison between the calculated value using the leakage method and the experimental value for a turbine flow meter with a 6 constant bladed angle rotor. The operational blades Reynolds number was between 500 and 5000 for flow rate between 2 to 20 lb/sec. respectively.

Figure 97 The comparison between the calculated value using the leakage method and the experimental value for a turbine flow meter with a 6 constant bladed angle rotor. The operational blades Reynolds number was between 275 and 2100 for flow rate between 2 to 20 lb/sec. respectively. There was good agreement in the laminar operational zone and a disagreement in the transition zone.

Figure 98 The comparison between the calculated value using the leakage theory and the experimental value for a turbine flow meter with 6 constant bladed angle rotor. The whole operational range was in laminar zone with a good agreement between calculated and experimental results. The operational blades Reynolds number was 122 to 600 for flow rate between 2 to 20 lb/sec. respectively.

Figure 99 The comparison between the calculated value using the leakage method and the experimental value for a turbine flow meter with a 6 constant bladed angle rotor. The operational blades Reynolds number was

between 146 and 1500 for flow rate between 2 to 20 lb/sec. respectively. There was good agreement in the laminar operational zone and a disagreement in the transition zone.

Figure 6.1 The reverse flow characteristic in the tip clearance area and the position of pressure tapping

Figure 6.2 The distribution of the circulation and its reduction $\Gamma - \Gamma_{c\ell}$ due to the swirl produced by tip clearance flow.

Figure 7.1 The displacement of the turbine rotor shaft e, from the bearing centre line under the action of the applied rotor weight w, for the case of heavily loaded rotor (Turbine flow meter Type A and B).

Figure II.1 The balance of forces acting on turbine flow meter rotor shaft for long bearing theory.

CONTENTS

CHAPTER 1 INTRODUCTION

1. Background

Over the past few years, the applications of turbine flow meters have increased rapidly. The main advantage of the turbine flow meter is its accuracy, about 1% over a wide range, its repeatability (.2%) and its physical size and the simplicity of its electronic system, which gives a digital output reading. However, the accuracy is questionable without calibration of the flow meter, especially when the fluid viscosity is different from the fluid which was originally used to calibrate the meter after manufacture. The minimum range of the turbine meter is mainly dependent on the viscosity of the fluid. This means that, using the same turbine meter, the transition from the non-linear to the linear part of the meter calibration curve moves toward high flow rates for increasing fluid viscosities (Fig. 12). Flow measurements with a turbine meter when the variation of the meter coefficient with changing fluid viscosity is known makes it possible to have an error in the measurement less than the 1% limitation. Therefore every meter should be individually calibrated, and at least 30 points on the calibration curve should be measured for each fluid of different viscosity which will be metered if there is not a precalculated calibration curve available. In this way linearity and repeatability are established. Any flow meter will be affected to some degree by a change in the viscosity of the fluid being measured. Although this problem can sometimes be overcome by using the drag of an external load on the meter to compensate for viscosity, a more accurate correction against the variable viscosity effect on the turbine flow meter is obtained by an investigation of blade geometry and performance. As a result of this investigation, it can be shown that various shaped calibration curves result for different viscosities. This indicates that the output is a function of both volumetric flow and viscosity, hence the turbine flow meter calibration data should include fluid viscosity. Each meter has an ideal continuous calibration curve or characteristic. Deviations from this curve mean that the meter is affected by several parameters, which include fluid viscosity, size and shape of the turbine meter blade, and bearing friction torque.

This research investigates these parameters and particularly the effect that the viscosity of the fluid has on the calibration curve. These parameters affect the turbine meter's main equation (eq. 5.19). The main problem in this research was to establish the influence of fluid viscosity in the turbine equation. This has been done by dividing the M.T.E. (main turbine equation) into several terms and studying the viscosity effect on each of these terms.

In order to understand the variation in the calibration curve of a turbine flow meter

due to changes in the fluid viscosity, it was necessary to start with a general equation, which could be applied for fluid dynamic characteristics of turbine flow meters and then improve it by including viscosity terms in the equation. TAN showed that for all meters the main turbine equation is (MTE)[1]

$$\frac{n}{Q} = A + \frac{B}{Q} - \frac{C}{Q^2} \tag{1.1}$$

TAN's (Ref. 86) experiments were mostly carried out on specially made research meters. He used water (approx. 20°C) as the test fluid and showed in his theory that there are two main groups of meters; as far as general behaviour is concerned, helical bladed rotors and constant blade angle rotors. TAN proved that helical blade rotors are less sensitive to the effect of tip clearance, inlet swirl, and velocity profile.

This research will study the effect of fluid viscosity on all hydrodynamic and geometrical components in the above equation. In order to understand the modified components, the terms in the above equation are studied separately. The value of A (Term 1) is the ideal magnitude (if the viscosity of test fluid is close to the viscosity of water) of $\frac{n}{Q}$ in a turbine flow meter, with negligible values for Terms 2 and 3 of the above equation. The value of "A" should be calculated for known viscosity, however,

$$A = f(\nu, C_L, C_D, \beta, \delta^*) \tag{1.2}$$

The hydrodynamic parameters are dependent on the fluid viscosity, so that

$$C_L = f_1(\nu) \tag{1.3}$$

$$C_D = f_2(\nu) \tag{1.3a}$$

$$\delta^* = f_3(\nu) \tag{1.4}$$

Term 1 can now be expressed as

$$A = f_4(\nu, \beta) \tag{1.5}$$

Term 2 $(\frac{B}{Q})$, is much more complicated.[2] The value of B will change with changes in tip clearance geometry, and u/U. Also this term will change its sign if the angle of attack at the tip becomes negative. TAN showed the importance of the geometry of the tip clearance. He changed the size of the tip clearance by turning down the rotor blades. In this research the hydrodynamic effects of the tip clearance flow are investigated. Term 2 is also a function of the following hydrodynamic components:

$$B = f_5(C_L, \nu, \frac{u}{U}, Q_c, \beta) \tag{1.6}$$

[1] This equation has been presented in different form in a later chapter (eqs. 5.15, 5.19, 5.20, 10.1)
[2] Concerned with tip clearance geometry (leakage), stated in eq. 1.10

Suppose the terms C_L, $\frac{u}{U}$, and Q_c are some function of viscosity as follows

$$C_L = f_1(\nu) \tag{1.7}$$

$$\frac{u}{U} = f_6(\nu) \tag{1.8}$$

$$Q_c = f_7(\nu, \text{ tip clearance geometry}, \beta) \tag{1.9}$$

Then term 2 of main turbine equation is

$$B = f_5(\nu, \beta, \text{ tip clearance geometry}) \tag{1.10}$$

The Term 3 is $\frac{C}{Q^2}$ where:[1]

$$C = f_8(\nu, T_d, T_{bear}) \tag{1.11}$$

The main interest of this research is to modify TAN's theory to allow to vary viscosity.

By writing the hydrodynamic parameters as functions of fluid viscosity or Reynolds number, and substituting them into the M.T.E., the M.T.E. can be used for any fluid viscosity.

The above will lead to a change in the M.T.E. A decision was made to select several different commercial meters, because TAN carried out most of his work on 'research' meters and has shown that his theory is applicable for meters operating in the low fluid viscosity range. (The difference between research and commercial turbine meters[2] has been explained in chapter 4.1.4). The investigation on commercial meters will also be more useful for practical applications of flow meters and of general use in established theory. Although there were a large number of experiments carried out on commercial meters by turbine meter producers (Ref. 15, 32), significant results were only produced from extensive investigation of research meters, and some inaccuracy in previous results (Salami's experiments, Ref. 97), were discovered. These inaccuracies will be discussed with suggestions as to their causes later in this work (Chapter 3).

1.1 Preliminary Review of the Existing Turbine Meter theoretical models and their Limitations

Although the turbine meter is an apparently simple axial machine, there is no existing theory which can be applied for estimating the whole range of the calibration curve of a turbine meter.

The hydrodynamic behaviour of the turbine meter is not completely understood. The significant characteristics of turbine meters are still to be analysed in detail, only then may a theory applicable for the whole operational range be derived. The meter coefficient

[1] This term is concerned with bearing friction torque as indicated in eq. 1.11
[2] See Table 9.1 page 93

(number of pulses per unit volume of fluid) can be calculated in a very simple way if ideal conditions are assumed. The ideal condition are those which neglect factors such as bearing friction and assume uniform flow through the meter annulus and no slip. Hence the flow rate is given by

$$Q = \pi r_0^2 \bar{L} \cdot n \left[1 - \left[\frac{r_h}{r_0}\right]^2 - \frac{4N (r_0 - r_h) \cdot t}{\pi r_0^2 \cos\beta}\right] \qquad (1.12)$$

The meter coefficient can be calculated from the above approximate equation. This equation is based on incompressible and bubble free flow conditions; it does not show the dependence of hydrodynamic forces and viscosity influence on the turbine blades. The rotor angular velocity is proportional to the fluid velocity or flow rate. Some theoretical models have been developed to explain the experimental results obtained from flow measurement through a turbine meter. For each of the theoretical models some assumptions have been made to simplify the calculations. In practice most of those assumptions are not justified because such ideal conditions are never realistic. According to the Hochreiters model (Ref. 24), the calibration curve should be linear throughout the flow range, which means the same meter coefficient is assumed at all flow rates, and even for zero flow rate. The calculation of the calibration curve for this model will never be near the achieved experimental results. Lee and Karlby (Ref. 36), derived their model from the Euler turbine equation and calculated the mechanical torque acting on the turbine blade. They assumed that the non-fluid forces (bearing friction, retarding force due to magnetic pick up), are negligible. This assumption cannot be true because these forces maintain a significant part of the Term 3 especially in the range of low flow rate of the M.T.E. and are occasionally useful for viscosity compensations. Another assumption of Lee and Karlby was that the angle of attack, α, is very small, so that there is no possibility of laminar separation of flow on the turbine blade. The skin friction is part of the total fluid friction. According to the experimental and theoretical calculation of this research and of the previous work (Ref. 86), the angle of attack, α, on the helical blade is much smaller than on the constant blade angle (Fig. 87). The results of the experiments of the present research show that the helical blade (Figs. 6 and 22) is not affected significantly by viscosity in comparison with the constant blade angle (Figs. 9, 12 and 12a). Lee and Karlby assumed that by keeping the value of T_D and T_{mech} as low as possible, the value of the meter coefficient would not vary by more than a small allowable quantity over a wide range of flow rates, not even when the viscosity is increased. This assumption could not be proved by the results of

the author's investigation, nor by Tan's result (Ref. 86) because of the effect of tip clearance, and of the viscous flow on the velocity distribution curve, the deviation angle, δ^* and on the drag coefficient, C_D, which all affect the three terms of the main turbine equation. Term 1 depends on the flow rate, and has a magnitude 44 to 83 times Term 2, and 20 to 180 times Term 3, from very high to very low flow ranges. Any change in Term 1 of the main turbine equation affects the calibration curve much more than a change in any of the other terms. However, the effect of viscosity on the last two terms determines the minimum operating flow rate in a turbine meter of small size and low capacity.

The calculation of the hydrodynamic torque is complicated because of the effect of the axial velocity distribution curve in upstream position of the blade and its variation with viscosity changes. In general, the turbine blades are influenced by the hydrodynamic torque and the bearing torque, which are in turn affected by viscosity changes. Lee and Karlby divided the turbine flow meters range into three different zones, laminar, transition and turbulent.

1.1.1 The magnitude of skin friction coefficient for the laminar zone, or the region of low Reynolds' number

Lee and Karlby used the relation between skin friction drag and Reynolds' number for a flat or thin symmetrical aerofoil in two dimensional flow. This relationship obeys the Blasius law

$$C_f = \frac{B_e^*}{Re_{blad}^{1/2}} \tag{1.13}$$

The secondary effects which include the three dimensional flow effects, the cascade effects, the rotating effects, and the pressure effect, will make the above relationship considerably different. Lee and Karlby (Ref. 36), assumed that these effects could be minimised by a well-designed meter.

1.1.2 The magnitude of skin friction coefficient for the transition zone

The region is the one between fully laminar and fully turbulent flow over the blades. The boundary layer of the turbine blade is laminar at the front or upstream edge of the blade, becoming turbulent further downstream. The position of the transition point can be determined from its distance from the leading edge and will depend on the intensity of the turbulence in the external flow. According to Prandt-Schlichting for flat plate at

zero incidence, the value of skin friction drag coefficient can be calculated from the value of drag for turbulent flow subtracted from the value for transition flow:

$$C_f = B^*_{turb} - \frac{B^*_{trans}}{Re_{blade}} \tag{1.14}$$

The position of the transition point (distance from leading edge) depends on the intensity of turbulence and will be defined by the value of Reynolds number based on the above mentioned distance. B^*_{trans} can be defined as follows:

$$B^*_{trans} = (B^*_{turb} - \frac{B^*_e}{Re^{1/2}_{crit.}}) \tag{1.14a}$$

1.1.3 The magnitude of skin friction coefficient for fully turbulent flow, or region of high Reynolds number

For high Reynolds's number, the boundary layer is fully turbulent, the blade surface cannot be considered hydraulically smooth. The skin friction drag becomes a function of the square of the velocity and the drag coefficient is independent of the Reynolds' number

$$C_f = \frac{D}{\frac{1}{2} \cdot V_m^2 \cdot 2c\,(r_t - r_h) \cdot \rho} \tag{1.15}$$

Lee and Karlby assumed that T_{mech} for a well-designed meter is negligible and the hydrodynamic torque consists of a resistive torque due to the skin friction drag in the turbine cascade, and to all secondary fluid drags (expression for the drag coefficient due to kinetic energy in the secondary flow). The skin friction drag coefficient

$$C_f = B^*_{turb.} = \text{const.} \tag{1.16}$$

and the overall secondary drag coefficient

$$C_s = \frac{D_s}{\frac{1}{2} \cdot V_m^2\, 2c(r_t - r_h) \cdot \rho} \tag{1.17}$$

With substitution of (1.15) and (1.17) into (7.18)

$$\frac{\omega_a}{Q} = [\frac{\tan\theta_m}{rA_a} - \frac{K}{N \sin\theta_m} \cdot C_s] - K C_f \tag{1.18}$$

The value of C_f depends on the operational Reynolds' number and

$$K = \frac{Nc\,(r_t - r_h)}{r_m \cdot A_a} \cdot \frac{\sin \theta_m}{\cos^2 \theta_m} \tag{1.19}$$

The assumption that the skin friction drag coefficient attains a constant value for fully turbulent flow cannot be accepted because this coefficient also depends on the angle of attack. The drag coefficient is constant up to a certain value of α and above this value the coefficient starts to increase. This increase happens in fully turbulent flow. H. Schlichting (Ref. 66) found that the relation between C_f and Reynolds' number in the transition zone, making an allowance for initial laminar length and the Prandtl-Schlichting formula is

$$C_f = \frac{0.255}{\log Re^{2.58}} - \frac{A''}{Re} \tag{1.20}$$

$$A'' = Re_{critical}\,(C_{f_{turb}} - C_{f_{lam}}) \tag{1.21}$$

The velocity distribution in the meter annulus becomes "peakier" when the viscosity is increased (Fig. 53). The error[1] magnitude also increases with increasing viscosity. In general, the fluids with higher viscosities tend to have a larger deviation from the normal operational meter coefficient at high Reynolds' number than the fluids with lower viscosities. Up to a certain viscosity, as the flow rate is increased, the calibration curve shows a hump, which according to Lee and Karlby occurs at the change over from laminar to turbulent flow. However, the author's research has found that the hump is due to the compensation of the three terms of the M.T.E. A turbine meter with a large hub ratio should be less sensitive to Reynolds' number or viscosity increases because the velocity distribution will always be flat. A close analysis of Lee and Karlby's theory shows that calibration curves can be divided into two regions – linear for high Reynolds' number and non-linear for low Reynolds' number. These two regions are connected via a transition section which, for the same meter, moves towards the higher flow rates when the viscosity is increased. The applicability of the properties of a single aerofoil is doubtful for use in a rotating turbine blade, unless the following effects are considered:

(a) the effect of the rotor blades on each other (interference)

(b) the effect between the turbine blade and hub (cascade secondary vortices)

(c) the edge effect of rotating turbine blade and the turbine cascade

(d) the centrifugal forces on the blade boundary layers due to the rotation.

[1] Deviation of meter coefficient from m.c. at high Reynolds number

(e) the variation in Reynold's number with blade radius.

The effect of Reynolds' number or viscosity on the M.T.E. may also be seen by substituting (1.20) in (1.18). The fact that a decrease of Reynolds' number with an increase in the value of fluid viscosity increases the term outside the square brackets, i.e. an increase in the fluid viscosity leads to a rise in the deviation from the normal operational meter coefficient. The larger the fluid viscosity the greater the value of deviation. The effect of the tip clearance has not been shown in any connection to fluid viscosity.

In addition the value of A" in equation (1.20) depends on the position of the transition point, which depends on the Reynolds'[1] number. According to this model the shape of the calibration curves depend only on the state of the boundary layer on the turbine blades. According to Lee and Karlby's model, the boundary layer is turbulent in the region of high flow rate and where the calibration curve is flat. In the region of low flow rate the boundary layer should be laminar and the transition region will connect the non-linear and the linear parts. Six experimental points are required to calculate the three different operational zones, two in each zone. According to Lee and Karlby, the laminar and transition zones will intersect so that the calibration curve does not exhibit a hump as shown experimentally (Fig. 26). Therefore, Lee and Karlby's sharp intersection between the linear (high flow rate) and non-linear (low flow rate) regions of the theoretical calibration curve cannot be applied to the calibration curve obtained experimentally which shows a hump in the mid-range flow rate. They paid very little attention to the effects of viscosity and tip clearance which are according to Tan and the present author's approach, the reasons for the creation and disappearance of the hump in the calibration curve.

1.1.4 The Effect of Variation of Tip Clearance on Turbine Flow Meter Calibration Curve

Tan demonstrated in his experiment that by increasing the tip clearance by turning down the rotor, the measured calibration curves showed an increasing hump between the linear and non-linear sections. The hump has been produced as a result of the tip clearance flow and not as explained by Lee and Karlby as a result of the boundary layers condition.

However, the leakage theory has been demonstrated in Tan's model, which point out the significance of the tip clearance. According to Tan's theory and experimental results, increasing the tip clearance of a constant blade angle research meter reduces the operating range of the calibration curve, by moving the threshold of the linear region to a higher flow rate, and thus increasing the non-linear region. Tan showed that the volumetric value of the tip clearance is independent of the flow conditions. The author has

[1] Critical Reynolds number

found that the flow condition in the tip clearance depends entirely on the angle of attack and on viscosity changes. The angle of attack determines the direction of the flow, which can be co- or counter-directional to the main flow. In this research the flow in the tip clearance of the helically bladed rotor is found to be always in the same direction as the main flow. This is not the case in the constant blade angle rotor.

Tan has proved that changing the tip clearance will change the leakage factor, k, and leakage ratio, g, which in turn control the shape of the calibration curve in the lower flow range. These factors are purely empirical values and are constant if the test fluid is water or[has a viscosity very close to the viscosity of water. From this research it is shown that the k and g factors cannot remain constant for high fluid viscosities. The author has replaced k and g with empirical equation which can be used for the chosen fluid viscosity. This will be discussed in greater detail in Chapter 2.3 and App. I. According to Tan's theory the meter coefficient consists of the pulses per unit volume flow travelling through the rotor $(\frac{n}{Q_r})$[1], multiplied by the ratio[2] of Q_r/Q. Tan's model n/Q_r consists of three terms, T_1 to T_3. He calculated these values by fitting the best possible curve to the M.T.E.[3] He used the least squares method and took two experimental points to find the leakage factor k and the leakage ratio, g. This is purely empirical and only applicable for water. The author replaces these terms with a viscosity dependent function. The same is done for the hydrodynamic components like local velocity, u, the deviation angle, δ^*, and the velocity angle, θ, so that the Terms T_1, T_2, T_3, are calculated theoretically. Instead of taking the leakage factor and leakage ratio into consideration, the author has developed an alternative model for calculating the volumetric efficiency Q_r/Q. This is purely a theoretical model and replaces Tan's empirical approach (Chapter 6).

According to Salami's model the shape of the calibration curve depends on the upstream velocity profile. He fails to explain the existance of the hump, and also there is no explanation of tip clearance flow and its significance in his theory. Salami's (Ref. 97) experiments on research turbine meters were carried out on meters with photocell pick ups. There is some discrepancy in his experimental results, which is described in Chapter 3. Therefore the theory based on his experimental results is doubtful i.e. Salami's model does not explain theoretically the existance of the hump on the calibration curve nor does he investigate the effect of tip clearance size and flow, and the effect of increasing viscosity.

1.1.5 The Axial and Tangential force Produced on Turbine Blades

Comolet (Ref. 6) derived a main turbine equation which is in general very similar to

[1] Eq. 5.11
[2] Eq. 6.88 = 1 – g + k/Q
[3] The MTE could be stated using eq. 5.20 and/or eq. 1.1

those derived by Tan (Ref. 86) and Lee and Karlby (Ref. 36).

Comolet (Ref. 6) neglected the effect of tip clearance. According to Tan's turbine equation, (Ref. 86) shows that the amount of flow going through the tip clearance is not negligible and has a large influence on the rotational speed at low flow rates. This effect will be discussed later. Comolet (Ref. 6) has also analysed the influence of the hub on the axial forces.

Taking account of tip clearance produced a basic improvement in the turbine meter general equation. Comolet's equation (Ref. 6) consisted of calculating the axial, dA, and tangential, dT, forces on the blade, which gives (see Fig. 3) (with the assumption that α is very small).

$$\beta - \theta = 0$$

The value of dT_d on the blade element is as follows:

$$dT_d = r \cdot dR = \frac{\bar{\rho} \cdot c \cdot V_m^2}{2} (C_L \cos\theta_m - C_D \sin\theta_m) r \cdot dr \qquad (1.22)$$

According to Gerston's cascade measurement (Ref. 17) the value of C_D (a correction for his experimental data has been suggested in Chapter 5.2 to allow for Reynolds' number effect), is given by

$$C_D = \frac{4\dot{v}_H^* + t}{c} \qquad (1.23)$$

With the assumption that the flow on the boundary layer past the blade leading edge is turbulent, the displacement thickness is given by:

$$\frac{\delta_H^*}{c} = \frac{0.046}{Re^{1/5}} \qquad (1.24)$$

And, (assuming that $\alpha \approx 0$ which can be applied for helical bladed rotor), momentum thickness by:

$$\frac{\dot{v}_H^*}{c} = \frac{0.036}{Re^{1/5}} \qquad (1.25)$$

thus

$$C_D = \frac{4\dot{v}_H^* + t}{c} = \frac{0.144}{Re^{0.2}} + \frac{t}{c} \qquad (1.26)$$

$$C_L = \frac{0.144}{Re^{0.2}} + \frac{t}{c} + 2\left(\frac{0.02}{Re^{0.2}} + \frac{t}{c}\right) \qquad (1.27)$$

In order to study the axial forces, and their influence on the blades and the hub, the forces are calculated assuming that the axial fluid velocity is constant in the blade area, and that α is very small.

$$A_{F_{blades}} = \frac{\rho}{2} \cdot c \cdot N \cdot U^2 \int_{r_h}^{r_t} C_{Do} \left[1 + 2\left(\frac{r}{r_0}\right)^2 + \left(\frac{r}{r_0}\right)^4\right] \frac{dr}{r_0} \qquad (1.28)$$

Comolet regarded the hub as a flat plate (length W and width $2\pi r_h$). The blades are perpendicular to this plate and according to Schlichting, the inter-action of the flow in the root gives a factor of: ($\bar{\zeta}$ is the corner effect between hub and turbine blade)

$$\bar{\zeta} = -\frac{0.0052}{Re^{0.4}} \qquad (1.29)$$

$$C_{D_{hub}} = \left[1.89 + 1.62 \log\left(\frac{c}{k_s \cos\beta}\right)\right] - \frac{N \cdot 0.0052}{Re^{0.4}} \qquad (1.30)$$

The Comolet model is applicable only where the tip clearance effect may be neglected and where $\alpha \approx 0$. Meter type B approximates to this situation and, since its Reynolds' number is close to that of the standard type, it may be considered to act in the manner of the Comolet model. But in the case of constant bladed angle rotors, α is large and can increase up to 12 ° at which value it has a large influence on C_D and C_L, and will affect all three terms of the M.T.E. Also the tip clearance flow is significant and cannot be neglected. Neglecting the tip clearance effect, as Comolet does, introduces an unacceptable error into the M.T.E. Also Comolet did not consider the effect of viscosity on the calibration curve.

CHAPTER 2. AIM OF RESEARCH

The experimental results in the present research show that for constant (Fig. 9) and helical blade angle rotors (Fig. 6) the meter coefficient n/Q is affected by Reynolds' number through the variation in dynamic viscosity over the whole range of the turbine meter calibration curve. In order to appreciate the reason for this it has been necessary to examine the turbine equation divided into three parts as follows:

$$\frac{n}{Q} = \overset{\text{Term 1}}{A} + \overset{\text{Term 2}}{\frac{B}{Q}} - \overset{\text{Term 3}}{\frac{C}{Q^2}}$$

This is similar to the equations of Comolet (Ref. 6), Kalkhof (Ref. 32), Lee and Karlby (Ref. 36) and that of Tan (Ref. 86) which is the only one to include the term B/Q which is related to tip leakage losses.

Each of three terms on the RHS is a complex combination of turbine meter and fluid characteristics, as discussed in later Chapters. A change of any of these terms will affect the meter calibration curve in a particular way. In order to understand the effect of viscosity it is necessary to consider the following points:

2.1 The physical meaning and the significant parameter in the different terms of MTE

Term 1. The ideal[1] value of the turbine meter coefficient $(\frac{n}{Q})$ is equal to the Term 1 of the above equation:

$$\frac{n}{Q} = A$$

This could be the case when the fluid velocity is proportional to the rotational speed (Eq. 7.20) and/or the values of B/Q plus C/Q^2 to compensate the drop in the value of A, which occurs by increasing the value of fluid viscosity (see Fig. 62), for helically bladed rotor. For the constant bladed rotor the above can happen only in the high flowrate with the condition of small value of B/Q and C/Q^2 (see Fig. 81a, 82).

"A" is dominant in the above equation and depends mainly on deviation angle δ*, lift and drag coefficient C_L and C_D and velocity distribution, which change with increasing fluid viscosity.

Term 2. $\frac{B}{Q}$: this term, which was proposed by Tan (Ref. 86) to cover the effect of tip-clearance and leakage, is a function of fluid viscosity and the leakage factor k (see App. I) The drag coefficient and the velocity profile in the meter annulus are affected by an increase of fluid viscosity which will change the magnitude of this term. Tan (Ref. 86) has shown

[1] The ideal value of A could not be achieved for the meters used in this research

the effect of tip clearance on this term (Fig. 25)

Term 3. $\frac{C}{Q^2}$: this term depends mainly on the total torque acting on the turbine blades (Eqs. 7.15). T_d (Eq. 7.8) and T_{bear} (eq. 7.23) depend on fluid viscosity. ($T_{bear} = T_{mech}$)

The above three terms have been calculated in this research and also a comparison between the experimental and the theoretical results has been made, which led to satisfactory agreement.

2.2 The effect of Balance, Compensation or Reduction of the three terms of the main turbine equation upon the calibration curve

It is desirable that the sum of three theoretically calculated terms in the M.T.E. shall give good agreement to experimental values of n/Q, since the relative magnitude of the three terms can then be compensated for changes in viscosity or other variables. Knowledge of the variation in the three terms can then be used to produce the geometry which will give a constant meter coefficient over the widest possible range of flow for fluids of high viscosity. Reduction of the Term 2 or 3 separately has the following results on the calibration curves:

1. A reduction in Term 2 due to a decrease in tip clearance or an increase in viscosity[1] causes a drop in the meter coefficient at low flow rate (Fig. 16). This pushes the lowest reliable range of the turbine meter towards the higher flow rates and the working range becomes smaller.

2. A reduction in Term 3, by balancing the mechanical (eq. 7.21) and hydrodynamical torques (eq. 7.15), or the effect of fluid viscosity on Term 2 which causes a hump on the calibration curve (Fig. 9, 12 ν = 12, 21, 47 cSt).

The experimental results have shown (Figs. 6 and 22) that the turbine meter with helical blades (Fig. 11) is less sensitive to the effect of fluid viscosity than that with a constant blade angle rotor (Fig. 10). The reason for this advantage might be one of the following points:

1. The angle of attack α, is small for the helical blades in comparison with the constant blade angle rotor (Ref. 86). Thus the hydrodynamic torque is small and hence will reduce Term 3. Also the tip clearance flow is co-directed with the main flow. Therefore, the variation in fluid viscosity affects mainly Term 1 which will be compensated with Term 2 and the calibration curve will be flat. The increase of fluid viscosity would not change the shape of the calibration curve greatly when the other Term 3 is negligible or has a compensating effect with the other two terms.

[1] Constant blade angle rotor

2. The velocity distribution over the blade area contributes towards a uniform force acting on the blade which does not change its magnitude with increasing fluid viscosity. (Equation 1.28). Besides there is no negative lift because the angle of attack is small and positive.

It was essential to predict theoretically the calibration curve obtained from numerical calculations of the magnitude of the hydrodynamic components with changing fluid viscosity. The above components are lift coefficient, C_L, drag coefficient, C_D, angle of attack, α, velocity angle, θ, and angle of deviation, δ *. Changes in turbine meter geometry such as blade angle, β, hub and tip clearance ratio, blade chord and thickness, and rotor bearing types (plain or ball bearing) will be made and their effect on the above components evaluated.

2.3 The theoretical leakage model based on tip clearance hydrodynamic behaviours

The main turbine equation introduced in Chapter 1 (eq. 1.1) has been derived by Lee and Karlby and altered by Tan to include the effect of tip clearance.

Tan developed his theory after adjusting the M.T.E. to fit his experimental results. This research has modified Tan's theory to make allowance for the effect of fluid viscosity on M.T.E. (Tan restricted his experiments to water only). The author has divided the M.T.E. into 2 main parts (eq. 5.15) which are:

a) The ratio of angular velocity to the flow through the rotor is (n/Q_r). The n/Q_r (eq. 5.10) has been calculated for type B turbine flow meters (representative of helically bladed angle rotor) and type C (representative of constant bladed angle rotor). T_1, T_2, T_3 had to be precalculated (eqs. 5.12, 5.13, 5.14) in order to determine n/Q_r (eq. 5.11). T_1, T_2 and T_3 vary with fluid viscosity and consequently the number of pulses produced by them will vary. The theoretical and the experimental values of the meter coefficient of n/Q for varying fluid viscosity are shown in figures 88-99.

b) Q_r/Q is influenced by the leakage or tip clearance flow which affects the calibration curve. Three different methods have been introduced in this work to calculate Q_r/Q.

1) The leakage method based on calculations of g (leakage ratio) and k (leakage factor) as a function of flow rate and fluid viscosity (chapter 8 app. I).
2) Displacement and momentum thickness based on boundary layer theory (Chapter 5.1)
3) The calculation of energy losses at the tip of the blade, based on the flow conditions in the tip clearance area (turbine flow meter volumetric efficiency, (Chapter 6).

When the experimental calibration curve has been determined the empirical values of A, B, C (eq. 1.1), g, k, T_1, T_2 and T_3 (eq. 5.20) can be obtained by using the method of least squares (App. I).

There is good agreement between experimental results and calculated values for the helical blade rotor and not such a good agreement for the constant blade angle rotor. This is not only because of leakage affecting the tip clearance flow. Any disturbance in the tip clearance flow will also affect n/Q_r therefore, n/Q. The calculation of this volumetric ratio Q_r/Q, (for uniform flow), is performed by integrating the flow through the blades from the blade hub to the blade tip and from the blade hub to the turbine casing respectively.

$$\frac{Q_r}{Q} = (1 - \frac{Q_c}{Q}) \qquad 2.1$$

The value of Q_c (eq. 5.17a) is the tip clearance flow and can be determined by the calculation of boundary layer thickness using Gersten's theory (eq. 5.16) which is described in chapter 5. Alternatively a more complicated method of this calculation is to apply the momentum equation in the turbine meter cascade and calculate the Q_c value by finding the energy losses in the turbine meter tip clearance (chapter 6).

The determination of the Q_r/Q ratio based on the volumetric efficiency of the turbine meter, can be used when there is not a good agreement between the empirical leakage method and the experimental results.

CHAPTER 3 AN ANALYSIS OF THE PREVIOUS EXPERIMENTS ON THE EFFECT OF THE FLUID VISCOSITY ON THE TURBINE METER CALIBRATION CURVE

At the beginning of this research programme there were three different experimental results available from the former researchers which may be divided into the following groups:

3.1 The experimental result on the research Turbine meter with Photocell pick-up

To explore the effect of viscosity on the research flow meter (Fig. 21) was the aim of Salami's research programme.[1]

He worked on research turbine meters having a photocell pickup (Ref. 65). The reflected light beams on the turbine blade tip which came from a bulb attached to the turbine meter casing, were picked up from a photocell, which was placed close to the light. The pulses were counted in a counter with 100 mV threshold.

As some of the pulses were not countable because of this low amplitude there was a counting error, which led to inaccuracy in the measurement. In Figs. 21, 37, the result of missed pulses can be seen; they do not have a dot under the very weak pulses. Another effect at high flow rate for photo-cell pick ups is that because of the large number of pulses, a certain number of pulses may join together and the Schmidt-trigger cannot separate them for counting. In this research work, these effects have been discovered by installing a magnetic pick up on the research meter with the photocell pick up (Fig. 34). The pulses produced from the magnetic pick up of this meter (Fig. 39) are harmonic in shape compared with pulses produced from photo cell pick up for the same rotor (Figs. 36, 37). The above mentioned magnetic pick up on the research meter made it possible to check the number of the missing pulses, which were lost during counting with photo cell pick ups.

This can be seen in Fig. 20; the calibration curves were plotted once just by using the photo cell pick-up and another time by using the magnetic pick-up. It can be discovered that from a flow rate of 4 lb/sec.[2] upwards a certain number of pulses are missing, but the measurement was difficult for low flow rates in the case of the magnetic pick-up because of the low speed of the blades passing the magnetic field.

The results of the present research have shown that the maximum gradient (the slope of non-linear part), of the calibration curve (n/Q against Q) for low flow rates will decrease, with an increase in the fluid viscosity. The calibration curves for fluids of higher viscosity than water rise with Q at slower rate than that for water but reaches a higher saturation (asymptotic) level after intersecting the curve for water, which gave a similar calibration

[1] Salami used only 1 photo cell pick-up, therefore he received less pulses/rev.
[2] Q = 4lb/sec = 1.816 litre/sec

curve to the commercial meter with a constant blade angle (Fig. 19). Salami's results with missing pulses due to the photo cell pick up (Fig. 21) can be compared with the present results (Fig. 20) obtained by installing the magnetic pick up on the above meter. The similarity between the research meter (Fig. 19) and the commercial meter (Figs. 9, 12, 12a) can be seen in a comparison of the calibration curves of these two groups of research and commerical turbine meters (Salami's results: two different calibration curves for commercial and research meter, Figs. 21, 28). The above two groups of meters have similar geometrical devices with small bearing friction and constant blade angle.

If the tip clearance from one blade is larger than for the other two in the research meter the reflected light beam from the blade tip will almost disappear and does not reach the photo cell because the viscous fluid (see chapter 4 for fluid being used), is not sufficiently transparent. This is one of the reasons for having some pulses of very small amplitude. The second reason is because of the different electrical resistances of the bulbs and their position relative to the blade tip. There were 4 photo cells installed on the research meter each of them collected the reflected light beam from a 6 volt bulb. The reason for having 4 photo cell pairs was to have as many pulses as possible. This could be realised either by increasing the number of blades or alternatively increasing the number of pick ups. This affects the brightness of the beam, and may be the reason for having two different shapes of calibration curve for the constant blade angle rotor in the research turbine meter with photo cell pick-up (fig. 16), and the commercial meter and the same shape of blades with a magnetic pick-up (Fig. 12).

From the previous research, the number of pulses per unit volume for viscous flow was always less than the number of pulses per unit volume for water (Fig. 16). In current research programme, where a double check of accuracy was possible with the additional magnetic pick-up, the number of pulses per unit volume were above those of water from a certain flow rate (Fig. 19).

3.2 The effect of the fluid viscosity on the calibration curve of a turbine meter obtained using a magnetic pick up

The magnetic pick up has some fundamental inherent characteristics, such as producing a magnetic field which can cause a reduction in rotational speed.

The lower rotational speed causes a weakness in the pulses produced. The number of pulses per unit volume can drop below the pulses produced by photocell pick up. (Fig. 20).

The experimental results in Salami's research on a commercial meter, which have

magnetic pickup, have been obtained for an Elliott 1½ ins. turbine meter. The experimental result can be seen in Fig. 28. In order to explain these results the author has discovered that Salami has worked in just a very small operational region. It was not possible to carry out tests at a very high and very low flow rates because of the following reasons:

(a) the pressure in the test line increased to the highest allowable extent of 70 psi, (4.83 bar) because head loss over the filter (Fig. 1) was very high. The results for the commercial meter were not complete because with an increase in viscosity there was a rapid pressure-rise (over 70 psi) across the main pump in the test line. The results for high flow rates for fluids with high viscosity could not therefore be achieved because the pump pressure control switch operated and cut off the power. The second restriction in his results was the limitation of the counter to (100 mV). Any pulses with a weaker amplitude could not be counted. Thus Salami has missed the turbulent zone, which was the end of the non-linear and the beginning of the linear part of calibration curves for the research meter. Only the humps in his curves could therefore be seen.

For fluids with high viscosities, high Reynolds' number and large flow rates could be achieved in the author's research programme by bypassing the filter in circuit, thus avoiding a large pressure drop. The second limitation was avoided by counting the pulses with a counter having lower limitation threshold, or by amplifying the pulses' amplitude. The results of these improvements can be seen in Fig. 9 and 12). The blades Reynolds' number in Salami's results was between 20 and 20.10^3 and the Reynolds' number in the meter annulus was between 53 and 61.10^3. The discontinuity in the calibration curve was probably because of the switch over from two to four photocell pick-up readings. Salami assumed that this was the result of a changeover in the flow from laminar to transiation zone. Salami's experiments were carried out almost at low Reynolds' numbers (blade range $Re < 10^5$). Salami did not check the influence of tip clearance on his results.

3.3 The experimental result in Tan's research programme on a research meter

The experiments carried out in Tan's research programme, were with water. He proved that the flow going through tip clearance is not negligibly small and this achievement improved the M.T.E. Because of the cleanness of water (test fluid), Tan did not miss any pulses, so that his experimental results were reliable. The commercial use of turbine flow meters dictated an investigation not only with water, but also with fluids of different viscosities, to make the commercial range of turbine flow meters more reliable. That is the reason for completing the M.T.E. with hydrodynamic components

which change with different fluid viscosity, which has been done in the present research.

3.4 The experimental results in the Lee and Karlby research programme on a commercial meter

Lee and Karlby used a large turbine meter (16 ins. diameter helically twisted blade rotor). They achieved for high flow rates and low fluid viscosity the linear zone of the calibration curve, and the non-linear part of the calibration curve for high fluid viscosity and low flow rate on one calibration curve, i.e. they connected the two different test fluid viscosities on one calibration curve. Effectively, they were two different calibration curves which cover each other on high flow rates and divide into two different parts in the non-linear part of the calibration curve. This can be seen in the previous report[1] (Fig. 26). They maintained that the viscosity caused the hump on the calibration curve. But as a result of this research it is proved that the creation and disappearance of the hump is due to the influence of Term 2, and Term 3 of the M.T.E. The balance of these terms leads to the disappearance of the hump on the calibration curve, although the viscosity was very high and the meter was not viscosity compensated with an external load. Lee and Karlby have no Term 2 in their equation.

Lee and Karlby's experiments covered three different zones – laminar (pipe Re = 50-4000), transition (4000-9000) and turbulent (9000-10^6). The non-linear part of their results was connected to the linear part with a hump between them. The existence of the hump was due to fluid viscosity (Ref. 36), corresponding to Lee and Karlby's theory. Tan has proved that this hump is due to tip clearance. The experimental results in this research have shown that the hump exists up to a certain viscosity at which the values of Terms two and three will balance each other, and the hump will disappear. The meter calibration curve has been compensated for by providing the turbine meter with an external load which causes the hump to disappear sometimes on the calibration curve (Fig. 26).

Tan's experiments were in fully turbulent flow. The general aspects of his observation on the effects of tip clearance on the calibration curve were significant, because of his explanation of the existence of the hump on the calibration curves due to the large gap between the rotor tip and the casing was more logical than that of Lee and Karlby (Ref. 36). Also for turbulent flow, increasing the tip clearance increases the Term 2 of the main turbine equation (5.20), so that the number of pulses per unit volume increases by having a meter with larger tip clearance. Lee and Karlby assumed the hump in the calibration

[1] Author's Interim Report No. ME/75/18 published in October '75 in Department of Mechanical Engineering University of Southampton

curve was due to the changeover from non-linear (laminar) to the linear (turbulent) part of meter calibration curve. Tan's tests were mostly carried out in the region of high Reynolds' number, therefore he has not investigated the influence of drag and drag coefficient at low Reynolds' numbers. His general equation can be applied for transition and turbulent zone. Tan's experiments were generally with rotors ½ ins., ¾ ins and 1½ ins. hub diameter : pipe Reynolds' number varied from 25000-250000. In rotor upstream position the Reynolds' number was between 14300 and 22900 and the blades Reynolds' number was 8400-25300. Among the four research meters were two constant blade angle and two helical blade rotors. The rate of increase in meter coefficient with an increase in ν is smaller for helical blade rotors than for constant blade angle rotors. (Fig 9 for turbine meter with constant bladed angle rotor and Fig. 22 for helically bladed rotor). That could be the result of having no negative lift in the helical blade rotors. The angle of attack, α, is positive and small for the whole operation range. The discontinuity in the meter calibration curve can be seen in Tan's work, which was discussed earlier. Tan suggested this was the result of an increase in the angle of attack and stalling and unstalling phenomena.

Another viscosity experiment has been done by Fischer and Porter (Fig. 31-32) which was demonstrated in Paper 2-17-207 (Ref. 15). Their results are similar to those of Salami's (Fig. 27). The calibration curves in that paper are made for viscosities between 1 and 80 cSt.

CHAPTER 4. DESCRIPTION OF THE RIG

In this chapter the calibration rig will be briefly described. The schematic and control diagrams can be seen in Figs. 1 – 2. The main pump (positive displacement pump) driven by a 25 hp motor and an infinitely variable hydraulic transmission (Fig. 42), circulates fluid from the sump around the rig (Fig. 41). The flow passes through a filter and a bypass into a 10-inch (254 mm) diameter, 40 ft. (12192 mm) long pipe which contracts into a conical section. This is then connected to the 26 ft. (7925 mm) long test length, where the turbine-meter can be installed. At the end of the test length there are two pressure regulating valves. These motor-driven valves control the pressure in the test length (Fig. 47). A fine control valve with a smaller valve-seat and slower driving motor, is installed for fine pressure and flow rate adjustment. For very low flow rates, this valve was brought into operation. The pump could provide any flow rate by varying the drive until the required pump speed or turbine frequency was obtained. The flow converges gradually from 10 ins. (254 mm) to 2 ins (50.8 mm) or 1½ ins (38.1 mm) pipes through a conical section. During normal operation, the pump pressure is set for 68-72 psi (4.68–4.96 bar). This high pressure is necessary to prevent air bubbles in the test length and cavitation within the meter. The water flows finally through the diverter, either to the sump or to the weigh-tank, depending on the diverter position. The weigh-tank (Fig. 46) is situated on a weighing machine, which is capable of weighing up to 2000 lb (908 kg) within one ounce.

After the pump is started, the water begins to flow through the 10 ins. pipe, and test length, and through the diverter back to the sump. The meter is situated in the test length. The viscosity of the fluid is changed by dissolving powdered Celacol D 450 in it. The weigh-tank and fluid contents are weighed. The scale of the weighing machine can be preset to stop the flow into the tank at any required weight up to 1900 lb. (862.6 kg) by the activation of a photo-cell. The time for the collection of the required amount of fluid can be recorded using a timer counter to the nearest millisecond. Before the start of the measurement and after the required weight has been collected, the weigh-tank is weighed. The difference from the initial weight gives the weight of fluid collection. This collected amount, divided by the time taken, gives the measured flow-rate. The pulses divided by the flow-rate gives the meter coefficient. To begin the measurement, the timer counter is started manually and is stopped automatically by the photo-cell on the lever arm, when the required fluid has been collected. A direct reading viscometer, with concentric cylinders is used to measure the viscosity. During the test the solution temperature is

taken at regular intervals and their mean gives the test temperature. The viscosity of fluid is also checked regularly using the direct reading viscometer contraves (Rheometer 15, 30) to ensure that it has not changed appreciably.

The celacol solution was found to be Newtonian up to viscosity 400 cSt. A steady rise in room temperature did not change the viscosity of the solution significantly so that an extra correction factor was not needed.

4.1 Instrumentation

The liquid used for the experiments is collected in a sump, measuring 2 m. x 1.80 m. x .80 m. and containing 450 gallons (1700 litres) of liquid when full. The main pump (Fig. 42) sucks the liquid through a 3 ins. (76.2 mm) diameter steel pipe and discharges to a 10 ins. (254 mm) pipe through either the diaphragm valve or via the self cleaning filter (Fig. 43). The pressure of the pump is measured and controlled by a pressure switch at the end of the test length. The pressure switch will cut off the pump when a certain preadjusted pressure has been reached. The pressure loss will change when the filter is in-line, depending on the viscosity of the liquid, in order to produce a uniform flow. The flow can be diverted either into the sump or into the weighing tank after passing through a right angled brass bend and 2 way fish-tail diverter. The flow diverter is for directing the fluid into the sump or for diverting it into the weigh tank while the experimental points have to be taken (Fig. 44). A small pump (Fig. 49) can transfer the fluid from the weighing tank into the sump. Air vent valves are situated at the highest point of the 10 ins. (254 mm) pipe and connected together by a plastic transparent pipe. As an extra precaution to check for the presence of air bubbles, a perspex pipe is situated in the actual test length of the system. The perspex pipe connects the 2 vent discharges into the sump. The test length used for measuring are in 2 sizes, 1½ ins. (38.1 mm) and 2 ins. (50.8 mm) diameter.

4.1.1 Control Panels (Fig. 40)

The control panel is self explanatory. The speed control is interlocked with the main drive motor. Limiting switches are fitted for pressure control of the test length and the speed of the main pump. For circulating the flow, the diverter must always be in the sump position, when the panel is first switched on. There are 2 warning lights (fitted to the pressure and temperature gauge, of the main pump). These will light up if any excessive disturbance in pressure or temperature occur, and will shut down the pump. After the fault has been cleared, the CLEAR button is pressed. There is also a TEST button to

disconnect the system if the pressure or temperature is still out of allowable limit.

4.1.2 The Main Pump

The main pump is driven by a 25 hp motor, through a Kopp speed variator (Fig. 42). A toothed pick-up wheel is fitted on the output shaft of the Kopp variator, with a magnetic pick-up to count the rev/min. The limitation output is set for 300 – 2600 rev/min with a constant input speed of 1480. The speed of the pump is adjustable to the nearest 1 rev/min with an extra push button switch on the panel. By controlling the line pressure, the maximum and minimum flow rates obtained are 21 and 0.1 lb/sec. (9.53 and 0.0454 kg/sec). In comparison to the lowest achieved flow rate (0.2 lb/sec, 0.0908 kg/sec) in the previous research, the present modified rig is improved at lower flow rates (0.1 lb/sec, 0.0454 kg/sec). This has been achieved by fitting a fine adjustment valve in the test line. For very low flow rates the main valve is shut down and the line pressure is adjusted by diverting the flow and using the fine adjustment valve (Fig. 47). The relief valve on the main pump is set for 78 lb_f/in^2 (5.38 bar) to protect the pump against excessive pressure. There is also an equivalent switch on the main pump set for recommended temperature.

4.1.3 Test Length

The flow converges from 10 ins. (254 mm) pipe into 2 ins (50.8 mm) or 1½ ins (38.1 mm) diameter test length. A conical section is fitted to connect the 10 ins pipe to the test length. The test length diameter was always equivalent to the size of the turbine meter in use. The contraction of the 10 ins (254 mm) pipe to the test length diameter was necessary to achieve an almost uniform flow over the whole test length. The test length was made in several pieces ranging from 6 ins to 96 ins (152.4 to 2438.4 mm) to allow more meters to be tested in the length for double checking purposes and also for changing the position of the turbine meters over the whole test length.

4.1.4 Turbine meters

Two types of turbine meter bodies were used during these experiments, one with a perspex body designed by the author (Fig. 33) and a magnetic pick-up. Two holes were bored in the upstream and downstream positions of the meter for L.D.A. velocity measurement. The holes were for sending the laser beam through the meter's body. In the other meter, specially designed for the rig, a light from a 6 volt bulb is directed at the blade tips, which are painted white to reflect better. The reflected light beam was picked up by a photo electric cell and amplified by a pre-amplifier with a gain of 100. The light bulb

together with the photoelectric were all in one unit, mounted at the window on the meter's body (Fig. 34, 35). The output signal is converted into square waves (in a schmidt trigger set) and then counted by a timer. Four photo cells situated at each end of a pair of diameters of the turbine casing at right angles to each other. The rotors of the research meters have 3 blades; therefore, there are 12 pulses obtained for each revolution (Fig. 36, 37). For commercial meters a magnetic pick-up is used to count the rotational speed. (The output signal is shown in Fig. 39).

4.1.5 Control valves

Two motor driving valves were fitted parallel to each other, after the test length (Fig. 47). They are used for controlling the line pressure. One driving valve, with a bigger (2 ins (50.8 mm)) seat and faster motor was used for rough adjustment and the other with a smaller seat (¾ins (19 mm)) and slower motor, for fine adjustment. By having the smaller valve in operation it was possible to achieve an experimental point at a very low flow rate (0.1 lb/sec, 0.0454 kg/sec) with reasonable repeatability. Also it was possible with the fine adjustment valve to drive the meter at a certain rotational speed with an accuracy to the nearest of 1 pulse/sec. The valves are operated by a two-way motor. They can be operated from the panel, having two sets of limitation lights, and an indicator on the valves to show the position of the seats.

4.1.6 Flow diverter

After the control valves, the liquid flows through the diverter (Fig. 44) and then either into the sump or the weigh tank (Fig. 46), depending on its position. The diverter is actuated by 2 pull-type solenoids, one on each side of it (Fig. 2). Depending on which solenoid has been energised the flow is directed either to the weighing tank or the sump. A metal strip, painted black, is attached to the diverter. This strip blocks the light beam directed onto the photocell, when the liquid flows into the sump. The push button for starting the experiment (situated on the control panel) will change the position of the diverter into the weigh tank. Thus the strip will allow the light beam to fall on the photo-cell and so produce a signal which triggers a timer counter. After the preset amount of liquid has been collected, the diverter will go back to the original position, blocking the light beam and stopping the time counter.

4.1.7 Sump Tank

The sump tank has a capacity of 700 gallons (2646 litres) and is connected to 2 reservoirs. The first one consists of 3 bins connected together for preparing the viscous

fluid (Fig. 48). The cellcol powder is mixed with water, gradually thickening it. By adding this thick liquid to the sump the viscosity can be increased gradually.

To decrease the fluid viscosity there is a tank with a capacity of 500 gallons (2270 litres). A part of the sump liquid can be pumped away into another tank and the remainder diluted with water. Therefore, it is possible to run the experiment at every required viscosity.

4.1.8 Weigh Tank

The weigh tank has a capacity of approximately 2000 lb (908 kg). The weigh tank (Fig. 46) rests on the weighing machine without touching the ground (Fig 46). High and low level controllers are fitted inside the tank. The high level control prevents any overflow, by automatically switching the diverter into the sump. The low level control is a control for transfer pump while it is emptying the weigh tank for starting the new experiment. If the "low level" is reached a control switch operates the 3-way solenoid valve to a position, such that the fluid will circulate in the pump only, protecting it against running dry.

4.1.9 Weighing Machine

The weighing machine (Fig. 46) can measure up to 2000 lb (908 kg) of fluid with an accuracy of ± 1 ounce (28.375 grams). The maximum weight of liquid used for any one experiment could not be more than 1300 lb[1] because of the tank weight and the "low level" fluid amount. Before and immediately after each experiment the weight of fluid is measured and subtracted from the initial weight to calculate the exact weight of fluid used in the experiment. The required value could be set on the weighing machine. Initially, the arm of the weighing machine blocks the light beam going to a photo electric cell (Fig. 46), which is connected to a time counter. The time counter will stop immediately on reaching the required amount of fluid collection, as the weighing machine arm will lift and the light beam can be picked up by the photo electric cell. (The light beam on the photo cell will also activate the solenoid and the diverter will come back to the SUMP position). The weighing machine is calibrated every two months with standard weights. These standard weights are adjusted by the Weights and Measures Department to within ±10 grains (0.6479 grams).

4.2 Velocity Measurement Using Laser Doppler Anemometry

The velocity distribution over the turbine blade annulus, the angle of attack, α, and the deviation angle δ^*, and the velocity angle θ, upstream and downstream of the rotor,

[1] 1300 lb = 590 litres

are the unknown parameters which affect the main turbine equation and the drag and lift coefficients, which will be discussed later. This factor made it necessary to use a method for velocity measurement which does not disturb the flow as a pitot tube does. The Laser anemometer has been developed recently to measure velocities. The frequency of laser radiation scattered by a small particle moving in the test length, in the upstream and downstream positions of turbine rotor, varies in a manner dependent on the velocity and the scattering geometry (the Doppler effect) and can therefore be used for local velocity measurement. Thus for a given fluid velocity (Ref. 93):

$$\bar{\nu} = \nu_0 + \frac{2\bar{\mu} u \sin \hat{\theta}/2}{\lambda}$$

$\hat{\theta}$ = scattering angle of the measured region

u = velocity (m/s)

λ = wave length

ν_0 = frequency of pre shift

$\bar{\mu}$ = refractive index of measuring medium

$\bar{\nu}$ = frequency of Doppler shift

A laser beam is focussed onto a rotating scattering disc (Fig. 50-52). The scattered radiation is collected through a slit at an angle of $\bar{\alpha}$, to the main beam and provides the reference beam. The reference beam and the main beam are refocussed at the point in the turbine meter tube in the upstream or downstream position in which the velocity is to be measured.

The main and reference beams are focussed at their intersection point, defining the measurement region (a small ellipsoidal volume about 600 x 50 μm). The anemometer, mounted on the bed of a milling machine, is adjusted so that the measuring volume traverses the flow from the inside casing to the hub. This measurement has been done for the axial velocity components. The results for the axial velocity component are measured. The corresponding calculation of θ, α and δ^* must also be evaluated for every individual point between the hub and the casing of the turbine meter. For this purpose perspex turbine meter body has been designed with 2 holes in the upstream and downstream positions of the rotor to let the laser beam pass through the turbine casing.

4.3 Run and Calibration procedure

The rig can be used to calibrate any turbine flow meter up to 2 ins (50.8 mm) diameter at flow rates of up to 22 lb/sec (9.988 kg/sec) at 70 p.s.i. (4.83 bar). It can also be used to study the effect of viscosity temperature, swirl and velocity profile on the

calibration curve. Any liquid can be used, provided it does not attack the rig. The meter can be placed at any required position along the test length. By adjusting the frequency output or pump speed the flow meter can be set to any required flow rate. The time for collection of the liquid can be chosen between 50 sec. for the highest flow rate 22 lb/sec (9.988 kg/sec) and any longer time depending on the chosen flow rate and the capacity of the weigh tank (maximum 1300 lb, 590.2 kg). It was initially decided to vary the viscosity by the use of Methocel powder. This provided a certain number of difficulties, such as the non-Newtonian properties of the fluid. At higher concentration it was also difficult to mix a uniform solution even if the liquid was heated. Therefore, the Celacol D450 was finally chosen because of its Newtonian properties and the ease of cold water mixing. The mixed Celacol D450 liquid was also uniform (the same viscosity) all over the sump. The efficiency drop in the main pump with viscosity increase is corrected by reducing the line pressure (opening the by-pass valve (Fig. 43)). All the controls are operated from the panel. The experimenter has to take two weighing machine readings at the beginning and the end of any experiment. The rotational speed which varies approximately linearly with the flow rate, can be recorded in 3 different ways:

a) continuous reading of the frequency counter, which shows the produced pulses to the nearest 0.1 Hz. The lowest achieved frequency was the number of blades passing a photo cell or magnetic pick up per second. In the case of rotors with 3 blades, this was sometimes down to 3 pulses per second which was not desirable for the required accuracy;

b) reading the total number of pulses produced to find 1 experimental point on the calibration curve. The electrical noise produced by the flow diverter in changing its position from SUMP to weigh tank and back causes disturbance in the counter for the initial and end value, giving a false reading. These noise error pulses cannot be distinguished from the number of real pulses in the total;

c) reading the time interval for 1000 pulses and taking the average value. The time can be measured to the nearest millisecond and the disturbances can be cut off by ignoring the disturbed values of the first and last reading.

4.4 The Modification of the Test Rig to achieve more accurate Experimental Results for viscous fluids in the present research.

The calibration rig has been modified by the present author to achieve more reliable results. The aims of improvement were to avoid miscounting and to attempt a wider

operational range for every meter. Another attempt at improvement was to introduce a double frequency checking. This made it possible to discover the miscounting of pulses in two different ways:

a) the pulses produced by the research meter with a photo cell pick-up were checked in number with a magnetic pick-up installed on the same meter;

b) the number of pulses produced by the magnetic pick-up in the commercial meter was checked with the number of pulses produced by a second turbine meter in the same test line for the same flow rate.

All the pulses produced from the magnetic and photocell pick-ups were amplified; this was easier in the case of the commercial meter because of the harmonic shape of the pulses produced by the magnetic pick-up (Fig. 39). In the case of the research meter with photocell pick-up this procedure was more difficult because of the weak amplitude of the pulses, which were the same size as the noise level (Fig. 36). The amplification in this case led to a much greater number of pulses which were not only produced by reflection of the light beam on the passing blades but partly by the noise. The magnetic pick-up has helped in such cases to discover the correct number of pulses; the inaccuracy in the counting of the pulses made it impossible for Salami (Fig. 27, 28) to achieve reliable results at low flow rates (sometimes no results in the case of the commercial meter). The high pressure created by viscous flow could be overcome in this research by by-passing the filter. This was also one of Salami's difficulties in achieving a result at high flow rates.

A mini valve (Fig. 47) has been installed to operate the rig at very low flow rates, when the main driven valve at the end of the test line is shut. The slow movement of this mini valve has enabled low flow rates to be established. This valve also made it possible to make small variations around a doubtful experimental point so as to achieve more accurate results or for checking the previous one. The time counter was improved by minimizing the cut off time of the weighing bridge on the weighing machine.

It is also possible with the modifications carried out for this research, to determine the magnitude of the magnetic torque (negligible for 1 magnetic pick-up) produced due to the magnetic pick-up by running the rig with the research turbine meter in the test line, once with the photocell pick-up and once with the magnetic pick-up and subtracting the results from each other. In the previous research program there were four photocells used for counting the pulses. Using all four photocells produces four pulses from one

blade. In the case of the research meter with a three-bladed rotor, the pulses produced were very close to each other. This leads to miscounting because of the overlap of some of the pulses and the Schmidt trigger recorded two pulses for one. In this research programme, the four photocell pick-ups were changed over to two photocell pick-ups to extend the distance of pulses from each other to overcome the danger of overlapping.

The number of turbine flow meters for this research programme was increased from two (as in Salami's experiments) to six (Table 9.1). This was significant for the study of the effect of viscosity on turbine flow meters with different geometrical devices.

CHAPTER 5

THE ANALYZING OF DIFFERENT TERMS OF THE MTE

(Main Turbine Equation)

The main turbine equation derived by Lee and extended by Tan is only going to be usefully applicable to all turbine meters and all fluid viscosities if the hydrodynamic parameters such as C_D, C_L, u/U, Q_c, δ^* are theoretically investigated. The relationship between each of these parameters and the blades Reynolds' number or the fluid viscosity is analyzed in this research. If these relationships with Reynolds' number are derived for each of the hydrodynamic parameters, the relationship between Reynolds' number and a combination of hydrodynamic parameters may be derived. The various combination of hydrodynamic parameters may cause a variation in importance of terms in the MTE. This research is concerned with evaluating these relationships through an analysis of the calibration curve variations with different fluid viscosities in proprietary flow meters and comparing them with a theoretical model.

A study of the hydrodynamic parameters within the three terms in the MTE shows how each of these terms varies with the fluid viscosity, because these terms comprise hydrodynamic and geometrical parameters. Tan also considered the influence of tip clearance flow Q_c, which was neglected in the other published works, but he used only cold water as the test fluid, The increase of fluid viscosity will change the above parameters and cause variations in the calibration curves. Tan's theory can be modified by substituting viscosity dependent hydrodynamic parameters in the equation to make it acceptable for all fluid viscosities which have been used in this research. Also the calculation of Q_c in Tan's theory should be reconsidered because of its dependency on fluid viscosity. The change in Q_c with viscosity is caused by an increase in the boundary layer thickness and by variation in the angle of attack, α. The local universal axial fluid velocity in the passage between the hub and casing of a turbine flow meter is given by (Ref. 68):

$$u = \frac{1}{4\eta}\frac{dp}{dx}\left[(r^2{}_o - r^2) - (r_o^2 - r_h^2)\ \frac{\ln\frac{r}{r_o}}{\ln\frac{r_h}{r_o}} \right] \qquad (5.1)$$

The driving torque (Fig. 3) acting on the turbine blades (Ref. 86) is given by:

$$dT_d = \tfrac{1}{2}\rho \,.\, N \,.\, W \,.\, u^2 \,.\, r \,.\, dr \left[\frac{C_L \,.\, \mathrm{Sin}\,\alpha}{\mathrm{Cos}\,\beta \,.\, \mathrm{Cos}\,\theta_m} - \frac{C_D \tan\theta_m}{\mathrm{Cos}\,\beta \,.\, \mathrm{Cos}\,\theta_m} \right] \qquad (5.2)$$

The angle of attack is

$$\alpha = \beta - \theta_m \tag{5.3}$$

Thus

$$\text{Sin}\,\alpha = \text{Sin}\,\beta\ \text{Cos}\,\theta_m - \text{Cos}\,\beta\ \text{Sin}\,\theta_m \tag{5.4}$$

$$v_e = u \tan [\beta - (\theta_o + \delta^*)] \tag{5.5}$$

with v as inlet swirl velocity in tangential direction;

$$\tan \theta_m = \frac{2\pi rn}{u} + \frac{v_e}{2u} - \frac{v}{2u} \tag{5.6}$$

Dividing (5.4) by $\text{Cos}\,\beta\ \text{Cos}\,\theta_m$ gives

$$\frac{\sin \alpha}{\text{Cos}\,\beta\ \text{Cos}\,\theta_m} = \tan \beta - \tan \theta_m \tag{5.7}$$

with substitution of the equation (5.5) into (5.6) and then into (5.7) it follows

$$\tan \beta - \tan \theta_m = \tan \beta - \frac{2\pi rn}{u} - \tfrac{1}{2} \tan [\beta - (\theta_o + \delta^*)] + \frac{v}{2u} \tag{5.8}$$

Equation (5.7) with the extension described in equation (5.6) and equation (5.8), together with equation (5.1) will be substituted into equation (5.2). Equation (5.2) is integrated from hub to the tip of the blade so that:

$$T_d = \tfrac{1}{2}\rho \,.\, N \,.\, W \,.\, \Big[\frac{U_m^2 r_o^{\,2}}{2} \int_{r_h}^{r_t} \frac{C_L}{U_m \,.\, r_o^{\,2}} \,[2 \tan \beta - \tan [\beta - (\theta_o - \delta^*)]] \Big]$$

$$. \Big[[(r_o^{\,2} - r^2) - (r_o^{\,2} - r_h^{\,2}) \frac{\ln \frac{r}{r_o}}{\ln \frac{r_h}{r_o}}] \frac{\Delta p_{blade}}{4\eta \,.\, \Delta x} \Big]^2 \, r\,dr$$

$$- \pi \,.\, n\, U_m^{\,2}\, r_o^{\,3}\, C_L \,.\, \rho \,.\, N \,.\, W. \int_{r_h}^{r_t} \frac{1}{\Delta x} \,[(r_o^{\,2} - r^2) - (r_o^{\,2} - r_h^{\,2}) \frac{\ell n \frac{r}{r_o}}{\ell n \frac{r_h}{r_o}}] \frac{\Delta p_{blade}}{4U_m \,.\, \eta}] \frac{r^2 \,.\, dr}{r_o^{\,3}}$$

$$+ \tfrac{1}{2}\rho \,.\, C_L \,.\, N \,.\, W. \int_{r_h}^{r_t} \frac{v}{\Delta x\, U_m^2} \Big[[(r_o^2 - r^2) - (r_o^{\,2} - r_h^{\,2}) \frac{\ell n \frac{r}{r_o}}{\ell n \frac{r_h}{r_o}}] \frac{\Delta p_{blade}}{4\eta} \Big] \frac{r\,dr}{r_o^{\,3}}$$

$$-\tfrac{1}{2}U_m \rho r_0^2 N.W. \int_{r_h}^{r_t} \frac{C_D \tan\theta_m}{\cos\beta \cos\theta_m} \left[\left[(r_0^2 - r^2) - (r_0^2 - r_h^2) \frac{\ell n \frac{r}{r_0}}{\ell n \frac{r_h}{r_0}} \right] \frac{\Delta p_{blade}}{4\eta U_m} \right]^2 \frac{rdr}{r_0^2}$$

(5.7a)

The rotation speed of the rotor can be solved from the above equation (Appendix I) which is:

$$n = \frac{1}{2\pi r_0 B(\nu)} A(\nu) + C(\nu) - D(\nu) - \frac{T_{total}}{\tfrac{1}{2}\rho . C_L . N.W. \pi . U_m . r_0^3 B(\nu)} \tag{5.8}$$

The flow through the rotor is

$$Q_r = \pi r_0^2 U_m \int_{r_h}^{r_t} (2r - \frac{N.t}{\pi}) \left[\left[(r_0^2 - r^2) - (r_0^2 - r^2) \frac{\ell n \frac{r}{r_0}}{\ell n \frac{r_h}{r_0}} \right] \frac{\Delta p_{blade}}{4U_m \eta . \Delta x} \right] \frac{dr}{r_0^2}$$

(5.9)

The pulses per unit volume of flow through the rotor is given by:

$$\frac{n}{Q_r} = \frac{A(\nu)}{2\pi^2 r_0^3 . B(\nu)E(\nu)} - \left[\frac{D(\nu)}{2C_L \pi^2 r_0^3 B(\nu)E(\nu)} - \frac{C(\nu)}{2\pi r_0^3 B(\nu)E(\nu)C_L} \right]$$

$$- \frac{2T_{total} \cdot [E(\nu) + Q_c]^2}{\rho . C_L . N.W.B(\nu) . E(\nu) r_0 Q^2} \tag{5.10}$$

Equation (5.10) can also be written in the following form:

$$\frac{n}{Q_r} = [T_1 - T_2 - \frac{T_3}{Q^2}] \tag{5.11}$$

where

$$T_1 = \frac{A(\nu)}{2\pi^2 r_0^3 . B(\nu)E(\nu)} \tag{5.12}$$

$$T_2 = \frac{D(\nu)}{2C_L . \pi^2 . r_0^3 B(\nu) . E(\nu)} - \frac{C(\nu)}{2\pi r_0^3 B(\nu) . E(\nu) . C_L} \tag{5.13}$$

$$T_3 = \frac{2T_{total} [E(\nu) + Q_c]^2}{\rho . C_L . N.W.B(\nu) . E(\nu) . r_0} \tag{5.14}$$

The values of $A(\nu)$, $B(\nu)$, $C(\nu)$, $E(\nu)$ are defined in Appendix I. The total number of pulses per unit volume or meter coefficient will be

$$\frac{n}{Q} = \frac{n}{Q_r} \cdot \frac{Q_r}{Q} \tag{5.15}$$

The flow through the rotor can be calculated using equation (5.11) by having the value of axial fluid velocity, u, lift and drag coefficient (C_L, C_D) and the deviation, δ^*, taken from Rhoden's measurement in the same range of blade Reynolds' number (Ref. 96). The volumetric ratio of flow through the rotor divided by the meter annulus flow can be either determined empirically by taking Tan's leakage theory (Ref. 86) and extending it to cover changes due to the variation in the fluid viscosity (Fig. 65, 84). The leakage ratio, g, (Fig. 64, 82) and the leakage factor, k (Fig. 66, 84) have been empirically determined for different fluid visocisites. These values have been calculated using the least square method for different blade Reynolds' number (Fig. 66, 84, 85). Thus Tan's function $1 - g + k/Q$ has been determined for different fluid viscosities. The values of T_1, T_2, T_3 (equations 5.12, 5.13, 5.14) have been calculated (see Appendix I). Thus values which are determined for different fluid viscosities (Fig. 58, 59, 61) can be combined with the Tan's leakage model for different fluid viscosities. Thus the calibration can be determined for any fluid viscosity if the leakage factor k and g are determined. This method is a semi-empirical way to evaluate the turbine meter equation. This method will have a correction effect on the calibration curves and can be considered as correction leakage factor for the flow through the turbine meter rotor. Alternatively, there is another theoretical model to evaluate this correction which is based on volumetric efficiency.

The second part of equation 5.15 (Q_r/Q) introduces the volumetric efficiency of a turbine flow meter. The volumetric efficiency can also be calculated by subtracting the tip clearance flow Q_c from the total turbine meter passage flow, Q. Thus the tip clearance flow needs to be known.

5.1 The evaluation of tip clearance flow due to the growth of the boundary layer thickness at the tip of the turbine blades.

A first approximation for the total volumetric flow through the turbine meter annulus can be made adding an integration of the flow between the hub and the blade tip, to an integration of the flow between the tip and the meter casing (the tip clearance flow). The actual flow rate is the fluid which passes the turbine flow meter rotor plus outside

effects such as the boundary layer effect and the tip clearance flow. Experimental results have been used as a semi-empirical calculation to evaluate the growth of the boundary layer thickness. The boundary layer thickness should be calculated at the blade trailing edge in order to evaluate the significance of the boundary layer effects on the calibration curve. For the determination of energy losses due to the boundary layer it is sufficient to know the values of the displacement and momentum thicknesses, which are according to Gersten (Ref. 17), displacement thickness

$$\delta^*_H = \frac{\bar{\bar{K}}}{Re^{.2}_{blade}} c \tag{5.16}$$

and the momentum thickness is

$$\dot{v}_H = \frac{\bar{\bar{\bar{K}}}}{Re^{.2}_{blade}} c \tag{5.17}$$

The constant factor, $\bar{\bar{K}}$ has been checked in the present experimental result. The author's approach is more realistic and makes the equations (5.16, 5.17) more accurate in practice. The experimental conditions in Gersten's Experiment are not comparable with those of this research (higher Reynolds' number and different blade shape). The consideration to make Gersten's equation more applicable for this research was as follows: The blades Reynolds' number at the peak of the hump in the calibration curve represents the maximum number of pulses per unit volume. The hump in the curve gradually moves towards the higher flow rate and disappears completely above a certain fluid viscosity (Fig. 12). The creation and disappearance of the hump are caused by the existence of a co-directional tip clearance flow. This statement is valid for both helically and constant blade angle rotors because the effect of viscosity will change the calibration curve of all groups of meter on the same way but different degree of intensity. A reduction of the tip clearance flow tends to flatten the hump until it disappears completely. The same effect can be achieved by decreasing the tip clearance. This was proved in Tan's experimental and theoretical results (see Fig. 25).

At a position where there is no tip clearance flow, the displacement thickness is equal to the size of tip clearance. The boundary layer thickness is for zero tip clearance flow exactly the size of tip clearance. For this case the n/Q is equal to n/Q_r or the flow through the meter annulus is passing only the blade area. Also, the Reynolds' number can be

calculated for this point. Therefore the $\bar{K}$ value can be calculated for any turbine meter. When a sheared flow (tip clearance and main flow) is turned through an angle, the vorticity vector, which is initially normal to the flow direction, will have a component along the main flow. The value of the constant factor $(\bar{K})$, $(\bar{\bar{K}})$ in equations 5.16 & 5.17 can be calculated for any turbine meter. Although the boundary layer near the turbine meter casing can cause unusual conditions, the principles of turbulent boundary layer can be applied to this situation with the addition of the above mentioned modification.

The actual value of the tip clearance flow will contribute to some extent to improve agreement between the calculated and empirical results. When sheared flow is turned through an angle, the vorticity vector, which was initially normal to the direction of flow, will give a component along the main flow and may be applied to the wall boundary layer.

The boundary layer thickness can be calculated accurately for flow with low swirl, but a change in the axial fluid velocity will affect the calculation to a large extent.

At high swirl, the calculation will be unreliable. The change of the blade force in the boundary layer region may also have a significant effect on the calculation of the boundary layer thickness. The development of the boundary layer is also dependent on the non-symmetrical and three dimensional nature of the flow. The evaluation of the change in the outlet velocity angle near to the tip clearance can be made using the secondary flow theory for a rotating cascade. A recalculation of the flow shows that the effect of boundary layer on the main flow is not great, but taking them into consideration will improve the agreement between the experimental results and the theoretical calculation. A shear force is exerted on the blade tip in the direction of rotation by the fluid in the tip clearance. The change in this force is small when there is a change in velocity profile across the blade between the hub and turbine meter casing. The simplicity of tip clearance flow for a helically bladed rotor is because these meters have a co-directed tip clearance flow relative to main flow with a negligible boundary layer thickness due to operation at high Reynolds number region and a smooth turbine meter casing. In case of constant blade angle rotors which operate at a greater angle of incidence which has a marked effect on the pressure distributions across the blade tip. The shape of this pressure distribution determines the direction of the flow around the blade tip.

The velocity profile across the annulus up and down stream of the blade can be divided into the mainstream and the tip clearance regions, (boundary layer region) provided that the shear in the mainflow is not too large. In the earlier research work the tip clear-

ance flow has either been neglected or considered purely co-axial without being affected in any way by the blade rotation and the pressure distribution across its tip (Ref. 86). The volumetric calculation of the tip clearance flow with the assumption of co-axial direction to the main flow is only acceptable for fluids with a viscosity close to that of water. For higher fluid viscosities the calculation of the tip clearance flow is much more complicated for the following three reasons:

a) The boundary layer effect:

The main turbine equation (5.15) should include the growth of boundary layer thickness on the turbine meter hub, blades surface and blade tip (or tip clearance area), which will increase with the fluid viscosity. Alternatively the tip clearance flow can be calculated from the pressure distribution on both sides of the blade which contains the effect of increasing fluid viscosity.

b) The rotational effect:

The blade tip flow will have a three dimensional flow characteristic. (Fig. 5c). This rotational effect is more emphasised if the calculation is based on volumetric efficiency as explained in the next chapter.

c) The pressure distribution effects:

According to the simplified theory (Ref. 86), the volumetric integration of tip clearance flow will always be a positive value. According to the experimental results and empirical calculation of Term 2 in the MTE, this term will approach zero for certain fluid viscosities and eventually become negative. This means the tip clearance flow is directed against the main flow through rotor (Fig. 79). The number of blades has no side effect in regard to solidarity of the rotor because the commercial meters have only relatively small numbers of blades (6 to 8). Therefore, the solidity of the rotor blade cannot be significant in practice in altering the flow regime through the tip clearance area.

A change in the value of tip clearance flow will cause a variation in the magnitude of the flow through the rotor. A reduction in Q_c increases the numerical value of the empirical calculation of Q_r. The direction of the flow in the tip clearance is determined by the pressure distribution across the blade tip. The boundary layer thickness and drag coefficient increase when operating in the range of low Reynolds' number. The velocity profile inside the tip clearance can be calculated theoretically in 3-dimensional flow conditions which are caused by rotational effects of the turbine rotor. The velocity

components are, u, v, w, and r is the radius of the turbine rotor with angular velocity and v is the kinematic viscosity (Appendix III). The tip clearance flow in regard to the growth of boundary layer is:

$$Q_c = U \int_{r_t}^{r_0} 2\pi r \frac{u}{U} dr - U \int_{r_0-\delta_x}^{r_0} 2\pi r \frac{u}{U} dr \qquad (5.17a)$$

Therefore

$$Q_c = \frac{2}{\delta^2_x}(r_0^3 - r_t^3)\left[\frac{(r_0^3 - r_t^3)}{36\delta^2_x}(6-k) - \frac{(r_0^2 - r_t^2)}{10\delta_x}\right.$$

$$\left.(4-k) - \frac{k}{8}(r_0 - r_t)\right] - \frac{2}{\delta_x}(3r_0^2 - 3r_0 + \delta^2_x)$$

$$\left[\frac{3r_0^2 - 3r_0 + \delta^2_x}{36\delta_x}(6-k) - \frac{(2r_0 - \delta_x)}{10}(4-k) - \frac{k}{8}\delta_x\right] \qquad (5.17b)$$

To achieve good accuracy in the calculation of Q_c it is necessary to check that the velocity component in the circumferential direction is negligible, otherwise the calculation based on equation 5.16 should be carried out to obtain the absolute velocity component in the tip clearance and hence to calculate the theoretical value of the Q_c. The calculation of Q_c (equation5.17b)is based on the displacement thickness δ_x in the axial direction and is one method of calculating the second term of equation 5.15. Two alternative methods will be described in the next chapter which are:

a) The empirical method based on leakage theory,

b) The theoretical method based on volumetric efficiency.

5.2 The calculation of the main turbine equation (M.T.E.)

The calculation of the MTE has been carried out for different fluid viscosities to predict the calibration curves, and fluid viscosity effects on the above curves.[1] These effects can be investigated theoretically on the main turbine equation and its three terms.

The calculation is as follows:

The flow through the meter annulus was divided into the flow through the blades Q_r, and through the tip clearance Q_c.

$$Q = Q_r + Q_c \qquad (5.18)$$

[1] Fig 6, 9, 12, 12a, 22

$$\frac{n}{Q} = \frac{n}{Q_r}\left(1 - \frac{Q_c}{Q}\right) \tag{5.19}$$

Q_c, as explained in Chapter 5.1, can be calculated either by using the semi-empirical leakage theory or using a purely theoretical method, which will be described in Chapter 6. The leakage method first used in Tan's theory is used to give the best possible fit to the calibration curve for water as the test fluid. According to his theory T_1, T_2 and T_3 were constant values for a certain flow rate. Using equation 5.11 multiplied by the leakage correction factor, $1 - g + k/Q$, he[1] determined his Main Turbine Equation as follows :

$$\frac{n}{Q} = T_1(1-g) - T_2(1-g) + \frac{T_1 k}{Q} - \frac{T_3(1-g)}{Q^2} \tag{5.20}$$

Tan used his experimental points to determine the values of the leakage factor k and the leakage ratio g using the least squares method. In this work, Tan's method has been modified to be more theoretical, by calculating equation 5.11 separately. T_1, T_2, T_3 have been calculated. The hydrodynamic components used in this calculation were functions of fluid viscosity, so that T_1, T_2, T_3 were also functions of fluid viscosity. According to equation 5.11, the number of pulses produced by the flow through the turbine rotor is dependent on the determination of the value of T_1 to T_3, so that n/Q_r can be calculated for any fluid viscosity. Also the value of the leakage factor and leakage ratio have been calculated empirically (Appendix I) (Figs. 64, 66, 82, 83, 84). Therefore, equation 5.15 is known for all fluid viscosities.

The calculation of the meter coefficient has been made in the following manner:

a) The values of T_1, T_2, T_3 in equations (5.12), (5.13), (5.14) respectively were calculated using a computer program. For calculating the flow through the turbine rotor, Q_r, the volumetric flow rate was integrated from r_h to r_t, and in a similar way the calculation of the flow through the tip clearance, the volume of the flow was integrated from r_t to r_0. The integration of Q_r was carried out in 10 steps, and that of Q_c in 5 steps. For the calculation of Q_c, the blade Reynolds' number is determined, also the displacement and momentum thicknesses in order to evaluate the boundary layer thickness in the axial and radial directions, and the velocity distribution in the tip clearance area (Appendix III). The value of the tip clearance flow is then calculated using equation 5.16. The displacement thickness in the rotational direction is neglected in this equation.

b) The values of C_D and C_L have been taken from equations (6.35) and (6.36). The

[1] Tan ignored some of the terms as negligible

method of calculation is described in Chapter 6.

c) The values of (u/U) have been taken from Laser Doppler Anemometry measurements up to a viscosity of 47 cSt. The velocity profile for viscosity 47 cSt upwards was calculated using equation (5.1). The results show good agreement throughout the viscosity range. For fluids with very low viscosities close to that of water, Tan's empirical approach, using the power law equation (Ref. 86, equation 4.7) shows good agreement between his experimental results and his proposed equation (Ref. 86).

The determination of the velocity profile using Laser Doppler anemometry has been explained in Chapter 4.2.

d) The deviation angle, δ^*, as a function of blade Reynolds' number can be either taken from the Graphs in Rhoden's calculations (Ref. 96) which varies between 1° and 3° depending on the Reynolds' number. Alternatively, through momentum considerations, the friction is the cause of the pressure drop and flow deviation to the cascade in the downstream direction, so that: (Ref. 17)

$$\Delta^* = \frac{2\delta^*_H + t}{s \cos\beta} \tag{5.21}$$

$$\theta^* = \frac{2\dot{v}_H}{\cos\beta} \tag{5.22}$$

For small deviation angles δ^* (1 to 3 degrees)

$$\cos\delta^* = 1 \tag{5.23}$$

According to Fig. 3

$$\beta = \delta^* + (\theta_0 + \varphi) \tag{5.24}$$

$$\cos\beta = \cos(\theta_0 + \varphi) - \delta^* \sin(\theta_0 + \varphi) \tag{5.26}$$

$$a = 0.092\, c\, Re_0^{-0.2} + t \tag{5.27}$$

$$\frac{2\Delta^* - \Delta^{*2}}{(1-\Delta^*)^2} = \frac{2.56\,\sigma\, Re_0^{-0.2}}{1\text{-}2.56\, Re_0^{-0.2}} \tag{5.28}$$

by assumption that $\Delta^{*2} \approx 0$ and for

$$b = 2.56\ Re_0^{-0.2} \tag{5.29}$$

$$c = 1 - 2.56\ Re_0^{-0.2} \tag{5.30}$$

$$\frac{2\Delta^*}{1-\Delta^*} = \frac{2a}{\cos\beta(1-2a/\cos\beta)} = \frac{2a}{\cos\beta - 2a} = \frac{b}{c} \tag{5.31}$$

$$\cos\beta = \frac{2(ac+ab)}{b\,.\,s} \tag{5.32}$$

with substitution of the equation 5.26 into 5.32

$$\cos(\theta_0+\varphi) - \delta^* \sin(\theta_0+\varphi) = \frac{2(ac+ab)}{b\,.\,s} \tag{5.33}$$

$$\delta^* = \cot g(\theta_0+\varphi) - \frac{2(ac+ab)}{s\sin(\theta_0+\varphi)} \tag{5.34}$$

The cross-section of the turbine blade is a parallelogram, which can be made similar to an aerofoil by rounding the leading corners and one of the trailing corners (assumption).

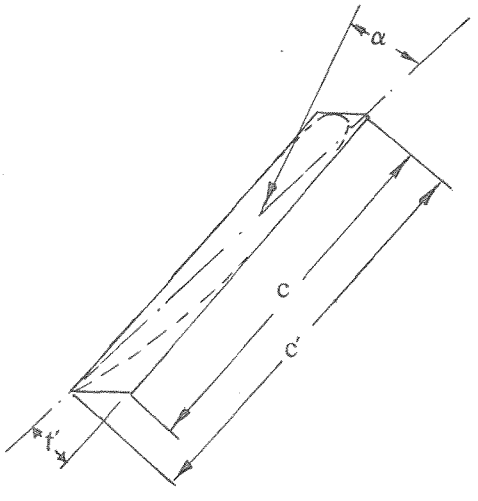

The maximum length for the above aerofoil would be: $c' = c + t'\cos\beta$

The above assumption will enlarge the angle of attack by

$$\bar{\epsilon} = \frac{t'\cos\beta}{c} \tag{5.35}$$

In the case of very thin turbine blades, the value of ϵ is very small and the change in α due to ϵ would be negligible. However, this assumption could lead to theoretical results for relatively thick turbine blades because of the increase of α caused by $\epsilon \neq 0$. This assumption will make the calculated value of the hydrodynamic torque larger than the actual value.

CHAPTER 6

THE VISCOSITY EFFECT ON THE HYDRODYNAMIC PARAMETERS AND THE TIP CLEARANCE LOSSES

The total energy losses in the turbine rotor are divided into losses arising from the existence of the boundary layer and the mixing losses in the wake flow, (the bearing friction is included). The mixing losses may be determined by solving the momentum equation between the blade trailing edge and a point far downstream, where the wake is completely uniform. For the evaluation of energy losses due to the boundary layer it is sufficient to know the value of the momentum thickness and the displacement thickness (eqs. 5.16 and 5.17). The second term in the MTE which takes the tip clearance flow into account shows reasonable agreement between experiment which is an indirect way of examining of tip flow, and theory in the simple case of co-directional flow (where the tip clearance flow is in the same direction as the flow through the rotor blades). An acceptable empirical method (leakage model) has been formulated to predict the calibration curve for the counter-directional flow. The angle of attack, α, is small and positive in the helically bladed rotor. This angle can be much larger or even negative for a constant angle bladed rotor depending on the flow condition. The magnitude and the sign of this angle will affect the pressure distribution at the blade tip and will determine the direction of the flow in the tip clearance.

There is a co-directional flow in the tip clearance and turbine blades for positive angles of attack and a counter-directional for negative angles of attack. Apart from term 2 there were no major difficulties in calculating the other terms of the MTE, which show good agreement between the values based on experimental results and those based on theoretical calculation. The calculation of the different terms in the MTE made it necessary to determine the effect of fluid viscosity on the hydrodynamic component involved in T_1, T_2 and T_3. Also in order to understand more about the fluid dynamic flow conditions in the tip clearance area it was essential to consider the tip clearance losses and to approach the real tip clearance volumetric values.

6.1 The Effect of Fluid Viscosity on Drag and Lift Coefficient

The thickness of the boundary layer, δ, increases from the leading edge of the turbine blade to the trailing edge. It increases with increasing viscosity of the fluid and even for low viscosity the shearing stress is an important factor because of the large velocity gradient in the boundary layer. The frictional force within this zone is much greater than

outside it. According to Prandtl's boundary layer theory only a thin zone of fluid field close to the walls takes the friction forces. The rest of the fluid field will be governed by potential flow (i.e. for incompressible fluid in regard to the Navier stock's equation, the velocity vector is the gradient of the potential φ. Therefore the friction term will disappear in the mentioned equation). Thus, the theory associated with fluids of low viscosity is less complex. The turbine cascade has a boundary layer thickness which is small and therefore avoids creating separation on the blade. The losses in the flow through the cascade depend upon the geometry of the cascade, the blade angle, the angle of attack, α, and angle of deviation, δ *. The coaxial cylindrical geometry may be transferred to a parallel plane geometry so that the turbine blades may be observed in a two-dimensional cascade. (Fig. 3). The boundary layer thickness over the blade is very small because the pressure drop predominates and therefore there is only a small separation (Turbine Cascade). The loss coefficient, C_{loss}, increases for a small blade spacing ratio (more blades) so that the loss coefficient for small deflections is proportional to the number of the blades.

The blade Reynolds' number similarly affects the loss coefficient in the cascade and the drag on a single aerofoil because in both cases the influence of Reynolds' number is via the boundary layer. In general the turbine cascade has a larger deviation and smaller loss coefficient relative to the pump cascade (Ref. 66).

The loss coefficient is affected by blade Reynolds number, the pressure distribution over the blade area in a turbine flow meter is such that no substantial flow separation is produced so the losses are only those of the boundary layer. The variation of losses is, in this case, like the change of drag coefficient of a flat plate at zero incidence, so that for laminar flow it is in proportion to $Re^{-1/2}$ and for turbulent flow it is in proportion to $Re^{-1/5}$. Re number depends on blade chord length, axial velocity and viscosity. The value of C_{loss} is also dependent on the position of the transition point, which moves on the blade by increasing the Reynolds number. The drag over the blade area in the cascade is important for theoretical calculation of the pressure distribution over the blade. The pressure drop over the cascade has a significant influence on the friction and also leads to separation in the flow. For estimating the fluid friction in the cascade it may be considered that the frictional forces are in the boundary layer near the wall. The rest of the flow field is considered as frictionless potential flow.

The losses in the cascade are as follows:

(a) From the boundary layer on the blade (and also pressure drop on the contour

of the blade).

(b) From mixing in the wake flow behind the cascade on the trailing edge of the blade.

The change in velocity in both magnitude and direction, and the pressure drop contribute to the energy loss of the flow. By means of the flow through the cascade the fluid force is transferred to the turbine blade (Kutta-Joukowsky),

$$\Gamma = s \cdot v_e \tag{6.1a}$$

$$L = \rho \cdot U \cdot \Gamma \tag{6.2a}$$

$$\Gamma = s\,U\,(\tan\theta_0 - \tan\theta_i) \tag{6.3a}$$

In comparison with ideal frictionless flow the influence of the friction increases the magnitude of V_0 and the value of C_L given by

$$C_L = 2\frac{s}{c}\cos^2\theta_m(\tan\theta_0 - \tan\theta_i) \tag{6.1}$$

By flowing around each side of the profile the boundary layer produces a disturbed section at the trailing edge by turbulent or laminar mixing. The profile friction is the reason for energy losses which are in the form of kinetic energy. This means that the velocity changes its magnitude and direction due to the influence of friction

$$\Delta p_{loss} = \frac{D\cos\beta}{s} \tag{6.2}$$

$$\Delta p_{loss} = \frac{\rho}{2} \cdot V_i^2 \cdot C_D \cdot \frac{c}{s} \cdot \cos\beta \tag{6.3}$$

The calculation of the laminar or turbulent boundary layer from the leading to trailing edge of the blade is necessary to estimate the value of the losses in the boundary layer. The mixing losses may be calculated from the blade trailing edge to the place behind the wake flow, where the flow is completely uniform. For calculating the energy losses it is enough to determine the displacement thickness, δ_H^* and the momentum thickness, $\dot{v}_H$

$$\delta_H^* = \int_{r_h}^{r_t} [1 - \frac{v_n}{v_0}]\, dr \tag{6.4}$$

$$\dot{v}_H = \int_{r_h}^{r_t} \frac{v_n}{v_0} \left[1 - \frac{v_n}{v_0}\right] dr \tag{6.5}$$

From the assumption that the boundary layer on the blade leading edge is turbulent it follows that the displacement thickness (Ref. 17) on the blade trailing edge in downstream position is

$$\delta^*_H = \frac{0.046}{Re_{blade}^{1/5}} \cdot c \tag{6.6}$$

and the momentum thickness is

$$\dot{v}_H = \frac{0.036}{Re_{blade}^{1/5}} \cdot c \tag{6.7}$$

The Momentum Observation shows (Ref. 66) that friction is the cause of the pressure drop and deviation of flow from the cascade downstream direction so that the dimensionless displacement Δ^* and momentum thickness θ^* will be:

$$\Delta^* = \frac{2\,\delta^*_H + t}{s\cos\beta} = \frac{0.092 \cdot c \cdot Re_{blade}^{-0.2} + t}{s\cos\beta} \tag{6.8}$$

$$\theta^* = \frac{2\,\dot{v}_H}{s\cos\beta} = \frac{0.072 \cdot c \cdot Re_{blade}^{-0.2} + t}{s\cos\beta} \tag{6.9}$$

for

$$\delta = 0.092 \cdot c \cdot Re_{blade}^{-0.2} \tag{6.9a}$$

then

$$\Delta^* = 1.28\,\sigma\, Re_{blade}^{-0.2} + \frac{t}{s\cos\beta} \tag{6.10}$$

$$\theta^* = \sigma\, Re_{blade}^{-0.2} + \frac{t}{s\cos\beta} \tag{6.11}$$

Because of displacement influence of the boundary layer the stream velocity in the plain blade trailing edge is larger than the velocity at a great distance downstream where the wake flow becomes uniform

$$v_m = \frac{v_{oid}}{1 - \Delta^*} \tag{6.12}$$

At this place, the pressure is smaller (far downstream the pressure is larger), so that from the Bernoulli equation it follows that

$$p_o = p_{oid} - \frac{\rho}{2} v_{oid}^2 \left[\frac{1}{(1-\Delta^*)^2} - 1 \right] \tag{6.13}$$

The momentum equation in the y-direction (see fig. 4) is

$$\rho \sin\theta_{oid} \cos\theta_{oid} \int_{r_h}^{r_t} v^2(y)\, d\left(\frac{y}{s}\right) = \rho \sin\theta_o \cos\theta_o v_o^2 \tag{6.14}$$

dividing by ρv_m^2 and rearranging LHS it follows

$$\cos\theta_{oi} \sin\theta_{oid} \left[1 - \int_{r_h}^{r_t} \frac{v(y)}{v_m} \left[1 - \frac{v(y)}{v_m} \right] d\left(\frac{y}{s}\right) - \int_{r_h}^{r_t} \left[1 - \frac{v(y)}{v_m} \right] d\left(\frac{y}{s}\right) \right] =$$

$$\cos\theta_o \sin\theta_o \left(\frac{v_o}{v_m}\right)^2 \tag{6.15}$$

The velocity calculated from potential theory at the blade trailing edge is larger due to displacement (and the pressure smaller) than for a distance further downstream position where the flow becomes uniform

$$v_o = \frac{v_{oid}}{(1-\Delta^*)} \tag{6.16}$$

$$v_{ix} = v_{oid_x} = v_{ox} = v_{oid} \cos\theta_{oid} = v_o \cos\theta_o \tag{6.17}$$

$$v_{oid} = v_o \frac{\cos\theta_o}{\cos\theta_{oid}} \tag{6.18}$$

$$v_m = v_o \frac{\cos\theta_o}{\cos\theta_{oid}} \cdot \frac{1}{1-\Delta^*} \tag{6.19}$$

$$\cos\theta_{oid} \sin\theta_{oid} (1 - \theta^* - \Delta^*) = \sin\theta_o \cos\theta_o \frac{v_o^2}{v_m^2} \tag{6.20}$$

$$\left[\frac{v_o}{v_m}\right]^2 = \frac{\cos^2\theta_{oid}}{\cos^2\theta_o} (1-\Delta^*)^2 \tag{6.21}$$

$$\operatorname{tg}\theta_{oid}\,(1-\theta^*-\Delta^*)=\operatorname{tg}\theta_o\,(1-\Delta^*)^2 \tag{6.22}$$

$$\frac{\operatorname{cotg}\theta_{oid}}{\operatorname{cotg}\theta_o}=\frac{(1-\theta^*-\Delta^*)}{(1-\Delta^*)^2}=\chi \tag{6.23}$$

Momentum eq. in x-direction is (see Fig. 4)

$$\rho\cos^2\theta_{oid}\int_{r_h}^{r_t} v^2(y)\frac{dy}{s}+p_m=\rho v_o{}^2\cos^2\theta_o+p_o \tag{6.24}$$

$$\frac{p_{oid}-p_m}{\frac{\rho}{2}v^2_{oid}}=2\cos^2\theta_{oid}\left[\frac{1-\theta^*-\Delta^*}{(1-\Delta^*)^2}-1\right] \tag{6.25}$$

$$\frac{p_{oid}-p_o}{\frac{\rho}{2}v^2_{oid}}=2\cos^2\theta_{oid}(\chi-1)-2\frac{\Delta^*-\Delta^{*2}}{(1-\Delta^*)^2} \tag{6.26}$$

The pressure magnitude at the blade trailing edge is obeying the Bernoulli equation

$$p_m=p_{oid}-\frac{\rho}{2}v^2_{oid}\left[\frac{1}{(1-\Delta^*)^2}-1\right] \tag{6.27}$$

The potential theoretical magnitude from potential theory is

$$\frac{p_{oid}-p_m}{\frac{\rho}{2}v^2_{oid}}=\frac{2\Delta^*-\Delta^{*2}}{(1-\Delta^*)^2}-2(\chi-1)\cos^2\theta_{oid} \tag{6.28}$$

So the pressure loss equals the energy loss, Δg, which is

$$\Delta g=p_{oid}+\frac{\rho}{2}v^2_{oid}-(p_o+\frac{\rho}{2}v_o^2) \tag{6.29}$$

The total non dimensional energy losses are as follows:

$$\frac{\Delta g}{\rho v^2_{oid}}=\left[\frac{1}{(1-\Delta^*)^2}-1\right]-2(\chi-1)\cos^2\theta_{oid}-(\chi^2-1)\sin^2\theta_{oid} \tag{6.30}$$

$$\frac{v_o}{v_{oid}}=\sqrt{\cos^2\theta_{oid}+\chi^2\sin^2\theta_{oid}} \tag{6.31}$$

$$\Delta g = c_{loss} \cdot \frac{\rho}{2} v_0^2 \sin^2 \theta_0 \tag{6.32}$$

$$v_{ox} = v_0 \cos \theta_0 \tag{6.33}$$

The cascade loss coefficient is

$$C_{loss} = \frac{1}{\cos^2 \theta_{oid}} \frac{2\Delta^* - \Delta^{*2}}{(1-\Delta^*)^2} - 2(\chi^2 - 1) - (\chi^2 - 1) \tan \theta_{oid} \tag{6.34}$$

$$C_D = C_{loss} \frac{s}{c} \cos^3 \theta_m \tag{6.35}$$

$$C_L = C_D \cdot \frac{2[\tan \theta_{oid} - \tan \theta_0]}{C_{loss} \cos^2 \theta_m} \tag{6.36}$$

For low angle of attack, α, C_L increases linearly and C_D is constant. At higher values near the stall of α, C_L will start to decrease whilst C_D increases. The C_D/C_L ratio should be small initially.

$$\frac{\tan \theta_0}{\tan \theta_{oid}} = \chi \tag{6.37}$$

$$\chi = \frac{1 - \theta^* - \Delta^*}{1 - 2\Delta^*} \tag{6.38}$$

With substitution of the above two relations into the equations 6.34, 6.35 and 6.36, the value of C_D, C_L, and C_{loss} could be calculated. These values will be substituted in equation 7.24. The relation between the turbine driving torque and viscosity can be calculated.

Equations 6.34, 6.35 and 6.36, show the effect of viscosity on C_D and C_L which will change the T_1 and T_2 in the main turbine equation from a constant value (for one fluid) to a variable value, which changes the shape of the meter calibration curve. These factors are constant according to Tan (Ref. 86) for the particular case of one liquid at temperature between 17–21° C. T_3 will not be affected as much because it is much smaller than T_1 and T_2 and the lift and drag coefficients influence this term indirectly (velocity distribution will change with increase in fluid viscosity). For the reasons to be discussed later, variation of the fluid viscosity will affect the first two terms of the main turbine equation more than the third. The derived equations 6.34, 6.35 and 6.36 show the theoretical depend-

ence of C_D and C_L on Reynolds number or on fluid viscosity. The gradient of the turbine meter calibration curve for low flow rate (or in the laminar flow region) will decrease with increasing viscosity. According to Lee and Karlby the change over from the non-linear (laminar zone) to the linear part (turbulent zone) on the turbine meter calibration curve represents the transition zone. For the maximum point of the hump[1] of the calibration curve which is a point in the transition zone, the calculated value of the blade Reynolds' number was almost constant ($Re = 10^3$) for all calibration curves with varying viscosities from $\nu = 1 - 71$ cSt (Figure 12). The disappearance of the hump for blades Reynolds' number $Re = 10^3$ introduced the possibility of finding a more applicable value (eq. 5.16 and 5.17) than that suggested by Gersten[2] (Ref. 17)). In changing from the large gradient non-linear section of the calibration characteristics to the constant section, the meter coefficient traverses a hump. All the calibration curves for different viscosities had a maximum between the laminar and turbulent zones, in which the above calculation has been made. The existence of these humps could be the result of having a large tip-clearance (0.016 ins., 0.4064 mm), for the turbine meter. This is shown in the calculation by the balance between relative values of T_1, T_2 and T_3 and the MTE. The increase of viscosity will also raise the calibration curve for high flow rates in viscous fluids. This is the result of the increase of the deviation angle, δ^*, drag coefficient, C_D and the change of velocity distribution over the blade area which affects Term 1 of the main turbine meter equation. However, for high viscosities the hump in the calibration curve disappears at a certain viscosity, when Terms 1, 2 and 3 compensate each other (in contrast the Lee and Karlby theory would not explain the disappearance of the hump). The effect of the fluid viscosity on the different terms of MTE is described in chapter 8.

6.2 The Tip Clearance Losses due to Leakage Flow

It would appear that an ideal turbine meter characteristic may be best achieved when the tip clearance is small in order to minimise the tip clearance losses. According to this, one should design a rotor, where the blade tips almost rubbed on the casing. Tan has shown that an optimum case (widest flow range) occurs at an intermediate tip clearance and further decrease in tip clearance causes a fall in the value of meter coefficient at lower flows which decreases the operational range together with a loss of measurement repeatability in this region. Tan did calibrate a few turbine flow meters with turned-down rotors, giving his calibration curves for tip clearances (the size of the rotor diameter was 2 ins. (50.8 mm)), from 0.0007 to 0.03 ins (0.1778 to 0.762 mm). One could find

[1] The value of Reynolds number can be calculated by taking the data out of mentioned Fig. 12
[2] Eq. 6.6 and 6.7

out from his experimental results that the calibration with a clearance of 0.022 ins (0.5588 mm) had the widest operational range. However, in the case of turbine meters there will always be a problem in evaluating the leakage amount and direction. This chapter gives an outline of the effect of the tip clearance on the main flow structure. An attempt is made to calculate the tip clearance flow and its effects on the main turbine equation. The tip clearance flow will have influence on the following components:

(1) The change of average lift by unloading the blade at the tip

(2) The induced drag by the formation of tip vortices

(3) The flow outlet angle near the tip

(4) The increase of the losses at the outlet (mixing)

(5) The separation caused by the passage secondary flow.

The tip clearance losses also depend on the blade Reynolds' number, space/chord ratio, tip clearance/chord ratio, the aspect ratio, the blade loading, the amount of vorticity.

The experimental part of the research has shown that the effect of the mechanics of the tip clearance flow is not always detrimental to the turbine flow meter calibration curve when the fluid viscosity is increased. In the case of a turbine flow meter with a helically bladed rotor the tip clearance flow will have a compensation effect on the calibration curve with an increase of fluid viscosity (Figure 62). For the small tip clearance the pressure difference was retained for a viscous flow and some of the bound vorticity could be carried across the blade tip (Ref. 99). The effect of viscosity on the diffusion of bound vorticity is significant at the blade tip. The losses in the turbine flow meter are mainly the profile loss, the losses due to the tip clearance drag and the secondary losses. Wolff (Ref. 98) (for turbine incompressible flow) looked into the overall losses associated with tip clearance and discovered they were independent of aspect ratio for large blade heights, but they increased with deflection and pressure rise (reverse flow for constant blade angle rotor) across the blades. The tip clearance flow has an effect on the lift force of the blades and, because of induced drag, causes the change in pressure distribution.

Mellor (Ref. 100) noted that over a rotor the change in displacement thickness and hence viscous dissipation of the work done in the boundary layer was related to the tip effects. He suggested that the passage efficiency will be based on the tip clearance and on the displacement thickness on the turbine hub. The boundary layer thickness will become

larger with the increase in clearance/chord ratio. The volumetric efficiency based on displacement thickness proposed by Mellor was

$$\eta_e = 1 - \frac{\delta_{tipx} + \delta_{hubx}}{r_o - r_h} = \eta_v \qquad (6.39)$$

Smith (Ref. 101) found that the losses are not as big as they appear in the above equation, because Mellor did not consider the change in the tangential force in the boundary layer and in the tip clearance. This force is smaller in the tip clearance area than in the rotor passage area. Therefore, the work input into the tip clearance area is reduced and the efficiency loss in the above equation is not as large as shown in the above equation. To produce a theoretical structure for the calculation of the tip clearance losses one should either take the above equation or use Tan's leakage model or try to determine the drag induced by tip clearance flow. Therefore it is advisable to divide the leakage into categories and produce an efficiency model of each one.

These categories can be explained as follows:

a) Due to the lack of any hydrodynamical forces in the tip clearance area the blade force cannot accelerate the flow outside the blade area or the fluid in the tip clearance and this causes energy losses. The volumetric efficiency can be calculated by estimating for the displacement thickness.

b) This model is the leakage loss for the case of normal flow in the tip clearance caused by the pressure differences across the blade. The tip clearance loss will be associated with the flux of kinetic energy.

Verra (Ref. 102) determined empirically a loss coefficient which was demonstrated in the following equation:

$$C_D = 1.13\, C_{loss} \frac{t}{2\ell} \quad C_L^{1.5}, C_f \qquad (6.40)$$

where C_f is the contraction factor in the tip clearance and ℓ is the mixing length.

c) In the case of a helically bladed rotor the shed vortex in the tip clearance will be almost linear across the blade passage. Therefore, in order to estimate the rotor efficiency and to calculate the meter coefficient for different fluid viscosities it is essential to calculate or measure the pressure difference across the turbine meter blades in the rotor passage in the upstream and downstream positions.

6.3 The Theory of Tip Clearance Flow

When fluid flows through the turbine meter cascade, it produces a pressure difference Δp across the blades. The turbine meter is analogous to an axial flow machine and the above pressures are those from the pressure and suction sides of the turbine blade.

The pressure distribution depends on the magnitude of the following components:

a) Skin friction drag, which depends on the Reynolds number of the blades

b) Pressure drag dependent on the blade shape

c) The angle of attack, α, determined by relative fluid velocity at the blade tip

d) Flow rate, Q, a function of axial fluid velocity

e) Angular velocity of the rotor, dependent on bearing friction force, hydrodynamic force or driving force.

The existence of the flow through the tip clearance depends entirely on the pressure difference across the blade at the tip. The energy necessary to maintain the flow through the tip clearance will be taken from the pressure difference at the tip across the thickness of the turbine blade.

In the case of an inviscid fluid, the velocity profile in the inlet and outlet of the tip clearance is the same since there is no drag in the tip clearance, and it follows that the pressure at these places will remain constant. The significant energy in the flow through the clearance will be kinetic energy of the fluid. In the case of real fluid the total energy necessary to maintain the flow through the gap is the sum of the energy loss for overcoming the drag in the tip clearance and the kinetic energy mentioned for an inviscid fluid.

In the case of frictionless fluid this pressure difference will be balanced due to existence of the tip clearance flow. In the case of real fluid the available pressure energy from Δp will be transformed into kinetic energy in the tip clearance flow less the drag losses which will be dissipated as heat energy. The pressure equalisation at the tip of the turbine blade will affect the pressure distribution on the whole blade surface. Not only the overpressure on the pressure side of the turbine blade but also the under pressure on the suction side of the blade will be reduced towards the turbine blade tip. This change in the pressure distribution on the blade surface caused by the tip clearance flow will be reduced with an increase in the tip clearance drag. A small tip clearance (large contraction effect) will result in a small variation in local pressure profile close to the blade tip and vice versa. The force on the turbine rotor is due to the interaction between the turbine blades and fluid flow. It depends on the pressure and velocity distribution on the

turbine blade surface. The tip clearance flow will affect the load or power on the blades in such a way that a large increase in the power of the blade or a larger flow rate will be equivalent to a reduction in the tip clearance drag relatively. The above affect can be achieved by a change in the tip clearance geometry or modification of the blade shape to minimise the tip clearance effect. The above changes can balance the clearance flow effects on the turbine blade power. The fluid velocity within boundary layer is always less than that of the main flow.

The value of the angle of incidence α, can be kept constant for a constant velocity profile over the blade span (from hub to tip). When the angle of incidence is positive the second term of the MTE is added to the first term, but for negative angles of incidence it is subtracted from the first term. For certain values of Term 1 and 2 there is a compensation effect with Term 3 allowing the flow meter to have a linear calibration characteristic over the required operational range. The value of the angle of attack can be reduced by having a blade with a helical pitch distribution. The helical pitch can be chosen to approach the optimum value of this angle for which the angle of attack α, is very small and remains positive for the whole operational range. The influence of this is shown for a constant blade angle rotor (Fig. 5c (i)) with a large angle of incidence, α, which can vary from a large positive value (see chapter 8) to a large negative value. This is dependent on the large variation in axial fluid velocity. Also the variation in α for a helically bladed rotor (Fig. 5c(ii)) is important for the value of lift and drag coefficients and therefore for the magnitude of T_1 and T_2. The angle of attack was small and positive in the helically bladed rotor. Therefore, the values of C_L and C_D were not much affected by the fluid viscosity and the tip clearance flow would not change direction from the main flow through the turbine blades (Fig. 5c(ii)).

The change in the angle of attack for Q constant and changing the viscosity or ν constant and changing the flow rate, is entirely dependent on the magnitude of the axial fluid velocity. Therefore, the magnitude of α is dependent on the operational range of a meter. The flow meters with a large increase in u and blade Reynolds' number will have a large increase in the value of α.

6.4 The Pressure Distribution and Momentum Equation in the Tip Clearance

For the fluid flow in the tip clearance close to the blade tip the absolute velocity is $\bar{c}$, the tip rotational velocity is $r_t\omega_a$, and the relative velocity is v as shown in figure 5c. The tip clearance velocity $\bar{v}$ over the blade is given by the vector equation:

$$v = \bar{v}' + \bar{c} - r \cdot \omega_a \tag{6.41}$$

For simplification, $\bar{v}'$ will be assumed perpendicular to the turbine blade chord. Rotor tip velocity determines the value of the normal component v sin α of the relative velocity, v. The direction of rotation determines the direction of v sin α. The $\bar{v}'$ component (produced by $\bar{\Delta}p^*$) can in the case of a constant angle bladed rotor be in the opposite direction to v sin α (depending on the sign of the angle of attack). A negative angle of attack causes a reverse flow through the tip clearance. In the case of a helically bladed rotor $\bar{v}'$ is in the same direction as v sin α.

The tip clearance losses written as: (with $\bar{\zeta}$ as tip clearance coefficient)

$$\frac{\Delta p^*}{\gamma} = \bar{\zeta} \frac{\bar{v}'^2}{2g} \tag{6.42}$$

is a function of blade thickness, tip clearance Reynolds number, and the product of the tip clearance size ($r_o - r_t$) and the blade chord multiplied by the number of blades. The rotor tip velocity should be taken into consideration because it determines the direction of velocity components. The energy (expressed as a fall in head) loss associated with the tip clearance flow is:

$$\frac{\Delta p}{\gamma} = \frac{\bar{\Delta} p^*}{\gamma} + \frac{v_n^2}{2g} \tag{6.43}$$

This is the sum of the tip clearance losses due to drag (pressure head), $\frac{\bar{\Delta} p^*}{\gamma}$ and the kinetic energy for a frictionless fluid. The kinetic energy of a real fluid is greater than that of an inviscid fluid of the same flow rate. The reduction in the pressure difference on the blade tip due to the existence of the tip clearance flow can be calculated by taking the coefficient, ζ, instead of $\bar{\zeta}$ (v_n instead of $\bar{v}'$) which gives the following equation:

$$\frac{\bar{\Delta} p^*}{\gamma} = \zeta \frac{v_n^2}{2g} \tag{6.44}$$

$$\frac{\bar{\Delta} p^*}{\gamma} = \frac{\zeta}{1+\zeta} \left(\frac{\Delta p}{\gamma}\right)_{tip} = f(c, Q, n) \tag{6.45}$$

For infinite clearance ($r_o - r_t = \infty$) $\zeta \to 0$ and $\bar{\Delta} p^* \to 0$. For ($r_o - r_t$) = 0

$$\lim_{\zeta \to \infty} \left(\frac{\zeta}{1+\zeta}\right) = 1 \text{ and } \bar{\Delta} p^* = \Delta p \tag{6.46}$$

[1] Ship propeller

Therefore the velocity distribution in the clearance is not only dependent on the pressure distribution on the tip but also depends on the geometry of the tip clearance (blade chord and thickness) or ζ. Due to the tip clearance flow there can be a reduction of the over-pressure on the pressure side and decrease in the underpressure on the suction side of the blade towards the blade tip. The streamline of the relative flow on the pressure side will be diverted towards the clearance and on the suction side will move away from the clearance. Therefore, there can be unsteady flow created downstream of the blade which can produce a vortex in the main flow close to the blade tip. The pressure loss coefficient of clearance can be approximately claculated by the following equation:

$$\bar{\zeta} = \frac{p_{1\,tip} - p_{2\,tip}}{\gamma \bar{v}'^2/2g} = \left(\frac{p_{1\,tip} - p_{2\,tip}}{\gamma}\right) \Big/ \frac{1}{2g} \left[\frac{Q_c}{\pi [2r_0 (r_0 - r_t)]}\right]^2 \qquad (6.47)$$

$$\bar{v}'^2 = \frac{1}{\sqrt{\bar{\zeta}}} \sqrt{\frac{2g\,(p_{1\,tip} - p_{2\,tip})}{\gamma}} \qquad (6.48)$$

$$\bar{\zeta} = \zeta \frac{t}{c \cos\beta} = \zeta' \frac{\bar{v}'^2}{(\bar{v}' + v \sin\alpha)^2} \qquad (6.49)$$

Figure 6.1 The reverse flow characteristic in the tip clearance area and the position of pressure tapping

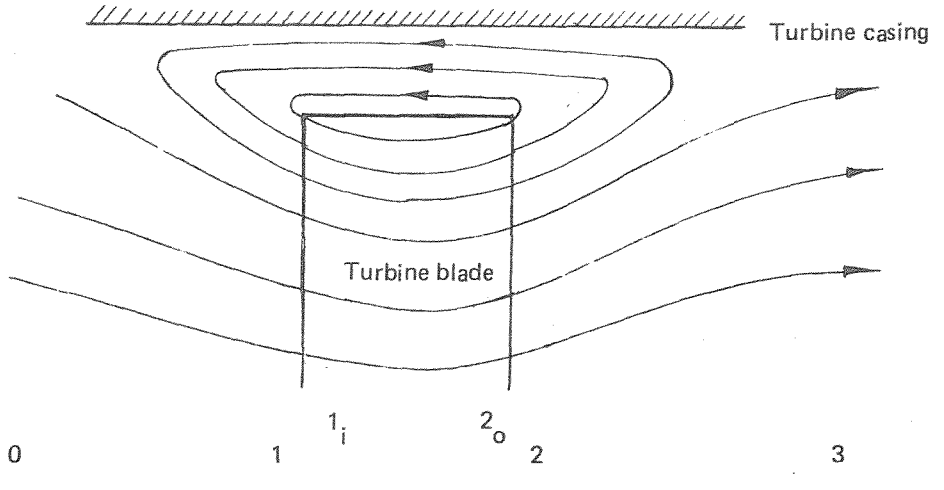

The tip clearance is a region of no energy flux due to mechanical means except the kinetic energy produced by drag in the tip clearance area. In this area the flow is either co-directional with the main flow or back-flow occurs. The direction of tip clearance flow depends on the velocity triangle as explained earlier. If $\bar{v}'$ is larger than $v \sin\alpha$,

then there is back flow through the clearance. This occurs when there are negative angles of attack, α. If main flow and tip clearance flow are co-directional there will be a pressure balance at the blade tip. The fluid flows in the tip clearance will reach the blade downstream pressure with a delay. The maximum value of pressure differences will be:

$$\Delta p_{tip} = p_{1\,tip} - p_{2\,tip} = \Delta p_{blade} \approx \frac{\rho v_1^2}{2} \tag{6.50}$$

with $v_3 = v_0 = u$ and $v_2 = v_1$. The boundary layer growth on the blade is relatively small for turbine cascade (Ref. 66). The pressure downstream of the rotor is given by:

$$p_{3\,total} = p_{2\,total} = p_3 + \frac{\rho}{2} v_0^2 = p_{2\,tip} + \frac{\rho}{2} v_1^2 \tag{6.51}$$

The tip clearance outlet pressure is equal to $p_{1\,tip}$ or $p_{2\,tip} = p_{C\ell}$ (depends on tip clearance flow direction) and the velocity $\bar{v}$ and the flow condition for the first approximation with zero loss

$$\frac{\rho}{2} \bar{v}^2 + p_{1\,tip} = p_{3\,total} = p_{2\,tip} + \frac{\rho}{2} v_1^2 \tag{6.52}$$

$$\frac{\rho}{2} \bar{v}^2 = \Delta p_{blade} + \frac{\rho}{2} v_1^2 \tag{6.53}$$

$$\Delta p_{blade} / \frac{\rho}{2} v_1^2 = \bar{\zeta} \tag{6 54}$$

from equation (6.53):

$$\frac{\bar{v}^2}{v_1^2} = \frac{\Delta p_{blade}}{\frac{\rho}{2} v_1^2} + 1 \tag{6.55}$$

Thus

$$\bar{v} = \sqrt{v_1^2 (\bar{\zeta} + 1)} \tag{6.56}$$

The tip clearance area is:

$$A_{C\ell} = \pi (r_0^2 - r_t^2) \tag{6.57}$$

The clearance flow is:

$$Q_c = \bar{v}\, A_{c\ell} = \bar{v}\,(r_0^2 - r_t^2)\,\pi \tag{6.58}$$

or

$$Q_c = v_1 \sqrt{\bar{\zeta} + 1}\, A_{c\ell} \tag{6.59}$$

The ratio of tip clearance flow to the turbine meter annulus flow will be:

$$\frac{Q_c}{Q} = \varphi' \frac{v_1 \sqrt{1+\bar{\zeta}}}{v_0} \tag{6.60}$$

The flow rate through the rotor is given by:

$$Q_r = v_1 \cdot A_a - (v_1 + \bar{v})\, A_{c\ell} = v_0 \cdot A_a \tag{6.61}$$

$$\frac{Q_c}{Q_r} = \varphi' \frac{\sqrt{1+\bar{\zeta}}}{1+\varphi\,(1+\sqrt{1+\bar{\zeta}})} \tag{6.62}$$

For the flow in the cross section 0, 1, 3 the momentum equation can be applied between 1 and 3 (with T as axial thrust):

$$T - A_a\,(p_3 - p_0) = 0 \tag{6.63}$$

Using the momentum equation for the corss section between 0 and 1: ($v_0 = v_3$)

$$A_a(p_{1\,tip} - p_0) = -A_a\,(p_0 - p_{1\,tip}) = \rho\, v_0^2 A_a - \rho v_1^2 A'_a - \rho \bar{v}^2 A_{c\ell} \tag{6.64}$$

By using the same equation between 1 and 3

$$T - A_a\,(p_3 - p_{1\,tip}) = \rho v_0^2 A_a - \rho v_1^2 A'_a - \rho \bar{v}^2 A_{c\ell} \tag{6.65}$$

$$p_0 - p_3 = p_{0_{total}} - p_{3\,total} = \Delta p_{total} \tag{6.66}$$

$$p_{1\,tip} - p_{2\,tip} = p_{1\,total} - p_{2\,total} = \Delta p_{blade} \tag{6.67}$$

$$p_{3\,total} = p_{2\,total} \tag{6.68}$$

$$\bar{\Delta} p^* = \Delta p_{blade} - \Delta p_{total} = p_{1\,total} - p_{0\,total} \tag{6.69}$$

$$\bar{\Delta} p^* = (p_{1\,tip} - p_0) + \left(\frac{\rho}{2} v_1^2 - \frac{\rho}{2} v_0^2\right) \tag{6.70}$$

Because of the tip clearance flow (which changes direction depending on the sign of the angle of incidence), and the momentum interaction between this flow and the main

flow upstream of the blade the static pressure downstream of the blade may be reduced to $\bar{\Delta}p^*/\Delta p_{blade}$.[1]

$$A_a \cdot \bar{\Delta}p^* = A_a(p_{1\,tip} - p_0) + A_a \cdot \frac{\rho}{2} v_1^2 - A_a \cdot \frac{\rho}{2} v_0^2 =$$

$$- A_a \cdot \frac{\rho}{2} v_1^2 + \frac{\rho}{2} \cdot A_a v_0^2 \left(2 \frac{A'_a}{A_a} - 1\right) + \frac{\rho}{2} \bar{v}^3 A_a \frac{A_{c\ell}}{A_a} \qquad (6.71)$$

$$\frac{\Delta p_{total}}{\frac{\rho}{2} v_1^2} = \frac{\Delta p_{blade}}{\frac{\rho}{2} v_1^2} - \frac{\bar{\Delta}p^*}{\frac{\rho}{2} v_1^2} \qquad (6.72)$$

$$\frac{\Delta p_{total}}{\frac{\rho}{2} v_1^2} = \bar{\zeta}\left[1 - \varphi'\left(2 - \varphi' + \frac{2(1-\varphi')(1+\sqrt{1+\bar{\zeta}})}{\bar{\zeta}}\right)\right] \qquad (6.73)$$

The flow through cross section 1 is

$$v_1 \cdot A_a - (v_1 + \bar{v}) A_{c\ell} = v_0 A_a \qquad (6.74)$$

$$\frac{v_0}{v_1} = 1 - \left(1 + \frac{\bar{v}}{v_1}\right) \frac{A_{c\ell}}{A_a} = 1 - (1 + \sqrt{1+\bar{\zeta}})\,\varphi' \qquad (6.75)$$

$$\frac{\Delta p_{blade}}{\Delta p_{total}} = \eta_p = \frac{1}{(1-\varphi')^2} \frac{1}{1 + 2\frac{1+\sqrt{1+\bar{\zeta}}}{\bar{\zeta}}} \qquad (6.76)$$

From equations 6.71 and 6.75 it follows:

$$\frac{\bar{\Delta}p^*}{\frac{\rho}{2} v_1^2} = -1 + \frac{v_0^2}{v_1^2}\left[2(1-\varphi') - 1\right] + \frac{\bar{v}^2}{v_1^2} \cdot \varphi' \qquad (6.77)$$

From equations 6.75 and 6.56 it follows:

$$\frac{\bar{\Delta}p^*}{\frac{\rho}{2} v_1^2} = -1 + \left[1 - (1 + \sqrt{1+\bar{\zeta}})^2 \varphi'^2\right]\left[2 - 2\varphi' - 1\right] + (1+\bar{\zeta})\varphi' \qquad (6.78)$$

$$\frac{\bar{\Delta}p^*}{\frac{\rho}{2} v_1^2} = 1 + \left[1 - (2 + \bar{\zeta} + 2\sqrt{1+\bar{\zeta}})\varphi'^2\right]\left[1 - 2\varphi'\right] + (1+\bar{\zeta})\varphi' \qquad (6.79)$$

[1] In case of reverse flow the discharge head will be multiplied by an index of $\bar{\Delta}p^*/\Delta p_{blade}$

$$\frac{\bar{\Delta}p^*}{\frac{\rho}{2}v_1^2} = 1 + [1 - 2(1 + \frac{\bar{\zeta}}{2} + \sqrt{1+\bar{\zeta}})\varphi'^2][1 - 2\varphi'] + (1+\bar{\zeta})\varphi' \quad (6.80)$$

The hydrodynamic power transferred from the fluid to the rotor is:

$$\eta_{blade} N_{blade} = \Delta p_{blade} \cdot Q = \Delta p_{blade}(Q_c + Q_r)$$

$$\eta_{blade} \cdot N_{blade} = \Delta p_{blade} (1 + \frac{Q_c}{Q_r}) Q_r \quad (6.81)$$

$$Q_c = v \cdot A_{c\ell} = v_1 \sqrt{1+\bar{\zeta}} \cdot \pi(r_0^2 - r_t^2) \quad (6.82)$$

$$Q_r = A'_a v_0 \quad (6.83)$$

$$\frac{Q_c}{Q_r} = \frac{A_{c\ell}}{A'_a} \cdot \frac{v_1\sqrt{1+\bar{\zeta}}}{v_0} \quad (6.84)$$

From equation 6.74 and 6.75 it follows:

$$\frac{Q_c}{Q_r} = \frac{\sqrt{1+\bar{\zeta}}}{1-(1+\sqrt{1+\bar{\zeta}})\varphi'} \quad \frac{\varphi'}{1-\varphi'} \quad (6.85)$$

$$\eta_{blade} N_{blade} = \Delta p_{blade} [\frac{\sqrt{1+\bar{\zeta}} \cdot \varphi'}{1-(1+\sqrt{1+\bar{\zeta}})\varphi'(1-\varphi')} + 1] Q_r \quad (6.86)$$

The hydrodynamic power transferred from the rotor to the fluid is:

$$\eta_p = \frac{\Delta p_{blade}}{\Delta p_{total}} \quad \text{pressure efficiency} \quad (6.87)$$

$$\eta_v = \frac{Q_r}{Q} \quad \text{volumetric efficiency} \quad (6.88)$$

$$\eta_{c\ell} = \frac{Q_r \Delta p_{blade}}{Q \Delta p_{total}} \quad \text{clearance losses} \quad (6.89)$$

$$\eta_{c\ell} = \frac{Q_r}{Q_r + Q_c} \cdot \frac{\Delta p_{blade}}{\Delta p_{total}} = \eta_p \cdot \eta_v \quad (6.90)$$

$$\eta_{c\ell} = \frac{1}{(1 + \frac{Q_c}{Q_r})} \cdot \frac{\Delta p_{blade}}{\Delta p_{total}} \quad (6.91)$$

$$\eta_{c\ell} = \eta_p \cdot \eta_v \tag{6.92}$$

From equations 6.54 and 6.80 and 6.72

$$\frac{\Delta p_{total}}{\frac{\rho}{2} v_1^2} = \bar{\zeta} - 1 - [1 - 2(1 + \frac{\bar{\zeta}}{2}\sqrt{1+\bar{\zeta}})\varphi'^2\ (1-2\varphi')\ ](1+\bar{\zeta})\varphi' \tag{6.93}$$

From equations 6.91, 6.85 and 6.93 it follows that:

$$\eta_{c\ell} = \frac{1}{1 + \frac{\sqrt{1+\bar{\zeta}}}{1-(1+\sqrt{1+\bar{\zeta}})\varphi'} \cdot \frac{\varphi'}{1-\varphi'}} \cdot \frac{\bar{\zeta}}{\bar{\zeta} - 1 - [1 - 2(1+\frac{\bar{\zeta}}{2}\sqrt{1+\bar{\zeta}})\varphi'^2(1-2\varphi')(1+\bar{\zeta})\varphi']} \tag{6.94}$$

The normal component in the velocity triangle i.e. v_n is given by:

$$v_n = v' + v \sin\alpha \tag{6.95}$$

$$\frac{\bar{\Delta} p^*}{\gamma} = \zeta \frac{v_n^2}{2g} = \zeta' \frac{\bar{v}'^2}{2g} \tag{6.96}$$

$$\zeta = \zeta' \frac{\bar{v}'^2}{(v' + v \sin\alpha)^2} \tag{6.97}$$

6.5 The Calculation of the Volumetric Efficiency of the Turbine Rotor

As explained earlier, in the case of a turbine flow meter with a constant blade angle rotor the angle of attack will be positive up to a certain value of viscosity or Reynolds' number. This will change its sign with increasing viscosity ($\alpha < 0$, $\zeta' < \zeta$). If $v \sin\alpha = -\bar{v}'$ then there will be no tip clearance flow (Figure 5c(i)). For $|v \sin\alpha| > \bar{v}'$ the tip clearance flow will change its direction, i.e. the flow will be towards the pressure side of the tip. Therefore the variation in the flow in the tip clearance due to a change in viscosity will be determined by the shape of the blade and the installation arrangement, e.g. straightness, sharp edges, or the eccentricity of the bearing. The latter will change the tip clearance flow pattern. Therefore, the clearance coefficients, $\bar{\zeta}$, cannot be kept constant over the blade tip. The tip clearance circulation is as follows:

$$\Gamma_{c\ell} = \int_{r_h}^{r_t} \frac{\Delta p}{\rho v_o}\, dr \approx \int_{r_h}^{r_t} \frac{\zeta}{1+\zeta}\, d\Gamma \tag{6.98}$$

When the tip clearance approaches infinity, $\zeta \approx 0$ and $\Gamma_{c\ell} \approx 0$ (Ship's propeller case). When the tip clearance is zero $\Gamma_{c\ell} = \Gamma_{\text{boundary layer}}$, the boundary layer thickness will be zero. In the case of real fluids $\zeta > 0$ and $0 < \Gamma_{c\ell} < \Gamma_{\text{blade}}$. IF the drag increases the values of $\Gamma_{c\ell}$ and Γ_{bound} will be approximately the same.

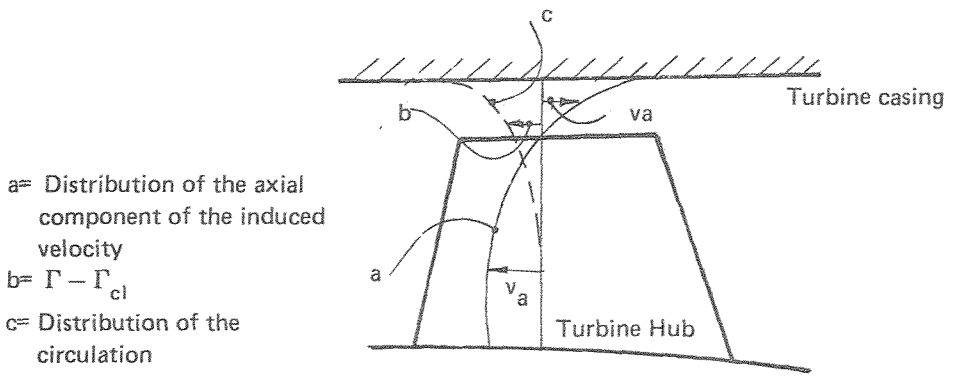

Fig. 6.2 The distribution of the circulation and its reduction $\Gamma - \Gamma_{cl}$ due to the swirl produced by tip clearance flow.

The tip clearance tangential circulation will increase towards the blade tip so that $\Gamma - \Gamma_{c\ell}$ will decrease. The change or reduction in the circulation effect is dependent on the distance from the tip and from the blade shape. In the case of zero clearance the value of hydrodynamic torque affecting the turbine blade will be:

$$T_d = N \cdot \rho \cdot \int_{r_h}^{r_t} \int_{0}^{c} v \cdot r \cdot d\Gamma \, dr \qquad \text{with zero clearance} \qquad (6.99)$$

$$T_{di} = N \cdot \rho \int_{r_h}^{r_t} \int_{0}^{c} v\, r\, (v_s - v_p)\, d \cdot \Gamma_{c\ell}\, dr \quad \text{with clearance} \quad (6.100)$$

The hydrodynamic torque for a rotor in a turbine cascade with a given size of tip clearance will be:

$$T_d = \tfrac{1}{2} U^2 .N.W.\rho \quad [C_L \left(\frac{2\pi}{L} - \frac{\omega_a}{U}\right) \int_{r_h}^{r_t} r dr - C_D \int_{r_h}^{r_t} \frac{\tan \theta_m}{\cos \beta \cos \theta_m} r \, dr] \qquad (6.101)$$

The tip clearance efficiency $\eta_{c\ell}$, will be

$$\eta_{c\ell} = \frac{T_{di}}{T_d} = \frac{1}{1 + \dfrac{\sqrt{1+\bar{\zeta}}}{1-(1+\sqrt{1+\bar{\zeta}})\varphi'} \dfrac{\varphi'}{1-\varphi'}} \cdot \frac{\bar{\zeta}}{\bar{\zeta} - 1 - [1 - 2(1 + \dfrac{\bar{\zeta}}{2}\sqrt{1+\bar{\zeta}})\varphi'^2 . (1-2\varphi')(1+\bar{\zeta})\varphi']} \tag{6.102}$$

For $\varphi'^2 \approx 0$

$$\frac{T_{di}}{T_d} = \frac{(1+\varphi')\,\bar{\zeta}}{(\bar{\zeta} - 1)} \cdot \frac{1}{\varphi'} \tag{6.103}$$

From equation 6.48 it follows:

$$\bar{\zeta} = \frac{1}{1 - \dfrac{T_d}{T_{di}}(1 + \dfrac{1}{\varphi'})} = \zeta \frac{t}{c \,.\, \cos\beta} \tag{6.104}$$

From equations 6.97 and 6.104 it follows:

$$\zeta = \frac{c \,\cos\beta}{t\,[\,1 - \dfrac{T_d}{T_{di}}(1 + \dfrac{1}{\varphi'})\,]} = \zeta' \frac{\bar{v}'^2}{(\bar{v}' + v \sin\alpha)^2} \tag{6.105}$$

Equation 6.103 may be substituted into equation 6.105

$$\zeta' = \frac{c \,.\, \cos\beta\,(\bar{v}' + v \sin\alpha)^2}{t \,.\, \bar{v}'^2\,[\,1 - \dfrac{T_d}{T_{di}}(1 + \dfrac{1}{\varphi'})\,]} \tag{6.106}$$

From equation 6.7 and 6.9 it follows

$$\zeta' \frac{\bar{v}'^2}{(\bar{v}' + v \sin\alpha)^2} = \frac{(p_{1\,tip} - p_{2\,tip})[2r_o\,(r_o - r_t)\,]^2}{\dfrac{\rho}{2}\,Q_c^{\,2}} \tag{6.107}$$

$$Q_c = \sqrt{\frac{\Delta p_{blade}}{\dfrac{\rho}{2}\zeta'}}\,[2\pi r_o \,.\, (r_o - r_t)\,]\,(1 + \frac{v \sin\alpha}{\bar{v}'}) \tag{6.108}$$

The solution for $\bar{v}'$ (in rotational direction) could be obtained from the velocity profile

between turbine blade tip and a moving flat surface (turbine casing). The boundary condition will be:

$$r = r_0 \qquad \bar{v}' = 0 \tag{6.109}$$

$$r = r_t \qquad \bar{v}' = r_t \omega_a \tag{6.110}$$

The velocity profile according to Schlichting (Ref. 66) will be:

$$\bar{v}' = \frac{r_0 - r}{r_0 - r_t} \cdot r_t \omega_a - \frac{r_0^2}{2\eta} \frac{\Delta p}{\Delta x} \frac{r_0 - r}{r_0 - r_t} \left[1 - \frac{r_0 - r}{r_0 - r_t}\right] \tag{6.111}$$

With substitution of 6.111 into 6.108 it follows:

$$Q_c = \sqrt{\frac{\Delta p_{blade}}{\frac{\rho}{2}\zeta'}} \cdot 2\pi r_0 \cdot (r_0 - r_t) \cdot [(1 + v \sin\alpha) / [\int_{r_t}^{r_0} \frac{r_0 - r}{r_0 - r_t} \cdot r_t \cdot \omega_a \, dr - \int_{r_t}^{r_0} \frac{r_0^2}{2\eta} \frac{\Delta p_{blade}}{\Delta x} \frac{r_0 - r}{r_0 - r_t} \left(1 - \frac{r_0 - r}{r_0 - r_t}\right) dr \,]\,] \tag{6.112}$$

The value of Q_c[1] can be calculated by measuring the pressure loss over the turbine rotor. This theoretical model together with the basic turbine equation can be used to calculate the number of pulses produced by flow through the turbine rotor (eq. 5.11). This gives a theoretical main turbine equation, which should be applicable for the calculation of the calibration curve for any fluid viscosity in the required operational flow range. In the case of negative values of α the theoretical value of Q_c changes the direction of flow in the tip clearance. Also the effect of fluid viscosity (which will change the velocity profile in the tip clearance) will alter the flow in the gap between the blades and turbine casing. The derivation of the second term of equation 5.15, which is the volumetric efficiency is the aim of the theoretical calculation of tip clearance flow described in this chapter. Although this part has been empirically calculated in the present research, the author has also tried to present a theoretical leakage model as an alternative to the empirical leakage model used previously. The conversion of the MTE to this theory means that Q_c (eq. 6.112) should be substituted into the following equation

$$\frac{n}{Q} = (T_1 - T_2 - \frac{T_3}{Q})(1 - \frac{Q_c}{Q}) \tag{6.113}$$

[1] Using the equation, 6.69, 6.85, 6.42, 6.96, and 6.112, one can determine ζ', $\bar{v}'$ and $v \sin\alpha$ and v_n respectively.

6.6 The Pressure Loss across the Turbine Blade

For the calculation of tip clearance flow, as has been shown in the last sub-chapter, the Δp_{blade} (pressure drop across the turbine blade) should be calculated for meters with different blade shapes.

There is a contraction and divergence of the flow when the fluid enters and leaves the rotor hub, thus there is also the same effect for the flow in the blade inlet and outlet. Therefore, there is an acceleration and deceleration due to the change in the cross-sectional area of the rotor hub and turbine blade. Thus the losses, as explained earlier, will b e the mixing losses and the energy losses for rotor motion. It depends entirely on the magnitude of the different terms of the MTE (Chapter 8), whether or not it is desirable to keep the head loss small. The energy loss connected with the retarding torque is unchangeable once the size of the hub and the blade shape have been fixed. The only external change will be varying the size of the shaft diameter and the tip clearance size to have a better compensation effect between the different terms of the MTE. The same statement can be applied to the losses due to the change in area of the hub and also in the blade inlet and outlet. The mixing losses can be corrected if necessary by changing the size of the hub, the number of blades, the design of the rotor supporter and the flow straightener, and alteration to the inside casing (the peripheral edges to fix the rotor supporter). Any changes in area should be as gradual as possible to avoid disturbances in the flow. The commercial meters used for the experiment are one with a helically bladed rotor (flow meter type B) and one with a constant blade angle rotor.

The pressure tapping was far distant upstream, just before the turbine blade (.1ins (2.54 mm) in front of the blade), just inside the blade area (.1 ins (2.54 mm) from the blade edge in the leading edge), just before the blade outlet (.1 ins (2.54 mm) from the blade edge from the trailing edge), and immediately outside of the blade (.1 ins (2.54 mm) away from the blade trailing edge. Each of the tapping pressures were a combination of the average of 3 connections at 120° to each other on one plane. The pressure drop across the blade has been measured by averaging in a chamber the pressure in each plane for different flow rates. The pressure change due to the contraction and expansion effects were measured by installing a hub the same size in place of the turbine rotor. The pressure measurement was taken according to the Figs. 45 and 6.1 in the planes "0" and "3" where the upstream and downstream taps were situated. Apart from that the blade inlet and outlet pressures were measured with the tapping located just before and after the

blade inlet and outlet (.1 ins before blade inlet .1 ins after the blade outlet; see Fig. 45, location "1" and "2"). Also 2 other tappings were installed the same distance from the blade edge immediately after the blade inlet "1_i" and close to blade outlet "2_o". Thus the pressure difference across the blade is given by

$$\Delta p_{blade} = p_{1i} - p_{2o}$$

The hub losses are due to area contraction and expansion when the flow enters the meter annulus and leaves it respectively, which causes an acceleration and deceleration in the flow. Bernoulli's equation can be applied to the accelerated flow (due to hub) between "0" and "1"

$$\frac{\gamma \cdot H_{01}\,\pi}{2\,X_{01}\cdot\eta}\int_0^{r_0} p_1 \cdot r(r_0^2 - r^2)dr = \frac{\gamma}{\eta}(p_0 - p_1)\int_0^{r_0} p_0\,\frac{(r_0^2 - r^2)\pi}{2X_{01}}\,rdr$$

$$+\frac{\rho}{2}\left[\int_0^{r_0}\frac{\pi}{32}\left[\frac{p_0}{X_{01}\cdot\eta}(r_0^2 - r^2)\right]^3 rdr\right.$$

$$\left. - \int_{r_h}^{r_0}\frac{\pi}{32}\left[\left[(r_0^2 - r^2) - (r_0^2 - r_h^2)\right]\frac{\ell n\frac{r}{r_0}}{\ell n\frac{r_h}{r_0}}\cdot\frac{(p_0 - p)}{X_{01}\cdot\eta}\right]^3 rdr\right. \qquad (6.114)$$

The same equation can be applied between "2" and "3" in which the flow is slowed down. Thus

$$\frac{\gamma.H_{23}.\pi}{2\,X_{23}\,\eta}\int_0^{r_0} p_3\,r(r_0^2 - r^2)dr = \frac{\gamma}{\eta}(p_2 - p_3)\int_0^{r_0} p_3\,\frac{(r_0^2 - r^2)}{2X_{23}\,\eta}.\,rdr$$

$$+\frac{\rho}{2}\int_{r_h}^{r_0}\frac{\pi}{32}\left[(r_0^2 - r^2) - (r_0^2 - r_h^2)\frac{\ell n\frac{r}{r_0}}{\ell n\frac{r_h}{r_0}}\,\frac{p_2 - p_3}{X_{23}\,\eta}\right]^3 rdr$$

$$-\int_0^{r_0}\frac{\pi}{32}\left[\frac{p_3}{X_{23}\cdot\eta}(r_0^2 - r^2)\right]^3 rdr \qquad (6.115)$$

The pressure loss due to the existence of the hub will be the sum of the losses from the plane "0" to "3".

Applying the Bernoulli equation between "1_i" and "2_0" gives the Head loss on the turbine blade

$$\gamma \cdot H_{blade} \left[\int_{r_h}^{r_t} (2\pi r - N.t)\, u \cdot dr + \int_{r_t}^{r_0} 2\pi r \bar{v}' \, dr \right]$$

$$= \gamma \int_{r_h}^{r_t} (p_{1i} - p_{2o}) (2\pi r - N \cdot t) \left[\left[(r_0^2 - r^2) - (r_0^2 - r_h^2) \right. \right.$$

$$\left. \frac{\ell n \frac{r}{r_0}}{\ell n \frac{r_h}{r_0}} \quad \frac{\Delta p_{blade}}{4\eta} \right] dr$$

$$- \gamma \int_{r_h}^{r_t} \frac{v_e^2}{2g} (2\pi r - N.t) \left[\left[(r_0^2 - r^2) - (r_0^2 - r_n^2) \right. \right.$$

$$\left. \frac{\ell n \frac{r}{r_0}}{\ell n \frac{r_h}{r_0}} \quad \frac{\Delta p_{blade}}{4\eta} \right] dr \qquad (6.116)$$

The axial force acting on element at radius dr (Ref. 86)

$$\Delta p_{blade} (2\pi r - N.t)\, dr = \tfrac{1}{2} \cdot \rho \cdot N.W.\, u^2 \left[\frac{C_L \sin\alpha \tan\theta_m}{\cos\theta_m \cos\beta} + \frac{C_D}{\cos\beta \cos\theta_m} \right] dr \qquad (6.117)$$

The mean value for relative velocity angle is given by

$$\tan\theta_m = \frac{2\pi rn}{u} + \frac{\tan(\beta - \delta^*)}{2} \qquad (6.118)$$

According to the theoretical model for driving torque the relation between the mean velocity angle, θ_m, and axial velocity can be expressed as follows (Ref. 62)

$$\frac{\sin\alpha \tan\theta_m}{\cos\theta_m \cos\beta} = (\tan\beta - \tan\theta_m) \cdot \tan\theta_m \qquad (6.119)$$

with substitution of equation 6.118 in 6.119

$$\frac{\sin\alpha \tan\theta_m}{\cos\theta_m \cos\beta} = \frac{\tan^2(\beta - \delta^*)}{4} - \frac{(\pi rn)^2}{u} \qquad (6.120)$$

The drag coefficient has been assumed to be constant along the blade (Ref. 86), therefore by substituting equation (6.120) into equation (6.117)

$$\Delta p_{blade} = \tfrac{1}{2} \frac{\rho . N.W}{\int_{r_h}^{r_t} (2\pi r - N.t)\, u \, . \, dr} . \left[C_L \int_{r_h}^{r_t} \frac{\tan(\beta - \delta^*)}{4} u \, dr \right.$$

$$\left. - C_L \int_{r_h}^{r_t} \pi^2 n^2 u^2 r^2 \, dr + \int_{r_h}^{r_t} \frac{C_D . u^3 \, dr}{\cos\theta_m \cos\beta} \right] \qquad (6.121)$$

The pressure loss at the blade tip will be substituted in Q_c. The head loss across the turbine flow meter with a constant blade angle rotor is larger than for the helical bladed rotor. This is because the angle of attack is larger in a constant blade angle rotor, therefore the outlet velocity angle, θ_0, is larger, and the outlet swirl will be larger also. Tan has realised that the constant blade angle rotors have a larger blade loss. He proved this assumption by measuring the blade loss for constant and helical bladed rotors with an otherwise equivalent geometrical device. The total head loss is the pressure drop across the plane "0" and "3", when the rotor is in operation. The commercial meters (Type A, B) have a substantially larger head loss compared with the research meter (6.7 times greater Ref. 86), therefore the commercial turbine meters can be optimized in regard to their head loss, if the magnitude of T_1 to T_3 shows a significant change (less viscosity sensitivity with the variation in total head loss). The pressure recovery, due to flow deceleration as the fluid leaves the rotor can be calculated by the same method, applying the Bernoulli eq. between the plane "2" and "3". A large change in area or a bearing supporter with excessively thick vanes will reduce the pressure recovery. One should sub-divide the blade loss and installation losses (Type C) into two different categories with regard to viscosity sensitivity (the supporter edges). Although larger installations losses due to abrupt change in area and thicker bearing support vanes will cause less repeatability in calibration curves, larger blade losses will not affect the meter in the same way. The constant blade angle rotor with a greater blade loss is more sensitive to the viscosity effect. The blade loss increases with the increase in the number of blades, bearing torque and hub/tip ratio.

CHAPTER 7

A THEORETICAL MODEL FOR THE RESULTANT TORQUE IN A TURBINE FLOW METER

In order to study the forces acting on the blades, of turbine flow meters, it is necessary to find out, theoretically, the total torque with respect to the blade number, blade angle and hub ratio. A relationship between meter coefficient and flow rate can be obtained with respect to the blade forces or to the total torque. The magnitude of the resultant torque depends on the hydrodynamic torque, (the resultant torque due to hydrodynamic loads) which is a function of viscosity, reduced by the mechanical torque (the torque produced by mechanical friction). The vector sum of the torque arising from the lift of the blades and the torque arising from the drag of the blades produces a resultant hydrodynamic torque. Consider an annular differential area element of thickness dr and radius r if dT_d is the elemental driving torque:

$$dT_d = N \cdot r\,(dL \cos\theta_m - dD \sin\theta_m) \qquad (7.1)$$

The angular momentum approach to calculate the driving torque is an alternative method to the same equation as that arising from aerofoil theory. The results are approximately the same if a certain number of assumptions are accepted. The aim of this research is to find a theoretical model with the minimum assumptions. Although these assumptions simplify the theory, they presuppose an ideal flow condition, which is not always the case.

A turbine meter consists of a rotor with a turbine-like blade in which a permanent magnet[1] is embedded so that in many ways a turbine meter is similar to an axial-flow turbine. The outer case is made of non-magnetic stainless steel on which an inductive pick-up is installed. When the rotor passes the coil, an electrical impulse is generated, which imposes an almost constant load on the rotor. The Euler turbine equation applies here i.e. that flow produces a fluid force or torque on the turbine blade, which is proportional to the flow rate and the rate of change of whirl in the circumferential direction. An investigation of Reynolds' number and its relation to the hydrodynamic parameters (C_D, C_L, δ^*, u/U, ...) of the turbine meter is necessary to find out the meter behaviour for fluids with different viscosities. As the angular velocity of the rotor is approximately proportional to the axial fluid velocity or the flow rate, the inlet velocity distribution is important for its influence on the rotational speed and thus the accuracy of the measurement.

The velocity profile depends on the inlet pipe Reynolds' number. This is one of the

[1] Turbine meter used in this research

reasons for different calibration curves for the same meter using fluids of different viscosities. For fluids with a high viscosity and a low Reynolds number, there is a large deviation from the normal operational value (i.e. average number of pulses per unit volume at high flow rate).

The rotor speed depends on the geometrical properties of the meter and decreases when the viscosity is increased. There is a linear meter characteristic during the operation at high Reynolds number. The external load on the meter is mechanical, the "mechanical" torque being the journal friction torque (bearing friction). The bearing torque is a function of viscosity, rotational speed of the rotor, and the mechanical coefficient of friction, μ. The magnetic load due to the magnetic pick-up was for the meters used in this research, negligible.

The influence of viscosity, in the laminar and the transition zones, upon skin friction coefficient and hence on the hydrodynamic drag, is the cause of a large deviation from the average meter coefficient.

By definition, the forces acting upon the turbine blade are given by (see Fig. 3)

$$dL = C_L \frac{\rho}{2} \cdot v_m^2 \, c \, . \, dr \qquad (7.2)$$

$$dD = C_D \cdot \frac{\rho}{2} \cdot v_m^2 \, c \, . \, dr \qquad (7.3)$$

The mean velocity angle, θ_m, with respect to the axis, is responsible for the relation between actual lift and drag forces on the blade element. An increase of the angle of attack, α, leads to an increase in lift and a small increase of drag coefficient up to a certain point. After this point the drag increases rapidly with a slightly decreasing lift coefficient. The relation between lift and drag also varies with the viscosity and rotational speed of the turbine rotor.

For an angle of attack up to 25 degree Rubin et al. (Ref. 62) from their work of turbine meters have assumed that the lift coefficient[1] will be

$$C_L = c_1 \sin \alpha \qquad (7.4)$$

A good agreement between calculated and the experimental values for water support the evidence for this assumption. Substituting this with (7.2) and (7.3) in equation (7.1):

$$dT_d = \tfrac{1}{2} \, . \, \rho \, . \, N \, . \, W \, . \, U^2 \, . \, r \, . \, dr \left[\frac{c_1 \, k \sin \alpha}{\cos \theta_m \cos \beta} - \frac{C_D \tan \theta_m}{\cos \theta_m \cos \beta} \right] \qquad (7.5)$$

[1] Suggested lift coefficient by F. Weinig: Die stroemung un die Schaufel von stroemung machinen J.A.Barth Munchen 1935

now

$$\frac{\sin \alpha}{\cos \theta_m} = \sin \beta - \cos \beta \tan \theta_m \tag{7.6}$$

or

$$\frac{\sin \alpha}{\cos \theta_m \cos \beta} = \tan \beta - \tan \theta_m = \frac{r}{r_0} \left[\tan \beta - \frac{2\pi r_0 n}{U}\right] \tag{7.7}$$

with substitution of (7.7) in (7.5) and assuming that C_D is independent of α, then

$$T_d = \tfrac{1}{2} U^2 \,.\, N \,.\, W \,.\, \rho \left[c_1 \int_{r_h}^{r_t} \frac{r}{r_0} \left[\tan \beta - \frac{2\pi r_0 n}{U}\right] dr \right.$$

$$\left. - C_D \int_{r_h}^{r_t} \frac{\tan \theta_m}{\cos \beta \cos \theta_m} \,.\, rdr \right] \tag{7.8}$$

The second term of equation (7.8) is as follows (Ref. 62):

$$C_D \int_{r_h}^{r_t} \frac{\tan \theta_m}{\cos \beta \cos \theta_m} rdr = C_D \left[\frac{\omega_a}{U} \left(\frac{r_t^3 - r_h^3}{3}\right) + \left(\frac{\omega_a}{U}\right)^3 \left(\frac{r_t^5 - r_h^5}{5}\right) \right] \tag{7.9}$$

From equations (7.8) and (7.9) it can be seen that the magnitude of the hydrodynamic torque depends on the total area of the blade, the hub ratio and the blade angle and the fluid viscosity.

The dynamic behaviour of the turbine meter rotor is a function of the rotational movement of the rotor as a result of the law of angular momentum:

$$dT_d = \bar{\theta} \,.\, \dot{\omega}_a \tag{7.10}$$

The constant number of pulses for each particular flow rate means that angular rotor acceleration must be zero, therefore the sum of all torques acting on the turbine rotor should be zero (experimentally observed of ideal case or for very high flow rates). These torques consist of those which force the rotor to move and those opposing motion. The fluid flows almost axially into the turbine cascade and because of the blade angle will be deflected (Chapter 9) onto the rotor blade. Assuming that the fluid is in a cylindrical shell of radius r, thickness dr, between leading and trailing edges of the turbine meter blade the Euler equation is:

$$dT_{total} = \rho \cdot r \cdot v_e \cdot dQ \tag{7.11}$$

It is assumed that the flow entering the cascade is swirl free. At the turbine outlet it can be observed (Fig. 3) that the magnitude of the component of the swirl velocity is:

$$v_e = U \tan \theta_m - r_m \cdot \omega_a \tag{7.12}$$

$$n = \frac{U}{r_m} \tan \theta_m - \frac{v_e}{2\pi r_m} \tag{7.13}$$

with the assumption that tip clearance is small compared with the length of the blade. As a result of swirl free flow coming into the turbine cascade, the velocity component across the blade in the axial direction remains constant:[1]

$$T_{mech} = Q \cdot \rho \cdot r_m \cdot v_e - T_d \tag{7.14}$$

where

$$T_{total} = T_d - T_{mech} \tag{7.15}$$

so that

$$v_e = \frac{T_{mech}}{\rho \cdot Q \cdot r_m} + \frac{T_d}{\rho \cdot Q \cdot r_m} \tag{7.16}$$

$$\frac{n}{Q} = \frac{\tan \theta_m}{4\pi^2 r_m^3} - \frac{T_d}{4\pi^2 r_m^2 \cdot \rho \cdot Q^2} - \frac{T_{mech}}{4\pi^2 r_m^2 \cdot \rho \cdot Q^2} \tag{7.17}$$

In the above equation, term one depends on meter performance (Term One) and term two and term three are fluid and non-fluid forces. The turbine equation in the presented form of Lee and Karlby should be completed for the effect of tip clearance. This equation is justified when the above effect is negligible. T_{mech} is mainly a function of bearing friction and depends on rotor speed and fluid viscosity (eq. 7.23).

According to Lee and Karlby (Ref. 36), the magnitude of the mechanical torque is small but in a later discussion it can be seen that this torque is important for its influence on the third term of the main turbine equation, which can be useful for compensating the viscosity influence. The assumption that the non-fluid forces should be kept negligibly small is not necessarily valid because these forces could be used as an external load on the turbine for reducing the influence of viscosity.

[1] Taking r_m and θ_m in equation 7.12 and 7.13 is only calculation of the mean value

7.1 The Calculation of the Total Torque Produced by Rotational and Retarding or Brake Forces

The rotational torque acting on the blade for a constant rotational speed is the only angular momentum, which acts in rotational direction T_T (produced by hydrodynamic fluid forces). The retarding or brake torque T_{brake} is produced by the sum of all torques in the opposing direction i.e. all peripheral forces, which have an anti-movement sense. These are fluid drag component force and the bearing friction. The net torque is the difference between the rotational torque and the brake or retarding torque. The magnitude of the retarding forces should be calculated because of the effect of viscosity on them. The above torques affect the driving rotational torque of the main turbine equation.

7.1.1 The Calculation of the Hydrodynamic Torque

The calculation of the torque produced by forces in the rotational direction is according to the force diagram, see Fig. 3, and by substitution of the eq. 7.12 into 7.11. The resultant torque produced by hydrodynamic forces is given by

$$T_T = \rho . r_m . U^2 . A_a \left[\tan\theta_m \int_{A_a} \frac{r}{r_m} \left(\frac{u}{U}\right)^2 \frac{\tan\theta_i}{\tan\theta_m} \frac{dA_a}{A_a} - \frac{2\pi rn}{U} \int_{A_a} \left(\frac{r}{r_m}\right)^2 \frac{u}{U} \frac{dA_a}{A_a}\right] \qquad (7.18)$$

The above expression is the Euler angular momentum equation in terms of normalised dimensions. The area integrals are a function of Reynolds' number, so that

$$T_T = \rho r_m U^2 A_a \left[\aleph \tan\theta_m - \frac{\bar{\aleph} 2\pi rn}{U}\right] \qquad (7.19)$$

It can be proved from the above equation that for high Reynolds' number the rotational speed is proportional to fluid velocity or flow rate.

For high Reynolds' number $T_T \simeq 0$ (bearing friction is negligible).

$$\frac{\aleph}{\bar{\aleph}} \tan\theta_m = \text{constant} = \frac{2\pi rn}{U} \qquad (7.20)$$

$\aleph$ and $\bar{\aleph}$ are constant for high Reynolds' number.

7.2 The Calculation of Brake Torque Produced by Retarding Forces

The resisting torque is the sum of all the friction forces acting on the turbine blade in the peripheral direction. The friction forces consist of fluid drag and bearing friction.

7.2.1 The Calculation of the Torque caused by Journal Bearing Friction

The shaft of the turbine rotor takes up an eccentric position within the bearing clearance under the influence of the rotor weight which it carries. The amount of eccentricity adjusts itself until the load has been balanced by the pressure created because of the existence of viscous fluid in the shaft clearance. The pressure produced and the load capacity of the turbine bearing depends upon shaft eccentricity and rotational speed of the turbine rotor. The load capacity is also related to the fluid viscosity and the size of shaft clearance. The viscosity should be assumed to remain constant as the test fluid passes the load area maintaining isotherm condition.

Although the fluid viscosity will vary with temperature and pressure, this can be taken into the calculation for a specific condition. The error arising, when no allowance is made for viscosity changes due to variation in pressure or temperature will be minimised by calculating the viscosity at the mean temperature (Ref. 94a). The power loss which has been applied to the journal bearing in order to overcome the bearing friction is shown in Fig. 63. It appears to be difficult or even impossible to calculate the bearing torque under the operating condition for different size and type of bearing, therefore the calculation must be semi-empirical.

The bearing friction torque is a function of the load due to rotor weight, the hydrodynamic forces on the shaft and the rotational speed of the rotor. The Petrov equation is applied for the plain bearing running concentrically (Ref. 95)

$$T_{bear} = \eta \left[\frac{R^3 L^* n^2}{c^* \cdot 10^{-6}}\right] 10.44 \qquad (7.21)$$

The above equation is a relatively good approximation for a lightly loaded bearing. More accurate analysis is based on an approximation proposed by Reynolds and Sommerfeld for a bearing with eccentricity ratio of $\epsilon^* = e/c^*$.

If the friction coefficient is defined by

$$\mu = \frac{c^*}{R}\left[\frac{1+\epsilon^{*2}}{2\epsilon^*}\right] \qquad (7.22)$$

The bearing friction torque is

$$T_{bear} = 24\,\eta\,\pi\,nL^*\left[\frac{R^3}{c^{*2}}\right] \frac{\epsilon^*}{(2+\epsilon^{*2})(1+\epsilon^*)^{1/2}} \cdot e \qquad (7.23)$$

The above equation should be calculated in order to illustrate the influence of the fluid

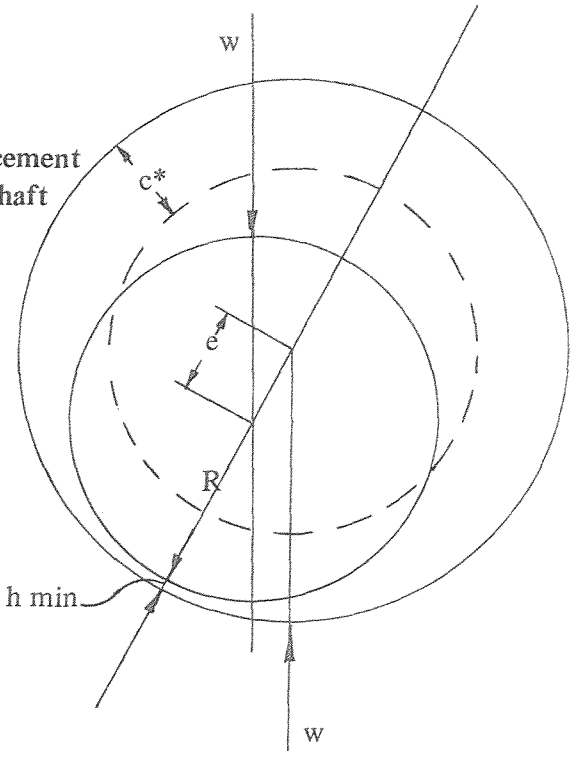

Fig. 7.1 The displacement of the turbine rotor shaft e from the bearing centre line under the action of the applied rotor weight w for the case of heavily loaded rotor (Turbine flow meter Type A and B)

viscosity on the bearing friction. Kalkhof (Ref. 32) assumed that the torque due to the bearing friction is approximately constant by neglecting the effect of variation in fluid viscosity.

However, Sommerfeld and Reynolds (Eq. 7.23) showed that for constant fluid temperature the bearing friction torque varies in proportion to fluid viscosity. It is reasonable to assume that most of the heat generated in the bearing will be carried away by the fluid and consequently a constant temperature condition may be deemed to exist in the rotor bearing. The commercial meters are mostly manufactured with plain bearings which make the calculation easier because the load distribution over the shaft is nearly uniform. The calculation for ball bearings is more complicated and the agreement between calculated and experiment is not good. The magnitude of bearing torque in the research meter (ball bearing) was significant to determine the value of Term 3 and compare it with the other two terms. The calculation of Term 3 in these meters has not been taken into consideration because this investigation was principally concerned with the commercial meter. The commercial turbine meter had either a relatively heavy rotor (Fig. 11) and large shaft diameter (rotor weight = 50 gram shaft diameter = 5 mm) or relatively light rotor (Fig. 10) and small shaft diameter (rotor weight = 10 gram shaft diameter = 1.5 mm). The bearing torque has been calculated for turbine flow meter type A (see chapter 9 and Table 9.1) according to equation (7.23) (see Appendix II and Fig. 71) for different fluid viscosities. The same calculation has been done for a lightly loaded

turbine meter with the Petrov approach (Fig. 86) which has proved to be a good approximation for the above meters. The bearing torque ratio of these two different rotors (helically and constant bladed) has been plotted in Fig. 72. It shows that for lower rotational speed or low flow rate the ratio can increase up to 30 times. The higher the fluid viscosity the larger the ratio. The effect of fluid viscosity on the flow meters becomes less significant for higher rotational speeds or higher flow rates. It is essential to find out how far the bearing torque has a viscosity compensation effect.

In such a case instead of applying an external load, the visocity of the fluid could increase the bearing torque. That makes unnecessary the existence of an external brake such as used by Lee and Karlby (which causes a disturbance in the flow) because a larger bearing torque will slow down the rotor and minimize the viscosity effect. Term 3 of the main turbine equation (eq. 5.20) contains the hydrodynamic torque and bearing friction torque so that the total torque is the hydrodynamic torque less the bearing friction torque. The rate of increase of bearing friction torque with respect to viscosity in turbine flow meter types A and B (Fig. 71) is much greater than with turbine flow meters type C and E (Fig. 86). At 1000 rpm for the turbine flow meter type A, for viscosity increase from 21 cSt to 170 cSt, the bearing friction torque will rise by about 43,72%. For a meter type C under the same conditions the increase will be 10,63%. For a meter type A the ratio of Term 3 for viscosity 47 cSt to that for water is 2.85. The equivalent ratio for type C is 7.69. Therefore the increase in Term 3 for the meter type C in changing from water to viscous fluid (ν = 47 cSt) is 2.57 times greater than with meter type A. Although for meter type C (with a smaller shaft and hence a smaller T_{bear}), the bearing friction torque increases more rapidly with viscosity, this steeper gradient cannot be used to decrease the viscosity effect in the first and second terms (Figs. 81a, b). The bearing torque exhibits a quite different behaviour in meter type A and B. Terms 1 and 2 compensate each other to a certain extent and the net effect will be a balance with the Term 3, so that in this case the bearing friction has a compensation effect (Fig. 62). Generally speaking one cannot say that the value of bearing friction always has a viscosity compensation effect. The usefulness of the bearing friction does however depend on the particular behaviour of the first two terms of the MTE.

7.2.2 The Calculation of Torque caused by Fluid Drag

This term is an important parameter for the calculation of the total torque because of the influence of the fluid viscosity. The viscosity increase affects the inlet velocity

distribution (see Fig. 53) and also C_D, which has been described in Chapter 6. The fluid drag torque is as follows:

$$T_D = \frac{\rho}{2} U^2 . N.W. (r_t - r_h) r_m \int_{A_a} C_D \cdot \frac{r}{r_m} (\frac{u}{U})^2 \frac{\tan \theta_m}{\cos \theta_m} \frac{dA_a}{A_a} \quad (7.24)$$

The above corresponds to the second term of the hydrodynamic torque on the turbine blade (eq. 7.5) i.e.

$$T_D = \rho . r_m . U^2 \bar{\bar{\aleph}} A'_a \quad (7.25)$$

for equilibrium

$$T_T = T_{brake} \quad (7.26)$$

with substitution of (7.18) and (7.25) into (7.26)

$$\frac{\omega_a}{Q} = \frac{\aleph \tan \theta_m}{r_m \cdot \bar{\aleph}} - \frac{\bar{\bar{\aleph}} A'_a}{\bar{\aleph} r_m A_a} - \frac{T_{bear}}{\bar{\aleph} \rho . Q^2} \quad (7.27)$$

The above equation is similar to the main turbine equation derived by Lee and Karlby (Ref. 36). The equation 7.27 should be corrected for the effect of tip clearance because it assumes zero clearance. The viscosity effect has already been considered in this equation with the factors $\aleph$, $\bar{\aleph}$, $\bar{\bar{\aleph}}$ which are functions of fluid viscosity and blade Reynolds number.

The first term in equation 7.27 is large in comparison with terms 2 and 3 in the equation which are respectively viscosity and bearing friction torque dependent terms. For $\frac{r\omega_a}{U} = 0$ the value of the fluid velocity, for which the rotor starts to rotate is

$$U_0 \approx \sqrt{\frac{T_{bear}}{\bar{\aleph}_0 \cdot \rho . r_m . A_a (\frac{\aleph_0}{\bar{\aleph}_0} . \tan \theta_m - \frac{\bar{\aleph}_0}{\bar{\aleph}} \frac{A'_a}{A_a})}} \quad (7.28)$$

In the equation 7.27 the first 2 terms are dependent upon Reynolds' number and are much larger than term 3 from 7.27.

$$\Phi = \frac{\aleph}{\bar{\aleph}} \tan \theta_m - \frac{\bar{\bar{\aleph}}}{\bar{\aleph}} \frac{A'_a}{A_a} \quad (7.29)$$

The eq. 7.29 shows the first 2 terms of equation 7.27 which are functions of Reynolds number and vary with fluid viscosity (Fig. 29).

7.3 The Determination of the Deviation of the Meter coefficient from "Normal Operational Value" and its Relation to Reynolds' number.

The value of the deviation of the meter coefficient from the 'normal operational value' (number of pulses per unit volume at high Reynolds numbers) is a function of Reynolds Number or viscosity. The driving torque is characterized by the flow rate at which the rotor starts to move. The effect of Reynolds number leads to a certain calibration curve for each kind of turbine meter. The main turbine equation, described in Chapter 5, the deviation can be calculated for different values of fluid viscosity. The influence of viscosity, which is a part of the Reynolds' number, on the deviation of a turbine meter is large in the laminar and transition zones and less for turbulent flow.

With substitution of equations (7.28) and (7.29) into (7.27)

$$\frac{r_m \omega_a}{U} = \Phi \left[1 - \frac{\overline{\aleph}_0}{\aleph} \frac{\Phi_0}{\Phi} \left(\frac{U_0}{U} \right)^2 \right] \tag{7.30}$$

$$\frac{r_m \omega_a}{U} = \Phi \left[1 - \delta \left(\frac{U_0}{U} \right)^2 \right] \tag{7.31}$$

For each rotor size, shape and turbine geometry, ϕ will exhibit a characteristic variation with Reynolds number which is similar to the relation between meter coefficient and flow rate.

The normal operational value $\phi = \frac{r\omega_a}{U}$, is defined as the asymptotic value of ϕ at high Reynolds' number. The corresponding proportional deviation in each point to the above value is then defined as: ($\frac{r.\omega_a}{U}^*$ =a certain meter coefficient in which zero error is assumed).

$$\epsilon = \frac{\frac{r\omega_a}{U}}{\frac{r\omega^*_a}{U}} - 1 \tag{7.32}$$

$$\epsilon = \frac{\Phi \left[1 - \delta \left(\frac{U_0}{U} \right)^2 \right]}{\frac{r\omega^*_a}{U}} - 1 \tag{7.33}$$

$$\phi = \frac{\Phi}{\frac{r\omega^*_a}{U}} \tag{7.34}$$

$$\epsilon = \phi \left[1 - \delta \left(\frac{Q_0}{Q} \right)^2 \right] - 1 \tag{7.35}$$

The starting flow rate value corresponding to equation (7.28) is a function of fluid density and Reynolds number or viscosity.

$$Q_0 = \sqrt{\frac{T_{bear} \cdot A_a}{\bar{\aleph}_0 \rho \cdot r_m \Phi_0}} \tag{7.36}$$

$$Q_0 = \sqrt{\frac{\zeta'(Re)}{\rho}} \tag{7.37}$$

substitution of 7.37 in 7.35

$$\epsilon = \phi \left[1 - \frac{\psi(Re)}{\rho Q^2} \right] - 1 \tag{7.38}$$

$$\psi = \zeta' \cdot \delta \tag{7.39}$$

The transition region (see Fig. 30) moves towards higher flow rates as the viscosity increases. The reliable range (as defined by that region with $\epsilon < 0.5\%$ is therefore confined to higher flow rates as the viscosity is increased). The value of $\psi(Re)$ is approximately constant (physikalische Bundesanstalt in W. Germany) so that the equation (7.38) becomes

$$\epsilon = \phi \left[1 - \left(\frac{Q_0}{Q} \right)^2 \right] - 1 \tag{7.40}$$

For high Reynolds' number ($Re \geq 10^5$) (see Fig. 29, 30) the value of ϕ is independent of Reynolds' number. As the Reynolds' number decreases the value of ϕ increases up to the laminar operational zone. In this zone the value of ϕ decreases again, because of increase of C_D, which is itself caused by the decrease in Reynolds' number (Ref. 32). The increasing of viscosity reduces the operational range of the turbine meter, because of $\varphi(Re)$ at low flow rates. Therefore, the turbine meter should be viscosity compensated at low Reynolds' number by an external load (Ref. 36), if the Term 1 and 2 are appropriate (see chapter 8).

CHAPTER 8

THE EFFECT OF FLUID VISCOSITY ON THE DIFFERENT TERMS OF THE MAIN TURBINE EQUATION

As described in Chapter 5, in order to find the magnitude of the three terms in the MTE (eq. 5.20) and the variation of these terms with fluid viscosity (Figs. 58 to 62 for turbine meter type B and Figs. 77, 78 and 79 for turbine meter type C), it was necessary t o know the effect of fluid viscosity on hydrodynamic parameters. The effect of fluid viscosity has been investigated for two groups of flow meters with different blade shapes. (Table 9.1).

(a) Turbine flow meter with helically bladed rotor (Type A, B).

(b) Turbine flow meter with constant blade angle bladed rotor (Type C, D, E).

The Term 1 of MTE can be subdivided into the following components:

$$\text{TERM 1} = T_1 (1-g) - T_2 (1-g) \qquad (8.1)$$

T_1 and T_2 can either be calculated as independent components corresponding to equations (5.12) and (5.13) so that the flow through the turbine rotor (eq. 5.11) can be calculated, or alternatively one can determine Term 1 of equation 5.20 with the influence of leakage ratio. T_1 and T_2 are calculated for a meter of type B (Fig. 54, 55) either as a function of flow rate or as a function of fluid viscosity (Figs. 58 and 59). The same calculation has been done for a meter of type C in which the meter coefficient is either plotted against the flow rate (Fig. 73 and 74) or against fluid viscosity (Figs. 77 and 78). The values of T_1 and T_2 have been plotted against viscosity change in the range 1 to 170 cSt. Test fluids with viscosities of 1, 21, 47, 71 and 170 cSt have been used. The meters type B and C were representative for the group (a) (with helically bladed rotor) and group (b) (with constant blade angle rotor). The experimental and the theoretical results for the two groups of meter should be analysed separately to find how the fluid viscosity affects the terms of MTE and how the effect of viscosity can be reduced. Therefore one should consider the variation of each individual term in MTE with changes in fluid viscosity to understand the hydrodynamic importance of them and the extent they can influence the calibration curve for the test fluid viscosity, in order to appreciate the applicability of a chosen meter for the given purpose. This research has divided the turbine flow meters into the previously mentioned groups a and b because of their different geometrical parameters (different blade shapes, different sizes in the rotor shaft and weight, group a being heavier than group b). These differences led to different flow characteristics and different responses to the

change in the fluid viscosity.

The variation of the different terms in MTE can be categorised as follows:

1) The first term of the MTE varies with viscosity as shown in Figs. 62 and 81a. For the group b meters with constant angle blade angle rotors there is an approximately constant increase in the value of Term 1, which ends in a roughly parabolic shape for high viscosity (Fig 81a). The graphs are drawn for different fluid viscosities by keeping the flow rate constant. It can be seen that an increase in viscosity causes a steady rise in Term 1 of the MTE, but the effect on Term 2 and Term 3 and their balance determines the gradient of the calibration curve for low flow rates, and later the creating and disappearance of the hump on the calibration curve. For a flow meter of type B, with a helically bladed rotor, the first part of Term 1, i.e. $T_1 = f(Q, \nu)$, has been calculated and plotted against flow rate (Fig. 54) and fluid viscosity (Fig. 58). T_1 is influenced by axial fluid velocity, blade angle, deviation angle, δ^*, and lift coefficient C_L. The second part of the Term 1, T_2, (with a retarding effect on T_1), can be considered separately when calculating the flow through the rotor according to equation 5.10 or as Term 1 in the MTE. T_1 has been calculated and plotted against flow rate Q (Fig. 55 for a turbine meter with a helical bladed rotor) and (Fig. 73) for a turbine meter with constant angle bladed rotor). T_2 has been plotted against the fluid viscosity for helically bladed rotor (Fig. 59) and constant angle bladed rotor (Fig. 78).

2) The value of Term 2 is a combination of the effect of viscosity on the tip clearance flow and tip clearance size. Increasing the value of tip clearance size creates a hump on the calibration curve even for a fluid with a low viscosity (water). Term 2 of the MTE has a compensation effect on term 1 especially on T_2. This term is $(\frac{T_1 k}{Q})$ demonstrating the effect of tip clearance flow on the MTE. Term 2 has been plotted against the flow rate for different fluid viscosities (Fig. 56 for helically bladed angle rotor) and (Fig. 75 for constant bladed angle rotor). Also Term 2 as a function of fluid viscosity has been plotted for different flow rates for helically bladed rotor (Fig. 60) and those of a constant bladed angle rotor (Fig. 79). This term behaves quite differently for the two different types of rotor with respect to the fluid viscosity.

Term 2 in the MTE is significant because it decreases the sensitivity of a turbine meter to fluid viscosity in the case of a constant angle bladed rotor. However, this compensation effect is not sufficient to produce a calibration curve acceptable for various viscosity ranges (Fig. 81a, b). This compensation effect is sufficient in the case of helically bladed

angle rotors and the variation due to the increase of fluid viscosity will be reduced to an acceptable minimum change in calibration curve (Fig. 62).

As explained, the viscosity increase caused a variation in the value of Q_c or on Term 2 in the main turbine equation. This variation causes an increase in Term 2 up to a certain viscosity and the decrease of it after passing a maximum (ν = 20 cSt). The above is the explanation of creating a hump and its increase up to a certain viscosity from which it starts to decrease and disappear by a certain viscosity (Fig. 79 ν = 60 cSt), and the tip clearance flow is by this viscosity approximately zero. Term 2 could become negative for continuing increase in viscosity. The negative value of Term 2 signifies the existence of a reverse flow in the tip clearance area. After Term 2 becomes negative the Term 2 and 3 reducing the calibration curve together in the same direction which will push down the calibration curve.

3) Term 3, shows the effect of driving and retarding forces acting on the turbine blades. This term is relatively small in comparison to the other two terms of MTE, but it is essential to consider its influence upon the MTE, especially in the range of low flow rates, in which this term starts to increase. This term has been plotted against the flow rate for different fluid viscosities (Fig. 57 for helically bladed rotors) and (Fig. 76 for constant blade-angle rotors). Also Term 3 as a function of fluid viscosity has been plotted for different flow rates for a helically bladed rotor (Fig. 61) and for a constant bladed angle rotor (Fig. 80).

The value of Term 3 is dependent on the magnitude of hydrodynamic and bearing torque. The value of this term was very small for the constant blade angle rotor because of small bearing torque. The constant bladed angle rotors cannot be well matched to the fluid flow direction over the radius of blades unlike helical blade rotors. Therefore, the axial width must be kept small. Due to the above reason the constant bladed angle rotors are lighter and the bearing is not loaded due to the weight of the rotor as much as it is in helically-bladed rotors. This term is much bigger in the helical bladed rotor (a rotor having a large bearing torque). The helical bladed rotor has the advantage of a better balance between Term (1 + 2) and Term 3 in the MTE (see Chapter 8.1.4) so that the effect of viscosity is minimal. The balance between Term (1 + 2) and Term 3 in the MTE for the constant blade angle rotors produces a hump in the meter coefficient at low flow rates and up to a certain viscosity, (above this viscosity Term 2 changes sign and Term 2 + 3) is then subtracted from Term 1.

If the theoretical relationship between C_D, C_L, δ^*, $\frac{u}{U}$, Q_c for different fluid viscosities is known, the variation of the calibration curve with the increase of fluid viscosity can be calculated. Also the value of T_2 should decrease[1] at much lower viscosities by optimising the geometrical device to approach a meter with wider operational range.

The helical bladed rotor used in this research programme had a large bearing friction and is less sensitive to the effect of viscosity for reason given in sub chapter 8.1 and 8.2.

The bearing friction of helical rotors was roughly 28 times that for the constant blade angle rotors. The bearing friction forces have the effect of a retarding torque on the tested helically bladed totor, which is identical to an external load and is viscosity compensated.

Commercial turbine meter used in this research with helically bladed rotor have a blade chord approximately 4 times larger than the otherwise identical constant blade angle rotors. This is the reason that for the same fluid velocity and viscosity, the blade Reynolds number could be 4 times larger for a helical blade rotor than for a constant blade angle rotor. A high Reynolds number means that the rate of change in C_L with blades Reynolds number is much smaller for helically bladed rotors, and therefore the rotor has a constant hydrodynamic torque. This torque varies for constant blade angle rotors which is one of the reasons for a greater variation in the calibration curve.

The tip clearance of the constant blade angle rotor (Type C) is 1.327 times bigger than a flow meter of type A. Smaller tip clearance has the same effect as having a larger T_{bear} or an external load, which was, as explained, viscosity compensated.

8.1 The Sensitivity of a helical bladed angle rotor with increasing fluid viscosity

The characteristics of a helical bladed rotor (group a) which will be discussed in this chapter, is quite different from that of the constant blade angle rotor (group b). Even helically-bladed rotors with different helical pitches, operating in the same fluid have slightly different meter coefficients (see MTE Term 1). One could consider a certain number of turbine rotors that are identical in all respects but that of helical pitch to identify the rotor with the optimum helical pitch, defined as that being the least sensitive to different fluid viscosities.

The helical bladed rotor is not very sensitive to the effect of tip clearance[2] flow (Figure 6, 22). The increase of tip clearance does not change the meter coefficient as

[1] This will flatten the calibration curve for low flow rate

[2] The tip clearance did not change the calibration curve significantly a lower Q

much as for the constant blade angle rotor. This has been observed in Tan's experimental results: Tan's experiments were carried out for water in the range of high Reynolds number (Re = 100 to 150.10^4). Increasing the fluid viscosity will reduce the Reynolds number. The above Reynolds numbers in the operational range were nearly twice those of the constant blade-angle rotor. The operation in range of higher Reynolds numbers will reduce the effect of the change in velocity profile in turbine meter with the increase in viscosity. To identify the difference between the two groups of meters, the following points should be considered:

(a) The change in the local axial fluid velocity is smaller, this keeps the variation of Θ_i, , and u, and v_e on a smaller scale, because of the larger Re numbers in the operational range for the helically bladed rotor. (The local axial velocity u, is almost constant. Even for higher fluid viscosity the Reynolds numbers are high enough to keep u close to the average value).

The local axial fluid velocity, u, is slightly larger on the rotor hub and will not change from the blade tip towards the hub because of a more turbulent shape of velocity profile. This is due to operation in higher blades Reynolds number for this group of meters (Type A and B). (For Q = 9.8159 lb/sec. u = 2.7915 m/s, Hel. Pitch L = 3.9596", frequency = 210 f/sec. v_e = 0.1806 m/s, $2\pi rn$ = 4.1893 m/s, Θ_i = 56.28°, β = 56.28°, β = 57.52°, χ = 1.24°).

ν cSt)	δ^* (degree)	v_e (m/s)	u (m/s)	Θ_i = degree	α = degree
water	0.09	0.1806	2.7915	56.28	1.24
21	0.11	0.1579	2.7791	56.44	1.08
47	0.13	0.1331	2.7654	56.57	0.95
71	0.138	0.1123	2.7529	56.69	0.83
170	.141	0.0758	2.7299	56.91	0.61

Table 8.1 The variation of deviation angle δ^*, axial fluid velocity u, velocity inlet angle Θ_i and angle of attack, α, for different fluid viscosity, ν, in helically bladed angle rotor (Type B).

δ^* is smaller in the helically bladed rotor because of higher blades Reynolds numbers (Ref. 96) and u is larger so that :

$$v_e = u \tan (\beta - \delta^*) - 2\pi rn$$

is larger. The change in δ^* and u are not the only factors contributing to an increased swirl v_e. The blade angle, β, will also increase from the hub to the blade tip by a factor of 2.37 thereby increasing v_e by the same factor.

This angle in helically bladed rotors depends on helical pitch. The increase of blade angle from the hub to the tip of the blade also contributes to slightly larger term 1 and 2 in helically bladed rotors. The reduction in u, caused by fluid viscosity increases, results in the small rise of the velocity inlet angle Θ_i. This small change will reduce the angle of attack for higher fluid viscosity, but will remain positive also for higher fluid viscosity. This is the reason for co-directional flow through the meter annulus and for tip clearance. The value of term 2 will rise with the increase in fluid viscosity as the flow becomes more steady. The meter's operational range will be reduced because of the rise in the value of T_2 with the fluid viscosity increase.

The meter calibration curve will tend to flatten as the value of Term 2 = $(T_1 \cdot k/Q)$ rises, thus producing a wider operational range, at low flow rates.

(b) The tip clearance flow will not be affected by boundary layer thickness in the case of a good installation condition (i.e. no leading edges or any disturbance which can cause swirl in the flow). The operations were carried out in a relatively higher Reynolds numbers range in comparison with the constant blade-angle (Helically bladed angle rotors blades Reynolds number = 150 x 10^4 to .9 x 10^4 and constant blade angle rotors blades Reynolds number = 12 x 10^4 to 0.07 x 10^4 for viscosity between water and 170 cSt). The boundary layer thickness is relatively small and it can be neglected for Reynolds number in the above operational range.

(c) The contribution of drag in helically bladed rotors depends mostly on the pressure drag, which would not vary significantly with changes in Reynolds number or viscosity increases (for helically bladed rotors for viscosities from water to 170 cSt: the drag will be doubled for the same flow rate Q = 4 lb/sec (1.81 litre/sec) and for the same viscosity increase the drag will increase to 8 times the initial value). This is the result of having much thicker blades in helically bladed rotors (blade thickness = 0.031 inches (.787mm)) compared with the constant blade angle rotor (blade thickness = 0.015 inches (.381mm)). The thicker blades will cause more kinetic energy losses in the turbine cascade outlet because of the wake in the flow and the mixing losses in the cascade outlet.

(d) The total torque acting on the turbine blade is the driving torque less the bearing friction torque. The total torque will increase by a factor of 2.58, from ν = 21, to ν = 170 cSt. At the same time the bearing friction torque will increase by a factor of 1.44 for the same change in viscosity. The bearing friction torque in the case of a helically bladed rotor has been calculated for a heavily loaded bearing and takes the eccentricity

and the weight of the rotor into consideration. For a vertically mounted meter the above consideration remains the same except the bearing friction reduces because the load will be carried only on lower side of the shaft, on which the rotor is standing. This kind of installation will affect the shaft eventually only in one point (at the ball end of the shaft) but it might exert side ways loading on the shaft in same configuration. The total torque for constant blade-angle rotors will increase for the viscosity range 21 to 170 cSt by a factor of 19, and therefore the helically bladed rotors are less sensitive to the change in viscosity. The total torque for helically bladed rotors at a viscosity of 21 cSt is 7.36 times the total torque for a constant blade-angle rotor. Increasing the fluid viscosity to 170 cSt will increase the level of the total torque of a constant blade angle rotor to the same level as a helically bladed rotor.

8.1.1 The effect of the fluid viscosity upon Term 1 in the MTE for a helically bladed rotor

As mentioned earlier the term 1 is sub-divided into two parts (eq. 8.1). This sub-division is necessary to calculate the flow through the rotor only. The first part of term 1 which is $T_1 = f(Q, \nu)$ is shown as a function of flow rate for different fluid viscosities (Figure 54), and the viscosity dependency of these meters (Type B) are demonstrated for different flowrates (Figure 58). The increase in T_1 for a specific fluid viscosity is small for the whole operational range of flow rate. For this group of meters T_1 has a non-linear part up to flow rate of 4 lb/sec (1.81 litre/sec) which gradually becomes linear. The increase in T_1 in the range of flow rates 0.5 lb/sec to 22 lb/sec (.23 litre/sec to 9.98 litre/sec) does not exceed the pulses per volume boundaries (see Fig. 58). The increase in T_1 was 1.89% for water : 2.1% for viscosity 47 cSt and 2.25% for ν = 170 cSt. The values of T_1 against different fluid viscosities have been plotted in Figure 58. The increase in T_1 relative to water for Q = 6 lb/sec (2.72 litre/sec) was for ν = 21 cSt .94% for ν = 47 cSt was 3.23% and for ν = 170 cSt was 8.5%. The gradient of the curves against the fluid viscosity are relatively large in spite of small increase of T_1 for different flow rates (Figure 58).

8.1.2 The effect of fluid viscosity upon the Term 2 in the MTE for a helically bladed rotor

The Term 2 which demonstrates the influence of the tip clearance flow is not only dependent on the geometry or the size of the tip clearance but also on the tip clearance flow condition and hydrodynamic component affecting these conditions. (i.e. the

pressure distribution across the blade, the velocity distribution in the tip clearance area and the angle of attack, α). The change in the hydrodynamic components, which is due to viscosity variation, affects the amount and direction of the flow through the tip clearance area. The flow through the tip clearance has been explained in detail in chapter 6.

The term $2=(\frac{T_1 k}{Q})$ has been plotted as a function of flow rate for different fluid viscosities (Figure 56) and as a function of fluid viscosity for different flow rates (Figure 60). The increase in this term with the decrease of flow rate Q is largely because of Q in the denominator. The leakage factor k is approximately constant with change in flow rate (Figure 66), because the change in Reynolds number due to change in the flow rate used is almost negligible compared to the Reynolds number change due to the viscosity changes . The second component, which causes a change in the value of Term 2, is T_1 which as has been explained in the section 8.2.1 does not change much with Q.

8.1.3 **The effect of fluid viscosity upon the Term 3 in the MTE for a helically bladed rotor**

Term 3 includes the hydrodynamic and retarding forces acting on the turbine blades. These forces have been described in detail in chapter 7.

T_3, which is the term 3 without the influence of leakage ratio has been theoretically and empirically calculated (Figure 61). There was a good agreement between the theoretical and the experimental results. The increase in this term for high flow rates is negligible. The fluid viscosities up to 50 cSt, which is the usual range for meters used in industry (Ref. 32), the rise of this term is small, less than ½ pulse per unit volume. In the range of low flow rates and because it will be divided by Q^2, Term 3 is becoming larger. This term is most significant in the region of very small flow rates (2 to 4 lb/sec (.908 to 1.816 litre/sec), see Figure 57). The increase in $T_{bearing}$ for helically bladed rotors (heavily loaded rotors with larger shaft diameter) as a function of fluid viscosity is demonstrated in Figure 71. The calculation of bearing torque is described in chapter 7 and appendix II. The slope of the curves of $T_{bear} = f(\nu)$ is much larger than for those with constant blade angle rotor (Figure 86).

Term 3 has a compensation effect in helically bladed rotor meters because of the characteristics of the other terms (Figure 62). Therefore this term can only be introduced as the viscosity compensating term under certain conditions. The degree of compensation effected by varying term 3 will clearly be dependent on the change of

magnitude with fluid viscosity which can make the combination of term 1 + 2. Term 3 will be quite inadequate as a compensation mechanism. The change in bearing torque for meters with this condition will not contribute very much to reduce the viscosity effect on the calibration curve.

8.1.4 The effect of fluid viscosity on leakage factor, k, leakage ratio, g, and correction leakage factor for a helically bladed angle rotor

The leakage factor, k, and leakage ratio, g, have been plotted against the blade Reynolds number (Figure 66). The change in k over the operating flow rate range is negligible. The gradient of $g = f(Re_{blade})$ will become steeper with increasing fluid viscosity. The operational Reynolds number range is larger for lower fluid viscosities. (Flow rate range 6 to 18 lb/sec. (2.72 to 8.172 litre/sec)). There was a rise in the value of the leakage factor, k, with increasing fluid viscosity. The leakage ratio, g, will drop with an increase in the flow rate. The gradient of the slope of calibration curve increases with an increase in the value of fluid viscosity. The decrease in the value of g with increasing viscosity is much smaller if the flow rate remains constant and high. Moving to the right along the dotted line (Figure 66), means an increase in the value of $(\frac{u}{U})$ and moving on the full line upwards means reducing speed of the rotor. The speed reduction for lower Reynolds number range and higher fluid viscosity is greater. This means that there is a higher volumetric efficiency for lower fluid viscosity.

This increasing of efficiency is an advantage of helically bladed rotors, caused by the equivalent flow direction through the tip clearance and the flow through the rotor. This behaviour is completely different in the case of constant blade-angle rotors because of the much more complex tip clearance flow (Figures 79, 81a, b).

8.2 The Sensitivity of Constant Blade Angle Rotors with increasing fluid viscosity

According to the experimental results of previous research (Ref 86), the increase in the tip clearance will cause a gradual rise in the turbine meter calibration curve in the overall operational range for water. The calibration curve for low flow rates will rise to a certain meter coefficient corresponding to the optimized tip clearance. The turbine meter with the optimized tip clearance has the widest operational range. Further increase in the tip clearance will create a hump on the calibration curve. For the flow meters of type C and D the precalculated optimized size of the tip clearance was approximately coincident with the clearance measured on the meter (0.0146 inches). The above optimization has been made only for low fluid viscosities or water. The

increasing fluid viscosity means a reduction in the blade Reynolds number or the movement of the flow condition from turbulent towards laminar flow (Re_{blade} = 120 x 10^3 for water to Re_{blade} = 730 for ν = 170 cSt). the decrease in Reynolds number will reduce the load affecting the turbine blades. This reduction will cause a more co-directional type of flow between the main and the tip clearance flow, which will raise the value of the meter coefficient to a certain viscosity; (according to the results of the present research this particular value is about ν = 21 cSt).

The calibration curve will rise up to the above mentioned viscosity for low flowrates because of the increase in the Term 2 = ($T_1 \cdot k/Q$). Further increase in the fluid viscosity will increase the boundary layer thickness which will effectively reduce the relative effect of tip clearance and the tip clearance flow. This will force down the calibration curve because of the decrease in the value of k. The above term has been reduced for ν = 47 cSt to the viscosity level of water. The change in angle of attack, from a positive value (α = 3.98° for water) to a negative value (α = 4.5° to −6.84° for very high fluid viscosity (ν = 71 to 170 cSt), will change the sign of the term $\frac{T_1 k}{Q}$ in the same sense. This sign change in Term 2 will affect the calibration curve. The Term 2 which is normally added to term one of the MTE (Figure 5Ci) will be subtracted for all viscosities above a certain value, which will effectively lower the calibration curve. This will reduce the range of the turbine meter for low flow rates so rapidly that the reading will suddenly drop to an unreliable value.

The operation of the constant blade-angle rotor for lower Reynolds number has the following characteristics :

(a) As the velocity profile changes from a flat shape for lower fluid viscosity to a parabolic one for higher fluid viscosity, the value of local axial velocity u will gradually start to decrease, which causes an increase in the inlet fluid velocity angle, Θ_i. (Θ_i will change from 26.0 degrees in water to 36.8 degrees (Meter Type C) in a viscosity of 170 cSt). With this increase in Θ_i, and negligible swirl the angular velocity will not be reduced significantly. The deviation angle will decrease at the same time so that v_e remains constant and negligible. The increase in the value of inlet velocity angle will reduce the angle of attack. A further increase in u moves the angle of attack to a negative value, which changes the sign of Term 2.

(b) The blade angle, β, is smaller in comparison with the helically bladed rotor so that T_1 and T_2 are smaller. (The ratio T_1/meter coefficient, and T_2/meter

coefficient are, for test fluid water, 1.27 and .3103 for helically bladed rotor and 1 and .0165 for constant blade-angle rotor, respecticely). The variation of Term 2 which has a quite different behaviour from that of the helically bladed rotor. T_2 cannot compensate for the effect of fluid viscosity and is larger than that of rotors with helical blades.

(c) The bearing torque was small for the constant blade angle rotor under test. The rotor could be considered as lightly loaded. The calculation of the bearing torque can be carried out using the Petrov approximation. The bearing torque was nearly constant for meters of type C and D over the whole viscosity range up to 170 cSt.

The total torque (for ν = 170 cSt) which consists of the driving torque less the bearing friction torque, was approximately equal for the tested helical and constant blade-angle rotors so that the following conclusion can be justified:

While the bearing friction torque in the tested helical bladed rotors rose by a factor of 1.44 (from ν = 21 to ν = 170) the total torque remained constant for the same viscosity range. Therefore the driving torque increases more rapidly at higher fluid viscosities.

(d) The blades used in the tested constant blade angle rotor were half as thick as used in the helically bladed rotor so that the pressure drag caused by wake in the flow of the blades trailing edge is negligible. The drag will be in this case more dependent on skin friction drag, which is Reynolds number (or viscosity) dependent.

8.2.1 The effect of fluid viscosity upon Term 1 in the MTE for a constant blade-angle rotor

For the reason mentioned in section 8.1.1 Term 1 was sub-divided into T_1 and T_2, which are shown as a function of fluid viscosity and flow rate for the constant blade-angle group of meters (Figures 73 and 77 for T_1 and Figures 74 and 78 for T_2). The increase in T_1 for constant fluid viscosity is small for the whole operational range of flow rate. This change in T_1 was approximately 3% over a range of .5 lb/sec (.22 litre/sec) to 22 lb/sec (9.98 litre/sec). The value of T_1 has been calculated for various fluid viscosities for this group of meters. For a constant flow rate of 6 lb/sec (2.72 litre/sec), and using a fluid with viscosity ν = 21 cSt the T_1 will increase by 4.28% relative to T_1 for water. The rise in T_1 related to water for the same flow rate will be 9.58% for ν = 47 cSt and 13.38% for ν = 71 cSt and 16.69% for ν = 170 cSt. The values of T_1 as a function of fluid viscosity (Figure 77) have been plotted for different flow rates. The gradient of the slope of calibration curve for the meter with constant blade angle rotor

is 1.56 times larger than for the meter with a helically bladed rotor for the viscosity range up to 70 cSt. The reason for greater percentage increase for constant blade angle rotors is that in the outlet velocity triangle Θ_o will increase with an increase in fluid viscosity, the angle of attack is larger in constant blade angle rotors so is the deviation angle δ^*, (this angle can rise up to 3 degrees). The axial fluid velocity, u, was smaller due to operation in the blades lower Reynolds number region (smaller blade chord), therefore the outlet velocity angle, Θ_o, was larger for constant blade angle rotors. The sum of outlet velocity angle, Θ_o, and deviation angle, δ^*, subtracted from blade angle β^1 in T_1 (equation 5.12). A viscosity increase will cause a rise in the value of $(\Theta_o + \delta^*)$ which has a faster increase for constant blade angle rotors than helically bladed rotors, therefore the gradient of the slope in T_1 for the meter described in this section is larger than that for helically bladed rotors.

8.2.2 **The effect of fluid viscosity upon the Term 2 in the MTE for a constant blade-angle rotor**

The Term 2 which represents the influence of tip clearance flow exhibits completely different behaviour from those with helical blades. The tip clearance flow for constant blade angle rotors is more sensitive to the site of tip clearance (Ref. 86) (only conclusive for low viscosity). An increase in fluid viscosity will cause a rise in the calibration curve up to a certain viscosity. Term 2 will rise up to ν = 21 cSt and fall again for a further increase in fluid viscosity (Figure 75), Term 2 decreasing to the value for water. The curve demonstrating the values of Term 2 for water and ν = 50 cSt are coincident. A further decrease in Term 2 is due to a decrease in the angle of attack and will reduce this term until the angle of attack experiences a sign change. After reaching this point as explained before, the tip clearance flow will reverse its direction giving a negative value for Term 2. This has an essential influence on the MTE which means Term 2 has from this point a reducing effect on MTE instead of an additional, therefore there will be smaller gradients (slope of the curve) for larger fluid viscosity.

8.2.3 **The effect of fluid viscosity upon Term 3 in the MTE for a constant blade-angle rotor**

The hydrodynamic and retarding forces (Ref. 18 and 7.24) acting on the turbine blade and described in chapter 7 are the components of Term 3, which is given by

$$T_3 = \frac{\text{Term 3.}\ Q^2}{(1-g)} \qquad (8.2)$$

[1] β is increasing from the hub to the tip of the blade for helical blade angle rotor

T_3 has been calculated and compared with the experimental results. The agreement between the calculation based on Petrov's approximation for lightly loaded bearing friction and the experimental results was acceptable (Figure 80). The variation of T_3 is, up to a viscosity of ν = 70 cSt, less than .5 pulses/pound (.22 litre/sec) for flow rates over 6 lb/sec (2.72 litre/sec). This viscosity range will cover the industrial application. The addition of Terms 1 and 2 is demonstrated in Figure 81b as a function of fluid viscosity. The nature of the variation of these two terms will not allow Term 3 to have any compensating effect. It can be seen that for a flow rate of 18 lb/sec (8.17 litre/sec), Term 1 + 2 rise to 32.25 pulses/pound (71.03 pulses/litre), an increase of 1.5 pulses/pound (3.30 pulses/litre) (5%) over the value obtained with water.

Variation of T_3 for constant bladed angle rotor is not sufficient to be used to reduce the viscosity effects (Figure 80).

8.2.4 **The effect of fluid viscosity on leakage factor, k, and leakage ratio, g, and correction leakage factor for a constant blade-angle rotor**

By taking the experimental points into the calculation the values of k and g have been determined (App. I) for different fluid viscosities. For this type of meter the tip clearance flow is much more complicated, therefore it is much more difficult to analyse theoretically the magnitude of the leakage factor and ratio (Figures 83 and 84), and the leakage correction factor (Figure 85). The leakage ratio increases and passes a maximum value and drops again with increasing blade Reynolds number (Figure 82).

The g and k values have been calculated empirically to predict the calibration curve for all fluid viscosities. Therefore one should attach less importance to the theoretical explanation because the leakage model is found to be applicable for practical usage. Never the less a theoretical consideration of leakage (chapter 6) provides more understanding of tip clearance geometry and gives more information about the hydrodynamic behaviour of the tip clearance flow. The leakage correction factor plotted against fluid viscosity shows a sharp drop (Figure 85) up to a viscosity of 50 cSt and a gradual increase at higher viscosities, the gradient of this rise being inversely proportional to flow rate. The sum of Term 1 + 2 as a function of fluid viscosity has been shown (Figure 81b) and Term 1 separately (Figure 81a) to emphasise the importance of leakage term (Term 2). Also the theoretical and experimental results have been compared in this figure (Figure 81a). There is good agreement between the theory and experiment.

Term 1 has a rapid increase with an increase of fluid viscosity and will pass a maximum before a gradual decrease with further increase in fluid viscosity. By adding term 2 the curves show a different shape dependent on the flow rate (Figure 81b). A flow rate of 7 lb/sec (3.17 litre/sec) passes a maximum ν = 25 cSt) and drops rapidly for any further increase, in viscosity with a flow rate of 10 lb/sec (4.54 litre/sec) the rise is greater for high fluid viscosities. Finally, for a flow rate of 18 lb/sec (8.17 litre/sec) the graph is approximately linear after the first rise. The above hydrodynamic behaviour is due to an increase in axial fluid velocity which will increase the inlet velocity angle Θ_i and will move the angle of attack towards the negative value after reducing it. This will cause reverse flow in the tip clearance area, therefore a greater reducing effect for lower flow rates. This flow characteristic differs completely from the characteristic obtained for helically bladed rotors (Figure 62).

The sum of Term 1 + 2 as a function of fluid viscosity has been shown in Figure 62 to find out the significance of the leakage term (Term 2). A good agreement between experiment and theory can be seen in this figure. The decrease of Term 1 is dependent on the flow rate. The lower the flow rate, the larger the gradient of the fall. By adding term 2 to term 1, there is an obvious compensation effect on the curves. Therefore the sum of Term 1 and 2 in the calibration curve is much less sensitive towards the viscosity increase. The tip clearance flow has very similar flow characteristics almost independent of flow rate and fluid viscosity for both types of rotors. The angle of attack is small and remains approximately the same over the whole operational range. There is a gradual increase in the curves which become more linear. Term 3 contributes significantly towards the full compensation for fluid viscosity. Therefore having this kind of meter with the Term 1 and 2 characteristics described offers the capability to compensate the turbine meter completely against effects of fluid viscosity by the variation of the bearing torque. This can be done by applying an external load to the meter or by reducing the shaft diameter.

CHAPTER 9

An Analysis of the Present Experimental Results

The main objective of this research was to study the effect of viscosity on the meter calibration curve. To get satisfactory results, all the meters were tested under various operational conditions such as long test runs (more than 100 hours). The turbine flow meters were placed at various positions along the test length prior to starting the main tests. The change in the meter coefficient due to a change in the position of the turbine meter was negligible when compared with the effect of fluid viscosity and therefore the author has not paid much attention to it. The calibration performance of a turbine meter was dependent on its design characteristics, i.e. the blade shape, number of blades, the angle of attack, the size of the helical pitch, bearing design, also the bearing dimension and the fluid viscosity. A change in bearing friction was significant at lower flow rates because it caused a rapid change in the TERM 3 of the MTE.

When the viscosity of the test fluid is increased, the calibration curve is affected in two ways. Firstly, it causes a change in the shape of the calibration curve especially for low flow rates, and secondly, there is a rise in the calibration curve. In general, for a given flow rate increasing the fluid viscosity in a turbine flow meter causes an increase in rotational speed of the meter and therefore increases the meter coefficient. The percentage increase is dependent on the geometry of the meter and might be zero for helically bladed rotors with appropriate bearing design. The effect of tip clearance is small when the hub radius is large enough to produce a flat velocity distribution, therefore reducing the value of the negative lift force of the tip (for constant bladed angle rotor TYPE C). For all turbine flow meters are similar at low flow rates the gradient of the nonlinear part of the calibration curve will increase with an increase in the fluid viscosity.

The increase in the number of pulses per unit volume with the increase in the fluid viscosity seems surprising because it could be defined as an increase in the turbine efficiency. In fact, this is due to the

Table 9.1 Meters used in this research.

Type	Blade Angle	Helical Pitch	Blade No.	Blade Tip Radius	Bore Radius	Hub Radius	Pick Up Magn/ photo	Axial Width	Shaft Dia.	No. of Pick-ups	Blade Thickness
A		3.7512	6	0.709" 18.008mm	0.720 18.288mm	0.3820" 9.703mm	mgn "	0.560" 14.224mm	0.195" 4.953mm	1	0.049" 1.245mm
B		3.9596	8	0.8995" 22.847mm	0.9095" 23.101mm	0.3915" 9.944mm	mgn "	0.960" 24.384mm	0.185" 4.699mm	1	0.040" 1.016mm
C	30		6	0.6541" 16.61mm	0.6687" 16.985mm	0.2881" 7.318mm	mgn "	0.251" 6.375mm	0.070" 1.778mm	1	0.015" 0.381mm
E	31.5		6	0.6431" 16.335mm	0.6685" 16.98mm	0.2835" 7.201mm	mgn "	0.250" 6.35mm	0.072" 1.829mm	1	0.016" 0.406mm
Research	33.5		3	0.992" 25.197mm	1" 25.4mm	0.381" 9.677mm	mgn & photo-cell	0.437" 11.1mm	0.078" 1.981mm	1 4	0.073" 1.854mm
Research	30		3	0.992" 25.197mm	1" 25.4mm	0.381" 9.677mm	mgn	0.437" 11.1mm	0.078" 1.981mm	1	0.073" 1.854mm

hydrodynamic characteristics of the tip clearance area as explained in chapter 6. If one changes the fluid viscosity while keeping all other parameters constant the real variation in the meter calibration which is purely due to the change in fluid viscosity can be seen on the calibration curve. When the angle of attack becomes negative a negative lift force occurs which decreases the overall lift force. The angle of attack will change with the radius in the case of constant blade angle rotors because of the change in the local axial fluid velocity. The blade angle will increase in helical blade angle rotors from the hub to the tip, which minimises the effect of velocity profile and keeps the angle of attack small, positive and constant (small change in velocity triangle in upstream position of the blade). Therefore any change in the hydrodynamic characteristics of the flow (and in upstream and downstream position of the blade in the tip clearance area), will not affect the calibration curve because the negative force affecting the turbine meter with a helically bladed rotor is either zero or negligible.

This explanation is also adequate and appropriate for the blade tip area because for the turbine meter the blade height occupies a smaller percentage of the total rotor radius when compared with a real water turbine of the same hub/tip diameter ratio, because of the relatively large tip clearance of the turbine meter.[1]

The size of the tip clearance and the flow condition in the tip clearance area can be used to advantage causing a turbine meter to be insensitive to a change in fluid viscosity. However, the blade shape can keep the angle of attack to a favourable size for any given fluid viscosity. When the experimental results for two meters, Type A and B (Table 9.1), with equivalent geometrical characteristics except for their helical pitch, are compared it can be seen that the meter Type B is less sensitive to the effect of fluid viscosity (Figure 22) than the Turbine flow meter Type A, (Figure 6). The reason is that the helical pitch of meter B is adapted better to the angle of attack and an optimal flow condition has been reached. The turbine meters which have been used for the author's research programme were mostly commercial meters which have been listed in Table 9.1. As well as these meters, there were other commercial meters which show similar geometrical characteristics and therefore they have not been used for the theoretical consideration. The research meters (Figure 33 and 34)have also played an essential part in the theoretical and experimental investigation of this work.

The only modification to the research meter was the installation of an additional magnetic pick up (Figure 34) to detect missing pulses caused by the opaqueness of

[1] Therefore only a small difference in the tip clearance size will contribute significantly to the calibration curve.

the viscous test fluid. A viscosity change affects the meter with a constant blade angle rotor much more than that with a helically bladed rotor.

9.1 A Brief description of present experiments

This research has been developed from the previous experimental results explained in Chapter 3. Previous publications do not consider the effect of fluid viscosity and therefore their hypotheses were based on experiments carried out with water (Ref. 24, 36, 86). Experimental results were not sufficiently reliable to use as a basis for the theory (see Chapter 2.1).

Tan's theory is the latest and the most complete form for turbine flow meter behaviour and his experimental results were also repeatable. Tan's theory is based on experiments with water, using a research meter and therefore his theory must be expanded and made applicable to a wide range of fluid viscosities and also his experiments were mostly carried out on research meters.

Industrial demand forced the author to divert his research direction more into the field of the commercial turbine flow meters. The experiments on commercial turbine meters were carried out on 2" (50.8mm) rotor diameter, one with a helically blade angle rotor (Type B) and one with a constant blade angle rotor (Type D) and three 1½" (38.1mm) rotor diameters, one with a helical blade angle rotor (Type A) and two with constant blade angle rotors (Types C and $\overline{E}$). The turbine flow meter can be situated anywhere along the test length (from 40D to 90D). Usually there were 2 meters in operation, the one which was placed in the middle of the test length was used for the experimental values. The interaction of the meters was insignificant. The pulses produced by the second meter, which was situated at the end of the test length have been used to confirm and recheck the measure flow rate at certain pump speeds and to quickly distinguish the unreliable experimental values. (The air bubble might cause unreliable reading). By adjusting the pump speed of line pressure or the number of produced pulses, any required flow rate can be set. A line pressure of approximately 70psi[1] was used to prevent the creation of any air bubbles in the system (Chapter 4.3).

Tan has discovered the importance of increasing the tip clearance. In this work the significance of tip clearance flow, especially with an increase of fluid viscosity, has been demonstrated. One might consider that in the small area of the tip clearance the flow is negligible. The blade height is small relative to the hub radius, therefore any unusual flow conditions will affect not only the tip clearance flow but also the flow

[1] p = 70 psi = 4.83 bar

through the rotor. However the tip clearance flow does not contribute towards the number of pulses produced at high flow rates. The meter coefficient drops rapidly at low flow rates. An increase of fluid viscosity produces the hump in the calibration curve at low flow rates up to a certain fluid viscosity and any further increase will reduce the minimum flow rate. Tan has observed the same effect by increasing the tip clearance size in his experiments. This effect can be seen in figure 12, increasing the fluid viscosity has raised the whole calibration curve, which has been explained in chapter 8. The existence of the hump and its disappearance can be also seen in the viscosity range 47 to 71 cSt.

The calibration curve is clearly a complex function of several parameters (such as blade angle and shape, hub and aspect ratio etc.) and it would not be practicable to predict a specific improvement of the curve (e.g. a fractional change in the root mean square deviation from the ideal curve with almost constant meter coefficient as a result of a specific fractional change in a single parameter).

The experimental and theoretical results of this research have proved that a helically bladed rotor with an optimised pitch is insensitive to the effect of fluid viscosity (one can optimize the helical pitch before looking at bearing friction). The bearing friction of such a rotor can also have a viscosity compensation effect once all the above factors have been established. A further improvement can be achieved by variation of the tip clearance i.e. the optimum size for tip clearance is according to Tan's work (ref. 86) neither a large one nor a small one. This means that by having a rotor with the above mentioned geometrical components one can enlarge the operational range by increasing the tip clearance until the hump has completely disappeared. This approach for a certain fluid viscosity is not valid if the test fluid changes its viscosity by more than 10 to 20 cSt, because changing the viscosity in this range will cause a drop in the lower operational zone. This means that the tip clearance should be re-optimised for the new viscosity (or alternatively using rotors with equivalent geometry but different tip clearance size). If the calibration curve for a particular blade shape and bearing friction optimised rotor has a hump and is not completely flat at the lower range for a particular fluid viscosity one can raise the lower range of calibration curve, therefore enlarging the operational range, by decreasing the tip clearance until the calibration curve is completely flat. This is only possible when there is sufficient space between the blade tip and meter casing. A change in the tip

clearance size will alter the leakage factor, k and leakage ratio g which will be reflected in the calibration curve at the lower flow rates. As explained in chapter 8.1.3 only with particular hydrodynamic and geometric characteristics will the fluid viscosity effect in term 3 have a compensating effect on the calibration curve. Therefore it can be seen from the experimental results that if a rotor is hydrodynamically sensitive to the effect of viscosity an external load will also not be able to compensate for this. The experiments of this work carried out on turbine flow meters can be divided into two major groups :

(a) using research turbine flow meters

(b) using commercial turbine flow meters

9.2 The experimental results obtained using the research turbine flow meter

The research turbine flow meter with rotor having 3 constant angle blades was originally equipped with a photoelectric pick up (Fig. 35). Because some of the pulses were too small to trigger the Schmidt counter an additional magnetic pickup was installed to indicate the missing pulses (Fig. 37). As a result of this misreading, the calibration curves were shown to have a completely different shape with a change in fluid viscosity (Fig. 16). Improved results have confirmed that a constant blade angle rotor in commercial meters has a similar change with a change in fluid viscosity. Weak pulses reflected by the blade tip which were lost due to the opaqueness of the viscous test fluid could be detected by comparing the number of pulses detected by magnetic pick up and photocell pick up (Fig. 20). At very low flow rates the number of pulses obtained from the magnetic pick up is less than the number of pulses obtained from the photo cell pick up. The rotor for the research meter has only 3 blades and in the range of low flow rates the number of produced pulses was not sufficient. The speed of the blades was too slow to generate pulses of sufficient voltage to be detected by the counter. The missing pulses caused in this case a sudden drop in the calibration curve. For low flow rates the output from the pick-up was amplified but there was then the danger of noise being confused with the pulses, therefore the research meter was not used when the fluid viscosity was greater than 47 cSt.

9.3 The experimental results using the commercial turbine flow meter

The commercial turbine flow meter did have a similar calibration curve, compared to the research meter, at low fluid viscosities or water (if the geometrical device were similar). The commercial turbine flow meters were divided into the 2 major groups which are the constant blade angle rotor and helical bladed angle rotors. These two designs of

rotor have a different degree of sensitivity towards a change in fluid viscosity, which has been explained in great detail in chapter 8. The calibration curves of these two types of meter have been calculated by calculating the different terms in the MTE. The experimental results of the turbine flow meters TYPE A, B, C, D and E have been shown in Figs. 6, 22, 13, 12a and 9 respectively.

9.3.1 Analysis of the results of experiments into the effect of fluid viscosity upon the calibration curve of helically bladed angle rotors

Turbine flow meters of type A and B have been chosen for this analysis. For flow rate between 6 and 19 lb/sec. (2.72 and 8.62 litre/sec.) and a viscosity range of 1 – 170 cSt the change in the meter coefficient variation is less than ± .80% for a helically bladed rotor Type A with an average meter coefficient of 41.55 pulses/pound (92.33 pulses/litre). The change in the meter coefficient will be ± .33%, for a smaller flow rate range (10–19 lb/sec. (4.54–8.63 litre/sec.) and average m.c. = 41.44 pulses/pound (91.28 pulses/litre) see Fig. 6). The experimental result for turbine flow meter TYPE B which also has a helically bladed rotor was slightly better in the range of low flow rates (under 6 lb/sec (2.72 litre/sec.)), because the tip clearance/blade height ratio is .0196 compared with .0336 for a turbine meter of type A. Therefore a meter of type B the percentage area occupied by the tip clearance is less than that for a meter of Type A. which means that the meter B is closer to the optimum size of tip clearance. However an improvement in meter Type A also can be achieved by reducing the size of the tip clearance. The knowledge of tip clearance flow is only essential for low flow rates because the leakage factor and bearing friction have a negligible effect for high flow rates (over 6 lb/sec. (2.72 litre/sec.)).

However, when the viscosity increases, the leakage factor will increase which is equivalent to a decrease in the tip clearance. This will affect the calibration curve for lower flow rates. Therefore increasing the fluid viscosity will reduce the hump on the calibration curve. If there is a significantly large difference in the size of the tip clearance of the two meters the meter with the larger tip clearance will cause a larger hump on the calibration curve. The meter Type B with a helically bladed rotor has a smaller deviation of the meter coefficient in the flow rate range of 6–20 lb per sec. (2.72–9.08 litre per sec.) which is ±.77% for an average mc. of 28.80 pulses/lb (63.44 pulses per litre). In the range of flow rates between 8–20 lb/sec. (3.63–9.08 litre/sec) for an average m.c. of 28.85 pulses/lb. (63.55 pulses/litre) the deviation will be ±.48%.

The viscosity range for above mentioned deviation was between 1–170 cSt. When the deviation in the meter coefficient for meters of type A and B are compared (± .33% for meter type A and ± .48% for meter type B), it can be seen that although the meter type A has a much larger viscosity effect in the lower flow rate range (under 6 lb/sec. (2.72 litre/sec.)), it is slightly less sensitive in the higher flow rate ranges. Therefore although the bearing friction and the tip clearance site improved, meter Type B at lower flow rates range, these components seem to be insignificant at higher flow rates. For flow rates below 6lb/sec. (2.72 litre/sec.) the two types of meters show different characteristics, type A meter is more sensitive to the viscosity.

The effect of fluid viscosity produces a hump on the calibration curve. The hump will gradually disappear in the viscosity range of 47 and 71 cSt. The same observation can be made for a meter with the same bore diameter but with a constant bladed angle rotor.

The hump in the calibration curve progressively diminishes with decreasing tip clearance (Ref. 86) until optimum clearance the curve flattens out completely with the widest possible operational range. With further decreasing of tip clearance the curve remains the same shape but reaches the constant meter coefficient level at higher Q, thus leading to a reduced operational range (Fig. 25).

The behaviour of the calibration curve with respect to fluid viscosity is somewhat similar, a reduction in the hump size accompanying an increase in viscosity. The curve however, also systematically skews towards higher Q before the hump disappears altogether, i.e. along with a reduction in the size of the hump there is a shift of the maximum towards the higher Q (Fig. 12). The optimum tip clearance (constant meter coefficient over a wide operational range), is not independent of viscosity so that there is a different optimized tip clearance for each viscosity. The calibration curve like that for meters of Type A and B, decreasing the size of the tip clearance will flatten the low Q end of the calibration curve up to viscosity 50 cSt. If the viscosity of the fluid is higher than this value some improvement can be achieved by increasing the tip clearance and therefore raising the low Q end of the calibration curve. This improvement seems to be more essential for meter Type A rather than the meter Type B, because in the case of meter B the ideal size of tip clearance seems to be achieved.

9.3.2 Analysis of the results of experiments into the effect of fluid viscosity upon the calibration curve of constant bladed angle rotors

The representatives of this group were the turbine flow meter Types C, D, E. The

turbine flow meter Type C and E were of 1½ ins bore diameter (38.1 mm) and D was 2 ins rotor diameter (50.8 mm). The results are reflected in the Fig. 9, 12 and 12a. The meter C has been the centre of the theoretical and experimental consideration because its characteristics were representative of the complete group of meters. The experimental results for water as test fluid exhibit a flat calibration curve with a wide operational range (1.5 to 20 lb/sec – .68 to 9.08 litre/sec). Apart from raising the whole calibration curves with the increasing of the fluid viscosity, these meters all show quite similar changes. The differences are that the changes are on a much bigger scale than for the meters with helically bladed rotors. The linear part of the calibration curve will rise by 5.36% from 1 to 71 cSt, for flow rates between 10 –20 lb/sec. (4.54 – 9.08 litre/sec.). From ν = 71 cSt upwards, there is hardly any linear part on the calibration curve. Therefore, this kind of turbine meter is only useable in lower viscosity range (up to ν = 20 cSt) and, even in that range, the user should calibrate his meter for the fluid used. The increase in meter coefficient from 1 – 20 cSt for flow rates between 10 and 20 lb/sec (4.54 to 9.08 litre/sec) is about 2.19%. The variation in the meter coefficient is about ± 1.16% for flow rates between 10 and 20 lb/sec (4.54 to 9.08 litre/sec) and viscosity range between 1 – 20 cSt, the average meter coeffient being 30.61 pulses/pound (67.42 pulses/litre). The onset and disappearance of the hump with the increase in fluid viscosity can be seen. (The hump will disappear at viscosity approximately 60 cSt). The hump has been moved towards much higher flow rates in comparison with the helically bladed angle rotor. The location of the maximum point of the hump on the flow rate axis is as follows:

	ν = 1 cSt	ν = 21 cSt	ν = 47 cSt
Turbine flow meter Type A	1.51 lb/sec	1.65 lb/sec	3.72 lb/sec
	.69 litre/sec	.75 litre/sec	1.69 litre/sec
Turbine flow meter Type C	no hump	1.91 lb/sec	8.03 lb/sec
		.87 litre/sec	3.65 litre/sec

The turbine flow meter type C can only be used if the calibration curve is known and the fluid viscosity does not change during the operation more than 2 – 3 cSt. Even when the meter is calibrated for a certain fluid viscosity, say for 12 or 21 cSt for a flow range between 6 to 20 lb/sec (2.72 to 9.08 litre/sec), the deviation in the meter coefficient will be ± .73% for an average meter coefficient of 30.67 pulses/pound (67.56 pulses/litre) and ± .93% for an average meter coefficient of 31.16 pulses/pound (68.55 pulses/litre). For a viscosity of 170 cSt no linear part can be seen. The improvement might be achieved

by decreasing the tip clearance for viscosities between 12 – 47 cSt to give the meter a wider operational range. The turbine flow meter with a constant blade angle rotor will have less sensitivity for the larger rotor (Fig. 12a) because of larger aspect ratio and less tip clearance influence. The operation is mostly in the range of high blades Reynolds number and the rotor weight can contribute significantly toward the effect of viscosity compensation. The tip clearance/blade height ratio is also smaller in larger rotors, therefore the leakage will not be reflected on the calibration curve to the same degree as in flow meters with smaller rotors.

CHAPTER 10

CONCLUSION

10.1 The Summerising and the Discussion of the Present Work

The effect of fluid viscosity on different terms of the main turbine equation (eq. 5.20), affects the hydrodynamic characteristics of turbine flow meters and will be reflected in the calibration curve. In order to find the effect of fluid viscosity on the calibration curve, it was necessary to evolve a theoretical model, which could be used to fit the experimental results (Figs. 88 to 99 and Table I.1 to I.18). To build up a theory one should look for a pattern in the experimental calibration curves (Figs. 6, 9, 12, 22). Having observed patterns in the calibration curves for certain groups of meter one is able to identify a meter type (Chapter 8) by the change in the curve shape under varying viscosity conditions (Figs. 12 and 22). The pattern observed with the research meter is entirely consistent with those observed in commercial meters. Research showed, that the meters behave similarly with respect to the effect of fluid viscosity but with different degrees of sensitivity (i.e. although the meters with helically bladed rotors (Type A and B and Fig. 22 See Table 9.1), were much less affected by viscosity than meters with constant blade angle rotors (Type C, D and E Figs. 9, 12 and 12a), the shape of the calibration curves have changed with viscosity in a similar manner.

This research has sought to evaluate the parameters (T_1, T_2, T_3, eq. 5.12, 5.13, 5.14), which have led to the differing patterns of change with respect to viscosity, observed in meters of different geometry. (Fig. 58, 59, 61 for meter type B with helically bladed angle rotor and Fig. 77, 78, 80 for meter type C with constant bladed angle rotor). The geometrical parameter s such as blade angle, blade shape (Figs. 10 and 11), hub and aspect ratio (eq. 5.7a), tip clearance size (Chapter 6), and size and geometry of the bearing (Chapter 7.2.1, Figs. 63, 71, 86), have been studied as well as the hydrodynamical parameters such as blade angle velocity angle (eq. 5.6) lift and drag coefficient (eq. 6.34 and 6.35) and velocity profile (eq. 5.1 and LDA measurement) in order to calculate the different terms in the MTE (Chapter 5.2). These parameters were taken into the calculation of the calibration curves using the main turbine equation (eq. 5.15). This equation can be generally used for meters with different geometry proportions (helically and constant bladed angle rotors). Also it was essential to find how different geometrical parameters (blade angle, blade shape, tip clearance size and bearing design) will relate to fluid viscosity change. In other words how the calibration curve will vary if a particular change in one of

the geometrical parameters has been made (i.e. The change in the size of tip clearance to destroy the hump produced on the calibration curve due to viscosity increase or the change in the bearing friction required to produce a viscosity compensation effect). It is obvious that a straightforward improvement (i.e. a decrease in the degree of sensitivity) of a particular meter is difficult if not impossible because a particular change in one geometrical parameter can be an advantage in one way but a disadvantage in another way, e.g. increasing the bearing friction may be useful for compensation effect but it lowers the calibration curve at low flow rate, so that one should balance the advantage and disadvantage of changing a parameter in order to find a compromise. Also a certain change which can be used to improve a particular meter cannot be generally used as an improvement factor for all meters (i.e. the change in the size of tip clearance, which might advantageously alter the calibration curve of a turbine flow meter with constant blade angle rotor to reduce the hump produced due to the fluid viscosity, will increase the sensitivity of a helically bladed rotor because of the change in the leakage and eventual creation of unwanted swirl. The bearing friction which has a compensation effect in a helically bladed rotor is negligible in the case of the present experiments for constant bladed angle rotor and cannot contribute significantly towards viscosity compensation (Chapters 8, 9).

10.2 The Turbine Flow Meter Theoretical and Empirical Model

To find a way to approach the effect of viscosity on all those components one had to find a theoretical equation (eq. 5.15) which could be applied with an appropriate approximation to fit the experiments for all groups of turbine flow meters and consider the variation of this equation by calculating the different terms as a function of fluid viscosity (T_1, T_2, T_3, eq. 5.12, 5.13, 5.14 and g and k see eq. 5.20 and App. I). This will not give a statement on how every single parameter will be affected by fluid viscosity but it will show how the fluid viscosity increase will affect the 3 terms in the MTE. These terms are a combination of different parameters. The study in this research was mainly concerned with finding a suitable equation and by studying the separate terms to eliminate the discrepancy between the equation derived from the previous theoretical models (Refs. 32 and 36) and the experimental calibration curves. This was done by adopting Tan's theoretical approach (Ref. 86) and making allowance for viscosity change. Therefore the calculated terms of the modified turbine equation have been studied for different fluid viscosity.

The calculation of the different terms in MTE also demonstrates how important the external parameters are and to what extent they can improve the meter calibration perform-

ance. (Fig. 62 shows to what extent an external load can compensate the viscosity effect in a helically bladed rotor whilst Fig. 81b shows that the friction due to bearing torque cannot contribute significantly towards the viscosity compensation in a constant bladed angle rotor). The Euler turbine equation has been used to derive the turbine meter equation, which is for an axial flow machine. Tan improved this equation for the effect of tip clearance. A further development has been achieved in the present research to allow for fluid viscosity changes, by finding the theoretical relationship between hydrodynamic parameters like C_D, C_L, u, δ^*, and blades Reynolds number or fluid viscosity. The main turbine equation can be generally expressed in the following form

$$\frac{n}{Q} = (T_1 - T_2 \underset{n/Q_r}{} - \frac{T_3}{Q^2}) (1 - g + \underset{Q_r/Q}{} \frac{k}{Q}) \qquad 10.1$$

The first part of the above equation shows the achieved pulses of the flow through the turbine rotor and the second part shows the leakage flow or the turbine volumetric efficiency. Tan has converted this equation to the form showed in equation 5.20 by neglecting some of the terms (Ref. 86) and found the best value for A, B, C (eq. 1.1) using the method of least squares.

This research investigated the calculated value of T_1, T_2, T_3 (eqs. 5.12, 5.13, 5.14) g and k (App. I) as a function of flow rate and fluid viscosity. g and k were determined (Fig.82-85 for constant bladed angle rotor and Fig. 65 and 66 for helically bladed rotor), using the experimental points, so that a general equation could be found to represent the g and k variation with flow rate and fluid viscosity. The second part of equation 10.1 can be determined in one of 2 ways:

a) leakage method using g, k = f (ν, Q)

b) volumetric efficiency. The second part of equation 10.1 can be expressed (see eq. 5.15) as

$$\frac{Q_T}{Q} = (1 - \frac{Q_C}{Q}) \qquad 10.2$$

To calculate the tip clearance flow to enable the determination of leakage flow, there were two methods suggested in this research:

1) The determination of leakage flow based on boundary layer displacement and momentum thickness (Chapter 5).

2) The calculation of leakage flow based on tip clearance energy losses (Chapter 6).

For the method 1, Gersten's 'displacement' equations have been used (eqs. 5.16, 5.17) with a correction factor to make his empirical suggestion applicable for this research.

For method 2, a theoretical model has been produced to evaluate and determine the leakage flow.

Chapter 6 gives an outline of the effect of the tip clearance flow on the main flow structure. An attempt is made to determine the tip clearance flow and its effect on the MTE with viscosity increase. Also the direction of the tip clearance flow has been investigated. The existance of a reverse flow, for constant bladed angle rotor has been proved (Chapter 6.6).

10.3 The Viscosity Effect on the Flow Characteristic of a Helically Bladed Rotor and a Constant Blade Angle Rotor

According to the observed calibration curves the turbine flow meter can be divided into 2 major groups: helically and constant bladed angle rotors. These groups of meters have a quite different degree of sensitivity towards the fluid viscosity. The variation of the three terms in the MTE shows why these two groups behave differently with the viscosity change. Term 2 in the MTE represents the tip clearance flow (Fig. 60 for helically bladed rotor and Fig. 79 for constant bladed angle rotor). The helical blade angle rotor is less sensitive to the effect of fluid viscosity (Fig. 6,22) because of a very good adaptibility between velocity angle θ, and blade angle β, which make α positive and small and the tip clearance flow uniform and co-directed with the main flow through the turbine blade. There is no negative lift force acting on the blade. The angle of attack, α, is initially positive for low fluid viscosity in a constant blade angle rotor and with the increase in fluid viscosity, this angle becomes smaller and eventually changes sign. The change in the sign of this angle produces a negative lift force on the blade tip area, so that the increase in viscosity will change the meter performance of a constant bladed angle rotor much more (Fig. 9, 12, 12a) than it does in helical bladed rotors.

The tip clearance flow direction depends on the sign of the angle of attack α, (Fig. 5c). The direction of the tip clearance flow is along the flow through the turbine rotor, if α is positive (Fig. 5 cii), and is in the reverse direction if α is negative (Fig. 5 ci).

The sign of the angle of attack, α, depends on the pressure distribution across the turbine blade. The sign of this angle determines the direction of the flow in the tip clearance, and also the sign of the Term 2 in MTE. Positive angle of attack means positive Term 2,

which will be added to Term 1 (Fig. 62). This was advantageously used in meter Type A and B with helically bladed rotor (i.e. Term 1 and 2 have compensated each other). Negative angle of attack means the tip clearance flow is in the opposite direction to the main flow through the turbine rotor, and the Term 2 will be subtracted from Term 1 (Fig. 81b). The first two terms in meter Types C, D and E do not show any compensation. Although the turbine flow meter is a very complicated machine the designer can suggest roughly what the calibration curve against viscosity will look like if certain geometrical components have been predetermined (helical or constant blade angle rotor). If a meter is required to operate in an unknown fluid viscosity range, a meter design similar to the turbine meter Type A and B will satisfy the user's need (Fig. 6 and 22). For operation in much lower viscosity fluid, close to water, the meter type C, D and E will have slightly better calibration performance (Fig. 9, 12, 12a) and repeatability (.1 to.4%). When the viscosity of the fluid and the design of the rotor is determined, some improvement can be achieved by calculating the different terms in the MTE for that particular design and viscosity resulting from a small alteration in the turbine rotor. The calculated value will show if the possibility of an increase in accuracy and repeatability is given which can be achieved by changing the bearing torque or applying an external load or by a change in the blade geometry. When the calibration curve is experimentally determined some improvement in the meter calibration can be approached by changing the size of the tip clearance if it is necessary to reduce any hump which has been created due to viscosity increase. The calculation of T_1, T_2, T_3 and the empirical determination of g and k (The three Terms of the MTE) have been used to predict the calibration curve for every fluid viscosity.

Also the theoretical suggestion for the calculation of volumetric efficiency can be used to replace the mentioned semi-empirical leakage theory.

10.4 The Tip Clearance Flow Structure

It may be thought that the ideal characteristic of a turbine flow meter will be achieved when the tip clearance is small in order to minimize the losses in this area. In practice, the flow characteristics in the turbine tip clearance are much more complicated than that (i.e. a meter with very small tip clearance is not always performing ideally).

A theoretical model has been offered in this work, to calculate the tip clearance flow as a function of fluid viscosity and the angle of attack, α (Chapter 6). The tip clearance flow, which can be affected by the force acting on the turbine blade, induced drag, velocity outlet angle θ_0, and the blade tip mixing losses, depends on the pressure distribution across the

blade. The experimental part of this research has shown that the mechanics of tip clearance flow does not contribute significantly towards the calibration curve for very viscous fluid. The tip clearance flow will affect the lift force of the blades because the induced drag causes a change in pressure distribution. The volumetric efficiency has been calculated by estimating the value of displacement thickness in order to determine the drag induced by tip clearance flow. The tip clearance flow will be associated with the energy losses in the tip clearance area, which is due to the pressure distribution across the blade tip. The pressure distribution at the blade tip is dependent on skin friction drag, blade Reynolds number, blade shape, angle of attack and hydrodynamic force on the blade, and has been measured for both helically and constant blade angle rotors to determine the magnitude and direction of the flow in the tip clearance area. A reduction in the tip clearance drag is equivalent to the increase in blade force. Therefore, a change in the tip clearance goemetry or an alteration in blade shape could reduce the tip clearance effect. The value of angle of attack determines the direction of the flow. A small positive angle of attack minimizes the tip clearance effect and can be achieved by having an optimum helical pitch on the turbine blade. The velocity distribution in the tip clearance area was not only dependent on the pressure distribution but also on tip clearance geometry. The tip clearance flow has been evaluated by applying the momentum equation for tip clearance area. The tip clearance efficiency, which can be either expressed as the ratio of the induced hydrodynamic driving torque with zero tip clearance to the hydrodynamic draving torque (eq. 6.102) or the volumetric efficiency (eq. 6.91), could lead to an equation for determining the tip clearance flow (eq. 6.112). The value of Q_c has been calculated by measuring the pressure loss over the turbine blade. That produced a theoretical MTE for the calculation of the calibration curve for any fluid viscosity.

10.5 Future Work

The turbine meter can be made to possess a satisfactory calibration curve for different fluid viscosities if the hydrodynamic parameters and all, or at least most, geometrical parameters are optimized. The importance of such parameters as tip clearance size has been made clear in previous work (Ref. 86) whilst the importance of the viscosity effect and the flow characteristic, in the tip clearance has been emphasised by the present work. Whilst this research and other work (Ref. 32, 36) have sought to identify and evaluate most of the governing factors in the calibration curves of these instruments, there remain a number of problems. It was essential to be able to theoretically predict the calibration

curves via numerical calculation. As is clear from previous chapters, any changes in the turbine meter geometry will affect they hydrodynamic parameters, which in turn will change the meter calibration performance. Some of these geometrical parameters which can be optimized are as follows:

1) The helical pitch: According to the experimental results, the calibration curve can reduce significantly its sensitivity to the fluid viscosity for different helical pitches. The helical bladed rotor meter used in these experiments employed different helical pitches, from 3.75 to 6.28.[1]

The best calibration curve was obtained with a meter of 3.95 helical pitch. It seems that the size of helical pitch goes through an optimum, and thereafter, the sensitivity to fluid viscosity starts to increase.

2) The bearing friction: The design of bearings and hence the friction can be altered to increase the viscosity compensation effect on the calibration curve. This is only feasible if the calculated value for the three terms in MTE make enough allowance for the viscosity comepnsation.

3) The size of tip clearance: The hump produced on the calibration curve is either due to the size of the tip clearance or occurs when the fluid viscosity increases and can be optimized by increasing the diameter of the blade or, if this is not sufficient, an increase in bearing friction will reduce the meter coefficient, thus leading to an enlargement of the operational range.

4) Since a decrease in the bearing friction leads to an extended range of the calibration curve (i.e. by increasing the meter coefficient at lower flow rates), and since this improvement is at the expense of losing some viscosity compensation in a certain type of meter, it would be useful to study the optimum value of bearing friction).

5) An increase in pressure drag can be achieved by thickening the turbine blades or by increasing the solidity (i.e. increasing the number of blades) if the calculated T_2 is not big enough.

6) The alteration of blade angle, β, from the hub to the tip. This is necessary when it is required that T_1 should be changed. T_1 will increase when the blade angle increases from the hub to the turbine tip.

7) If a flat axial velocity distribution (operation at higher blades Reynolds number) is required an optimized hub ratio should be sought. An increase of the hub ratio will lead to an increase of the bearing load because of the increase in the rotor weight,

[1] Helical pitch for research turbine flow meter

which can reduce the operational range at lower flow rate.

8) If the hydrodynamic force acting on the blade has to be increased, the blade height ratio (smaller hub ratio) should be increased. This is linked with unloading of the turbine bearing or reducing the viscosity compensation effect and can produce a hump on the calibration curve and reduce the operational range.

The hydrodynamical parameters cannot always be directly changed and can only be optimized by changing some of the geometrical parameters. But one has always got to balance the advantage and disadvantage of an alteration in order to achieve an improvement of the calibration curve.

Having elucidated the important parameters to be changed in meter design, the problem is then to search for the combination of those parameters that gives the best operational performance. The optimization of a multivariable function, without knowledge of the theoretical functional form, is a case for iterative solution. The parameters (mentioned in 10.5.1 to 8), should be arranged in descending order of importance, and optimized individually whilst maintaining all other parameters constant. The optimum parameters are used in the optimization of the following parameters and when the process is complete it would need to be reiterated to consistency.

APPENDIX I

The calculation of the main turbine equation

The values $A(\nu)$, $B(\nu)$, $C(\nu)$ and $D(\nu)$ in the equation 5.8 are given by the following equations:

$$A(\nu) = \int_{r_h}^{r_t} \frac{C_L}{U_m^2 \cdot r_o^2} \left[2 \tan\beta - \tan\left[\beta - (\theta_o + \delta^*)\right]\right] \cdot \left[\left[(r_o^2 - r^2) - (r_o^2 - r_h^2) \frac{\ell n \frac{r}{r_o}}{\ell n \frac{r_h}{r_o}} \right] \frac{\Delta p_{blade}}{4\eta} \right] r^2 \, dr \qquad \text{I.1}$$

$$B(\nu) = \int_{r_h}^{r_t} \left[(r_o^2 - r^2) - (r_o^2 - r_h^2) \frac{\ell n \frac{r}{r_o}}{\ell n \frac{r_h}{r_o}} \right] \frac{\Delta p_{blade}}{4 U_m \eta} \frac{r^2 \, dr}{r_o^3} \qquad \text{I.2}$$

$$C(\nu) = \int_{r_h}^{r_t} \frac{v}{U_m^2} (r_o^2 - r^2) - (r_o^2 - r_h^2) \frac{\ell n \frac{r}{r_o}}{\ell n \frac{r_h}{r_o}} \Big] \frac{\Delta p_{blade}}{4\eta} \frac{r dr}{r_o^2} \qquad \text{I.3}$$

$$D(\nu) = \int_{r_h}^{r_t} \frac{C_D \tan\theta m}{\cos\beta \cos\theta m} \left[\left[r_o^2 - r^2 \right) - (r_o^2 - r_h^2) \frac{\ell n \frac{r}{r_o}}{\ell n \frac{r_h}{r_o}} \right] \frac{\Delta p_{blade}}{4\eta Um} \frac{r dr}{r_o^2} \qquad \text{I.4}$$

$$E(\nu) = \int_{r_h}^{r_t} (2r - \frac{N \cdot t}{\pi}) \left[\left[(r_o^2 - r^2) - (r_o^2 - r_h^2) \frac{\ell n \frac{r}{r_o}}{\ell n \frac{r_h}{r_o}} \right] \frac{\Delta p_{blade}}{4Um \eta} \right] \frac{dr}{r_o^2} \qquad \text{I.5}$$

The integration of the above equation has been taken from the blade hub to the tip. The tip clearance flow for a fluid with low viscosity is determined by integration from blade tip to the turbine casing. The uniform flow condition through the tip clearance has been assumed for this calculation. The boundary layer thickness has been calculated with regard to the velocity profile at the blade tip (Tip clearance area). The simpler method

of evaluating the boundary layer thickness is the Gersten equation 5.16. The calculation of tip clearance flow with respect to the boundary layer has been carried out by integrating from the tip of the blade to the turbine casing and subtracting from that turbine casing to the boundary layer thickness. The C_D, C_L, δ^* values are functions of fluid viscosity. The blade angle is obviously constant for a "constant bladed angle rotor" and a function of r for a helical bladed rotor. The drag coefficient is given by (eq. 6.35). The lift coefficient has been taken from equation 6.36. For the calculations of $A(\nu)$, $B(\nu)$, $C(\nu)$, $D(\nu)$ and $E(\nu)$ the sub-routine F4ACSL has been used. The inlet and outlet velocity angles θ_i and θ_0 are obtained by (either) measuring the axial and tangential fluid velocity (or) the rotational speed. The δ^* has been taken from Rhoden's (Ref. 96) measurement. The theoretical result and the empirical result of T_1 to T_3 could be compared with the experimental values.

Values of g and k have been found empirically for various fluid viscosities and flow rates. It is convenient to represent this data by some suitable function, least squares fitted. One is interested, for simplicity, only in inhomogeneous functions of the kind: dimensions in form

$$g, k = f(\nu, Q, \epsilon_1, \epsilon_2, ...) \qquad I.6$$

where k and g are subjected to Normal Law of Errors.

ν, Q — are variables not subjected to error

ϵ_1, ϵ_2 — are disposable constants

Thus for exact 'input' values of (ν, Q) or (ν_i, Q_i), there is an observed output g_i^{obs}, k_i^{obs} with a certain (unknown) variance or error probability. The least squares process compares g_i^{obs} or k_i^{obs} with g_i, k_i (ν, Q ..... ϵ_1, ϵ_2 .....) which we can call $g_i^{theor.}$ or $k_i^{theor.}$

The 'failure' of fit is

$$\Delta_{i_g} = g_i^{theor} - g_i^{obs} \qquad I.7$$

$$\Delta_{i_k} = k_i^{theor} - k_i^{obs} \qquad I.8$$

The least squares principle states that the best form of g, k is that which minimizes the sum of the squares of the residuals i.e. the least squares principle is:

$$\text{Min } [\Sigma \Delta^2_{i_{g,k}}] \qquad I.9$$

This assumes that all f_i^{obs}[1] have the same reliability. It may well be that certain domains of (ν, Q) space have led to more reliable g_i^{obs}, k_i^{obs} than others. Suppose for example g or k was a measurement of length, $\gamma_{ii} \to \gamma$

[1] $f_i^{obs} = g_i^{obs}$ or k_i^{obs}

e.g. g, k are a length from an origin O to one of a set of lines A, B, C, D, E

If the width of A is δ, B = 2δ, C = 2δ, D = δ, E = 3δ, then there are corresponding differences in the ability to define g_A and k_A or g_B and k_B. In fact the width represents an uncertainty. If the uncertainty in g_A or k_A is γ_{ii} then for g_B or k_B it is 2γ .....

The normal process here would be to assign 'weights' to the observations $g_{A,B}$, $k_{A,B}$ etc. Weights vary inversely as the square of the uncertainty therefore:

$$\omega_D = \omega_A = \frac{1}{\gamma} \qquad \omega_B = \frac{1}{4\gamma} = \omega_C \qquad \omega_E = \frac{1}{9\gamma} \qquad \text{I. 10}$$

The size of γ is not important in weighting since it will always cancel out so that weights are not absolute but relative i.e. the weights would be

$$\omega_D = \omega_A = 1 \qquad \omega_B = \omega_C = 1/4 \qquad \omega_E = 1/9 \qquad \text{I. 11}$$

The **Complete Least Squares Principle** is then:

$$\text{Min} \quad [\ \Sigma\ \omega_{i_{g,k}} \Delta_{i_{g,k}}{}^2\ ] \qquad \text{I. 12}$$

Clearly the theoretical values in I. 7 and I. 8 are unobtainable except through infinite measurements so they are replaced by g_i^{best} and k_i^{best}.

$$g_i^{\text{best}} = f(\nu_i, Q_i \ldots\ldots \epsilon_1^{\text{best}}, \epsilon_2^{\text{best}}, \ldots\ldots) \qquad \text{I. 13}$$

$$k_i^{\text{best}} = f(\nu_i, Q_i \ldots\ldots \epsilon_1^{\text{best}}, \epsilon_2^{\text{best}}, \ldots\ldots) \qquad \text{I. 14}$$

and

$$R_{i_g} = g_i^{\text{best}} - g_i^{\text{obs}} \qquad \text{I. 15}$$

$$R_{i_k} = k_i^{\text{best}} - k_i^{\text{obs}} \qquad \text{I. 16}$$

and minimise it to $\quad \text{Min} \quad [\ \Sigma\ \omega_{i_{g,k}} R_{i_{g,k}}{}^2\ ] \qquad \text{I. 17}$

It may well be that another functional form gives an even better minimum, but there is no general way of finding the functional form that minimizes the weighted square residuals. Nor is it necessarily true that the function that does minimize, is the physical function governing the experiment. One can only say that it gives a good fit. It is perfectly possible that the true physical function will give a worse fit than some artificial functions. Normally curve fitting is done for the following reasons:

1. Theory gives a functional form, but not certain constants in the equation. The curve-

fitting then gives the best values for those constants,

2. Theory may give several functional forms according to different assumptions. Curve fitting indicates the best form to take all other things being equal,

3. Curve-fitting to data where no functional form is presupposed but where a formula fit is a convenient representation of tabulated data. Here one indicates the error of fit one requires and chooses a function accordingly. Simple examples are polynomials, Fourier synthesis, Lagrange, Bessel and Hermite polynomials. The theory is generalized in the MINIMAX theory, Chebyshev, polynomial theory. There is no 'right' or 'proper' function. One is merely concerned with the most efficient (i.e. function with least coefficients) representation of observed data within a given error bar.

4. Polynomial curve-fitting over a short range with only a few coefficients.

   A. for establishing a stationary point.

The fitted polynomials at these two regions may be differentiated to find the maximum and minimum. A separate polynomial should be fitted in each case.

   B. data smoothing.

Here one is not interested in a single curve fit for the whole range but one is required to remove a certain amount of 'noise'. This is a mathematical process on digital data analogous to a smoothing circuit on a continuous chart recorder. The more a curve is smoothed the more information is lost so one is always balancing by deciding what level of noise one can accommodate. The process most often used in 'Lagrangian' smoothing and is related to Lagrangian interpolation (i.e. where one wants to find an intermediate value in a table of values of a function).

The aim here is to find a convenient formula to represent data within an acceptable error bar with the consideration of eq. I. 15, I. 16, I. 17 the approximate values of ϵ_j:

$$\epsilon_j^{\text{appr.}} = \epsilon_j^{\text{best}} - \delta\,\epsilon_j \qquad \text{I. 18}$$

$$g_i^{\text{best}} = f\,(\nu_i, Q_i, \ldots\ldots \epsilon_j^{\text{appr.}}) + \sum_j \frac{\partial g}{\partial \epsilon_j}\,\delta\epsilon_j \qquad \text{I. 19}$$

$$R_{i_g} = g_i^{\text{appr.}} - g_i^{\text{obs}} + \sum_j \frac{\partial g}{\partial \epsilon_j}\,\delta\,\epsilon_j \qquad \text{I. 20}$$

$$\text{Let} \quad h_{i_g} = g_i^{\text{appr.}} - g_i^{\text{obs}} \qquad \text{I. 21}$$

then

$$R_{i_g} = h_{i_g}^{obs} + \sum_j \frac{\partial g_i}{\partial \epsilon_j} \delta \epsilon_j \qquad \text{I. 22}$$

which is called a 'Reduced Equation of Condition'.

To minimize the equation I. 17, the value of $\sum_j \omega_{i_g} R^2_{i_g}$ should be differentiated with respect to the variables to be determined i.e. the $\delta\epsilon_j$. Therefore I. 17 is achieved when:

$$\frac{\partial}{\partial (\delta \epsilon_j)} \sum_i \omega_{i_g} R^2_{i_g} = 0 \qquad \text{for all } j \qquad \text{I. 23}$$

or
$$\sum_i \omega_{i_g} R_{i_g} \frac{\partial R_{i_g}}{\partial (\delta \epsilon_j)} = 0 \qquad \text{for all } j \qquad \text{I. 24}$$

or
$$\sum_i \omega_{i_g} (h_{i_g}^{obs} + \sum_j \frac{\partial g_i}{\partial \epsilon_j} \delta \epsilon_j) \frac{\partial g_i}{\partial \epsilon_\gamma} = 0 \text{ for all } \gamma \qquad \text{I. 25}$$

Let
$$v_{ij} = \frac{\partial g_i}{\partial \epsilon_j} \qquad \text{I. 26}$$

Then
$$\sum_i \omega_{i_g} (h_{i_g}^{obs} + \sum_j v_{ij} . \delta \epsilon_j) v_{i\gamma} = 0 \text{ for all } \gamma \qquad \text{I. 27}$$

For want of any other information we must take the weights ω_{i_g} as equal i.e. $\omega_{i_g} = 1$.

$g_i^{appr.}$ is known, as is g_i^{obs}

$v_{ij} = \frac{\partial g_i}{\partial \epsilon_j} \simeq \frac{\partial g_i}{\partial \epsilon_j}^{appr.}$ any error in this approximation is removed by the subsequent iterations that determine $\delta \epsilon_j$;

so v_{ij} is known.

i.e. eq. I. 27 is a linear equation in the unknowns $\delta\epsilon_j$. Since there is an equation for every γ, this equation is equivalent to n simultaneous linear equations (where n is the no. of coefficients ϵ_j). These equations are called the "normal equations".

They may be reduced to the following form:

$$\sum_j P_{\gamma j} \delta \epsilon_j = T_\gamma \qquad \text{I. 30}$$

where
$$P_{\gamma j} = \sum_i \omega_{i_g} v_{ij} v_{i\gamma} \qquad \text{I. 31}$$

$$T_\gamma = -\sum_i \omega_{i_g} h_i^{obs} v_{i\gamma} \qquad \text{I. 32}$$

Equation I. 30 is solved determinantly i.e.

$$\delta \epsilon = P^{-1} T \qquad \text{I. 33}$$

where $\delta\epsilon$ is the vector $\begin{pmatrix} \delta\epsilon_1 \\ \delta\epsilon_2 \\ \vdots \\ \delta\epsilon_n \end{pmatrix}$ T is the vector $\begin{matrix} T_1 \\ \cdot \\ T_\gamma \\ \cdot \\ T_n \end{matrix}$

P^{-1} is the inverse matrix of P.

The error in $\delta\epsilon_j$ is

$$\sigma_j = \left[\frac{\Sigma \omega_{i_g} R_{i_g}^2}{(N-n)} \cdot \frac{\hat{P}_{jj}}{|P|} \right]^{1/2} \qquad \text{I. 34}$$

where

N is no. of observations

n is no. of coefficients

P_{jj} is the minor of element jj in P

and P is the determinant of P

The solution of I. 33 gives values of $\delta\epsilon_j$ which then give new approximations to ϵ_j so that the process is reiterated until all $\delta\epsilon_j$ are negligible.

Sometimes the initial approximation is not good enough and the corrections are large enough to cause instability and the process does not converge. The way round this is to take

$$\epsilon_j^{new} = \epsilon_j^{old} + \delta\epsilon_j \times D \qquad \text{I. 35}$$

where D is a damping factor $0 < D < 1$.

It is possible to have functions that cannot converge and special methods need to be employed to

$$\text{Min } [\Sigma \omega_{i_g} R_{i_g}^2].$$

In the case of k as a function of z there is a Gaussian-like hump so one fits a general Gaussian of the form:

$$k = \epsilon_4 \left[\epsilon_3 + \exp\left[-\frac{(\nu - \epsilon_1)^2}{\epsilon_2}\right]\right] \qquad \text{I. 36}$$

Since there is nothing known theoretically about the form of the g and k function, one cannot regard them as a separable function of ν and Q.

i.e. in general

$$g \text{ or } k\ (\nu, Q) \neq f(\nu)\ f^*(Q) \qquad \text{I. 37}$$

In this case, however, it does look as if it approximates to a separable function. To make up for small deviations from separability we can include a mixing polynomial of the kind $(A + B\nu Q + C\nu^2 Q + D\nu Q^2 + E\nu Q^{-1} + F\nu^{-1} Q + \ldots\ldots)$

Since one has not an immense amount of information and since one wants to keep the g and k simple as possible one reduces these to $(A + B\nu Q)$. Throwing away all redundant disposable coefficients one is left with

$$k = \frac{(\epsilon_4 + \epsilon_5 \nu Q)}{(\epsilon_6 + Q)} \cdot \left[\epsilon_3 + \exp\left[\frac{-(\nu - \epsilon_1)^2}{\epsilon_2}\right]\right] \qquad \text{I. 38}$$

One should solve equation I. 30 so we need $P_{\gamma j}$ and T_{γ}

$$P_{\gamma j} = \sum_{i=1}^{N} \omega_{i_g} v_{ij} v_{i\gamma} \qquad \text{I. 39}$$

This program has put $\omega_i = 1$ i.e all observations are of equal weight for want of anything better.

$$v_{ij} \simeq \frac{\partial f_i^{\text{appr.}}}{\partial \epsilon_j} \qquad f = g \text{ or } k \qquad \text{I. 40}$$

In this program, $g_i^{\text{appr.}}$ and $k_i^{\text{appr.}}$ are defined for i = 1, NOBS (NOBS = no. of observations above).

$$v_{i1} = \frac{\partial f_i^{\text{appr.}}}{\partial \epsilon_1}$$

gives

$$v_{i1} = \frac{2(\epsilon_4 + \epsilon_5 \nu Q)}{(\epsilon_6 + Q)\epsilon_2} \cdot (\nu - \epsilon_1) \cdot \exp\left(\frac{-(\nu - \epsilon_1)^2}{\epsilon_2}\right) \qquad \text{I. 41}$$

Subroutine LSFERR takes v_{ij}, ω_i, k_i^{obs} and computes

$$P_{\gamma j}, T_{\gamma}$$

It then solves the matrix equation I. 33 to produce the array or vector $\delta\epsilon$ (see eq. I. 35). The damping factor was approximately 0.5 to start with until the coefficients got close

enough for stability and then D has been increased to speed the convergence. The equation I. 34 is a reasonable guide to the goodness of fit. The most efficient fit is that which gives the least value of ERROR for the least number of coefficients.

Thus:

PROGRAM 1 ERROR = 0.0966 K DATA
6 coeffs.

PROGRAM 2 ERROR = 0.0132 G DATA
6 coeffs.

If on K DATA we take the mixing term νQ out of the expression we get

PROGRAM 3 ERROR = 0.126 5 coeffs.

The efficiency of fit can be defined by multiplying ERROR by the number of coefficients. (EFF = Efficiency of fit). Thus:

PROGRAM 3 EFF = 0.126 x 5 = 0.63

PROGRAM 1 EFF = 0.0966 x 6 = 0.58.

Thus the 6th coefficient has improved on Program 3 by more than the previous 5 and so that coefficient may be considered an efficient addition. For each calibration curve 40 theoretical points have been calculated from the flow rate 24 lb/sec.[1] to 5 lb/sec.[2] in steps at 1 lb/sec.[3] and from 4.5 lb/sec.[4] to 1.5 in steps of .5 lb/sec.[5] and 1.5 lb/sec.[6] to .2 lb/sec.[7] in steps of .1 lb/sec.[8] For each viscosity, the value of T_1, T_2, T_3 and the blade Reynolds number and passage Reynold's number have been calculated and are tabulated at the end of this appendix. The theoretical value for the meter coefficient has been calculated for the above mentioned steps in flow rate. The calculation is carried out for meter Types A, B, C, and E. Turbine flow meters type A and B are representative of a meter with a helically bladed rotor and Turbine flow meters with constant blade angle rotor are represented by Types C and E. The geometrical device of each meter has been given at the top of the numerical results.

1. Q = 10.89 litre/sec
2. Q = 2.27 litre/sec
3. Q = .454 litre/sec
4. Q = 2.043 litre/sec
5. Q = .227 litre/sec
6. Q = 2.724 litre/sec
7. Q = .0908 litre/sec
8. Q = .0454 litre/sec

Pipe radius = 19.05 mm; Axial width = 14.224 mm; Tip radius = 18.008 mm; Meter radius = 18.288 mm; Hub radius = 9.703 mm; Blade thickness = 1.24 mm.

C00B3: JASU7IDEL :=))

TURBINE FLOW METER TYPE A 1.5INCH HELICAL BLADE ANGLE ROTOR HELICAL PITCH=3.7512

PIPE RADIUS = 0.7500 METER RADIUS = 0.7200 TIP RADIUS = 0.7090 HUB RADIUS = 0.3820 AXIAL WIDTH=0.560

NO OF BLADES =3.000 BLADE THICKNESS =0.049 NO OF PICKUP =1.000 VISCOSITY(CENTI-POISE)= 1.00

EXPERIMENTAL VALUE		THEORETICAL VALUE		BLADES	THEORETICAL VALUE				(PULSES PER POUND)	
Q	M.C.	Q	M.C.	RE-JO	T1	T2	T1K/Q	T3	PASS.RE	
19.3014	41.2216	24.0000	41.1757	398942.	53.1203	12.2204	0.2878	0.0119	166570.	
18.2015	41.2105	23.0000	41.1317	382320.	53.1185	12.2241	0.3003	0.0130	121296.	
17.7124	41.2013	22.0000	41.1382	365697.	53.1165	12.2280	0.3139	0.0142	116022.	
16.8124	41.2021	21.0000	41.1054	349075.	53.1143	12.2322	0.3289	0.0156	110749.	
15.8035	41.2511	20.0000	41.2034	332452.	53.1119	12.2367	0.3453	0.0172	105475.	
14.8501	41.2761	19.0000	41.2122	315829.	53.1093	12.2415	0.3635	0.0191	100201.	
13.8142	41.2374	18.0000	41.2221	299207.	53.1064	12.2468	0.3837	0.0212	94927.	
12.8300	41.2376	17.0000	41.2331	282584.	53.1031	12.2525	0.4065	0.0238	89654.	
11.8510	41.2251	16.0000	41.2455	265962.	53.0994	12.2587	0.4317	0.0269	84380.	
10.8524	41.2564	15.0000	41.2596	249339.	53.0953	12.2656	0.4604	0.0306	79106.	
9.9956	41.2810	14.0000	41.2756	232716.	53.0905	12.2731	0.4933	0.0351	73832.	
9.5412	41.3012	13.0000	41.2940	216094.	53.0850	12.2815	0.5313	0.0407	68559.	
8.9054	41.3078	12.0000	41.3154	199471.	53.0786	12.2910	0.5755	0.0478	63285.	
8.3412	41.4012	11.0000	41.3403	182849.	53.0710	12.3017	0.6279	0.0568	58011.	
8.2135	41.4081	10.0000	41.3698	166226.	53.0619	12.3140	0.6906	0.0688	52737.	
7.4512	41.4525	9.0000	41.4050	149603.	53.0508	12.3283	0.7674	0.0849	47464.	
6.8520	41.5121	8.0000	41.4476	132981.	53.0369	12.3452	0.8633	0.1075	42190.	
6.3012	41.5123	7.0000	41.4998	116358.	53.0191	12.3656	0.9866	0.1403	36916.	
6.1001	41.7056	6.0000	41.5645	99736.	52.9953	12.3909	1.1511	0.1910	31642.	
5.9024	41.5333	5.0000	41.6447	83113.	52.9619	12.4234	1.3813	0.2751	26369.	
5.4012	41.6127	4.5000	41.6913	74802.	52.9397	12.4436	1.5348	0.3396	23732.	
4.8627	41.5211	4.0000	41.7413	66490.	52.9119	12.4675	1.7266	0.4298	21095.	
4.3020	41.5897	3.5000	41.7918	58179.	52.8762	12.4963	1.9733	0.5614	18458.	
3.6014	41.7354	3.0000	41.8346	49868.	52.8286	12.5321	2.3021	0.7641	15821.	
3.0012	41.7345	2.5000	41.8461	41556.	52.7619	12.5781	2.7626	1.1003	13184.	
2.6021	41.8021	2.0000	41.7555	33245.	52.6619	12.6404	3.4532	1.7193	10547.	
2.3012	41.8254	1.5000	41.3113	24934.	52.4953	12.7318	4.6043	3.0565	7911.	
2.0143	41.8124	1.4000	41.1164	23272.	52.4477	12.7557	4.9332	3.5087	7383.	
1.6214	41.8254	1.3000	40.8337	21609.	52.3927	12.7823	5.3126	4.0693	6856.	
1.4045	41.8233	1.2000	40.4960	19947.	52.3286	12.8122	5.7553	4.7757	6328.	
1.1023	41.8127	1.1000	40.0017	18285.	52.2528	12.8461	6.2786	5.6835	5801.	
0.9021	41.7328	1.0000	39.3063	16623.	52.1619	12.8850	6.9064	6.8771	5274.	
0.6011	41.6526	0.9000	38.3145	14960.	52.0508	12.9302	7.6738	8.4902	4746.	
0.0000	0.0000	0.8000	36.8160	13298.	51.9119	12.9836	8.6330	10.7454	4219.	
0.0000	0.0000	0.7000	34.5168	11636.	51.7334	13.0480	9.8663	14.0548	3692.	
0.0000	0.0000	0.6000	30.7750	9974.	51.4953	13.1280	11.5107	19.1029	3164.	
0.0000	0.0000	0.5000	24.2356	8311.	51.1619	13.2309	13.8128	27.5082	2637.	
0.0000	0.0000	0.4000	11.3761	6649.	50.6619	13.3703	17.2660	42.9816	2109.	

TABLE I. 1 The experimental and the calculated results for Q (Flow rate), M.C. (meter coefficient) and the calculated values for Blades Reynolds number Re_{blade} and meter annulus Reynolds number Re_{pass} and the theoretical values for T_1, T_2, T_3 and Term 2 using leakage theory for

Turbine Flow Meter Type A 1.5 ins (38.1 mm)

Pipe radius = 19.05 mm; Axial width = 14.224 mm; Tip radius = 18.008 mm; Meter radius = 18.288 mm; Hub radius = 9.703 mm; Blade thickness = 1.24 mm

```
GOOR3:  JA567/DEL :=J0
GOOR3:        1  CARDS/TR LINES LEFT IN FILE

   TURBINE FLOW METER TYPE A 1.5INCH                    HELICAL BLADE ANGLE ROTOR  HELICAL PITCH=3.7512

   PIPE RADIUS =  0.7500   METER RADIUS =  0.7200   TIP RADIUS =  0.7090   HUB RADIUS =  0.3820   AXIAL WIDTH=0.560

   NO OF BLADES =6.00   BLADE THICKNESS =0.049   NO OF PICKUP =1.000   VISCOSITY(CENTI-POISE)= 21.00
EXPERIMENTAL VALUE      THEORETICAL VALUE      BLADES      T H E O R E T I C A L   V A L U E  (PULSES PER POUND)
     Q        M.C.        Q        M.C.       RE=RO        T1          T2          T1K/Q          T3          PASS.RE
19.5516     41.4134    24.0000    41.4542    19028.    53.7830     12.8367     0.5288      0.0209       6027.
18.5012     41.4057    23.0000    41.4567    18235.    53.7812     12.8536     0.5518      0.0227       5776.
17.4516     41.4038    22.0000    41.4596    17442.    53.7792     12.8716     0.5769      0.0249       5525.
16.5732     41.4043    21.0000    41.4632    16649.    53.7770     12.8909     0.6044      0.0273       5274.
15.5414     41.4141    20.0000    41.4676    15856.    53.7746     12.9116     0.6346      0.0301       5023.
14.5237     41.4585    19.0000    41.4728    15063.    53.7720     12.9339     0.6680      0.0333       4771.
13.5737     41.5439    18.0000    41.4790    14271.    53.7691     12.9581     0.7051      0.0371       4520.
12.6764     41.5437    17.0000    41.4864    13478.    53.7658     12.9843     0.7466      0.0416       4269.
11.5978     41.6170    16.0000    41.4954    12685.    53.7621     13.0130     0.7933      0.0470       4018.
10.5220     41.7378    15.0000    41.5061    11892.    53.7580     13.0445     0.8461      0.0535       3767.
 9.0238     41.7045    14.0000    41.5191    11099.    53.7532     13.0793     0.9066      0.0614       3516.
 9.0975     41.7429    13.0000    41.5347    10307.    53.7477     13.1181     0.9763      0.0712       3265.
 7.6979     41.6594    12.0000    41.5538     9514.    53.7413     13.1616     1.0577      0.0836       3014.
 7.2132     41.8556    11.0000    41.5771     8721.    53.7337     13.2110     1.1538      0.0994       2762.
 6.1765     41.7712    10.0000    41.6060     7928.    53.7246     13.2675     1.2692      0.1203       2511.
 5.6246     41.8264     9.0000    41.6419     7135.    53.7135     13.3333     1.4102      0.1485       2260.
 4.9574     41.8474     8.0000    41.6872     6343.    53.6996     13.4110     1.5865      0.1880       2009.
 4.2762     41.9391     7.0000    41.7446     5550.    53.6818     13.5048     1.8131      0.2455       1758.
 3.4061     42.1104     6.0000    41.8179     4757.    53.6580     13.6212     2.1153      0.3342       1507.
 2.4392     42.1293     5.0000    41.9109     3964.    53.6245     13.7709     2.5384      0.4813       1256.
 1.8353     41.2926     4.5000    41.9648     3568.    53.6024     13.8639     2.8205      0.5941       1130.
 1.3434     41.2790     4.0000    42.0219     3171.    53.5746     13.9758     3.1730      0.7520       1005.
 0.8604     39.3662     3.5000    42.0786     2775.    53.5389     14.1065     3.6263      0.9822        879.
 0.0000      0.0000     3.0000    42.1141     2378.    53.4913     14.2710     4.2307      1.3368        753.
 0.0000      0.0000     2.5000    42.0936     1982.    53.4246     14.4828     5.0768      1.9250        628.
 0.0000      0.0000     2.0000    41.8931     1586.    53.3246     14.7697     6.3460      3.0079        502.
 0.0000      0.0000     1.5000    41.0819     1189.    53.1580     15.1901     8.4614      5.5473        377.
 0.0000      0.0000     1.4000    40.7374     1110.    53.1104     15.3002     9.0657      6.1385        352.
 0.0000      0.0000     1.3000    40.2765     1031.    53.0554     15.4228     9.7631      7.1192        326.
 0.0000      0.0000     1.2000    39.6524      951.    52.9913     15.5605    10.5767      8.3552        301.
 0.0000      0.0000     1.1000    38.7940      872.    52.9155     15.7165    11.5382      9.9433        276.
 0.0000      0.0000     1.0000    37.5399      793.    52.8246     15.8953    12.6920     12.0314        251.
 0.0000      0.0000     0.9000    35.8590      714.    52.7155     16.1032    14.1023     14.8536        226.
 0.0000      0.0000     0.8000    33.2917      634.    52.5746     16.3489    15.8651     18.7991        201.
 0.0000      0.0000     0.7000    29.3280      555.    52.3961     16.6456    18.1315     24.5539        176.
 0.0000      0.0000     0.6000    22.8771      476.    52.1580     17.0136    21.1534     33.4206        151.
 0.0000      0.0000     0.5000    11.5959      396.    51.8246     17.4872    25.3841     48.1257        126.
```

TABLE I. 2 The experimental and the calculated results for Q (flow rate), M.C. (meter coefficient) and the calculated values for Blades Reynolds number Re_{blade} and meter annulus Reynolds number Re_{pass} and the theoretical values for T_1, T_2, T_3 and Term 2 using leakage theory for Turbine Flow Meter Type A 1.5 ins (38.1 mm)

Pipe radius = 19.05 mm; Axial width = 14.224 mm; Tip radius = 18.008 mm; Meter radius = 18.288 mm; Hub radius = 9.703 mm; Blade thickness = 1.24 mm

```
GOOR3;  #A567!DEL ;=00
```

TURBINE FLOW METER TYPE A 1.5INCH HELICAL BLADE ANGLE ROTOR HELICAL PITCH=3.7512

PIPE RADIUS = 0.7500 METER RADIUS = 0.7200 TIP RADIUS = 0.7090 HUB RADIUS = 0.3820 AXIAL WIDTH=0.560

NO OF BLADES =6.000 BLADE THICKNESS =0.049 NO OF PICKUP =1.000 VISCOSITY(CENTI-POISE)= 47.00

EXPERIMENTAL VALUE		THEORETICAL VALUE		BLADES	THEORETICAL VALUE (PULSES PER POUND)				
Q	M.C.	Q	M.C.	RE-NO	T1	T2	T1K/Q	T3	PASS.RE
18.7106	41.5139	24.0000	41.3477	8493.	53.7818	13.2213	0.8276	0.0394	2693.
17.7566	41.5282	23.0000	41.3552	8139.	53.7790	13.2464	0.8636	0.0429	2581.
16.8975	41.5209	22.0000	41.3596	7786.	53.7770	13.2733	0.9029	0.0469	2469.
16.0310	41.5636	21.0000	41.3671	7432.	53.7748	13.3021	0.9458	0.0515	2356.
15.1492	41.5606	20.0000	41.3758	7078.	53.7724	13.3330	0.9931	0.0568	2244.
15.2569	41.5851	19.0000	41.3860	6724.	53.7698	13.3663	1.0454	0.0629	2132.
15.3510	41.2355	18.0000	41.3979	6370.	53.7669	13.4023	1.1035	0.0701	2020.
14.3315	41.4101	17.0000	41.4119	6016.	53.7636	13.4415	1.1684	0.0786	1908.
14.3312	41.4723	16.0000	41.4283	5662.	53.7599	13.4843	1.2414	0.0887	1795.
13.4527	41.5209	15.0000	41.4477	5308.	53.7558	13.5313	1.3242	0.1010	1683.
12.3756	41.4833	14.0000	41.4706	4954.	53.7510	13.5833	1.4188	0.1159	1571.
12.4974	41.4341	13.0000	41.4978	4601.	53.7455	13.6411	1.5279	0.1344	1459.
12.1161	41.3443	12.0000	41.5305	4247.	53.7391	13.7061	1.6552	0.1578	1346.
11.2454	41.3486	11.0000	41.5698	3893.	53.7315	13.7797	1.8057	0.1877	1234.
11.1369	41.3275	10.0000	41.6175	3539.	53.7224	13.8641	1.9863	0.2272	1122.
10.9281	41.3557	9.0000	41.6757	3185.	53.7113	13.9622	2.2070	0.2805	1010.
9.9125	41.3757	8.0000	41.7472	2831.	53.6974	14.0781	2.4828	0.3550	898.
9.5436	41.6080	7.0000	41.8354	2477.	53.6796	14.2181	2.8375	0.4636	785.
9.0187	41.9541	6.0000	41.9434	2123.	53.6558	14.3917	3.3105	0.6310	673.
8.9816	41.3359	5.0000	42.0711	1769.	53.6224	14.6152	3.9725	0.9087	561.
8.1760	41.7729	4.3000	42.1384	1592.	53.6002	14.7559	4.4139	1.1218	505.
7.8112	41.7315	4.0000	42.2104	1416.	53.5724	14.9179	4.9657	1.4198	449.
7.3672	41.7324	3.5000	42.2415	1239.	53.5367	15.1158	5.6751	1.8545	393.
6.9589	41.8349	3.0000	42.2245	1062.	53.4891	15.3614	6.6209	2.5241	337.
6.5915	41.8626	2.5000	42.3554	885.	53.4224	15.6774	7.9451	3.6348	281.
5.5640	41.8325	2.0000	41.4590	708.	53.3224	16.1055	9.9314	5.6793	224.
5.3093	41.9110	1.5000	39.5683	531.	53.1558	16.7327	13.2418	10.0966	168.
4.3032	42.1767	1.4000	38.8085	495.	53.1032	16.8971	14.1877	11.5905	157.
4.5056	42.1597	1.3000	37.3100	460.	53.0532	17.0800	15.2790	13.4422	146.
4.1045	42.5585	1.2000	36.4301	425.	52.9991	17.2854	16.5523	15.7759	135.
3.8995	42.2532	1.1000	34.6776	389.	52.9153	17.5181	18.0570	18.7746	123.
3.4106	42.3679	1.0000	32.1329	354.	52.8224	17.7850	19.8627	22.7173	112.
3.0657	42.2691	0.9000	28.6398	318.	52.7113	18.0952	22.0697	28.0461	101.
2.7026	42.0390	0.8000	23.4432	283.	52.5724	18.4618	24.8284	35.4958	90.
2.3382	42.3081	0.7000	15.5029	248.	52.3939	18.9045	28.3753	46.3619	79.
1.3225	40.9262	0.6000	2.7031	212.	52.1558	19.4536	33.1049	63.1036	67.

TABLE I. 3 The experimental and the calculated results for Q (flow rate), M.C. (meter coefficient) and the calculated values for Blades Reynolds number Re_{blade} and meter annulus Reynolds number Re_{pass} and the theoretical values for T_1, T_2, T_3 and Term 2 using leakage theory for Turbine Flow Meter Type A 1.5 ins (38.1 mm)

Pipe radius = 19.05 mm; Axial width = 14.224 mm; Tip radius = 18.008 mm; Meter radius = 18.288mm; Hub radius = 9.703 mm; Blade thickness = 1.24 mm

GOOR5; 4A567/DEL ;=0)

TURBINE FLOW METER TYPE A 1.5INCH HELICAL BLADE ANGLE ROTOR HELICAL PITCH=3.7512

PIPE RADIUS = 0.7500 METER RADIUS = 0.7200 TIP RADIUS = 0.7090 HUB RADIUS = 0.3820 AXIAL WIDTH=0.560

NO OF BLADES =6.00) BLADE THICKNESS =0.049 NO OF PICKUP =1.000 VISCOSITY(CENTI-POISE)= 71.00

EXPERIMENTAL VALUE		THEORETICAL VALUE		BLADES	THEORETICAL VALUE (PULSES PER POUND)				
	M.C.	Q	M.C.	RE-NO	T1	T2	T1K/Q	T3	PASS.RE
19.3509	41.5705	24.0000	41.2344	5630.	53.7730	13.4968	1.0726	0.0694	1783.
18.5087	41.4055	23.0000	41.2920	5395.	53.7762	13.5278	1.1192	0.0756	1708.
16.0300	41.4207	22.0000	41.3108	5161.	53.7742	13.5610	1.1701	0.0826	1634.
14.5091	41.4540	21.0000	41.3108	4926.	53.7721	13.5965	1.2258	0.0906	1560.
12.9562	41.4706	20.0000	41.3223	4692.	53.7697	13.6346	1.2871	0.0999	1486.
10.3320	41.6257	19.0000	41.3355	4457.	53.7671	13.6757	1.3548	0.1107	1411.
11.2509	41.5475	18.0000	41.3507	4225.	53.7641	13.7201	1.4301	0.1234	1337.
9.1130	41.6547	17.0000	41.3683	3988.	53.7609	13.7685	1.5142	0.1383	1263.
8.0599	41.7160	16.0000	41.3886	3753.	53.7572	13.8213	1.6088	0.1562	1188.
8.0051	41.5984	15.0000	41.4122	3519.	53.7530	13.8793	1.7161	0.1777	1114.
7.4054	41.7593	14.0000	41.4396	3284.	53.7483	13.9434	1.8387	0.2040	1040.
6.3259	41.6343	13.0000	41.4716	3050.	53.7428	14.0147	1.9801	0.2365	966.
6.2254	41.7059	12.0000	41.5090	2815.	53.7364	14.0948	2.1451	0.2776	891.
5.3130	41.8458	11.0000	41.5529	2580.	53.7288	14.1856	2.3401	0.3304	817.
5.4041	41.8158	10.0000	41.6043	2346.	53.7197	14.2897	2.5741	0.3998	743.
5.0556	41.8023	9.0000	41.6645	2111.	53.7086	14.4107	2.8602	0.4935	669.
4.6646	41.8544	8.0000	41.7340	1877.	53.6947	14.5538	3.2177	0.6246	594.
4.5153	42.3280	7.0000	41.8119	1642.	53.6768	14.7264	3.6774	0.8158	520.
3.7225	41.8012	6.0000	41.8922	1408.	53.6530	14.9407	4.2902	1.1105	446.
3.4421	41.7365	5.0000	41.9527	1173.	53.6197	15.2163	5.1483	1.5991	371.
3.0656	41.4397	4.5000	41.9563	1056.	53.5975	15.3874	5.7203	1.9741	334.
2.5346	40.3966	4.0000	41.9169	938.	53.5697	15.5897	6.4354	2.4985	297.
1.1419	36.4439	3.5000	41.7914	821.	53.5340	15.8339	7.3547	3.2634	260.
0.3669	34.0577	3.0000	41.4382	704.	53.4864	16.1368	8.5805	4.4418	223.
0.0000	0.0000	2.5000	40.7955	586.	53.4197	16.5266	10.2966	6.3962	186.
0.0000	0.0000	2.0000	39.1417	469.	53.3197	17.0547	12.8707	9.9941	149.
0.0000	0.0000	1.5000	34.7163	352.	53.1550	17.8284	17.1610	17.7673	111.
0.0000	0.0000	1.4000	33.0649	328.	53.1034	18.0312	18.3868	20.3961	104.
0.0000	0.0000	1.3000	30.9401	305.	53.0505	18.2568	19.8011	23.6546	97.
0.0000	0.0000	1.2000	28.1661	282.	52.9864	18.5102	21.4512	27.7613	89.
0.0000	0.0000	1.1000	24.4764	258.	52.9106	18.7973	23.4013	33.0383	82.
0.0000	0.0000	1.0000	19.4584	235.	52.8197	19.1265	25.7415	39.9763	74.
0.0000	0.0000	0.9000	12.4476	211.	52.7086	19.5091	28.6016	49.3535	67.
0.0000	0.0000	0.8000	2.3221	188.	52.5697	19.9614	32.1768	62.4630	59.

TABLE I. 4 Experimental and the calculated results for Q (flow rate), M.C. (meter coefficient) and the calculated values for Blades Reynolds number Re_{blade} and meter annulus Reynolds number Re_{pass} and the theoretical values for T_1, T_2, T_3 and Term 2 using leakage theory for Turbine Flow Meter Type A 1.5 ins (38.1 mm)

Pipe radius = 19.05 mm; Axial width = 14.224 mm; Tip radius = 18.008 mm; Meter radius = 18.288 mm; Hub radius = 9.703 mm; Blade thickness = 1.24 mm.

GOORS: JASO7|DEL :-00

TURBINE FLOW METER TYPE A 1.5INCH HELICAL BLADE ANGLE ROTOR HELICAL PITCH=3.7512

PIPE RADIUS = 0.7500 METER RADIUS = 0.7200 TIP RADIUS = 0.7090 HUB RADIUS = 0.3820 AXIAL WIDTH=0.560

NO OF BLADES =6.00 BLADE THICKNESS =0.049 NO OF PICKUP =1.000 VISCOSITY(CENTI-POISE)=170.00

EXPERIMENTAL VALUE		THEORETICAL VALUE		BLADES	THEORETICAL VALUE (PULSES PER POUND)				
Q	M.C.	Q	M.C.	RE=NO	T1	T2	T1K/Q	T3	PASS.RE
17.2570	41.5815	24.0000	41.4346	2348.	54.6894	14.2756	1.1458	0.0750	745.
16.1537	41.5252	25.0000	41.4781	2250.	54.6876	14.3234	1.1956	0.0816	714.
15.2121	41.5089	22.0000	41.4718	2152.	54.6856	14.3745	1.2499	0.0892	682.
14.2776	41.4825	21.0000	41.4658	2054.	54.6535	14.4292	1.3094	0.0979	651.
14.2591	41.5777	20.0000	41.4601	1956.	54.6611	14.4880	1.3749	0.1080	620.
14.0008	41.5547	19.0000	41.4548	1859.	54.6735	14.5513	1.4473	0.1196	589.
13.1208	41.4270	18.0000	41.4501	1761.	54.6755	14.6198	1.5277	0.1333	558.
12.5412	41.4319	17.0000	41.4461	1663.	54.6723	14.6943	1.6175	0.1494	527.
11.9078	41.4574	16.0000	41.4429	1565.	54.6686	14.7757	1.7186	0.1687	496.
11.2593	41.4578	15.0000	41.4407	1467.	54.6644	14.8650	1.8332	0.1919	465.
10.3756	41.4077	14.0000	41.4397	1370.	54.6597	14.9638	1.9642	0.2203	434.
10.4650	41.4183	13.0000	41.4401	1272.	54.6542	15.0738	2.1152	0.2555	403.
10.3479	41.4365	12.0000	41.4422	1174.	54.6476	15.1972	2.2915	0.2999	372.
9.4315	41.4394	11.0000	41.4460	1076.	54.6402	15.3372	2.4998	0.3569	341.
9.1593	41.4356	10.0000	41.4515	978.	54.6311	15.4976	2.7498	0.4318	310.
8.3606	41.4392	9.0000	41.4582	880.	54.6200	15.6840	3.0553	0.5331	279.
7.3945	41.3172	8.0000	41.4662	783.	54.6061	15.9045	3.4373	0.6747	248.
6.7462	41.3579	7.0000	41.4647	685.	54.5862	16.1706	3.9283	0.8813	217.
7.1724	41.3407	6.0000	41.4473	587.	54.5644	16.5007	4.5830	1.1995	186.
6.7462	41.6579	5.0000	41.3730	489.	54.5311	16.9254	5.4996	1.7273	155.
6.1621	41.3365	4.5000	41.2930	440.	54.5089	17.1891	6.1107	2.1325	140.
5.6325	41.5273	4.0000	41.1559	391.	54.4811	17.5008	6.8745	2.6989	124.
4.2015	41.2603	3.5000	40.3998	342.	54.4434	17.8771	7.8566	3.5251	109.
5.5424	40.8308	3.0000	40.4218	293.	54.3978	18.3440	9.1660	4.7980	93.
3.2324	40.4639	2.5000	39.4765	245.	54.3311	18.9447	10.9992	6.9092	78.
2.9629	40.0912	2.0000	37.4262	196.	54.2311	19.7584	13.7491	10.7956	62.
2.4949	37.3358	1.5000	32.2536	147.	54.0644	20.9508	18.3321	19.1921	47.
2.2577	38.8393	1.4000	30.3634	137.	54.0168	21.2632	19.6415	22.0318	43.
1.3154	38.0081	1.3000	27.9317	127.	53.9619	21.6110	21.1524	25.5517	40.
0.0000	0.0000	1.2000	24.8238	117.	53.8978	22.0013	22.9151	29.9877	37.
0.0000	0.0000	1.1000	20.6386	108.	53.8220	22.4438	24.9983	35.6878	34.
0.0000	0.0000	1.0000	15.0958	98.	53.7311	22.9511	27.4981	43.1823	31.
0.0000	0.0000	0.9000	7.3212	88.	53.6200	23.5407	30.5535	53.3115	28.

TABLE I. 5 The experimental and the calculated results for Q (flow rate), M.C. (meter coefficient) and the calculated values for Blades Reynolds number Re_{blade} and the meter annulus Reynolds number Re_{pass} and the theoretical values for T_1, T_2, T_3 and Term 2 using leakage theory for Turbine Flow Meter Type A 1.5 ins (38.1 mm)

Pipe radius = 25.4 mm; Meter radius = 23.101 mm; Axial width = 24.384 mm; Hub radius = 9.944 mm; Blade thickness = 10.16 mm; Tip radius = 22.8473 mm.

```
000R3;  3A567$DEL :=00

    TURBINE FLOW METER TYPE B 2INCH                          HELICAL BLADE ANGLE ROTOR   HELICAL PITCH=3,9596

    PIPE RADIUS =  1,0000   METER RADIUS =  0,9995   TIP RADIUS =  0,8995   HUB RADIUS =  0,3915   AXIAL WIDTH=0,960

    NO OF BLADES =3,000    BLADE THICKNESS =0,400   NO OF PICKUP =1,000   VISCOSITY(CENTI-POISE)=170,00
```

EXPERIMENTAL VALUE		THEORETICAL VALUE		BLADES	T H E O R E T I C A L	V A L U E	(PULSES PER POUND)		
Q	M.C.	Q	M.C.	RE-NO	T1	T2	T1K/Q	T3	PASS.RE
19.3685	28,9320	24,0000	29,2000	8896.	40,3136	12,6996	1,6650	0,0790	2668.
17.5631	28,9777	23,0000	29,1766	8516.	40,3118	12,7865	1,7374	0,0861	2557.
18.6065	28,9715	22,0000	29,1527	8146.	40,3098	12,8794	1,8164	0,0941	2445.
16.9323	28,9733	21,0000	29,1235	7776.	40,3076	12,9787	1,9029	0,1032	2334.
15.9499	28,8341	20,0000	29,1039	7405.	40,3052	13,0855	1,9980	0,1138	2223.
15.6178	28,9064	19,0000	29,0791	7035.	40,3026	13,2006	2,1032	0,1261	2112.
15.3226	29,0234	18,0000	29,0541	6665.	40,2997	13,3251	2,2200	0,1405	2001.
14.6299	28,9055	17,0000	29,0290	6295.	40,2964	13,4605	2,3506	0,1575	1890.
14.4785	28,8778	16,0000	29,0041	5924.	40,2927	13,6083	2,4975	0,1779	1779.
13.4338	28,9120	15,0000	28,9795	5554.	40,2886	13,7708	2,6640	0,2024	1667.
12.5071	28,9115	14,0000	28,9555	5184.	40,2838	13,9503	2,8543	0,2323	1556.
11.7590	28,8929	13,0000	28,9326	4814.	40,2783	14,1501	3,0739	0,2694	1445.
11.3623	29,0434	12,0000	28,9113	4443.	40,2719	14,3745	3,3300	0,3162	1334.
10.9679	28,9323	11,0000	28,8920	4073.	40,2643	14,6288	3,6327	0,3763	1223.
10.5695	28,9560	10,0000	28,8757	3703.	40,2552	14,9203	3,9960	0,4553	1112.
10.0701	28,9967	9,0000	28,8629	3332.	40,2441	15,2591	4,4400	0,5621	1000.
9.6185	28,8025	8,0000	28,8542	2962.	40,2302	15,6597	4,9950	0,7114	889.
8.4562	28,8353	7,0000	28,8485	2592.	40,2124	16,1433	5,7086	0,9292	778.
7.9274	29,0765	6,0000	28,8407	2222.	40,1886	16,7432	6,6600	1,2647	667.
7.3340	29,0155	5,0000	28,8110	1851.	40,1552	17,5150	7,9920	1,8212	556.
6.4596	28,9769	4,5000	28,7704	1666.	40,1350	17,9943	8,8800	2,2484	500.
5.9424	29,0057	4,0000	28,6389	1481.	40,1052	18,5607	9,9900	2,8456	445.
5.5931	28,8845	3,5000	28,5254	1296.	40,0695	19,2446	11,4172	3,7167	389.
5.0015	28,8357	3,0000	28,1901	1111.	40,0219	20,0930	13,3200	5,0589	333.
4.6817	28,9953	2,5000	27,4699	926.	39,9552	21,1846	15,9840	7,2848	278.
4.3504	28,3709	2,0000	25,7394	741.	39,8552	22,6634	19,9801	11,3825	222.
4.0838	28,7370	1,5000	21,2628	555.	39,6806	24,6304	26,6401	20,2355	167.
3.9570	28,5522	1,4000	19,5563	518.	39,6410	25,3981	28,5429	23,2295	156.
3.4550	28,2156	1,3000	17,5538	481.	39,5860	26,0301	30,7385	26,9407	145.
3.0339	27,8367	1,2000	14,4646	444.	39,5219	26,7395	33,5001	31,6179	133.
2.7390	27,7064	1,1000	10,6020	407.	39,4461	27,5436	36,3274	37,6280	122.
2.3460	27,0247	1,0000	5,3200	370.	39,3552	28,4655	39,9601	45,5298	111.

TABLE I. 10 The experimental and calculated results for Q (flow rate), M.C. (meter coefficient) and the calculated values for blades Reynolds number and meter annulus Reynolds numbers, Re_{pass} and the theoretical value for T_1, T_2, T_3 and Term 2 using the leakage theory for Turbine Flow Meter Type B 2 ins (50.8 mm) diameter.

Pipe radius = 25.4 mm; Meter radius = 23.101 mm; Axial width = 24.384 mm; Hub radius = 9.944 mm; Blade thickness = 10.16 mm; Tip radius = 22.8473 mm

COOR3; #A567(DEL :=0)

TURBINE FLOW METER TYPE B 2INCH HELICAL BLADE ANGLE ROTOR HELICAL PITCH=3,9596

PIPE RADIUS = 1,0000 METER RADIUS = 0,9095 TIP RADIUS = 0,8995 HUB RADIUS = 0,3915 AXIAL WIDTH=0,960

NO OF BLADES =3,000 BLADE THICKNESS =0,400 NO OF PICKUP =1,000 VISCOSITY(CENTI-POISE)= 74,00

EXPERIMENTAL VALUE		THEORETICAL VALUE		BLADES	THEORETICAL VALUE (PULSES PER POUND)				
Q	M.C.	Q	M.C.	RE=NO	T1	T2	T1K/Q	T3	PASS.RE
19.7206	28,9321	24,0000	29,0729	20416,	39,2196	11,3254	1,2352	0,0584	6129,
18,3411	28,9734	23,0000	29,0625	19565,	39,2177	11,3808	1,2889	0,0635	5873,
17,4013	29,1229	22,0000	29,0517	18714,	39,2158	11,4421	1,3475	0,0695	5618,
16,3261	28,9539	21,0000	29,0413	17864,	39,2136	11,5077	1,4116	0,0762	5363,
15,9351	28,9125	20,0000	29,0315	17013,	39,2112	11,5781	1,4822	0,0840	5107,
15,5299	28,9248	19,0000	29,0217	16162,	39,2086	11,6540	1,5602	0,0931	4852,
15,2178	28,9627	18,0000	29,0126	15312,	39,2057	11,7362	1,6469	0,1038	4597,
14,7178	28,9381	17,0000	29,0043	14461,	39,2024	11,8255	1,7438	0,1163	4341,
13,8169	28,9501	16,0000	28,9971	13610,	39,1987	11,9231	1,8528	0,1313	4086,
13,3916	29,0555	15,0000	28,9912	12760,	39,1946	12,0303	1,9763	0,1494	3830,
13,3584	28,3863	14,0000	28,9870	11909,	39,1898	12,1487	2,1174	0,1715	3575,
12,8336	28,9306	13,0000	28,9851	11058,	39,1843	12,2806	2,2803	0,1989	3320,
12,1958	28,9658	12,0000	28,9861	10208,	39,1779	12,4286	2,4704	0,2334	3064,
11,3983	28,9330	11,0000	28,9910	9357,	39,1703	12,5964	2,6949	0,2778	2809,
11,5098	28,9318	10,0000	29,0007	8507,	39,1612	12,7888	2,9644	0,3362	2554,
11,2551	28,9251	9,0000	29,0165	7656,	39,1501	13,0124	3,2938	0,4150	2298,
10,7534	29,1581	8,0000	29,0398	6805,	39,1362	13,2767	3,7055	0,5252	2043,
10,5138	29,0051	7,0000	29,0714	5955,	39,1164	13,5958	4,2349	0,6860	1788,
10,3183	29,1316	6,0000	29,1098	5104,	39,0946	13,9917	4,9407	0,9338	1532,
9,7937	29,1997	5,0000	29,1444	4253,	39,0612	14,5010	5,9288	1,3446	1277,
9,4097	29,1553	4,5000	29,1494	3828,	39,0390	14,8172	6,5876	1,6600	1149,
8,8285	29,1763	4,0000	29,1383	3403,	39,0112	15,1910	7,4111	2,1010	1021,
8,5491	29,1052	3,5000	29,0589	2977,	38,9735	15,6423	8,4698	2,7441	894,
7,9777	29,1019	3,0000	28,8721	2552,	38,9279	16,2021	9,8814	3,7351	766,
7,5629	29,1512	2,5000	28,4180	2127,	38,8612	16,9224	11,8577	5,3785	638,
7,0254	29,1627	2,0000	27,2812	1701,	38,7612	17,8982	14,8221	8,4039	511,
6,4409	29,1263	1,5000	24,0390	1276,	38,5946	19,3281	19,7628	14,9402	383,
6,0442	29,1601	1,4000	22,8579	1191,	38,5469	19,7027	21,1744	17,1508	358,
5,3065	29,0878	1,3000	21,2846	1106,	38,4920	20,1198	22,8032	19,8908	332,
4,8103	29,2497	1,2000	19,1994	1021,	38,4279	20,5879	24,7035	23,3441	306,
4,3902	29,1558	1,1000	16,4015	936,	38,3521	21,1185	26,9493	27,7814	281,
2,9723	28,6925	1,0000	12,5631	851,	38,2612	21,7268	29,6442	33,6155	255,
2,8139	28,4598	0,9000	7,1536	766,	38,1501	22,4339	32,9380	41,5006	230,

TABLE I. 9 The experimental and calculated results for Q (flow rate), M.C. (meter coefficient) and the calculated values for blades Reynolds number and meter annulus Reynolds numbers, Re_{pass} and the theoretical value for T_1, T_2, T_3 and Term 2 using the leakage theory for Turbine Flow Meter Type B 2 ins. (50.8 mm) diameter.

Pipe radius = 25.4 mm; Meter radius = 23.101 mm; Axial width = 24.384 mm; Hub radius = 9.944 mm; Blade thickness = 10.16 mm; Tip radius = 22.8473 mm.

```
00083;  $A567IDEL ;=JJ
```

TURBINE FLOW METER TYPE B 2INCH HELICAL BLADE ANGLE ROTOR HELICAL PITCH=3,9596

PIPE RADIUS = 1,0000 METER RADIUS = 0,9095 TIP RADIUS = 0,8995 HUB RADIUS = 0,3915 AXIAL WIDTH=0,960

NO OF BLADES =3,000 BLADE THICKNESS =0,400 NO OF PICKUP =1,000 VISCOSITY(CENTI-POISE)= 47,00

EXPERIMENTAL VALUE		THEORETICAL VALUE		BLADES	THEORETICAL VALUE (PULSES PER POUND)				
Q	M.C.	Q	M.C.	RE-NO	T1	T2	T1K/Q	T3	PASS.RE
19.2575	28.7197	24.0000	28.3500	32134.	38.6233	10.7851	1.0696	0.0577	9649.
18.7054	28.7129	23.0000	28.3439	30795.	38.6215	10.8308	1.1161	0.0629	9247.
18.1145	28.7358	22.0000	28.3381	29456.	38.6195	10.8796	1.1668	0.0687	8845.
17.4623	28.7046	21.0000	28.3326	28117.	38.6173	10.9318	1.2224	0.0754	8443.
16.8396	28.7719	20.0000	28.3275	26779.	38.6150	10.9878	1.2835	0.0831	8041.
16.4451	28.7311	19.0000	28.3230	25440.	38.6123	11.0483	1.3511	0.0921	7639.
15.7079	28.8249	18.0000	28.3192	24101.	38.6094	11.1137	1.4261	0.1026	7237.
15.5543	28.7379	17.0000	28.3163	22762.	38.6061	11.1848	1.5100	0.1150	6835.
15.0051	28.7790	16.0000	28.3145	21423.	38.6025	11.2625	1.6044	0.1299	6433.
14.5654	28.7536	15.0000	28.3141	20084.	38.5983	11.3478	1.7113	0.1478	6031.
13.9364	28.3517	14.0000	28.3154	18745.	38.5935	11.4421	1.8336	0.1696	5629.
13.2666	28.7365	13.0000	28.3188	17406.	38.5880	11.5471	1.9746	0.1967	5227.
12.6304	28.3491	12.0000	28.3250	16067.	38.5816	11.6649	2.1392	0.2309	4825.
11.9662	28.3312	11.0000	28.3344	14728.	38.5740	11.7985	2.3336	0.2748	4423.
11.4349	28.3517	10.0000	28.3479	13389.	38.5650	11.9516	2.5670	0.3325	4021.
11.0114	28.9141	9.0000	28.3660	12050.	38.5538	12.1296	2.8522	0.4105	3619.
10.3415	28.9391	8.0000	28.8392	10711.	38.5400	12.3400	3.2088	0.5195	3216.
9.2784	29.9097	7.0000	28.9167	9372.	38.5221	12.5940	3.6672	0.6785	2814.
9.3591	28.9275	6.0000	28.9439	8034.	38.4983	12.9092	4.2784	0.9235	2412.
8.8957	28.9044	5.0000	28.9545	6695.	38.4650	13.3146	5.1340	1.3299	2010.
8.3760	28.9091	4.5000	28.9320	6025.	38.4427	13.5663	5.7045	1.6419	1809.
7.9157	28.7574	4.0000	28.3906	5356.	38.4150	13.8639	6.4175	2.0780	1608.
7.5964	28.9013	3.5000	28.7763	4686.	38.3792	14.2231	7.3343	2.7141	1407.
7.3669	28.7454	3.0000	28.5254	4017.	38.3316	14.6688	8.5567	3.6942	1206.
6.8425	28.3396	2.5000	27.9712	3347.	38.2650	15.2422	10.2681	5.3196	1005.
6.3665	28.3394	2.0000	26.6691	2678.	38.1650	16.0190	12.8351	8.3119	804.
5.9407	28.9168	1.5000	23.1777	2008.	37.9983	17.1573	17.1134	14.7768	603.
5.5051	28.9158	1.4000	21.8679	1874.	37.9507	17.4555	18.3358	16.9631	563.
5.1694	28.9216	1.3000	20.1313	1741.	37.8957	17.7874	19.7463	19.6732	523.
4.7590	28.3575	1.2000	17.9746	1607.	37.8316	18.1601	21.5918	23.0887	482.
4.4052	28.3724	1.1000	15.0324	1473.	37.7559	18.5825	23.5365	27.4774	442.
4.0911	28.3327	1.0000	11.0207	1339.	37.6650	19.0667	25.6701	33.2477	402.
3.7554	28.3029	0.9000	5.4001	1205.	37.5538	19.6296	28.5224	41.0465	362.

TABLE I. 8 The experimental and calculated results for Q (flow rate), M.C. (meter coefficient) and the calculated values for blades Reynolds number and meter annulus Reynolds numbers, Re_{pass} and the theoretical value for T_1 , T_2 ,T_3 and Term 2 using the leakage theory for Turbine Flow Meter Type B 2 ins. (50.8 mm) diameter.

Pipe radius = 25.4 mm; Meter radius = 23.101 mm; Axial width = 24.384 mm; Hub radius = 9.944 mm; Blade thickness = 10.16 mm; Tip radius = 22.8473 mm

COORS: MAS67!DEL :=J0

TURBINE FLOW METER TYPE B 2INCH HELICAL BLADE ANGLE ROTOR HELICAL PITCH=3,9596

PIPE RADIUS = 1,0000 METER RADIUS = 0,9095 TIP RADIUS = 0,8995 HUB RADIUS = 0,3915 AXIAL WIDTH=0,960

NO OF BLADES =3,000 BLADE THICKNESS =0,400 NO OF PICKUP =1,000 VISCOSITY(CENTI-POISE)= 21,00

EXPERIMENTAL VALUE		THEORETICAL VALUE		BLADES	THEORETICAL VALUE (PULSES PER POUND)				
Q	M.C.	Q	M.C.	RE=40	T1	T2	T1K/Q	T3	PASS.RE
18.7311	28.8249	24.0000	28.8935	71946.	38.2361	10.0751	0.7648	0.0323	21596.
17.2743	28.8398	23.0000	28.8915	68950.	38.2342	10.1057	0.7981	0.0351	20697.
17.9238	28.7385	22.0000	28.8398	65952.	38.2323	10.1364	0.8344	0.0384	19797.
16.3611	28.8156	21.0000	28.8887	62955.	38.2301	10.1733	0.8741	0.0422	18897.
14.7177	28.8767	20.0000	28.8382	59957.	38.2277	10.2108	0.9178	0.0465	17997.
12.5962	28.9747	19.0000	28.8384	56959.	38.2251	10.2513	0.9661	0.0515	17097.
11.4963	28.9875	18.0000	28.8894	53961.	38.2222	10.2951	1.0198	0.0574	16197.
10.7672	28.9872	17.0000	28.8916	50963.	38.2189	10.3427	1.0797	0.0643	15297.
9.8125	29.1057	16.0000	28.8951	47965.	38.2152	10.3947	1.1472	0.0726	14398.
8.7073	29.1653	15.0000	28.9003	44968.	38.2111	10.4518	1.2237	0.0826	13498.
8.3954	28.9671	14.0000	28.9070	41970.	38.2063	10.5150	1.3111	0.0948	12598.
7.4285	29.1739	13.0000	28.9155	38972.	38.2008	10.5852	1.4120	0.1100	11698.
6.6650	29.1413	12.0000	28.9308	35974.	38.1944	10.6641	1.5296	0.1291	10798.
6.2418	29.1043	11.0000	28.9483	32976.	38.1868	10.7535	1.6687	0.1536	9898.
5.7554	29.2194	10.0000	28.9715	29978.	38.1777	10.8561	1.8356	0.1859	8999.
4.9107	29.1941	9.0000	29.0014	26981.	38.1666	10.9752	2.0395	0.2295	8099.
4.1281	29.2507	8.0000	29.0407	23983.	38.1527	11.1161	2.2945	0.2905	7199.
3.5651	29.2422	7.0000	29.0916	20985.	38.1349	11.2861	2.6222	0.3794	6299.
2.9759	29.2545	6.0000	29.1569	17987.	38.1111	11.4971	3.0593	0.5164	5399.
2.5162	29.2351	5.0000	29.2368	14989.	38.0777	11.7685	3.6711	0.7436	4499.
2.2491	28.2117	4.5000	29.2795	13490.	38.0555	11.9370	4.0790	0.9180	4049.
0.0000	0.0000	4.0000	29.3186	11991.	38.0277	12.1362	4.5889	1.1618	3599.
0.0000	0.0000	3.5000	29.3423	10492.	37.9920	12.3767	5.2445	1.5175	3149.
0.0000	0.0000	3.0000	29.3224	8994.	37.9444	12.6751	6.1186	2.0654	2700.
0.0000	0.0000	2.5000	29.1668	7495.	37.8777	13.0589	7.3423	2.9742	2250.
0.0000	0.0000	2.0000	28.7295	5996.	37.7777	13.5790	9.1779	4.6475	1800.
0.0000	0.0000	1.5000	27.2454	4497.	37.6111	14.3410	12.2371	8.2618	1350.
0.0000	0.0000	1.4000	26.6498	4197.	37.5634	14.5406	13.1112	9.4842	1260.
0.0000	0.0000	1.3000	25.8659	3897.	37.5085	14.7629	14.1198	10.9994	1170.
0.0000	0.0000	1.2000	24.8194	3597.	37.4444	15.0124	15.2964	12.9091	1080.
0.0000	0.0000	1.1000	23.3977	3298.	37.3686	15.2951	16.6870	15.5628	990.
0.0000	0.0000	1.0000	21.4251	2998.	37.2777	15.6193	18.3557	18.5890	900.
0.0000	0.0000	0.9000	18.6163	2698.	37.1666	15.9961	20.3952	22.9494	810.
0.0000	0.0000	0.8000	14.4854	2398.	37.0277	16.4416	22.9446	29.0454	720.
0.0000	0.0000	0.7000	8.1555	2098.	36.8491	16.9793	26.2224	37.9368	630.

TABLE I. 7 The experimental and calculated results for Q (flow rate), M.C. (meter coefficient) and the calculated values for blades Reynolds number and meter annulus Reynolds numbers, Re_{pass} and the theoretical value for T_1, T_2, T_3 and Term 2 using the leakage theory for Turbine Flow Meter Type B 2 ins. (50.8 mm) diameter.

Pipe radius = 25.4 mm; Meter radius = 23.101 mm; Hub radius = 9.944 mm; Axial width = 24.384 mm; Blade thickness = 10.16 mm; Tip radius = 22.8473 mm

COORS: MA567[DEL ;=))

TURBINE FLOW METER TYPE B 2INCH HELICAL BLADE ANGLE ROTOR HELICAL PITCH=3.9596

PIPE RADIUS = 1.0000 METER RADIUS = 0.9095 TIP RADIUS = 0.8995 HUB RADIUS = 0.3915 AXIAL WIDTH=0.960

NO OF BLADES =3.000 BLADE THICKNESS =0.400 NO OF PICKUP =1.000 VISCOSITY(CENTI-POISE)= 1.00

EXPERIMENTAL VALUE		THEORETICAL VALUE		BLADES	T H E O R E T I C A L V A L U E (PULSES PER POUND)				
*	M.C.	Q	M.C.	RE=NO	T1	T2	T1K/Q	T3	PASS.RE
17.2405	28.5512	24.0000	28.5776	1510056.	37.2356	8.9740	0.3442	0.0282	453526.
17.3622	28.5928	23.0000	28.5316	1447137.	37.2357	8.9806	0.3591	0.0307	434629.
17.4067	28.5955	22.0000	28.5359	1384218.	37.2318	8.9878	0.3755	0.0335	415732.
17.3146	28.0422	21.0000	28.5908	1321299.	37.2296	8.9954	0.3934	0.0368	396835.
16.7101	28.5624	20.0000	28.5961	1258380.	37.2272	9.0035	0.4130	0.0406	377938.
16.1146	28.7001	19.0000	28.6020	1195461.	37.2246	9.0124	0.4348	0.0450	359041.
15.7938	28.6281	18.0000	28.6086	1132542.	37.2217	9.0219	0.4589	0.0501	340144.
15.3141	28.5911	17.0000	28.6159	1069623.	37.2184	9.0323	0.4859	0.0562	321247.
14.4241	28.5327	16.0000	28.6240	1006704.	37.2147	9.0436	0.5163	0.0634	302351.
12.4924	28.5984	15.0000	28.6331	943785.	37.2106	9.0560	0.5507	0.0722	283454.
12.0165	28.5926	14.0000	28.6432	880866.	37.2058	9.0698	0.5900	0.0828	264557.
11.6189	28.5732	13.0000	28.6546	817947.	37.2003	9.0851	0.6354	0.0961	245660.
11.0133	28.7175	12.0000	28.6673	755028.	37.1939	9.1022	0.6884	0.1127	226763.
10.7162	28.6484	11.0000	28.6814	692109.	37.1863	9.1217	0.7509	0.1342	207866.
9.8159	28.5634	10.0000	28.6969	629190.	37.1772	9.1440	0.8260	0.1624	188969.
8.5661	28.6355	9.0000	28.7135	566271.	37.1661	9.1700	0.9178	0.2004	170072.
8.2649	28.7395	8.0000	28.7304	503352.	37.1522	9.2007	1.0325	0.2537	151175.
7.7118	28.5547	7.0000	28.7454	440433.	37.1344	9.2377	1.1801	0.3313	132278.
7.2773	28.7071	6.0000	28.7527	377514.	37.1106	9.2836	1.3767	0.4510	113381.
7.0210	28.7551	5.0000	28.7372	314595.	37.0772	9.3427	1.6521	0.6494	94485.
6.1353	28.3499	4.5000	28.7095	283136.	37.0550	9.3794	1.8356	0.8017	85036.
5.7737	28.5468	4.0000	28.6548	251676.	37.0272	9.4228	2.0651	1.0147	75588.
5.7555	28.7473	3.5000	28.5511	220217.	36.9915	9.4752	2.3601	1.3253	66139.
3.5743	28.0648	3.0000	28.3533	188757.	36.9439	9.5401	2.7535	1.8039	56691.
3.3404	28.7781	2.5000	27.9600	157298.	36.8772	9.6237	3.3042	2.5976	47242.
3.3131	28.7673	2.0000	27.1117	125838.	36.7772	9.7369	4.1302	4.0588	37794.
4.3311	28.7483	1.5000	24.9989	94379.	36.6106	9.9029	5.5069	7.2157	28345.
3.0785	28.4356	1.4000	24.2336	88037.	36.5629	9.9463	5.9003	8.2833	26456.
2.7291	28.0582	1.3000	23.2607	81795.	36.5080	9.9947	6.3541	9.6067	24566.
0.0000	0.0000	1.2000	22.0040	75503.	36.4439	10.0491	6.8837	11.2745	22676.
0.0000	0.0000	1.1000	20.3494	69211.	36.3681	10.1106	7.5094	13.4176	20787.
0.0000	0.0000	1.0000	18.1211	62919.	36.2772	10.1812	8.2604	16.2353	18897.
0.0000	0.0000	0.9000	15.0375	56627.	36.1661	10.2653	9.1782	20.0435	17007.
0.0000	0.0000	0.8000	10.6248	50335.	36.0272	10.3603	10.3255	25.3676	15118.
0.0000	0.0000	0.7000	4.0387	44043.	35.8487	10.4774	11.8006	33.1332	13228.

TABLE I. 6 The experimental and calculated results for Q (flow rate), M.C. (meter coefficient) and the calculated values for blades Reynolds number and meter annulus Reynolds numbers, Re_{pass} and the thoeretical value for T_1, T_2, T_3 and Term 2 using the leakage theory for Turbine Flow Meter Type B 2 ins (50.8 mm) diameter.

TABLE I.11 Turbine Flow Meter Type C 1.5 ins (38.1 mm) diameter

TURBINE FLOW METER TYPE C 1.5INCH — CONSTANT BLADE ANGLE ROTOR BLADE ANGLE=30 DEGREE

PIPE RADIUS = 0.6687 METER RADIUS = 0.6687 TIP RADIUS = 0.6541 HUB RADIUS = 0.2881 AXIAL WIDTH=0.251

NO OF BLADES =6.00 BLADE THICKNESS =0.015 NO OF PICKUP =1.000 VISCOSITY(CENTI-POISE)= 1.00

EXPERIMENTAL VALUE		THEORETICAL VALUE		BLADES	THEORETICAL VALUE				(PULSES PER POUND)
Q	M.C.	Q	M.C.	RE=NO	T1	T2	T1K/Q	T3	PASS.RE
19.5950	30.2530	24.0000	30.2580	123405.	30.5162	0.3834	0.1289	0.0038	138795.
18.3509	30.2606	23.0000	30.2590	118263.	30.5144	0.3858	0.1346	0.0041	133011.
17.3636	30.2547	22.0000	30.2601	113121.	30.5125	0.3885	0.1407	0.0045	127228.
16.3857	30.2409	21.0000	30.2614	107979.	30.5103	0.3913	0.1474	0.0049	121445.
15.3952	30.2432	20.0000	30.2628	102838.	30.5079	0.3944	0.1547	0.0055	115662.
14.4409	30.2683	19.0000	30.2644	97696.	30.5053	0.3977	0.1629	0.0060	109879.
13.5166	30.2641	18.0000	30.2663	92554.	30.5024	0.4012	0.1719	0.0067	104096.
12.6125	30.2953	17.0000	30.2685	87412.	30.4991	0.4051	0.1820	0.0076	98313.
11.6025	30.2954	16.0000	30.2710	82270.	30.4954	0.4093	0.1934	0.0085	92530.
10.7902	30.3226	15.0000	30.2739	77128.	30.4912	0.4140	0.2063	0.0097	86747.
9.9291	30.3231	14.0000	30.2773	71986.	30.4865	0.4191	0.2210	0.0111	80964.
9.0880	30.3196	13.0000	30.2813	66844.	30.4810	0.4248	0.2381	0.0129	75180.
8.2305	30.3370	12.0000	30.2861	61703.	30.4746	0.4312	0.2579	0.0152	69397.
7.3970	30.3517	11.0000	30.2918	56561.	30.4670	0.4385	0.2813	0.0180	63614.
6.4866	30.3336	10.0000	30.2987	51419.	30.4579	0.4468	0.5095	0.0218	57831.
5.6207	30.3790	9.0000	30.3072	46277.	30.4468	0.4565	0.3439	0.0269	52048.
4.3364	30.3640	8.0000	30.3177	41135.	30.4329	0.4680	0.3868	0.0341	46265.
4.2294	30.3306	7.0000	30.3308	35993.	30.4151	0.4818	0.4421	0.0445	40482.
3.6084	30.3549	6.0000	30.3475	30851.	30.3912	0.4989	0.5158	0.0606	34699.
3.2353	30.3526	5.0000	30.3685	25709.	30.3579	0.5210	0.6189	0.0873	28916.
2.8765	30.3942	4.5000	30.3809	23138.	30.3357	0.5347	0.6877	0.1078	26024.
2.4704	30.3390	4.0000	30.3945	20566.	30.3079	0.5509	0.7737	0.1364	23132.
2.2097	30.3316	3.5000	30.4098	17997.	30.2722	0.5704	0.8842	0.1782	20241.
1.8816	30.3381	3.0000	30.4189	15426.	30.2246	0.5947	1.0316	0.2425	17349.
1.5603	30.2962	2.5000	30.4207	12855.	30.1579	0.6259	1.2379	0.3493	14458.
1.2612	30.3055	2.0000	30.3914	10284.	30.0579	0.6681	1.5473	0.5457	11566.
1.0447	30.1656	1.5000	30.2541	7713.	29.8912	0.7301	2.0631	0.9702	8675.
0.8683	30.1136	1.4000	30.1941	7199.	29.8436	0.7463	2.2105	1.1137	8096.
0.6938	29.5933	1.3000	30.1132	6684.	29.7887	0.7643	2.3805	1.2916	7518.
0.5683	28.6221	1.2000	30.0030	6170.	29.7246	0.7846	2.5789	1.5159	6940.
0.4508	26.2955	1.1000	29.8505	5656.	29.6488	0.8076	2.8133	1.8040	6361.
0.0000	0.0000	1.0000	29.6358	5142.	29.5579	0.8340	3.0947	2.1828	5783.

Pipe radius = 16.985 mm; Tip radius = 16.6141 mm; Meter radius = 16.985 mm; Axial width = 6.3754 mm; Hub radius = 7.3177 mm; Blade thickness = .381 mm.

TABLE I.12 Turbine Flow Meter Type C 1.5 ins. (38.1 mm) diameter

C0083: #A567|DEL :=00

TURBINE FLOW METER TYPE C 1.5INCH — CONSTANT BLADE ANGLE ROTOR BLADE ANGLE=30 DEGREE

PIPE RADIUS = 0.6687 METER RADIUS = 0.6687 TIP RADIUS = 0.6541 HUB RADIUS = 0.2881 AXIAL WIDTH=0.251

NO OF BLADES =6.000 BLADE THICKNESS =0.015 NO OF PICKUP =1.000 VISCOSITY(CENTI-POISE)= 21.00

EXPERIMENTAL VALUE		THEORETICAL VALUE		BLADES	THEORETICAL VALUE (PULSES PER POUND)				
Q	M.C.	Q	M.C.	RE-NO	T1	T2	T1K/Q	T3	PASS.RE
18.4488	31.5032	24.0000	31.3464	5904.	31.7396	0.8527	0.4305	0.0210	6609.
17.6547	31.2494	23.0000	31.3498	5658.	31.7378	0.8643	0.4492	0.0229	6334.
17.0037	31.2637	22.0000	31.3537	5412.	31.7858	0.8768	0.4696	0.0250	6058.
16.0560	31.3544	21.0000	31.3581	5166.	31.7837	0.8900	0.4920	0.0275	5783.
15.6379	31.3815	20.0000	31.3632	4920.	31.7815	0.9043	0.5166	0.0303	5508.
15.4770	31.3568	19.0000	31.3691	4674.	31.7787	0.9197	0.5437	0.0335	5232.
14.4615	31.3318	18.0000	31.3759	4428.	31.7757	0.9364	0.5739	0.0374	4957.
14.1954	31.4390	17.0000	31.3836	4182.	31.7725	0.9545	0.6077	0.0419	4682.
13.7093	31.4395	16.0000	31.3929	3936.	31.7688	0.9743	0.6457	0.0473	4406.
13.1295	31.5015	15.0000	31.4035	3690.	31.7646	0.9960	0.6887	0.0538	4131.
12.4554	31.4321	14.0000	31.4160	3444.	31.7599	1.0200	0.7379	0.0618	3855.
12.0114	31.5112	13.0000	31.4306	3198.	31.7544	1.0468	0.7947	0.0717	3580.
11.4795	31.5012	12.0000	31.4480	2952.	31.7480	1.0768	0.8609	0.0841	3305.
11.3223	31.5043	11.0000	31.4687	2706.	31.7404	1.1108	0.9392	0.1001	3029.
10.0125	31.5934	10.0000	31.4935	2460.	31.7313	1.1498	1.0331	0.1211	2754.
9.0111	31.6081	9.0000	31.5234	2214.	31.7202	1.1951	1.1479	0.1495	2478.
8.1011	31.6015	8.0000	31.5597	1968.	31.7063	1.2487	1.2914	0.1892	2203.
7.0011	31.6537	7.0000	31.6037	1722.	31.6884	1.3134	1.4759	0.2472	1928.
6.1250	31.6827	6.0000	31.6564	1476.	31.6646	1.3937	1.7218	0.3364	1652.
5.0011	31.6976	5.0000	31.7161	1230.	31.6313	1.4970	2.0662	0.4844	1377.
4.5911	31.6931	4.5000	31.7457	1107.	31.6091	1.5611	2.2958	0.5981	1239.
4.1122	31.7068	4.0000	31.7703	984.	31.5813	1.6369	2.5828	0.7569	1102.
3.5110	31.7141	3.5000	31.7803	861.	31.5456	1.7284	2.9517	0.9886	964.
3.0187	31.7024	3.0000	31.7541	738.	31.4980	1.8419	3.4437	1.3456	826.
2.5112	31.6876	2.5000	31.6581	615.	31.4313	1.9879	4.1324	1.9377	688.
2.0123	31.3199	2.0000	31.2834	492.	31.3313	2.1858	5.1655	3.0276	551.
1.5123	30.6055	1.5000	30.1936	369.	31.1546	2.4757	6.8874	5.3825	413.
1.4163	30.0077	1.4000	29.7658	344.	31.1170	2.5517	7.3793	6.1789	386.
1.1510	29.4526	1.3000	29.2068	320.	31.0521	2.6362	7.9470	7.1660	358.
0.3441	25.7078	1.2000	28.4659	295.	30.9980	2.7311	8.6092	8.4101	330.
0.0000	0.0000	1.1000	27.4666	271.	30.9222	2.8387	9.3919	10.0087	303.

Pipe radius = 16.985 mm; Tip radius = 16.6141 mm; Meter radius = 16.985 mm; Axial width = 6.3754 mm; Hub radius = 7.3177 mm; Blade thickness = .381 mm

TABLE I. 13 Turbine Flow Meter Type C 1.5 ins. (38.1 mm) diameter

COORS: #A567[DEL :=00

TURBINE FLOW METER TYPE C 1.5INCH CONSTANT BLADE ANGLE ROTOR BLADE ANGLE=30 DEGREE

PIPE RADIUS = 0.6687 METER RADIUS = 0.6687 TIP RADIUS = 0.6541 HUB RADIUS = 0.2881 AXIAL WIDTH=0.251

NO OF BLADES =6.000 BLADE THICKNESS =0.015 NO OF PICKUP =1.000 VISCOSITY(CENTI-POISE)= 47.00

EXPERIMENTAL VALUE		THEORETICAL VALUE		BLADES	THEORETICAL VALUE (PULSES PER POUND)				
Q	M.C.	Q	M.C.	RE-NO	T1	T2	T1K/Q	T3	PASS.RE
18.5755	31.5061	24.0000	32.0149	2638.	32.7492	1.1337	0.4554	0.0560	2953.
17.9353	31.6431	23.0000	32.0103	2528.	32.7474	1.1512	0.4752	0.0610	2830.
17.4717	31.6458	22.0000	32.0055	2418.	32.7454	1.1700	0.4968	0.0667	2707.
16.7132	31.7113	21.0000	32.0004	2308.	32.7433	1.1901	0.5205	0.0732	2584.
16.1560	31.7609	20.0000	31.9950	2199.	32.7409	1.2117	0.5465	0.0807	2461.
15.8431	31.8742	19.0000	31.9891	2089.	32.7385	1.2350	0.5752	0.0894	2338.
15.2215	31.8628	18.0000	31.9827	1979.	32.7353	1.2602	0.6072	0.0996	2215.
14.3409	31.7738	17.0000	31.9757	1869.	32.7321	1.2876	0.6429	0.1117	2092.
13.6582	32.0156	16.0000	31.9679	1759.	32.7284	1.3175	0.6831	0.1261	1969.
12.4988	31.9223	15.0000	31.9591	1649.	32.7242	1.3503	0.7286	0.1435	1846.
11.8754	31.8410	14.0000	31.9488	1539.	32.7195	1.3866	0.7807	0.1647	1723.
11.2549	31.8909	13.0000	31.9367	1429.	32.7140	1.4271	0.8407	0.1910	1600.
10.6060	31.8960	12.0000	31.9218	1319.	32.7075	1.4724	0.9108	0.2242	1477.
10.0509	31.9870	11.0000	31.9030	1209.	32.7000	1.5239	0.9936	0.2668	1353.
9.3012	32.1245	10.0000	31.8782	1099.	32.6909	1.5828	1.0930	0.3228	1230.
8.7080	31.9383	9.0000	31.8443	989.	32.6798	1.6514	1.2144	0.3985	1107.
8.0488	31.9332	8.0000	31.7954	879.	32.6659	1.7324	1.3662	0.5044	984.
7.3589	32.0452	7.0000	31.7205	769.	32.6480	1.8302	1.5614	0.6588	861.
6.5061	32.0442	6.0000	31.5977	660.	32.6242	1.9515	1.8216	0.8967	738.
5.8132	32.5013	5.0000	31.3780	550.	32.5909	2.1076	2.1859	1.2912	615.
5.3348	32.5268	4.5000	31.1989	495.	32.5687	2.2046	2.4288	1.5940	554.
4.8603	32.5282	4.0000	30.9567	440.	32.5409	2.3191	2.7324	2.0175	492.
4.3225	32.2415	3.5000	30.5354	385.	32.5052	2.4575	3.1228	2.6351	431.
3.8127	32.0519	3.0000	29.8351	330.	32.4573	2.6291	3.6432	3.5866	369.
3.0935	31.9117	2.5000	28.7482	275.	32.3909	2.8499	4.3719	5.1647	308.
2.8146	31.7415	2.0000	26.5369	220.	32.2909	3.1490	5.4648	8.0699	246.
2.0124	31.5349	1.5000	21.4770	165.	32.1242	3.5873	7.2865	14.3464	185.
1.4093	31.4413	1.4000	19.7123	154.	32.0766	3.7021	7.8069	16.4691	172.
1.0533	31.0392	1.3000	17.4989	143.	32.0217	3.8299	8.4075	19.1005	160.
0.7718	30.2308	1.2000	14.6759	132.	31.9575	3.9734	9.1081	22.4163	148.
0.7298	30.3453	1.1000	11.0046	121.	31.8818	4.1360	9.9361	26.6772	135.
0.3990	29.7948	1.0000	6.1186	110.	31.7909	4.3225	10.9297	32.2795	123.

Pipe Radius = 16.985 mm; Tip radius = 16.6141 mm; Meter radius = 16.985 mm; Axial width = 6.3754 mm; Hub radius = 7.3177 mm; Blade thickness = .381 mm

TABLE I. 14 Turbine Flow meter Type C 1.5 ins (38.1 mm) diameter

COORS: W.SO7(DEL :-0)

TURBINE FLOW METER TYPE C 1.5INCH CONSTANT BLADE ANGLE ROTOR BLADE ANGLE=30 DEGREE

PIPE RADIUS = 0.6687 METER RADIUS = 0.6687 TIP RADIUS = 0.6541 HUB RADIUS = 0.2881 AXIAL WIDTH=0.251

NO OF BLADES =6.000 BLADE THICKNESS =0.015 NO OF PICKUP =1.000 VISCOSITY(CENTI-POISE)= 71.00

EXPERIMENTAL VALUE		THEORETICAL VALUE		BLADES	THEORETICAL VALUE (PULSES PER POUND)				
K	M.C.	N	M.C.	RE=NO	T1	T2	T1K/Q	T3	PASS,RE
19.4564	31.8024	24.0000	32.2017	1750.	33.3538	1.3402	0.2669	0.0788	1955.
18.3015	31.8212	23.0000	32.1829	1677.	33.3520	1.3618	0.2785	0.0858	1873.
18.1687	31.8528	22.0000	32.1625	1604.	33.3500	1.3849	0.2912	0.0938	1792.
17.7122	31.8723	21.0000	32.1404	1531.	33.3479	1.4096	0.3050	0.1029	1710.
17.2011	31.8566	20.0000	32.1162	1459.	33.3455	1.4361	0.3203	0.1135	1629.
16.5735	31.8343	19.0000	32.0896	1386.	33.3428	1.4646	0.3371	0.1258	1548.
15.8929	31.8724	18.0000	32.0601	1313.	33.3399	1.4956	0.3559	0.1401	1466.
15.8728	31.8826	17.0000	32.0272	1240.	33.3367	1.5292	0.3768	0.1571	1385.
14.5755	31.9715	16.0000	31.9901	1167.	33.3330	1.5659	0.4004	0.1773	1303.
14.1125	31.8363	15.0000	31.9478	1094.	33.3288	1.6063	0.4271	0.2018	1222.
13.2023	31.8712	14.0000	31.8992	1021.	33.3241	1.6508	0.4576	0.2316	1140.
13.7617	31.7702	13.0000	31.8422	948.	33.3186	1.7005	0.4928	0.2686	1059.
12.3015	31.9331	12.0000	31.7745	875.	33.3121	1.7562	0.5338	0.3153	977.
12.9169	31.8552	11.0000	31.6924	802.	33.3046	1.8194	0.5823	0.3752	896.
12.0702	31.9747	10.0000	31.5903	729.	33.2955	1.8918	0.6406	0.4540	815.
11.5023	31.8315	9.0000	31.4598	656.	33.2844	1.9759	0.7118	0.5605	733.
11.1402	31.9473	8.0000	31.2865	583.	33.2705	2.0754	0.8007	0.7093	652.
10.7048	31.9574	7.0000	31.0458	510.	33.2526	2.1955	0.9151	0.9265	570.
10.3265	31.9963	6.0000	30.6909	438.	33.2288	2.3445	1.0676	1.2610	489.
9.3147	31.3419	5.0000	30.1246	365.	33.1955	2.5362	1.2812	1.8159	407.
9.0374	31.8310	4.5000	29.6097	328.	33.1733	2.6552	1.4235	2.2418	367.
8.7716	31.7069	4.0000	29.1137	292.	33.1455	2.7959	1.6015	2.8373	326.
8.7555	31.7622	3.5000	28.2684	255.	33.1098	2.9657	1.8302	3.7059	285.
8.4580	31.6346	3.0000	26.9768	219.	33.0621	3.1765	2.1355	5.0441	244.
8.1015	31.5233	2.5000	24.3467	182.	32.9955	3.4476	2.5623	7.2635	204.
7.9913	31.5322	2.0000	20.9343	146.	32.8955	3.8149	3.2029	11.3493	163.
7.7315	31.2511	1.5000	12.4698	109.	32.7286	4.3530	4.2706	20.1765	122.
7.6424	31.1556	1.4000	9.6009	102.	32.6812	4.4940	4.5756	23.1618	114.
7.0114	30.9012	1.3000	6.0406	95.	32.6263	4.6510	4.9276	26.8622	106.
6.7154	30.8925	1.2000	1.5473	88.	32.5621	4.8272	5.3382	31.5258	98.

Pipe radius = 16.985 mm; Tip radius = 16.6141 mm; Meter radius = 16.985 mm; Axial width = 6.3754 mm; Hub radius = 7.3177 mm; Blade thickness = .381 mm

TABLE I. 15 Turbine Flow Meter Type C 1.5 ins (38.1 mm) diameter

COOR3: MA567IDEL :=00

TURBINE FLOW METER TYPE C 1.5INCH — CONSTANT BLADE ANGLE ROTOR BLADE ANGLE=30 DEGREE

PIPE RADIUS = 0.6637 METER RADIUS = 0.6687 TIP RADIUS = 0.6541 HUB RADIUS = 0.2881 AXIAL WIDTH=0.251

NO OF BLADES =6.000 BLADE THICKNESS =0.015 NO OF PICKUP =1.000 VISCOSITY(CENTI-POISE)=170.00

EXPERIMENTAL VALUE		THEORETICAL VALUE		BLADES	THEORETICAL VALUE (PULSES PER POUND)				
I	M.C.	N	M.C.	RE-NO	T1	T2	T1K/Q	T3	PASS.RE
19.3132	32.1112	24.0000	32.5392	730.	35.3098	1.8714	-0.8555	0.0739	816.
18.3225	32.0721	23.0000	32.4370	700.	35.3080	1.9047	-0.8858	0.0805	782.
18.1144	31.8713	22.0000	32.3394	669.	35.3060	1.9402	-0.9184	0.0880	748.
18.2912	31.8331	21.0000	32.2757	639.	35.3038	1.9782	-0.9533	0.0965	714.
16.3914	31.3622	20.0000	32.1851	609.	35.3014	2.0191	-0.9909	0.1064	680.
15.3115	31.6011	19.0000	32.0366	578.	35.2988	2.0631	-1.0312	0.1179	646.
14.2161	31.5101	18.0000	31.9791	548.	35.2959	2.1107	-1.0747	0.1314	612.
13.5022	31.4011	17.0000	31.8612	517.	35.2926	2.1625	-1.1215	0.1473	578.
12.2134	31.3917	16.0000	31.7515	487.	35.2889	2.2191	-1.1721	0.1663	544.
11.2182	31.1016	15.0000	31.5378	456.	35.2848	2.2813	-1.2265	0.1892	510.
10.2213	30.8501	14.0000	31.4277	426.	35.2800	2.3499	-1.2852	0.2172	476.
10.2302	30.6020	13.0000	31.2481	396.	35.2745	2.4264	-1.3481	0.2519	442.
9.3001	30.5315	12.0000	31.0453	365.	35.2681	2.5122	-1.4149	0.2956	408.
8.2321	30.1212	11.0000	30.8143	335.	35.2605	2.6095	-1.4849	0.3518	374.
7.2231	29.6311	10.0000	30.5487	304.	35.2514	2.7211	-1.5560	0.4257	340.
7.1123	29.5313	9.0000	30.2403	274.	35.2403	2.8507	-1.6238	0.5256	306.
6.3145	29.1014	8.0000	29.3734	243.	35.2264	3.0040	-1.6789	0.6652	272.
5.2516	28.7512	7.0000	29.4492	213.	35.2086	3.1890	-1.7016	0.8688	238.
5.1111	28.3011	6.0000	28.9364	183.	35.1848	3.4185	-1.6473	1.1826	204.
4.1512	27.9001	5.0000	28.3256	152.	35.1514	3.7138	-1.4091	1.7029	170.
3.3210	27.3512	4.5000	27.9845	137.	35.1292	3.8972	-1.1452	2.1023	153.
2.3235	26.9022	4.0000	27.6297	122.	35.1014	4.1139	-0.6971	2.6607	136.

Pipe radius = 16.985 mm; Tip radius = 16.6141 mm; Meter radius = 16.985 mm; Axial width = 6.3754 mm; Hub radius = 7.3177 mm; Blade thickness = .381 mm

TABLE I. 16 Turbine Flow Meter Type E 1.5 ins (38.1 mm) diameter

DOORS; MASS/DEL :-01

TURBINE FLOW METER TYPE E 1.5INCH — CONSTANT BLADE ANGLE ROTOR BLADE ANGLE=30 DEGREE

PIPE RADIUS = 0.6637 METER RADIUS = 0.6687 TIP RADIUS = 0.6541 HUB RADIUS = 0.2881 AXIAL WIDTH=0.251

NO OF BLADES =6.000 BLADE THICKNESS =0.015 NO OF PICKUP =1.000 VISCOSITY(CENTI-POISE)= 47.00

EXPERIMENTAL VALUE		THEORETICAL VALUE			THEORETICAL VALUE (PULSES PER POUND)				
Q	M.C.	Q	M.C.	BLADES RE-NO	T1	T2	T1K/Q	T3	PASS.RE
16.5755	31.9361	24.0000	32.0351	2645.	33.0590	1.1570	0.2161	0.0330	2953.
17.7558	31.9331	23.0000	32.0721	2535.	33.0572	1.1746	0.2255	0.0359	2830.
17.7132	31.9313	22.0000	32.0583	2424.	33.0552	1.1934	0.2357	0.0393	2707.
17.4717	31.9256	21.0000	32.0434	2314.	33.0551	1.2135	0.2469	0.0431	2584.
16.5642	31.9142	20.0000	32.0273	2204.	33.0507	1.2351	0.2595	0.0475	2461.
16.1330	31.8942	19.0000	32.0099	2094.	33.0461	1.2584	0.2729	0.0527	2338.
15.8431	31.8842	18.0000	31.9910	1984.	33.0451	1.2836	0.2881	0.0587	2215.
15.2215	31.8623	17.0000	31.9702	1873.	33.0419	1.3110	0.3050	0.0658	2092.
15.1215	31.7703	16.0000	31.9472	1763.	33.0382	1.3409	0.3241	0.0743	1969.
13.5176	31.7969	15.0000	31.9215	1653.	33.0340	1.3737	0.3457	0.0845	1846.
13.3409	31.7738	14.0000	31.8926	1543.	33.0293	1.4100	0.3704	0.0970	1723.
12.4948	31.9328	13.0000	31.8597	1433.	33.0238	1.4505	0.3989	0.1125	1600.
11.9421	32.0526	12.0000	31.8216	1322.	33.0174	1.4959	0.4321	0.1320	1477.
11.3754	31.5410	11.0000	31.7768	1212.	33.0098	1.5473	0.4714	0.1571	1353.
11.2649	31.5991	10.0000	31.7228	1102.	33.0007	1.6063	0.5186	0.1902	1230.
10.5660	31.5960	9.0000	31.6562	992.	32.9896	1.6748	0.5762	0.2348	1107.
10.5090	31.5570	8.0000	31.5709	882.	32.9757	1.7559	0.6482	0.2971	984.
9.7080	31.7580	7.0000	31.4569	771.	32.9578	1.8537	0.7408	0.3881	861.
9.5488	31.7310	6.0000	31.2951	661.	32.9340	1.9751	0.8643	0.5282	738.
9.3589	31.7051	5.0000	31.0460	551.	32.9007	2.1312	1.0371	0.7606	615.
8.5061	31.6342	4.5000	30.8537	496.	32.8785	2.2281	1.1524	0.9390	554.
7.7068	31.5502	4.0000	30.6159	441.	32.8507	2.3427	1.2964	1.1884	492.
7.0603	31.5182	3.5000	30.2633	386.	32.8150	2.4811	1.4816	1.5523	431.
6.6024	31.5311	3.0000	29.7304	331.	32.7674	2.6527	1.7286	2.1128	369.
5.7532	31.2512	2.5000	28.8590	275.	32.7007	2.8736	2.0743	3.0424	308.
4.3535	31.0392	2.0000	27.2670	220.	32.6007	3.1727	2.5928	4.7538	246.
4.4926	30.8136	1.5000	23.8289	165.	32.4340	3.6111	3.4571	8.4512	185.
4.1716	30.6508	1.4000	22.6629	154.	32.3864	3.7260	3.7041	9.7016	172.
3.8553	30.5134	1.3000	21.2151	143.	32.3315	3.8538	3.9890	11.2516	160.
3.7298	30.5453	1.2000	19.3865	132.	32.2674	3.9973	4.3214	13.2049	148.
3.5990	30.2548	1.1000	17.0309	121.	32.1916	4.1600	4.7143	15.7150	135.
3.1088	29.4934	1.0000	13.9248	110.	32.1007	4.3465	5.1857	19.0151	123.
2.8672	29.4551	0.9000	9.7127	99.	31.9896	4.5633	5.7619	23.4755	111.

Pipe radius = 16.985 mm; Tip radius = 16.6141 mm; Meter radius = 16.985 mm; Axial width = 6.3754 mm; Hub radius = 7.3177 mm; Blade thickness = .381 mm

TABLE I.17 Turbine Flow Meter Type E 1.5 ins (38.1 mm) diameter

GOOR3: HA567IDEL :=0)

TURBINE FLOW METER TYPE E 1.5INCH　　　CONSTANT BLADE ANGLE ROTOR　BLADE ANGLE=30 DEGREE

PIPE RADIUS = 0.6687　METER RADIUS = 0.6687　TIP RADIUS = 0.6541　HUB RADIUS = 0.2881　AXIAL WIDTH=0.251

NO OF BLADES =6.00)　BLADE THICKNESS =0.015　NO OF PICKUP =1.000　VISCOSITY(CENTI-POISE)= 71.00

EXPERIMENTAL VALUE		THEORETICAL VALUE		BLADES	THEORETICAL VALUE (PULSES PER POUND)				
Q	M.C.	Q	M.C.	RE-NO	T1	T2	T1K/Q	T3	PASS.RE
19.5883	30.3547	24.0000	31.3233	1739.	33.3565	1.2485	-0.7396	0.0449	1955.
17.6342	30.4056	23.0000	31.2684	1666.	33.3545	1.2695	-0.7676	0.0489	1873.
16.3651	30.5139	22.0000	31.2092	1594.	33.3525	1.2920	-0.7979	0.0534	1792.
15.0433	30.5346	21.0000	31.1452	1521.	33.3503	1.3160	-0.8305	0.0586	1710.
14.3310	30.5562	20.0000	31.0756	1449.	33.3480	1.3418	-0.8659	0.0646	1629.
13.0294	30.4030	19.0000	30.9998	1377.	33.3453	1.3696	-0.9043	0.0716	1548.
12.0680	30.3225	18.0000	30.9168	1304.	33.3424	1.3997	-0.9462	0.0798	1466.
11.5074	30.1559	17.0000	30.8254	1232.	33.3391	1.4324	-0.9919	0.0895	1385.
11.4332	30.1658	16.0000	30.7244	1159.	33.3355	1.4681	-1.0420	0.1010	1303.
10.5425	30.0359	15.0000	30.6119	1087.	33.3313	1.5074	-1.0971	0.1149	1222.
9.7519	29.3111	14.0000	30.4860	1014.	33.3265	1.5507	-1.1579	0.1319	1140.
9.0304	29.7091	13.0000	30.3439	942.	33.3210	1.5990	-1.2251	0.1530	1059.
8.4026	29.4551	12.0000	30.1825	869.	33.3146	1.6532	-1.2996	0.1795	977.
7.3452	29.1716	11.0000	29.9965	797.	33.3070	1.7147	-1.3821	0.2137	896.
7.1936	28.3064	10.0000	29.7810	724.	33.2930	1.7851	-1.4733	0.2585	815.
6.5025	28.6529	9.0000	29.5275	652.	33.2868	1.8670	-1.5732	0.3192	733.
6.2345	28.4064	8.0000	29.2252	580.	33.2730	1.9638	-1.6800	0.4040	652.
5.3230	28.1797	7.0000	28.8587	507.	33.2551	2.0806	-1.7881	0.5276	570.
5.4170	28.0290	6.0000	28.4066	435.	33.2313	2.2255	-1.8810	0.7182	489.
5.0116	27.7355	5.0000	27.8393	362.	33.1930	2.4120	-1.9124	1.0342	407.
4.5542	27.5350	4.5000	27.5016	326.	33.1737	2.5278	-1.8696	1.2767	367.
4.1999	27.2476	4.0000	27.1232	290.	33.1430	2.6647	-1.7442	1.6159	326.
3.3818	27.1356	3.5000	26.7060	254.	33.1122	2.8299	-1.4657	2.1105	285.
0.0000	0.0000	3.0000	26.2678	217.	33.0646	3.0349	-0.8893	2.8726	244.
0.0000	0.0000	2.5000	25.8744	181.	32.9980	3.2987	0.3117	4.1366	204.
0.0000	0.0000	2.0000	25.7536	145.	32.8980	3.6560	2.9751	6.4635	163.

Pipe radius = 16.985 mm; Tip radius = 16.6141 mm; Meter radius = 16.985 mm; Axial width = 6.3754 mm; Hub radius = 7.3177 mm; Blade thickness = .381 mm

TABLE I. 18 Turbine Flow Meter Type E 1.5 ins (38.1 mm) diameter

COORS; #A567/DEL :=00

TURBINE FLOW METER TYPE E 1,5INCH CONSTANT BLADE ANGLE ROTOR BLADE ANGLE=30 DEGREE

PIPE RADIUS = 0,6687 METER RADIUS = 0,6687 TIP RADIUS = 0,6541 HUB RADIUS = 0,2881 AXIAL WIDTH=0,251

NO OF BLADES =6,000 BLADE THICKNESS =0,015 NO OF PICKUP =1,000 VISCOSITY(CENTI-POISE)=170,00

EXPERIMENTAL VALUE		THEORETICAL VALUE		BLADES	THEORETICAL VALUE (PULSES PER POUND)				
A	M.C.	Q	M.C.	RE=NO	T1	T2	T1K/Q	T3	PASS.RE
19.9012	30.6501	24.0000	31.1285	726.	34.2524	1.7833	-1.2210	0.1197	816.
19.4101	30.6042	23.0000	31.0413	696.	34.2506	1.8158	-1.2632	0.1303	782.
18.7015	30.5451	22.0000	30.9475	666.	34.2486	1.8505	-1.3082	0.1425	748.
18.2113	30.4152	21.0000	30.8462	635.	34.2464	1.8876	-1.3563	0.1563	714.
17.5010	30.4111	20.0000	30.7364	605.	34.2441	1.9275	-1.4077	0.1724	680.
16.8025	30.4020	19.0000	30.6172	575.	34.2414	1.9706	-1.4627	0.1910	646.
16.1122	30.3122	18.0000	30.4870	545.	34.2385	2.0171	-1.5215	0.2128	612.
15.3014	30.2111	17.0000	30.3444	514.	34.2352	2.0677	-1.5845	0.2386	578.
14.6522	30.1011	16.0000	30.1873	484.	34.2316	2.1230	-1.6519	0.2693	544.
14.0522	29.7617	15.0000	30.0135	454.	34.2274	2.1837	-1.7237	0.3064	510.
13.0125	29.5611	14.0000	29.8201	424.	34.2226	2.2509	-1.7999	0.3518	476.
11.6501	29.3312	13.0000	29.6035	393.	34.2171	2.3256	-1.8801	0.4080	442.
11.2513	29.2055	12.0000	29.3594	363.	34.2107	2.4094	-1.9631	0.4788	408.
10.5022	28.9011	11.0000	29.0822	333.	34.2031	2.5045	-2.0466	0.5698	374.
9.8213	28.5512	10.0000	28.7652	303.	34.1941	2.6135	-2.1259	0.6895	340.
9.0123	28.3021	9.0000	28.3997	272.	34.1829	2.7402	-2.1919	0.8512	306.
7.9512	27.8902	8.0000	27.9753	242.	34.1691	2.8899	-2.2265	1.0773	272.
6.9018	27.3816	7.0000	27.4806	212.	34.1512	3.0707	-2.1928	1.4071	238.
5.3524	26.8813	6.0000	26.9061	182.	34.1274	3.2950	-2.0110	1.9152	204.
4.8154	26.2612	5.0000	26.2586	151.	34.0941	3.5836	-1.4939	2.7579	170.
4.2111	25.8523	4.5000	25.9253	136.	34.0718	3.7628	-0.9789	3.4048	153.
3.5123	25.3012	4.0000	25.6166	121.	34.0441	3.9745	-0.1437	4.3092	136.
0.0000	0.0000	3.5000	25.3926	106.	34.0083	4.2302	1.2429	5.6284	119.
0.0000	0.0000	3.0000	25.3913	91.	33.9607	4.5474	3.6389	7.6609	102.

Pipe radius = 16.985 mm; Tip radius = 16.6141 mm; Meter radius = 16.985 mm; Axial width = 6.3754 mm; Hub radius = 7.3177 mm; Blade thickness = .381 mm

APPENDIX II

The Sommerfeld Solution of the Bearing Theory

Load capacity of Sommerfeld equation under the action of load W the shaft of rotor is displaced a distance of e from the bearing centre line. The Reynolds approximation for pressure distribution on the bearing shaft is (Ref. 95):

(II.1)
$$P = \frac{6\eta\, U \,.\, R}{C^{*2}} \cdot \int_0^{2\pi} \frac{d\breve{\theta}}{(1+\epsilon\cos\breve{\theta})^2} - \frac{h_0}{c^*}\frac{d\breve{\theta}}{(1+\epsilon\cos\breve{\theta})^3} \qquad \text{(II.1)}$$

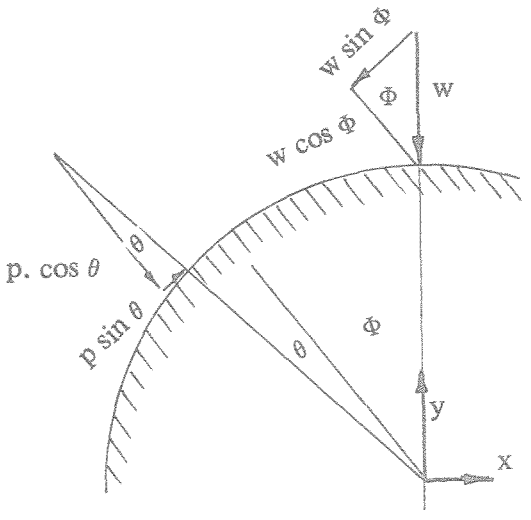

Fig. II.1. The balance of forces acting on turbine flow meter rotor shaft for long bearing theory.

The viscous fluid acts around the shaft and is directed to its centre. The equilibrium o of forces around the shaft is:

$$\int_0^{2\pi} L^* R \sin\breve{\theta}\, d\theta \,.\, p - W \sin\Phi = 0 \qquad \text{(II.2)}$$

$$\int_0^{2\pi} L^* R \cos\breve{\theta}\, d\breve{\theta} \,.\, p + W \cos\Phi = 0 \qquad \text{(II.3)}$$

Differentiating of (II.1) and substitution in (II.2) and (II.3) gives:

$$W \sin\Phi = \frac{12\eta\, nR^2 L^*}{c^{*2}} \int_0^{2\pi} \frac{\cos\breve{\theta}\, d\breve{\theta}}{(1+\epsilon\cos\breve{\theta})^2} - \frac{h_0}{c}\int_0^{2\pi} \frac{\cos\breve{\theta}}{1+\epsilon\cos\breve{\theta}}\, d\theta \qquad \text{(II.4)}$$

$$W \sin \Phi = 24\pi \cdot n L^* \left(\frac{R}{c^*}\right)^2 \frac{\epsilon}{(1-\epsilon^2)^{1/2}(2+\epsilon^2)} \tag{II.5}$$

The W cos $\breve{\theta}$ can be also calculated on the same way

$$W = [(W \cos \Phi)^2 + (W \sin \Phi)^2]^{1/2} \tag{II.6}$$

With substitution of (II.5) and the equivalent equation for W cos Φ into (II.6) is

$$W = 24. \pi\eta \, RnL^* \left(\frac{R}{c^*}\right)^2 \frac{\epsilon}{(1-\epsilon)^{1/2}(2+\epsilon^2)} \tag{II.7}$$

The journal friction force (Ref. 96)

$$Fj = \int_0^{2\pi} \tau_{Xj} L^* R d\breve{\theta} \tag{II.8}$$

$$Fj = \eta 2\pi \cdot n \cdot R \cdot L^* \left(\frac{R}{c^*}\right) \frac{4\pi(1+2\epsilon^2)}{(2+\epsilon^2)(1-\epsilon^2)^{1/2}} \tag{II.9}$$

Bearing shear stress is

$$\tau_{x\,B} = -\frac{h}{2R} \frac{dp}{d\breve{\theta}} \cdot \frac{2R\pi\eta}{h} \tag{II.10}$$

Bearing friction force becomes

$$F_B = 2\pi R \cdot \eta L^* \left(\frac{R}{c^*}\right) \frac{4(1-\epsilon^2)^{1/2}}{(2+\epsilon^2)} \tag{II.11}$$

The bearing torque will be (II.11) subtracted by (II.9) multiplied by shaft radius

$$T_{bear} = 24\pi\eta \cdot n L^* \left(\frac{R}{c^*}\right)^2 \frac{\epsilon}{(2+\epsilon^2)(1-\epsilon^2)^{1/2}} \, e \, . \tag{II.12}$$

APPENDIX III

Velocity Distribution in Tip Clearance Area

The friction at the blade tip imparts a tangential velocity component on to the fluid in the tip clearance. For calculation purposes the blades may be replaced by a rotating disc. The angular momentum of the fluid in the tip clearance is dependent upon the ratio of tangential to axial velocity component. The basic equation for the above motion is Prandtl's boundary layer equation which is the simplification of the Navier Stoke's equation. This is valid provided the ratio of tangential to the axial velocity is not very high. The typical velocity profile of such a rotating body at the blade tip exhibits a twist from axial to tangential direction. Therefore, the velocity will not only change the magnitude but also the direction of the flow between the casing of the rotor and the blade tip. At the blade tip the velocity is in the tangential direction only because of the friction between the fluid and the blade tip. Therefore, the angular velocity component of the blade tip is w, as it has no axial component. Outside the boundary layer the tangential velocity approach approaches zero and the absolute fluid velocity is the local axial velocity, u. Thus the resultant velocity component has a continuous change in direction until it is codirected to the axial velocity.

In the axial direction the Prandtl boundary layer equation of motion is:

$$u\frac{\partial u}{\partial x} + w\frac{\partial u}{\partial z} = \frac{UdU}{dx} + \frac{v^2\,dr}{rdx} + \frac{1}{\rho}\frac{\partial \tau_x}{\partial z} \qquad \text{III.1}$$

in tangential direction

$$u\frac{\partial v}{\partial x} + w\frac{\partial v}{\partial z} = -\frac{u\,.\,v}{r}\cdot\frac{dr}{dx} + \frac{1}{\rho}\frac{\partial \tau_y}{\partial r} \qquad \text{III.2}$$

The continuity equation is given by

$$\frac{\partial (ur)}{\partial x} + \frac{\partial (wr)}{\partial z} = 0 \qquad \text{III.3}$$

u,v,w are the velocity component in cartesian coordinate system and x, y lie in the tangential plane the simplified equation of the motion according to Schlichting boundary layer theory is given by

$$\frac{\partial u}{\partial x} + \frac{u\,\partial r}{r\,\partial x} + \frac{\partial w}{\partial z} = 0 \quad \text{continuity equation} \qquad \text{III.1a}$$

in x-direction

$$\frac{u\,\partial u}{\partial x} - \frac{v^2\,dr}{r\,dx} + w\,\frac{\partial u}{\partial z} = U\,\frac{dU}{dx} + v\,\frac{\partial^2 u}{\partial z^2} \qquad \text{III.2a}$$

in tangential direction

$$u\,\frac{\partial u}{\partial x} + \frac{u\,v\,dr}{dx} + \frac{w\,\partial v}{\partial z} = v\,\frac{\partial^2 v}{\partial r^2} \qquad \text{III.3a}$$

Within the boundary conditions

$$z = r_t \quad u = 0 \qquad \text{III. 4}$$

$$v = v_0 = r_t.\omega \qquad w = 0 \qquad \text{III.5}$$

$$z = r_0 - \delta \quad u = U \qquad v = 0 \qquad \text{III.6}$$

$$z = r \qquad u = U \qquad \text{III.7}$$

The momentum equation can be applied in the axial direction at the tip of the blade, so that the integration could be changed from $z = r_t$ to $z = r$ and reversing the condition from $z = r$ to $z = r_0 - \delta$ which is outside the boundary layer to the tip of the turbine blade. Integration of the equation (III.2a) and III.8 considering the continuity equation (III.1a) and shearing stress gives the momentum equation for the meter cascade.

$$U\,\frac{d\dot{v}_{Hx}}{dx} + U\,\frac{dU}{dx}\,(2\,\dot{v}_{Hx} + \delta^*_x) + \frac{1}{r}\,\frac{dr}{dx}\,(U^2\,\dot{v}_{Hx} + v_0\,\dot{v}_{Hy}) = \frac{\tau}{\rho} \qquad \text{III.9}$$

$$\delta_H^* = \int_{r_t}^{r} \left(1 - \frac{u}{U}\right) dr \qquad \dot{v}_H^* = \int_{r}^{r_0} \frac{u}{U}\left(1 - \frac{u}{U}\right) dr \qquad \text{III.10}$$

$$\dot{v}_{Hx_1} = \int_{r_t}^{r} \frac{u}{U}\left(1 - \frac{u}{U}\right) dr \qquad \dot{v}_{Hx_2} = \int_{r}^{r_0-\delta} \frac{u}{U}\left(1 - \frac{u}{U}\right) dr \qquad \text{III.11}$$

$$\dot{v}_{Hy_1} = \int_{r_t}^{r} (\frac{v}{v_0})^2 \, dr \qquad \dot{v}_{Hy_2} = \int_{r}^{r_0-\delta} (\frac{v}{v_0})^2 \, dr \qquad \text{III.12}$$

The velocity distribution in the meter axis at the blade tip is

$$\frac{u}{U} = 2t + 2t^3 + t^4 + k\frac{1}{6}(t - 3t^2 + 3t^3 - t^4) \qquad \text{III.13}$$

$$t = \frac{r - r_t}{\delta_x} \qquad \text{III.14}$$

$$k = \frac{\delta_x^2}{\nu} [\frac{dU}{dx} + (\frac{v_0}{U})^2 \frac{U}{r} \frac{dr}{dx}] \qquad \text{III.15}$$

$$t' = \frac{r - r_t}{\delta y} \qquad \text{III.16}$$

$$\frac{v}{v_0} = 1 - 2t' + 2t'^3 - t'^4 \qquad \text{III.17}$$

The boundary condition

$$t = 0 \quad r = r_t \quad u = 0 \quad \frac{\nu \partial^2 u}{\partial r^2} = U\frac{dU}{dx} - \frac{r_0^2}{r}\frac{dr}{dx}$$

$$t = 1 \quad r = r_t + \delta_x \quad u = U \quad \frac{\partial u}{\partial r} = 0 \quad \frac{\partial^2 u}{\partial r^2} = 0$$

$$t' = 1 \quad v = v_0 = r_t \cdot \omega \qquad \text{III.18}$$

$$t' = 1 \quad v = 0 \qquad \text{III.19}$$

The value of Q_c is as follows:

$$Q_c = U \int_{r_t}^{r_0} 2\pi r \frac{u}{U} dr - U \int_{r_0-\delta}^{r_0} 2\pi r \frac{u}{U} dr \qquad \text{III.20}$$

According to equation (III.13) for

$$Q_c = \int_{r_t}^{r_0} [\frac{2r^2}{\delta x} - \frac{2r^4}{\delta x} 3+ \quad \frac{r^5}{\delta x^4} + k\frac{1}{6}[\frac{r^3}{\delta_x} - \frac{3r^3}{\delta_x{}^2} + \frac{3r^4}{\delta_x{}^3}$$

$$- \frac{r^5}{\delta_x{}^4}] \ ] \ dr - \int_{r_0.-\delta_x}^{r_0} [\frac{2r^2}{\delta_x} - \frac{2r^4}{\delta_x{}^3} + \frac{r^5}{\delta_x{}^4} \quad +k \frac{1}{6} \ [\ \frac{r^2}{\delta_x}$$

$$- \frac{3r^3}{\delta_x{}^2} + 3 \frac{r^4}{\delta_x{}^3} - \frac{r^5}{\delta_x{}^4}] \ ] dr \qquad \text{III.21}$$

$$Q_c = 2[\frac{2}{3} \frac{r^3}{\delta_x} - \frac{2}{5} \frac{r^5}{\delta_x{}^3} + \frac{1}{6} \frac{r^6}{\delta_x{}^4} + \frac{k}{6}(\frac{1}{3} \frac{r^3}{\delta_x} - \frac{3}{4} \frac{r^4}{\delta_x} + \frac{3}{5} \frac{r^5}{\delta_x{}^3} - \frac{r^6}{\delta_x{}^4})]_{r_t}^{r_0}$$

$$- 2[\frac{2}{3} \frac{r^3}{\delta_x} - \frac{2}{5} \frac{r^5}{\delta_x{}^3} + \frac{1}{6} \frac{r^6}{\delta_x{}^4} + \frac{k}{6}(\frac{1}{3} \frac{r^3}{\delta_x} - \frac{3}{4} \frac{r^4}{\delta_x{}^2} + \frac{3}{5} \frac{r^5}{\delta_x{}^3} - \frac{r^6}{\delta_x{}^4})]_{r_0 - \delta}^{r_0}$$

III.22

$$Q_c = \frac{2}{\delta_x{}^2} (r_0{}^3 - r_t{}^3)(r_0 - r_t) \frac{r_0{}^2 + r_0 r_t + r_t{}^2}{6 \delta_x{}^2} (1 - \frac{k}{6}) - \frac{(r_0 + r_t)}{5\delta_x}$$

$$[2 - \frac{k}{2}] - \frac{2}{\delta_x} (3r_0{}^2 - 3r_0 + \delta_x{}^2) [\delta_x \frac{(3r_0{}^2 - 3r_0 + \delta_x{}^2)}{36 \delta_x{}^2}$$

$$(6 - k) - \frac{\delta_x(2r_0 - \delta_x)}{10 \delta_x} (4 - k) - \frac{k}{8} \delta_x] \qquad \text{III.23}$$

APPENDIX IV

Velocity Measurement using the Conventional LDA Systems

The LDA method has been intensively used in the measurements of velocity in various fluid conditions. A considerable number of optical set-ups have been developed in which three components of velocity are able to be measured simultaneously. However, the principle for LDA systems is rather straightforward and can be summarised as follows:

(a) Doppler Shift:

For moving particle illuminated by a plane electromagnetic wave, the scattered wave has a Doppler Shift as (Ref. 103), (see Figure 2).

$$\Delta\bar{\nu} = \bar{u} \cdot (\underline{r} - \underline{s})/\lambda = 2U_x \cdot \sin \bar{\alpha}/2$$

Fig. IV.1

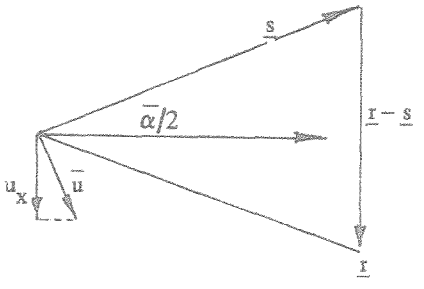

where u velocity vector for the moving particle

$\underline{s}$ propagation vector for incident wave

$\underline{r}$ direction of scattered wave

$\bar{\alpha}/2$ half angle between $\underline{s}$ and $\underline{r}$

λ wave length of incident wave.

Typical number may be seen in Table IV.1.

Table IV.1

	$\bar{\alpha}/2$	$\Delta\nu/u_x$ for λ = .6328 μm
Forward scatter	0°	0 MHz/(m/s)
Typical LDA	5°	0.27 MHz/(m/s)
Backscatter	90°	3.16 MHz/(m/s)

(b) Most common systems (Ref 104)

(i) Reference beam

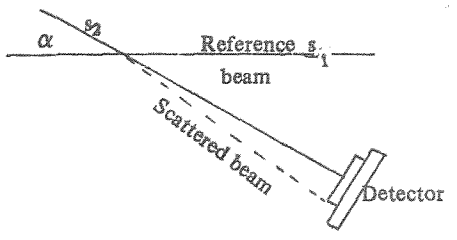

$$\nu_1 = \nu_0 + \bar{u} \cdot (\underline{r} - \underline{s})/\lambda$$

$$\nu_2 = \nu_0$$

$$\Delta\nu_0 = \nu_1 - \nu_2 = \bar{u} \cdot (\underline{r} - \underline{s}_1)/\lambda$$

Scattered and s_2 have no doppler shift. Therefore beating s_2 and scattered from s_1 and scattered from s_2 and scattered from $\underline{s}_1$ are identical.

(ii) Crossed beam system

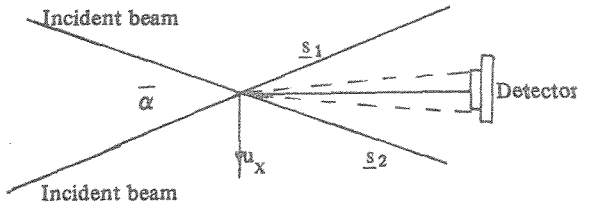

$$\nu_1 = \nu_0 + \bar{u} \cdot (\underline{r} - \underline{s}_2)/\lambda$$

$$\nu_2 = \nu_0 + u \cdot (\underline{r} - \underline{s}_2)/\lambda$$

$$\Delta\nu_0 = u \cdot (\underline{s}_2 - \underline{s}_1)/\lambda$$

(iii) Dual scattered system

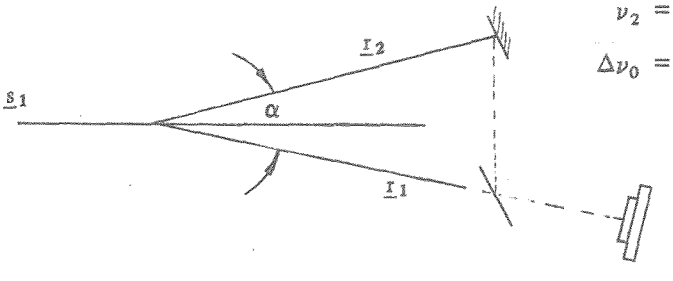

$$\nu_1 = \nu_0 + \bar{u} \cdot (\underline{r}_1 - \underline{s}_1)/\lambda$$

$$\nu_2 = \nu_0 + \bar{u} \cdot (\underline{r}_2 - \underline{s}_1)/\lambda$$

$$\Delta\nu_0 = \bar{u} \cdot (\underline{r}_1 - \underline{r}_2)/\lambda$$

All $\Delta\nu_0 = 2u_x \sin \bar{\alpha}/2 \cdot \lambda$

The above systems are basically "beating" two beams where one or both have been doppler shifted to isolate the shifted frequency, (ν_0), and hence to evaluate the velocity information of the particles in the fluid system.

(c) Signal processors

The typical signal in LDA systems is plotted as follows (Ref. 104)

Fig. IV.3

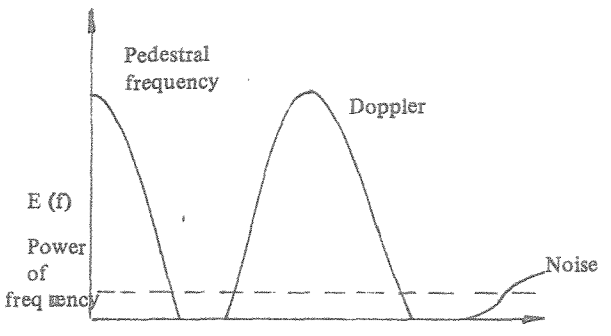

Fig. IV.4

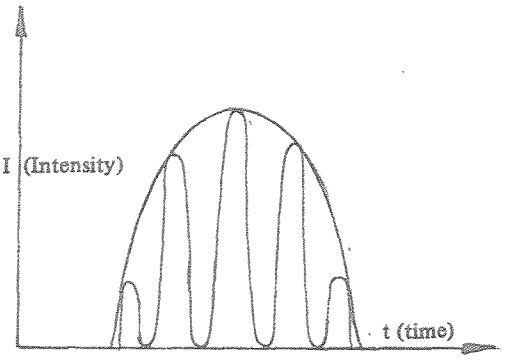

Figure IV.3 shows a typical LDA signal displayed in frequency domain. Figure IV.4 shows the ideal optical intensity signal in a crossed beam system as one scatterer passes through the intersection region.

(i) Spectrum analysis for Doppler frequency (Ref. 105)

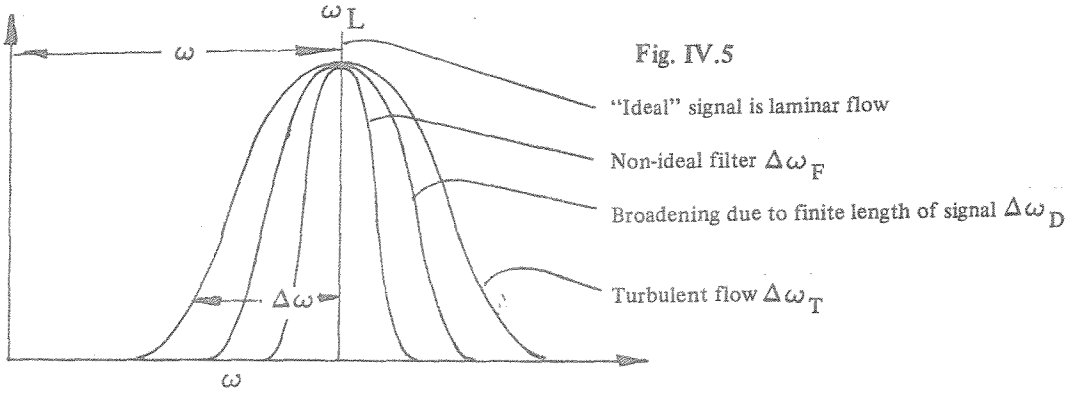

Fig. IV.5

where $\Delta\omega_F{}^2 + \Delta\omega_D{}^2 + \Delta\omega_T{}^2 = \Delta\omega$

Consequently, the ω_L gives the mean velocity and $\Delta\omega$ shows the intensity of turbulence, provided the $\Delta\omega_F$ and $\Delta\omega_O$ are known or can be estimated.

The typical results for ω_D estimated by Goldstein and Hagen (Ref. 106) are listed in Table IV.2.

Table IV.2

Transit time broadening	$\Delta\omega_D \approx 2 - 10\%$
Laser line broadening	$\Delta\omega_O \approx 10$–$100$ Hz
Brownian motion	$\Delta\omega_R \approx 10$ Hz
Velocity gradients	$\Delta\omega_{G_1} \approx 0$–$100\%$
Turbulent fluctuations	$\Delta\omega_T \approx 0$–30%

(ii) Types of signal processor

(a) Special techniques

Spectrum analyser

Analog correlator

Photon counting correlator

(b) Frequency to Voltage Converters

Tracker (D/A converter necessary for assessment of computer)

Counter

Filter Bank

Direct to Computer

The special techniques do not give an instantaneous velocity value. Spectrum analysers generally sweep through the frequency range of interest, displaying the frequencies present as peaks on some types of display. Correlators do not operate fast enough to give a good measurement when there are only a few Doppler cycles.

The tracker, counter, and filter bank, are all methods to obtain a nearly 'instantaneous' (dependent on the response time of instruments), conversion of the frequency to voltage. A fast analog to digital converter with subsequent computer data processing can also be used.

Since tracker, counter and photon correlator are the most popular systems engaged in the LDA technique, and hence the comparison of them is summarised as follows.

	Tracker	Counter
Required S/N ratio	Low	High
Dynamic range (Frequency)	Good	Very good
Slew rate	Good	Limited only by processing time ($>1\mu s$)
Capture bandwidth	Limited	Limited only by filters
Ease of use	Good	Fair
Cost	Medium	High

The information recorded in this list is estimated by using the instruments produced by Thermo-Systems Inc.

Photon correlator (Ref. 107).

The photon correlator is basically the same as a standard correlator with a special input section for pulse counting. The usual correlator has an A/D converter on the input and the

correlations are then made on the digital word. The advantage of using the photon correlator is to achieve the velocity information while the scattered signal is very weak or discrete. The major disadvantage of the photon correlator is the incapability of real time velocity measurement.

(d) Data analysis

The choice of the best method of data analysis depends on many, often interrelated factors, the single most important factor is the burst density.

Apart from burst density a few other factors have to be considered, they are:

(i) particle size (and number of density concentration)

(ii) spatial/temporal resolution

(iii) photocurrent signal to noise ratio

(iv) signal processing method

(v) signal validation method

(vi) type of information required

(i) mean velocity

(ii) fluctuation statistics

(i) Particle size:

The larger the size of particle, in general, gives good S/N ratio, but the large particle cannot follow the flow faithfully. Thus from Choa's (Ref. 108) method the typical size can be summarised as:

Particle	Fluid	Density ratio	Diameter (μm) f = 1kHz	10kHz
Silicon Oil	Air	900	2.6	0.8
PVC	H_2O	1.54	16	5.0

(ii) and (iii) may be minimized by specific instrument characteristics. (iv), (v). The correct selection of iv and v has to be done by considering the following points:

1) For high density burst:

The characteristics for high density burst signal is the output signal from a signal processor is a continuous voltage. It may have some dropouts because of signal validation circuitry. However, the dropout durations are usually short (< a few doppler cycles) so the velocity changes very little during these periods. The processor signal contains noise

due to the random addition of multiple particle signals. This noise is normally dominant, but in addition the processor signal will also contain noise where the input signal is a single pure sinosoid.

Edwards (Ref. 105), has demonstrated that the frequency demodulation method has little or no effect on the phase noise or the mean biases. However, in signal validation effects can be more important in the high density burst situation.

To obtain mean velocity information, the simple time average using a low pass filter is the normal procedure for obtaining the mean value for almost all measuring devices. However, for the fluctuation velocity spectrum, the phase noise or band width of photo current spectrum of processor filter has to be known or properly set. As regards the spectra, the phase noise spectra is added to the true velocity spectrum and it becomes dominant at high frequencies where the velocity spectrum is falling off rapidly.

2) Low burst density signals

The typical characteristic in the low burst density signals is the output signals are often discrete, and hence data biases occur due to:

number of fringes crossed

velocity

signal procesor biases

velocity (also significant for high burst density i.e. liquids) gradients across measuring volume.

The methods of taking data are normally (Ref. 103) standard analogue techniques when the signal is nearly continuous (Ref. 104), take individual data points as they occur. At very low turbulence intensity, most data processing techniques give the right answer. However, at very high turbulence intensity the method (Ref. 103) may work if signals of interest are essentially continuous and (Ref. 104) is necessary if at low data rates.

3) Remarks:

The above data processing methods are essentially a statistical representation of velocity information for measured fluid. For a very high turbulence intensity such as the separation of boundary layer or eddies measurements, the direction of velocity may be the major interest to measure. In these cases, the discussed methods cannot provide the direction f of velocity uniquely. Thus, a frequency shift (ω_s) needs to be imposed in the incident wave before it propagates into the fluid. Subsequently, the detected frequency shift (ω_{sd}) in comparison with (ω_d) which has been detected without pre-shifted incident wave will

give the direction of velocity in the fluid. The pre-shifted frequency normally provided by inserting a scattering disc or diffraction disc (or Bragg cell) in the optic path. With known direction of the disc the true Doppler shift may be obtained by

$$\omega_{ws} = \omega_d \pm \omega_s$$

as well as the direction.

BIBLIOGRAPHY

1. Biryukov, B.V. — "Errors in equipments for calibrating and testing turbine flow meters". *Measurements Techniques USSR.* 1968 page 1193.

2. Bolwell, A.J. — "Gas bearing improves efficiency of turbine flow meter". *Design News Vol. 24,* 1969. page 40.

3. Burgin, B.J. — "Turbine meter measurement on a transmission system" *Gas Vol. 49,* February, 1973. pp 30-32.

4. Calame, H. — "Die Erfassung von durchfluss und Menge nach volumetrische elektrischen, dynamischen Messverfahren". *Tech. Mitteilung,* June 1967, Heft 6/7, pp 272-277.

5. Campbell, W.B. Slattery, J.C. — "Flow in entrance of a tube". *Journal of Basic Engineering, Vol. 41,* March 1963.

6. Comolet, R. Fernez, L. — "Study of turbine type flow meter with helical blades" 4th Conference on Fluid Machinery, Budapest, 1972. pp. 251-266.

7. Davis, H. Kottas, H., Moody, A.M.G. — "The Influence of Reynolds number on the performance of Turbo machinery". Transactions on the ASME, July 1951, pp. 499-509.

8. Dijstelbergen, H.H. — "Performance of a swirl flow meter". *Journal of Physics E. Vol. 3,* pp. 886-887.

9. Dittrich, G. — "Das Messverhalten der Woltmann und Flugelradzahler" VID Berichte Nr. 86, 1964, pp. 109-114.

10. Dunlop, A.R. — "New Turbine type meters for custody transfer". *The Oil and Gas Journal,* Sep. 1958, pp 83-85.

11. Edge, R.M. — "The operation and calibration of a miniature turbine flowmeter with gases at low flow rate" *Journal of Physics E Vol. 1,* 1968, pp. 35-40.

12. Eggers, G. — "Woltmann Zahler fur Flussigkeiten". *Archiv fur Tech. Messen J.* 1235-1 May 1937. pp. 66-69.

13. Engelhardt, H. — "Stromungtechnische Grundlagen derTurbinen zahler" VDI Berichte Nr. 86, 1964, pp. 77-84.

14. Fernez, L. — "Etude de turbines debitmetriques a pales helicoidales" These de doctorat-ingenieur Universite de Paris VI.

15. Fischer & Porter Co. — "Selection guide for turbine flowmeters" Tech. Information 10C - 1 Dec 1967 10C - 2 Oct. 1971.

16. Fischer & Porter Co. — "Turbine flowmeters – Predictable performance" Tech. Information 10C - 8 Apr. 1969.

17. Gersten,K. "Experimentelle Beitrag zum Reibungseinfluss auf die Stromung durch ebene Schaufelgitter" *Abhandlung des Braunschweigischen wissenschaftlichen Gesellschaft.* Vol. 7, 1955, pp 93-99.

18. Gersten, K. "Der Einfluss der Reynoldszahl auf der Stromungsverlustre in ebene Schaufelgitter" Institut fur Stromungsmechnik. TH Braunschweig 1958, pp 5-19.

19. Grey, J. "Calibration of turbine flowmeters for cryogenic operation". *ARS Journal Feb. 1960,* pp. 192-193.

20. Grey, J. "Transient response of turbine flowmeter" *Jet Propulsion.* Feb. 1956, pp 98-99.

21. Griffiths, C. "The design and application of the insertion turbine flowmeter". *EFM Information,* pp 1-24.

22. Hengstenberg, J. "Aufbau und Eigenschaft von Volumenzahlern fur Flussigkeiten". *Tech. Mitteilung Heft 8,* August 1963, pp. 319-325.

23. Higson, D.J. "The transient performance of a turbine flowmeter in water". *J. Sci. Instrum. Vol. 41,* 1964, pp. 317-320.

24. Hochreiter, H.M. "Dimensionless correlation of coefficients of turbine type flow meters". Transaction of the ASME Oct. 1958, pp. 1363-1368.

25. Ives, G.O. "Proving liquid turbine meters". *Pipeline and Gas Journal* August 1970, pp. 56-61.

26. Jepson, P. "Current meter error under pulsating flow condition". *J. Mech. Eng. Vol. 9,* 1967. p. 45.

27. Jepson, P. "Effect of upstream velocity profiles on turbine meter registration". *J. Mech. Eng. Vol. 11.* pp. 503-510, 1969.

28. Jepson, P. "Method of measuring time const. of current meter and turbine type flowmeter". *J. Sci. Instr. J. of Physics E. Vol. 44,* pp. 17-20, 1967.

29. Jepson, P. "Transient response of a helical flowmeter". *J. Mech. Eng. Sci. Vol. 6, No. 4,* 1964, pp. 337-342.

30. Kalkhof, H.G. "Menge Messung von Flussigkeiten". *Hanser Verlag Munchen.* p. 7.

31. Kalkhof, H.G. "Zur Fehlerherve der Turbinenradzahler". *Erdol und Kohle Erdgas Petrochemie Nr. 10,* Oct. 1968, pp. 627-632.

32. Kalkhof, H.G. "Zur theorie der mittelbaren volumenzahler". Bopp und Reuther GmbH Mannheim, pp. 3-7.

33. Lakshminarayana, B. Horlock, J.H. — "Secondary flows and losses in cascade and axial flow turbomachines". *Inst. J. Mech. Sci. Pergamon Press, Vol. 5,* 1963. pp. 287-305.

34. Lee, W.F.Z., Evans, H.G. — "Densith effect and Reynold's number effects on gas turbine flowmeters". *Journal of Basic Engineering,* Dec 1965, pp. 1043-1060.

35. Lee, W.F.Z., Karlby, H. — "Metering Crude oil with a turbine has much to reco recommend it". *The Oil and Gas Journal Vol. 57,* No. 51, Dec. 1959, pp. 92-96.

36. Lee, W.F.Z., Karlby, H. — "A Study of viscosity effect and its compensation on turbine type flowmeter". *Journal of Basic Engineering 1959,* Paper No. 59-A-105, pp. 717-728, pp 1-9.

37. Lee, W.F.Z., Evans, H.J. — "A field method of determining gas turbine meter performance". *Journal of Basic Engineering,* Dec. 1970, pp. 724-731.

38. Lehmann, N. — "Turbinenzahler fur gross durchflussstarkern und hohe viskositat". *VDI Berichte Nr. 86* 1964, pp. 1112-1114.

39. Minkin, H.L., Hobart, H.F. — "Preliminary calibration on some head type and turbine type flowmeters". *National Aeronautics and Space Administration Tech. Note D. 577.*

40. Minkin, H.L., Warshawsky, I., Hobart, H.F. — "Performance of turbine type flow meters in liquid hydrogen". NASA TN-D3770, pp. 1-21.

41. Molnar, K. — "Electronic compensation of viscosity dependence of turbine flowmeter". *Microtecnic Vol. 27,* pp 372, 1973.

42. Muesmann, G. — "Zusammenhang der stromungseigungschaften des laufrades eines axial geblases mit denen eines binzel flugels". *Zeitung fur flugwissenschaften,* Dec. 1958, Heft 12, pp. 345-362.

43. Myles, D.J., Harrison, P. — "Turbine flowmeters". *Control,* June, 1963.

44. Howell, A.R., Carter, A.D.S. — "Fluid flow through cascades of aerofoils". *6th Int. Cong. App. Mech.* Paris 1946.

45. Dowdell, R.B., Liddle, A.H. — "Measurement of pulsating flow with propeller and turbine type meters". *Transaction of ASME 1953,* Vol. 75, pp 961-968.

46. Alspach, W.J., Miller, C.E., Flynn, T.M. — "Flow measurement Part 2: Meas. flow meters in cryogenics". *Mech. Eng. 1967.* Vol. 89, pp. 105-113.

47. Alspach, W.J. — "Considerations when using turbine type flow meters in cryogenic service". *Advance in Cryogenic Engineering,* Vol. 10, Sec. F-3, pp 246-252.

48. Himmelskamp, H. — Profiluntersuchung an einem Umlanfenden Propellor Mittelung aus dem Max Planck Institut fur Stromungs-forschung Goettingen, pp. 20-36, 1950.

49. Caldwell, B.J. — "Flow measurement Part 4: the fuel gas industry". *Mech. Eng.* 1967, Vol. 59, pp. 6-8.

50. Crosscombe, A.T. — "The turbo-meter: new measuring device for gas" *Canada Gas Journal* 1966, Vol. 59, pp. 6-8.

51. Grant, D.J. — "Precision flow measurement techniques for low thrust auxiliary propulsion liquid rockets". NASA-TM-X-55967, 1967.

52. Betz, A. — "Introduction to the theory of flow machines". Pergamon Press, London 1st. edition, p. 250.

53. Hallman, A. — "Pulsation errors in turbine flowmeters". *Control Engineering* 1965, Vol. 5, pp. 89-91.

54. Dijstelbergen, H.H. — "Rotameters and turbine flowmeters in pulsating flow measurement". Paper presented at a symposium on the measurement of pulsating flow University of Surrey, Guildford, 2-3 April, 1970, pp. 66-73.

55. Dijstelbergen, H.H. — "Dynamic response of turbine flowmeters". *Instrument Revue* 1966, pp. 241-244.

56. Bucknell, R.L. — "Calibration systems and turbine type flow transducers for cryogenic flow measurement". Advances in cryogenic engineering, 1963, Vol. 8, Sec. F-5, pp. 360-369.

57. Jeffs, A.T. — "Comparative tests of turbine flow meters with cryogenic fluids". RPE Technical Note No. 229, March 1964.

58. Bowers, K., Galley, R.L. Vincelett, P.S. — "Flow measurement in rocketry". *Instrument Control System Vol. 34,* 1961, pp. 638-640.

59. Prandtl, L., Tietjens, O.G. — "Applied Hydro-and Aeromechanics". Dover Publication, New York, pp. 201-207.

60. Pursley, W.C. — "Flow Measurement Memo". National Engineering Laboratory 1974.

61. Quarmby, A. — "A Calibration of a Turbine Flowmeter". *J. Roy. Aer. S. Vol. 70,* 1966. p. 725.

62. Rubin, M., Fox, W.G., Miller, R.W. — "Driving torques in a theoretical model of turbine meter". *Journal of Basic Engineering, Transaction of the ASME* 1965, pp. 1-8.

63. Ruegg, F.W. Shafer, M.R. — "Liquid Calibration Techniques". Transaction of the ASME October 1958.

64. Salami, L.A. "Turbine type flowmeter calibration". Dept. of Mech. Eng. University of Southampton, April 1971.

65. Salami, L.A. "Swirl effects on turbine type flow meters and effectiveness of different types of flow straighteners". Dept. Mech. Eng. University of Southampton, Report No. ME/72/3

66. Schlichting, H. "Boundary layer Theory". 1968.

67. Schlichting, H. "Three dimensional boundary layer flow". Conference IAHR – Belgrade, 1961.

68. Schlichting, H. "Anwendung der Grenzschicht theorie auf Stromungsprobleme der Turbomaschinen". Siemens Zeitschrift Heft 7, July 1959.

69. Schlichting, H. "Ergebnisse und Probleme von Gitteruntersuchungen" Zeitschrift fur Flugwissenschaft Heft 5, Oct. 1953.

70. Schlichting H. "Problems and Results of Investigation on Cascade Flow". *Journal of Aeronautical Sciences,* March 1954, pp. 163-178.

71. Scott, R.W.W. "Turbine flowmeters". Equipment surveys: Year Book 1967, pp. 688-699.

72. Shafer, M.R. "Performance Characteristics of turbine flowmeters". *Journal of Basic Engineering,* Transaction of the ASME Dec. 1962. pp. 1369-1379.

73. Shamp, F.F. "Metering cryogenic liquids". *Oil and Gas Journal* 1970, Vol. 8, pp. 112-114.

74. Sievert, G. "Entwicklungstendenzen in der Flussigkeitzahler technik". *Erdol Kohle Erdgas Petrochemie.* November 1963, Nr. 11.

75. Sive, R. "Turbine flowmeter in fuel oil service". *Instrumentation Technology, Vol. 20,* 1973. pp. 39-41.

76. Slavnits, B.N. "Method of testing turbine flowmeter for industrial liquids". *Measurements Techniques USSR. Vol. 16,* 1973, pp. 1658-1659.

77. Speidel, L. "Brechnung der Stromungsverluste von ungestaffelten ebene Schaufelgittern". *Ingenieur – Archiv. Heft 5,* 1954.

78. Steven, G.H. "Dynamic calibration of turbine flowmeters". *Instr. Contr. Vol. 43,* 1970, pp. 109-111.

79. Stringer, J.A., "UK pipeline turbine meters are used for custody transfer". *Oil and Gas Journal,* Vol. 65, pp. 145-146.

80. Strohmeier, W.O. "Turbine flowmeters: past, present and future". Fisher and Porter Co. Warminster, Penna. 18974.

81. Strohmeier, W.O. "Bearings for turbine flowmeter". *Instrumentation Technology, Vol. 19,* pp 39, 1972.

82. Strscheletzky, M. "Spaltverluste bei axial stromungsmaschinen". Forschung auf dem gebeit des ingenieurwesen Nr. 4, Band 21, 1955, pp. 101-106.

83. Stubbs, P.S. "Flow measurement in gas pipelines". *Gas World 1970,* Vol. 172, pp. 331-333.

84. Sunley, H.L.G., Simpkin, A.J., Townsend, W.G. "The effect of viscosity upon performance of turbine type flowmeters". *Spaceflight, Vol, 8.* 1966, p. 283.

85. Tan, P.A.K., Hutton, S.P. "Experimental, Analytical and Tip-clearance loss Studies in Turbine Type Flowmeters". *Proc. Int. Conf. Modern Develop. Flow Measurements,* Harwell, 21-23 September, 1971. Ed. C.G. Clayton. Pub. Peter Peregrinus Ltd., pp. 321-345.

86. Tan, P.A.K. "Experimental and analytical studies of turbine type flowmeter". Report No. 1 Feb. 1971, Ph.D. 1974. Report No. 2 July 1971, University of Southampton.

87. Thomson, R.E. Grey, J. "Turbine flowmeter performance model". Transaction of ASME. *Journal of Basic Engineering* Dec. 1970. pp. 712-723.

88. Werner, H. "Konstruktive Ausfuhrung und Eigenschaften von Turbinenzahler". *VDI Berichte Nr. 86,* 1964 pp. 91-103.

89. Withers, V.R., Chesters, D.A., Inkley, F.A. "Flow characteristics of turbine flowmeters". *Proc. Int. Conf. Mod. Develop. Flow Measure.* Sept. 1971, Ed. C.G. Clayton, Pub. Peter Peregrunus Ltd., pp. 305-319.

90. Woodrings, E.D. "Magnetic turbine flowmeters". *Instr. Contr.* Vol. 42, 1969, p. 133.

91. Yard, J.S. "Characteristics and uses of turbine flowmeters". *ISA Journal* May 1959. Vol. 6, No. 5, pp. 54-49.

92. Blackmore, C.S. "An investigation of confined turbulent swirling flow using an L.D.V." Ph.D. 1975, Dept. Mech. Eng. University of Southampton.

93. Bedi, P.S., Thew, M.T. "Flow measurement in the presence of strong swirl using a laser doppler anemometer". *Proc. Int. Conf. Mod. Develop. Flow Measure.* 1971. Ed. C.G. Clayton, pp. 61-77.

94. Ballantyne, A., Blackmore, C.S., Rizzo, J.E. — "Frequency shifting for laser anemometers by scattering". *Optics and laser technology,* August, 1974, pp. 170-173.

94a. Raimondi, A.A., Boyd, F. — "A solution for the finite journal bearing and its application". Contributed by ASLE committee on bearing and bearing lubrication presented by American Soc. of Lubrication Engineers, Pittsburgh, Pa. Apr. 1956, Part I, II, III.

95. Neale, M.F. Dowson, D., Duncan, A.B. — "Calculation Method for Steadily loaded pressure fed Hydrodynamic Journal Bearings". Sept. 1966, ITEM No. 66023. Eng. and Sci. Data Section I to IV.

96. Rhoden, H.G. — "Effect of Reynolds number on the flow through a cascade blades." *Aeronautical Research Council,* Report Memoranda No. 2919, 1956.

97. Salami, L.A. — "Scale and Reynolds number effects on some axial turbomachines". Ph.D. Thesis, 1971, Ch. 5, Mech Eng. Dept. University College Cardiff.

98. Wolf, H. — "Tip losses in linear cascade of blades". *Zeitschrift der Techniche Hochschule Dresden.* Vol. 2, p. 10, 1961.

99. Dean, R.C. — "The influence of tip clearance on boundary layer flow in a rectilinear cascade". *G.T.L. Reports 27-3* M.I.T. 1954.

100. Mellor, G.L., Strong, R.E. — "End wall effect in axial compressors". ASME Paper No. 16, FE – 16 1967, p. 435.

101. Smith, L.H. — Casing Boundary layer in multistage axial flow compressor: Flow research on blading". L.S. Dzung, Elsevier, 1970, pp. 330-335.

102. Vevra, M.H. — "Aero-Thermodynamics and flow in turbomachines". J. Wiley, and Son, Inc. New York, 1960. pp. 210-15.

103. Born and Wolf. — "Principle of Optics", Pergamon Press, (4th Ed. 1970). London.

104. Greated and Durrani. — "Laser Systems in Flow Measurement". Plenum Publishing Co. NY (1976).

105. Edwards, R.V., Hugus, J.C., French, M.J. & Dunning, J.W. Jr. (1971) — *J. Appl. Phys.* 42, pp.837.

106. Goldstein, R.J. and Hagen, W.F. (1976) — *Phys. Fluids,* 10, P. 1349.

107. Pike, E.R., Jackson, D.A., Bourke, P.J. and Page, D.I. (1968). — *J. Phys., E. Sci. Instru.* 1.

108. Chao, B.T. (1964) Ostereicheisches Ingeniur Archiv. 18, p. 7.

109. Edwards, R.W. (1975) In *Proc. of 4th Biennial Symposium on Turbulence in Liquids,* Rolla, Missouri, Sept.

Figure 1. Functional system diagram of test rig.

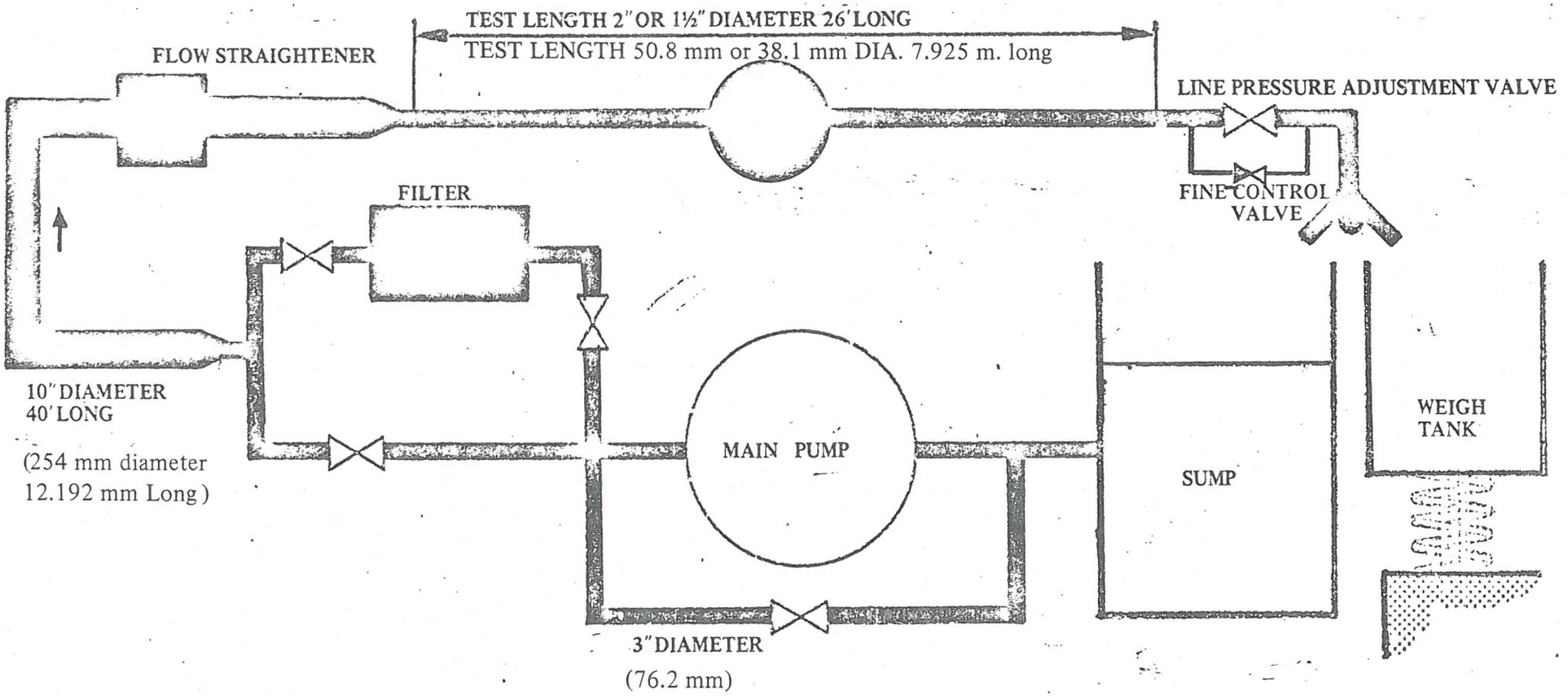

Figure 2. FUNCTIONAL AND CONTROL OF TEST RIG

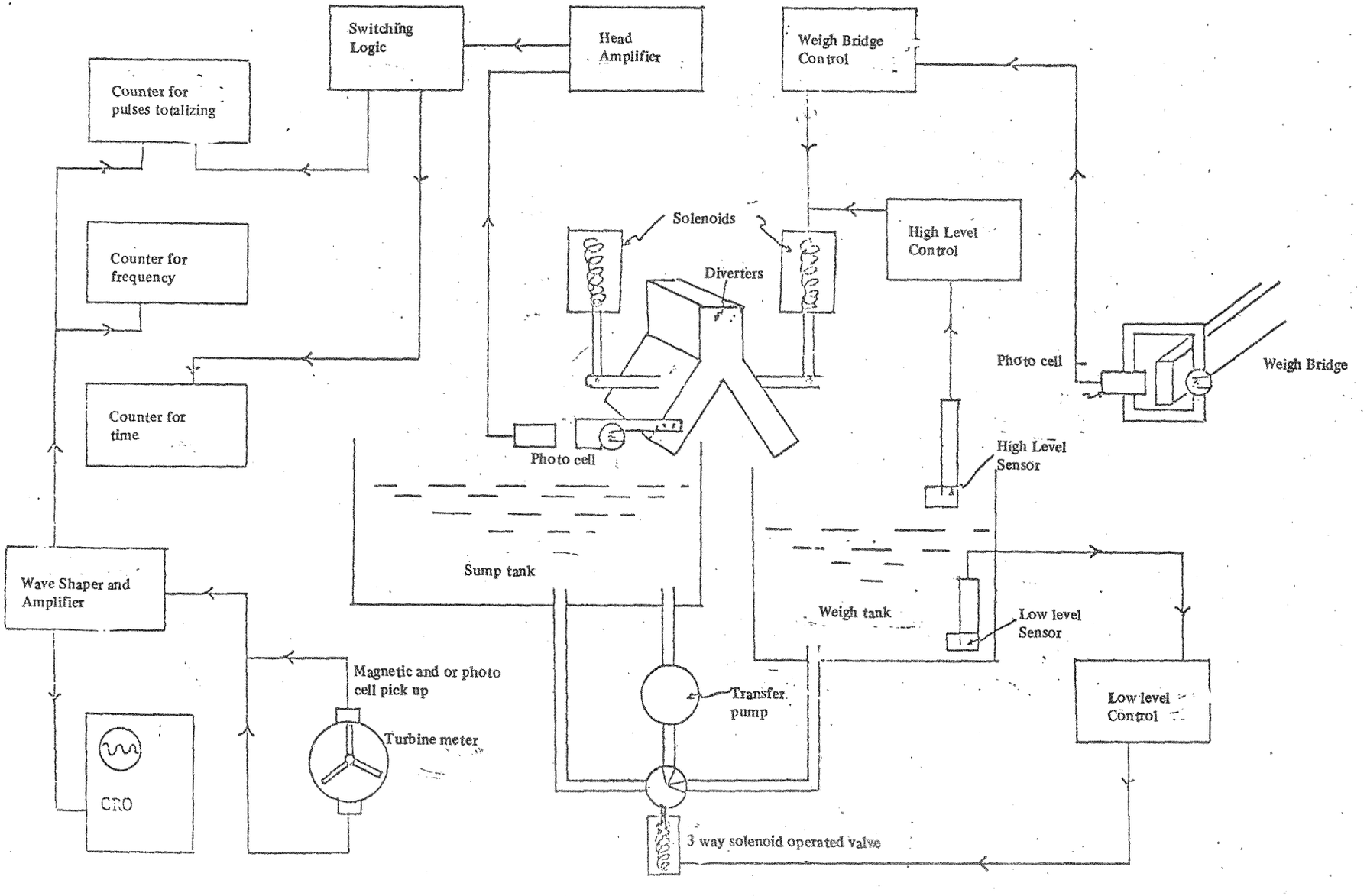

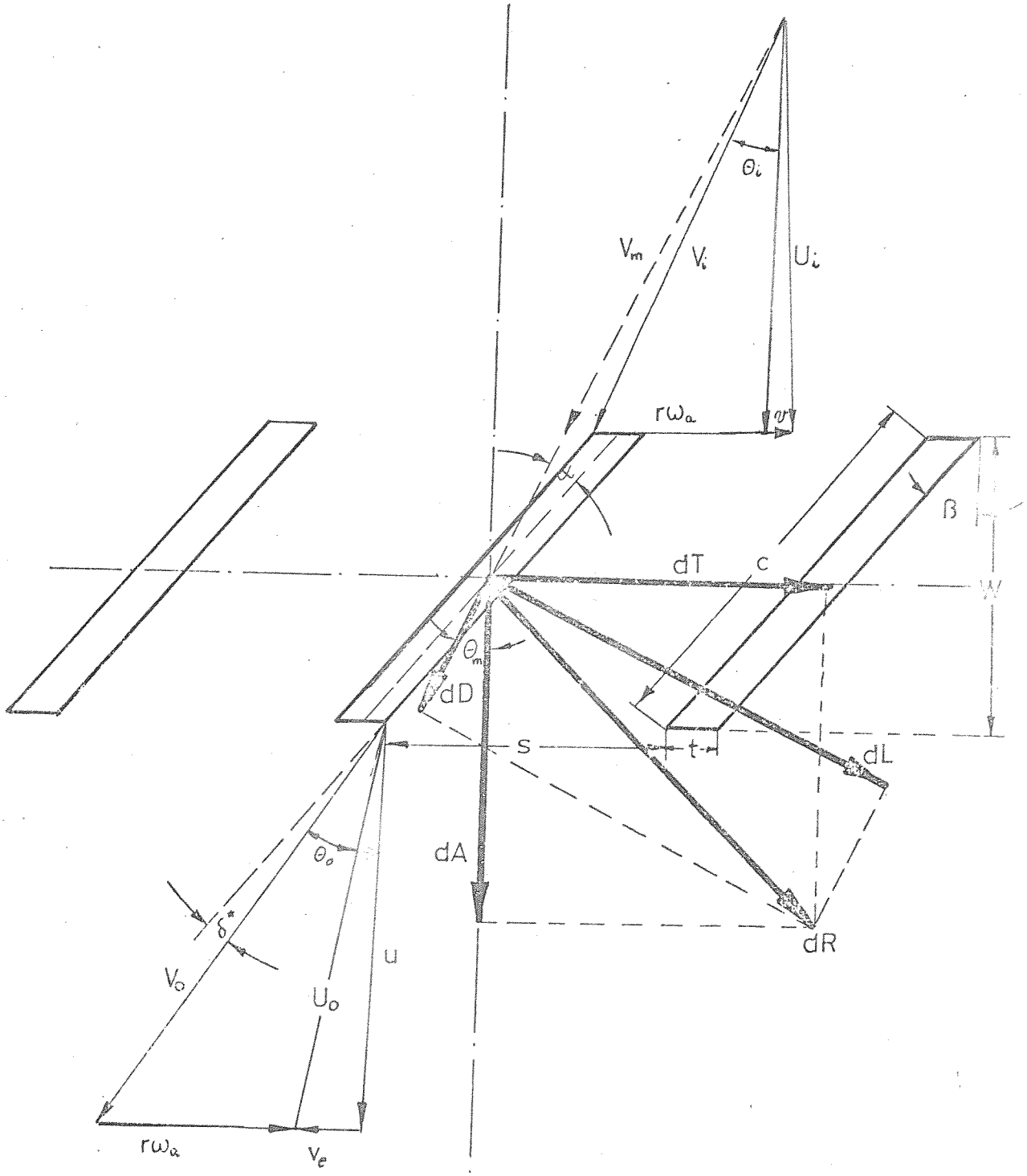

Fig. 3 Velocity diagram at radius r on elemental blade dr and the hydrodynamic forces acting on the blade. In the case of friction–less fluid, the resultant force dR is perpendicular to the direction of mean fluid velocity Vm

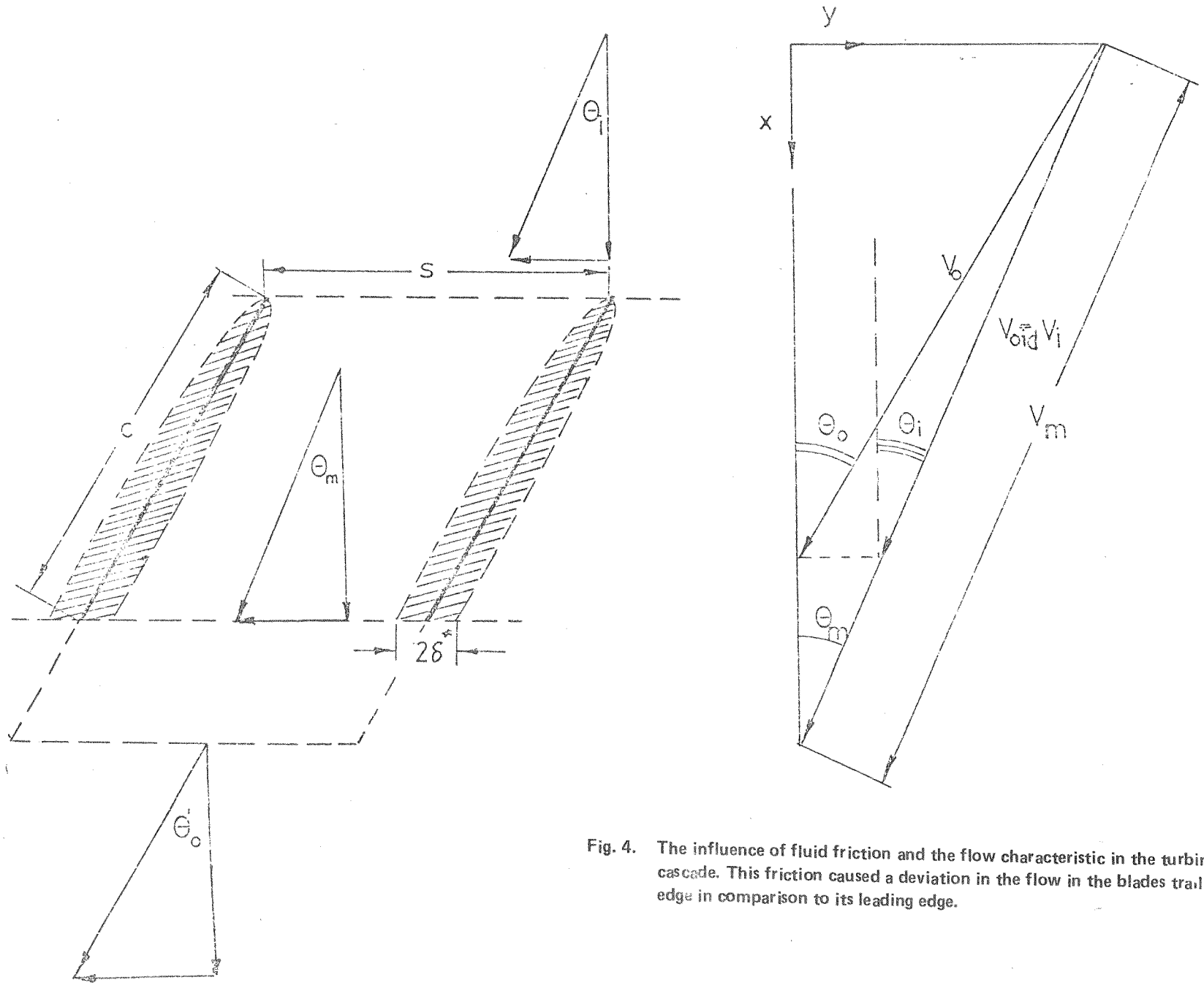

Fig. 4. The influence of fluid friction and the flow characteristic in the turbine cascade. This friction caused a deviation in the flow in the blades trailing edge in comparison to its leading edge.

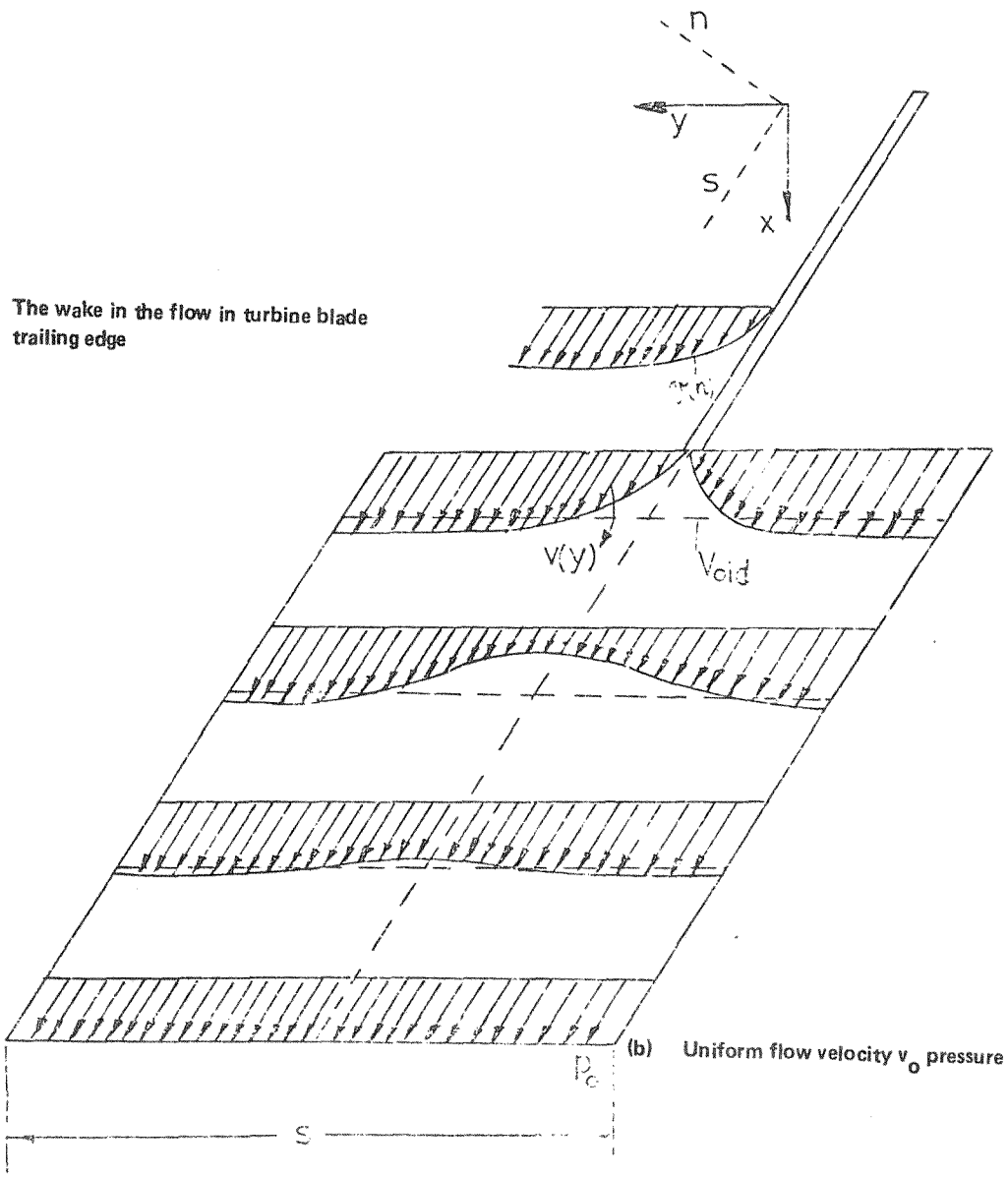

Fig. 5. The wake in the flow in turbine blade trailing edge

(a) Velocity inside of the boundary layer v(n) Velocity outside of the boundary layer v_m pressure p_m

(b) Uniform flow velocity v_o pressure p_o

Fig. 5C. The velocity diagram for tip clearance flow dependent on angle of attack.

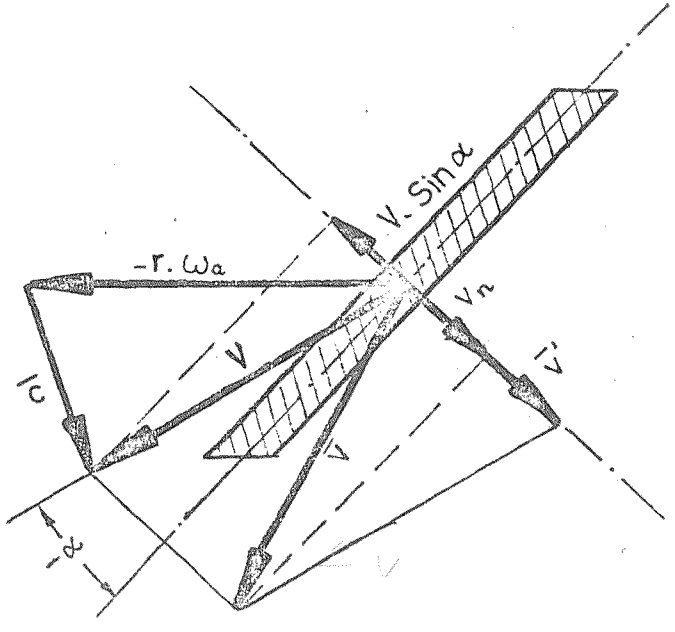

5Ci The demonstration of the flow in tip clearance at a negative angle of attack. The tip clearance flow dependence on the magnitude of V sin α against $-v_n$ which is either a co- or counter directional flow relative to the main flow. The constant bladed rotor had a negative angle of attack. The sign of this angle was dependent on the local axial fluid velocity.

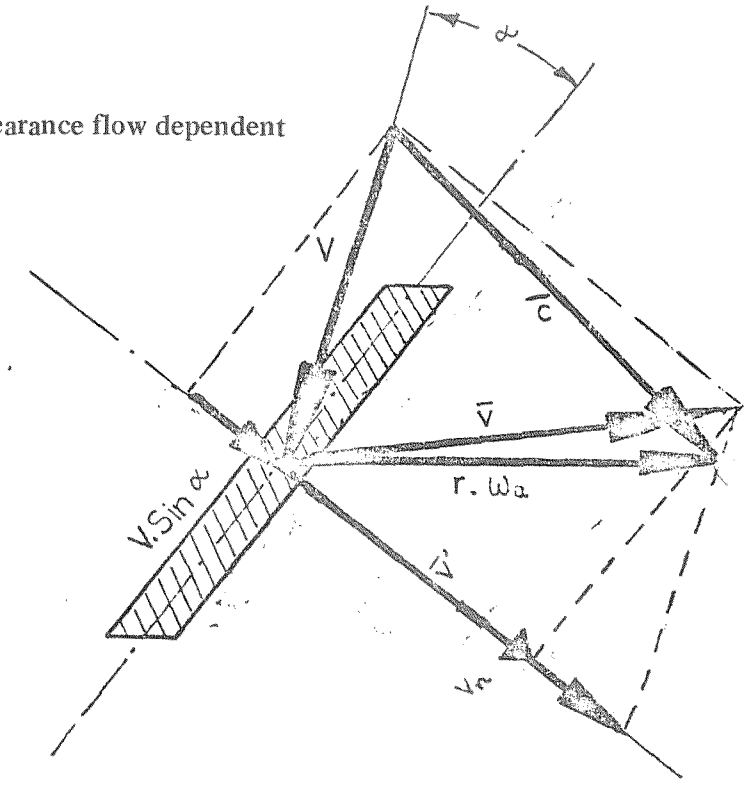

5Cii The demonstration of flow in the tip clearance with a positive angle of attack. In this case V sin α and v_n are co directed therefore there is no back flow in the tip clearance relative to the main flow.

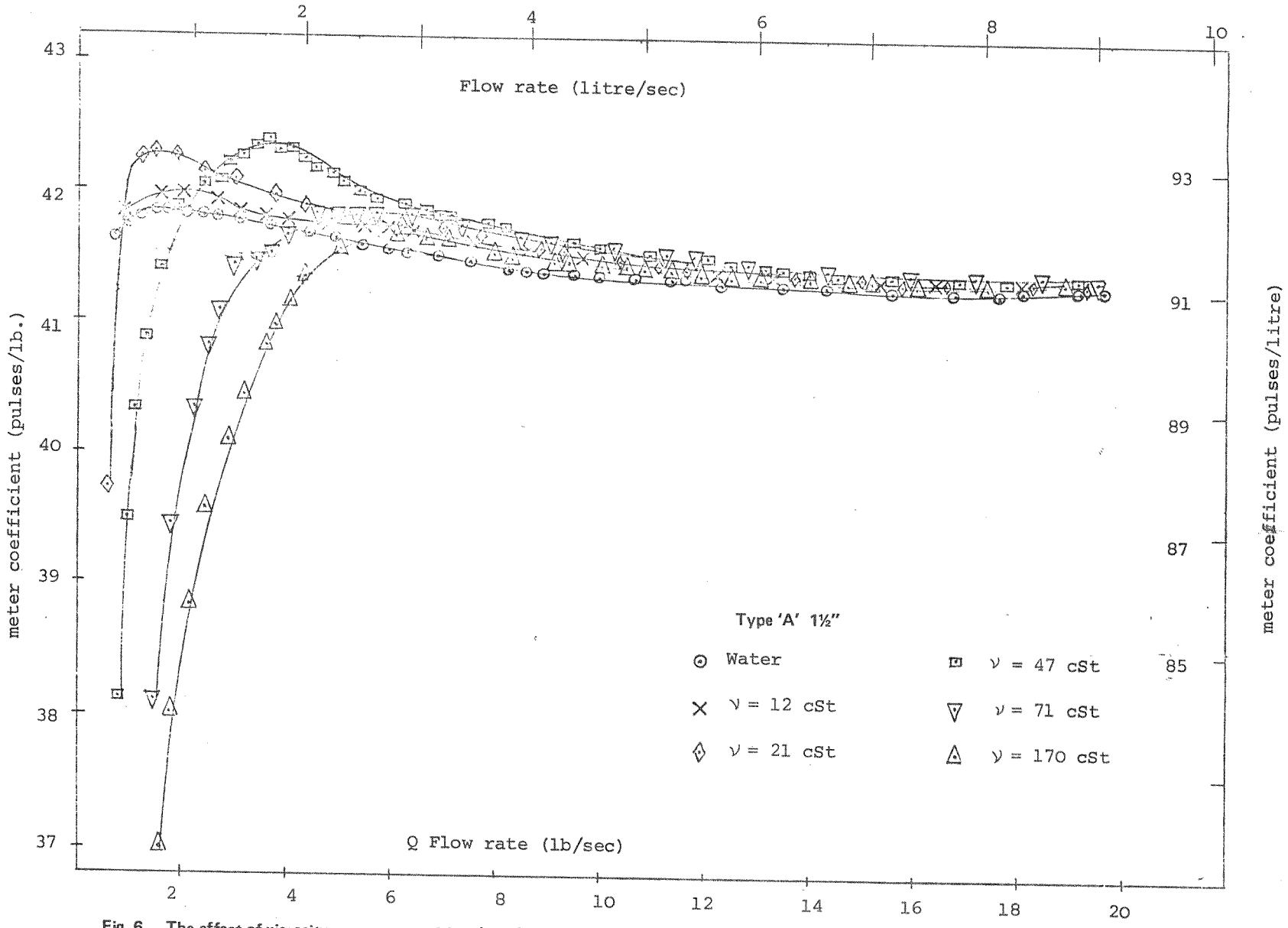

Fig. 6. The effect of viscosity on a commercial turbine flow meter with a 6 helical bladed angle rotor. The bearing friction was relatively large, the viscosity effect was relatively small for this type of flow meter.

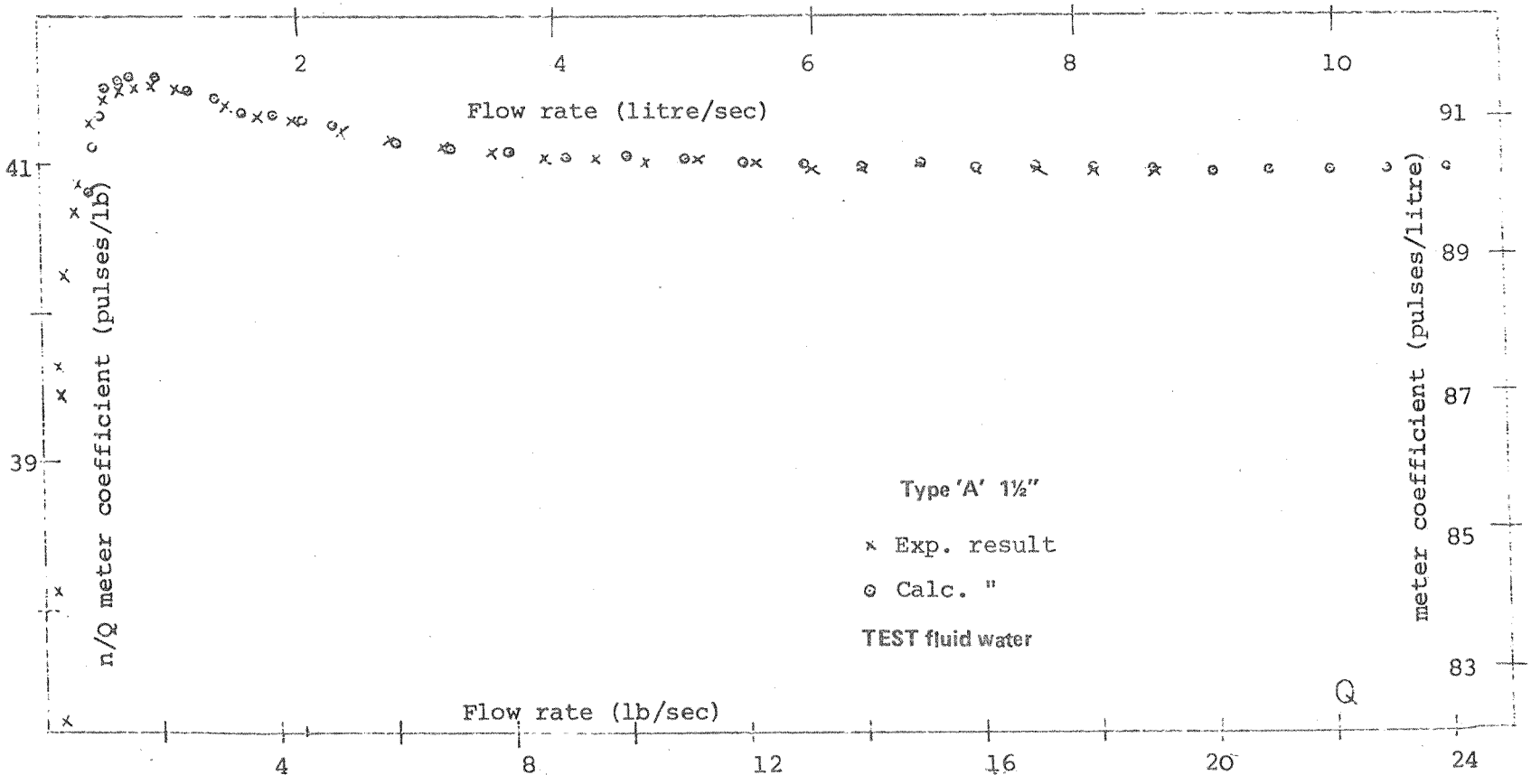

Fig. 7. The comparison between the experimental and calculated results on a commercial turbine flow meter with 6 helical bladed angle rotor.

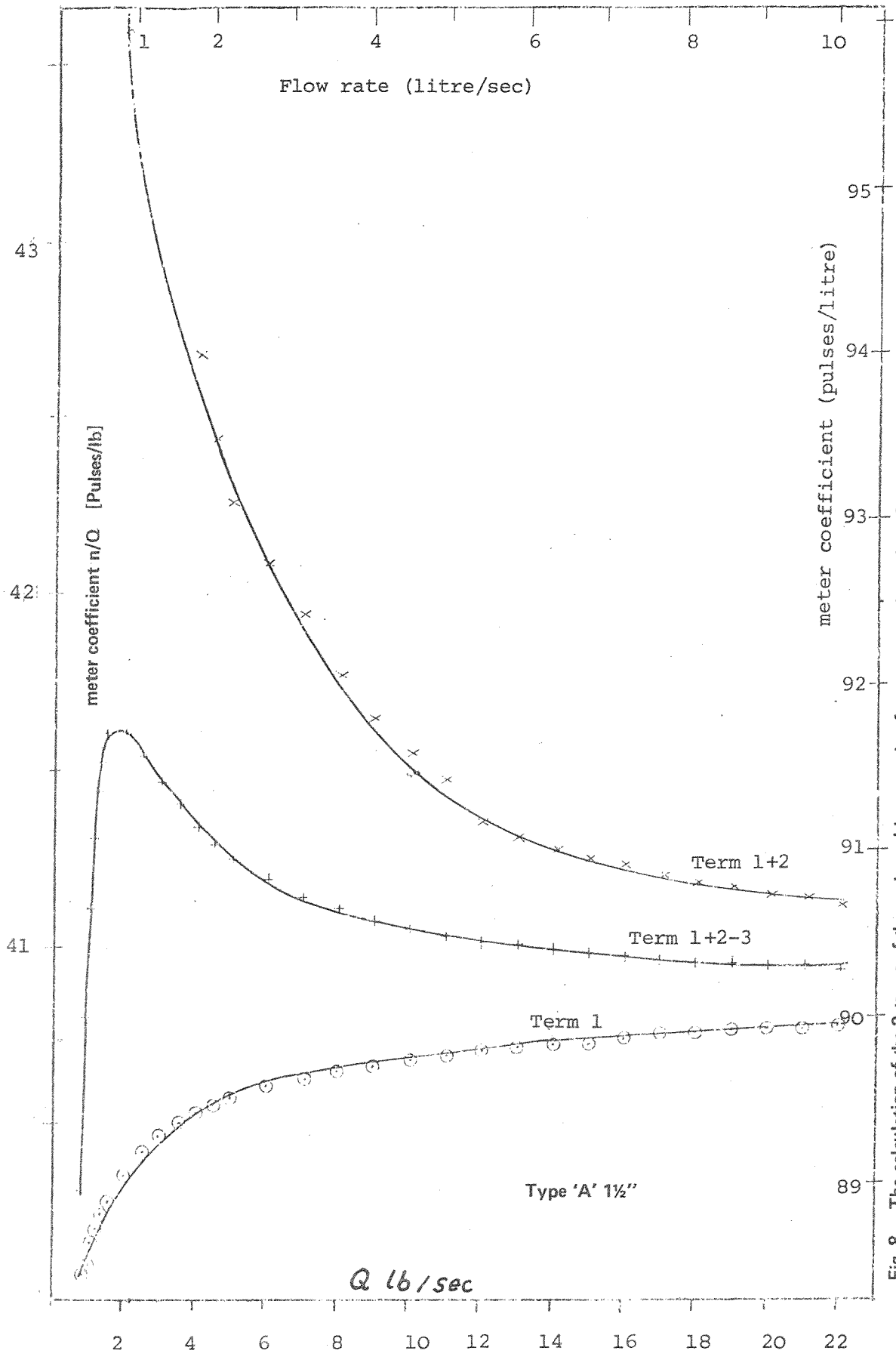

Fig. 8. The calculation of the 3 terms of the main turbine equation for a commercial turbine flow meter with 6 helical bladed angle rotor. (Water)

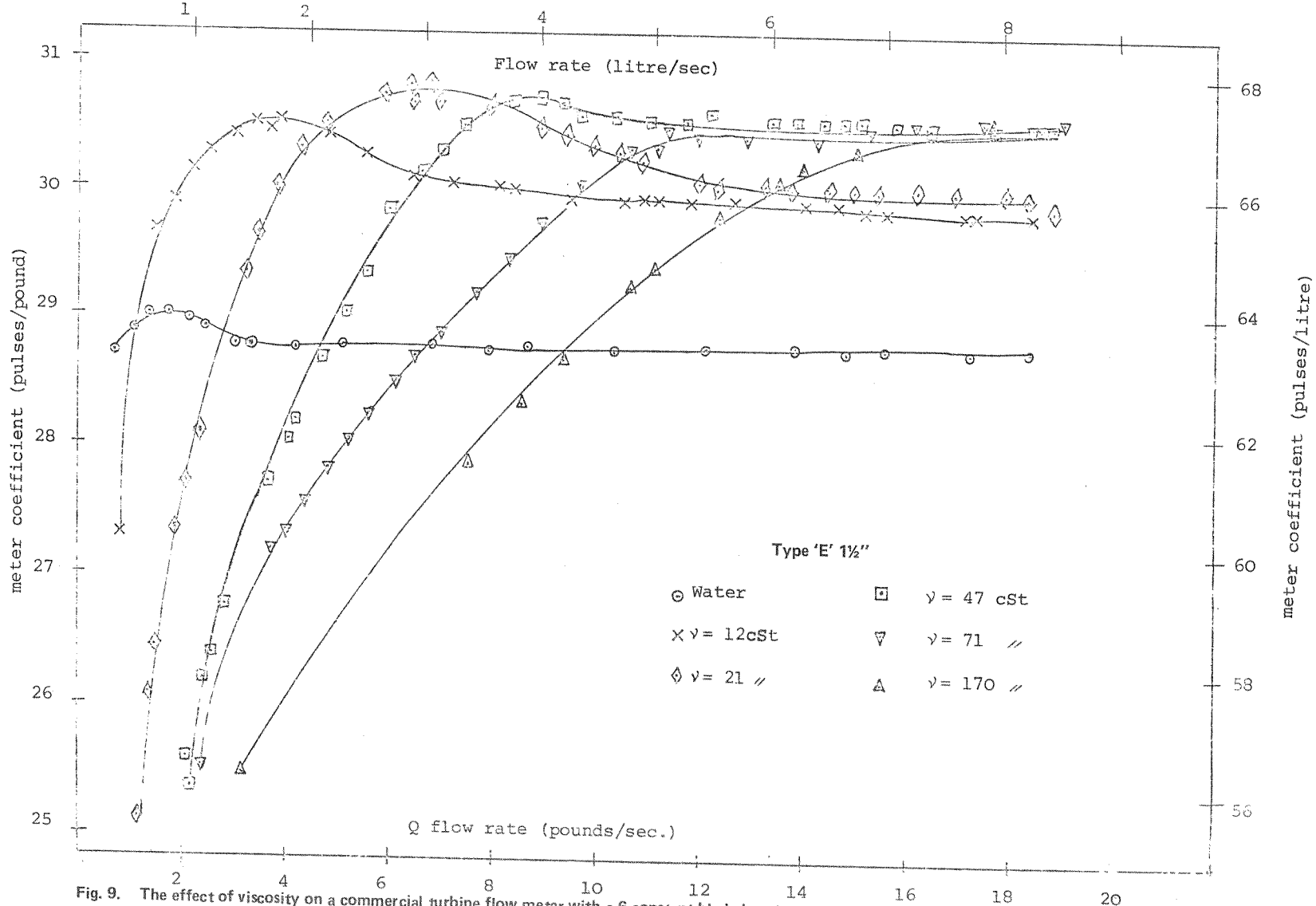

Fig. 9. The effect of viscosity on a commercial turbine flow meter with a 6 constant bladed angle rotor with small bearing friction and large viscosity influence

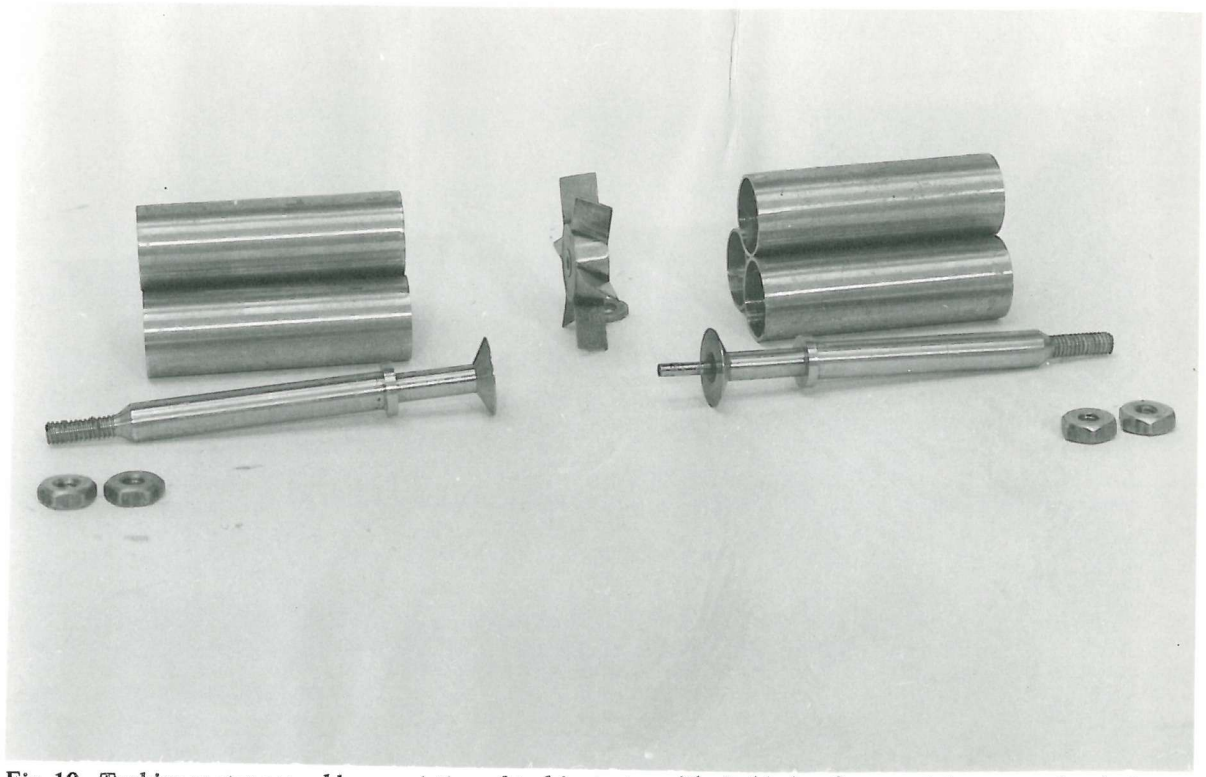

Fig. 10 Turbine meter assembly, consisting of turbine rotor with six blades, flow straightener, and a shaft with a plain bearing. (Constant angle blades) Type 'C' and 'E'

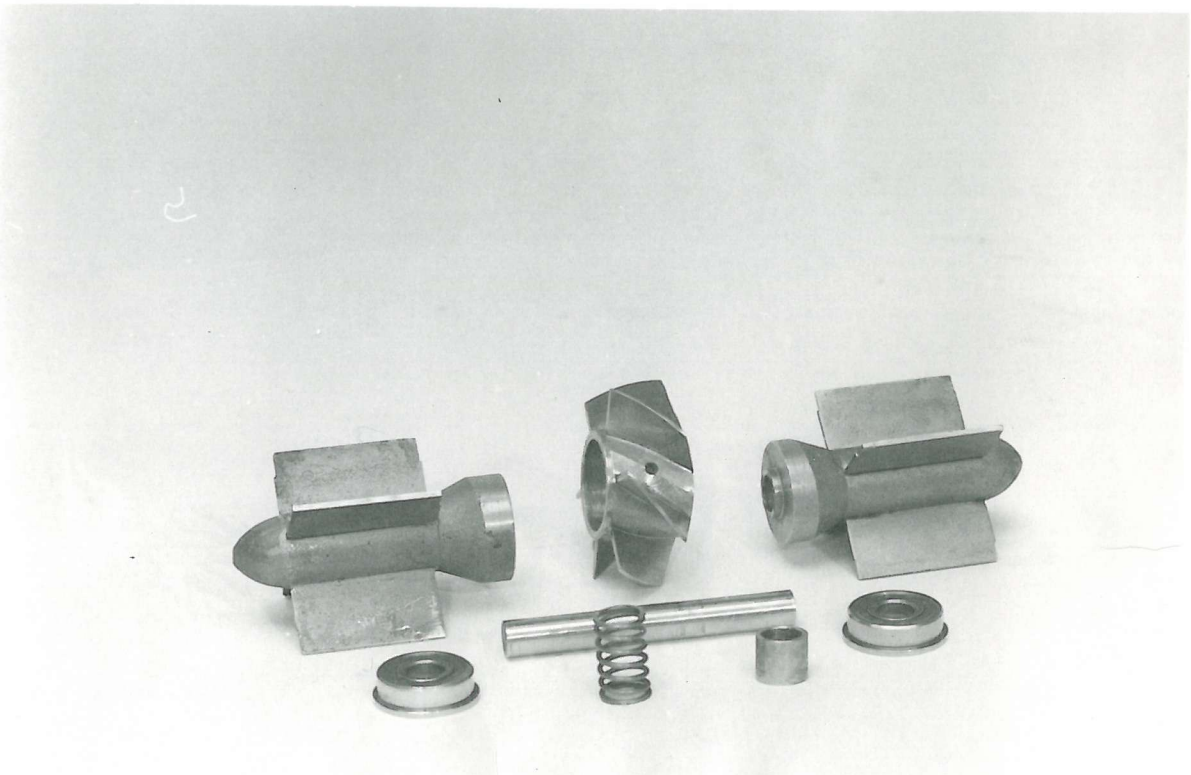

Fig. 11 Turbine meter assembly, consisting of turbine rotor with six blades, flow straightener, and a shaft with a plain bearing. (Helical angle blades) Type 'A'

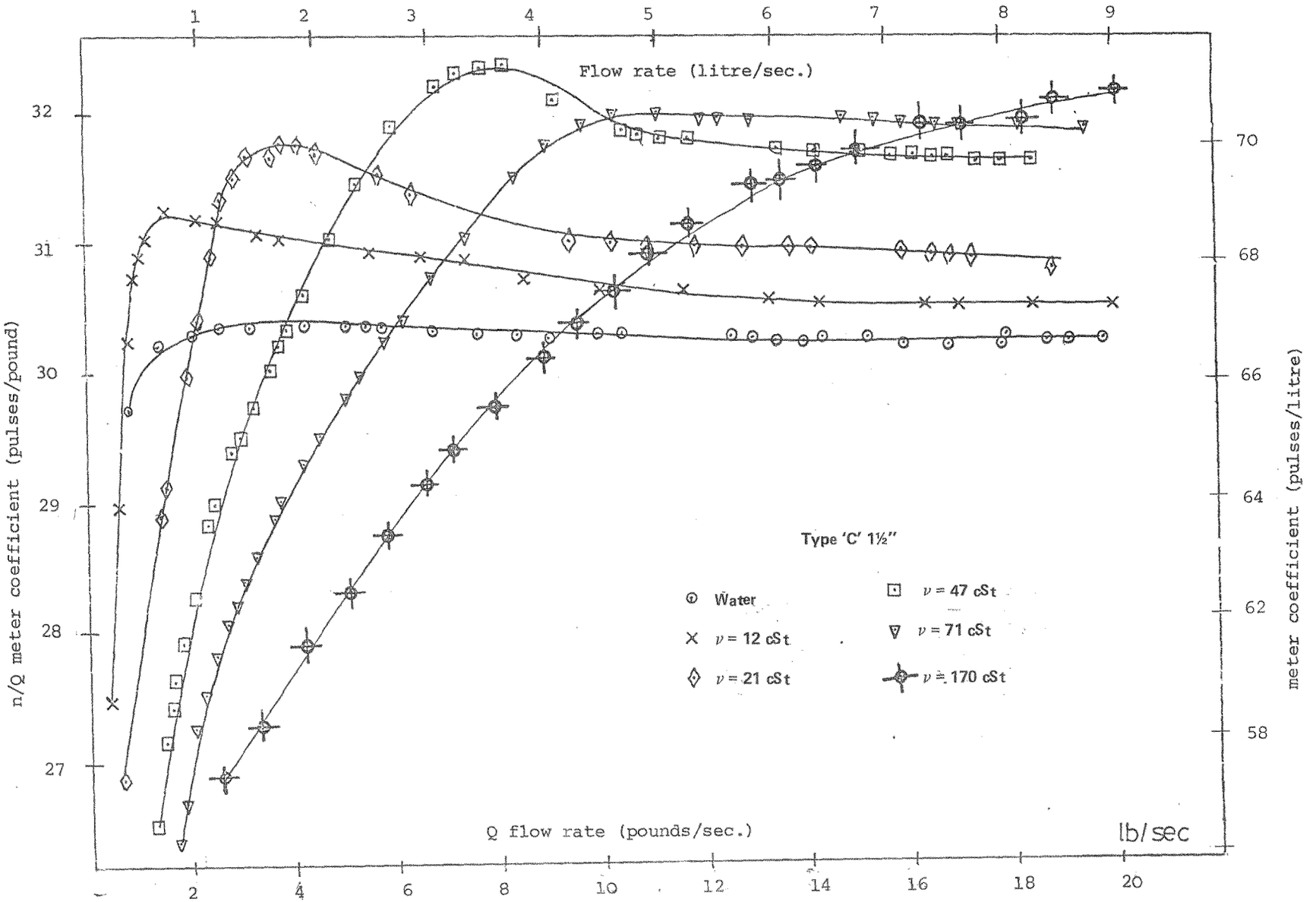

Fig. 12. The effect of viscosity on the constant angle blade rotor turbine flow meter, with small bearing friction. (These meters were more affected by viscosity of test fluid).

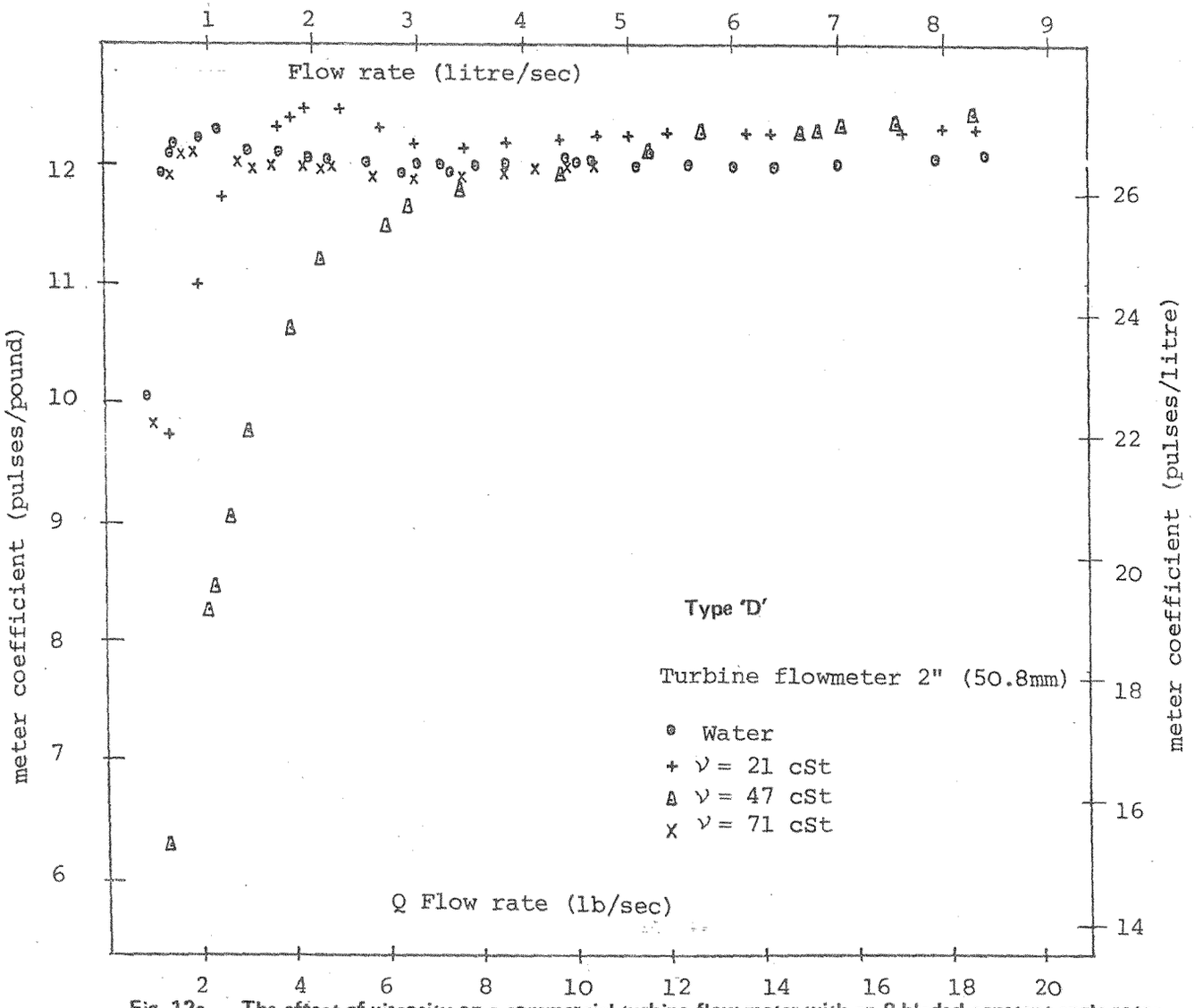

Fig. 12a. The effect of viscosity on a commercial turbine flow meter with an 8 bladed constant angle rotor

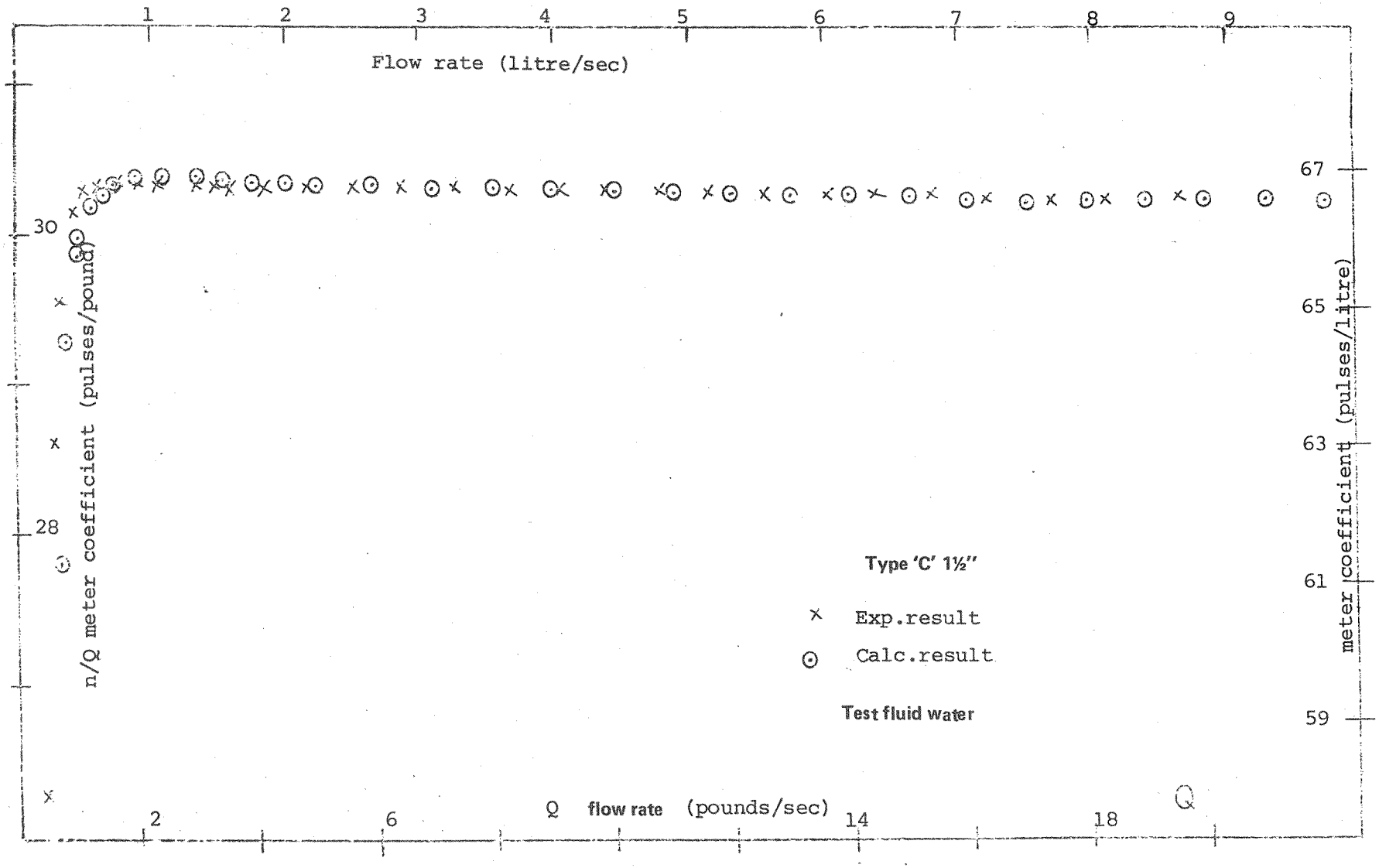

Fig. 13. The comparison between experimental and theoretical results on a commercial turbine flow meter with 6 constant bladed angle rotor

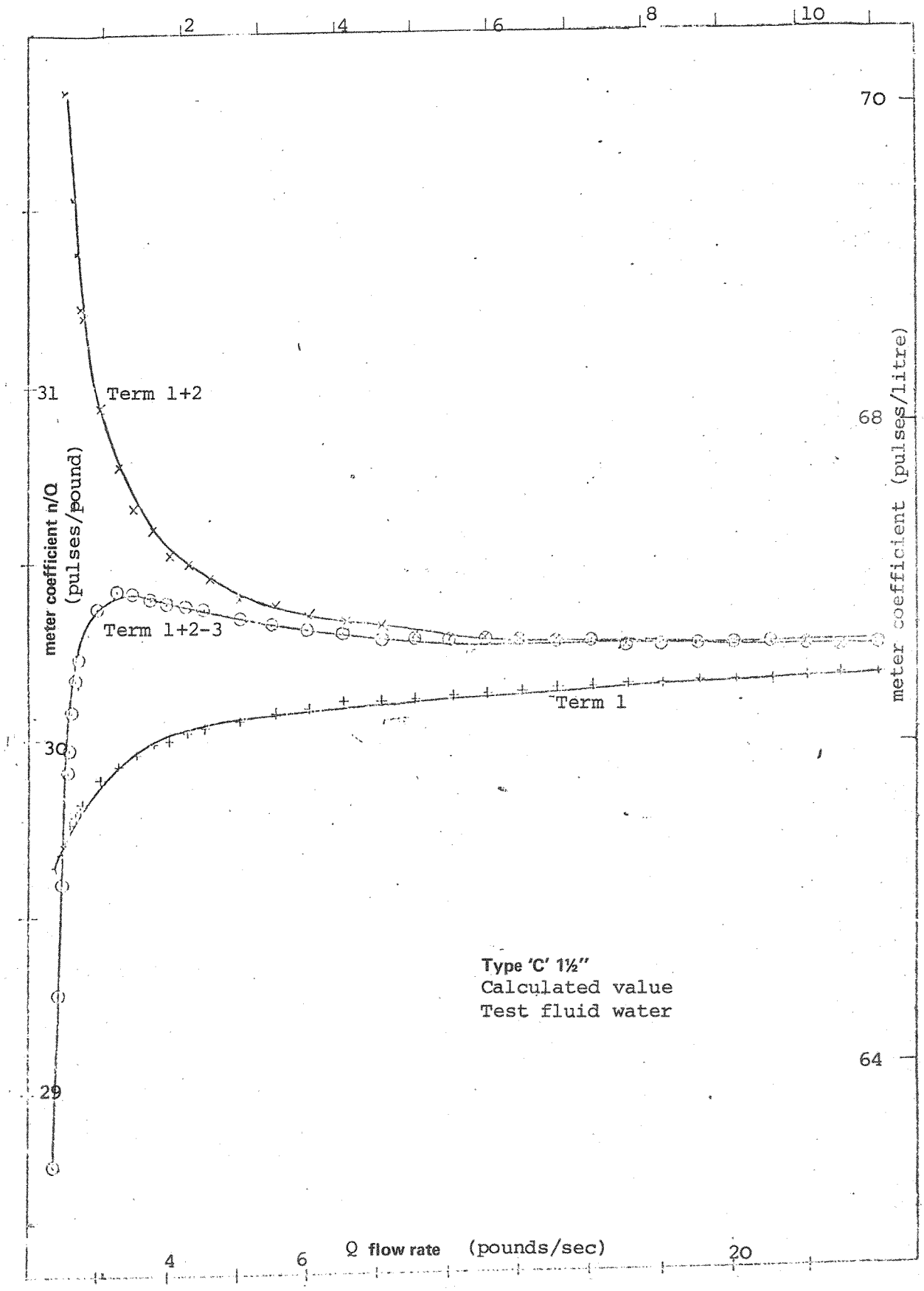

Fig. 14. The calculation of the 3 terms of the main turbine equation for a commercial turbine flow meter with a 6 bladed constant angle rotor

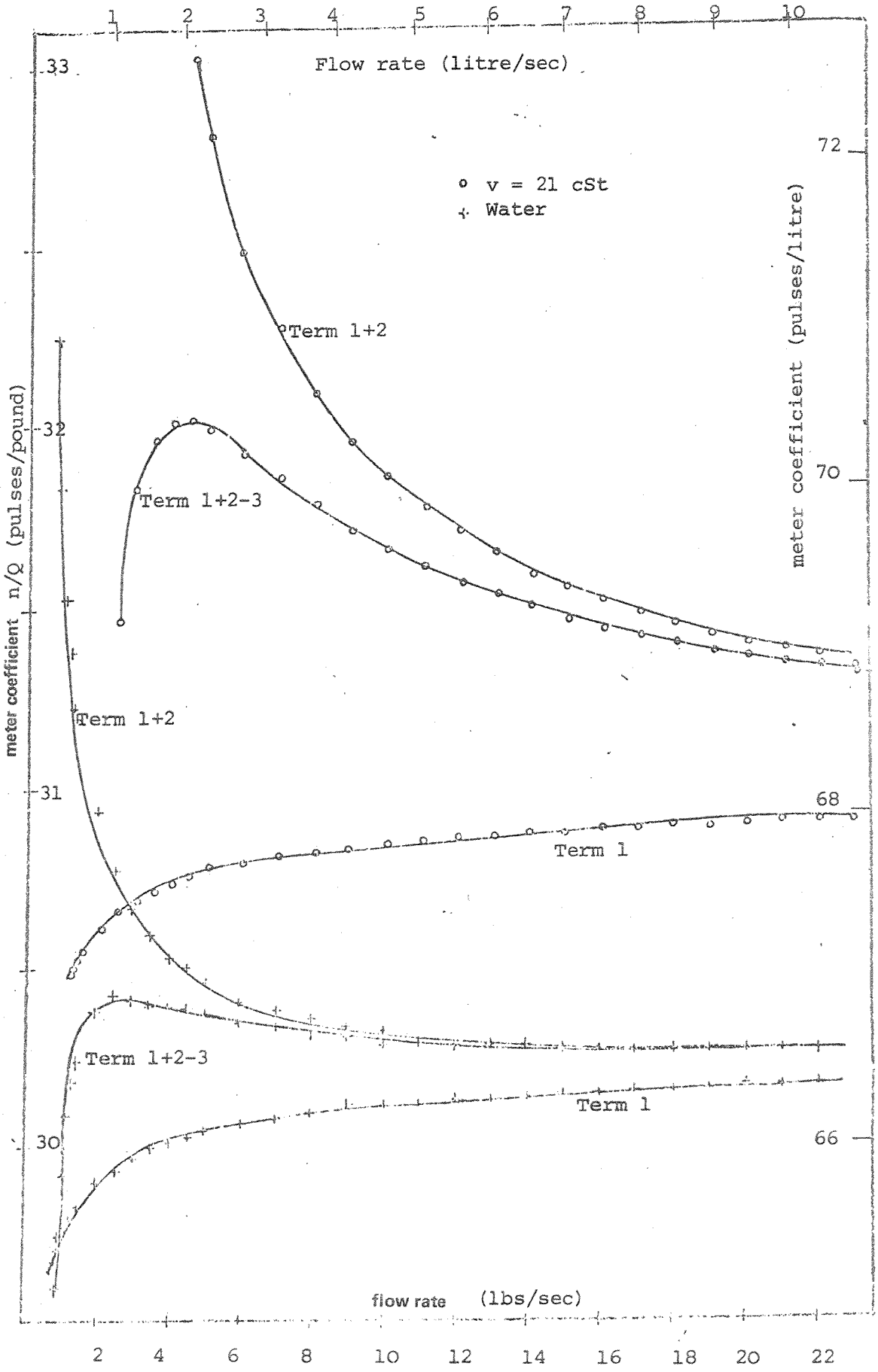

Fig. 15. The calculation of the 3 terms of main turbine equation for a commercial turbine flow meter Type 'C' with 6 bladed constant angle rotor and the first variation in the terms due to the increase in fluid viscosity up to ν = 21 cSt

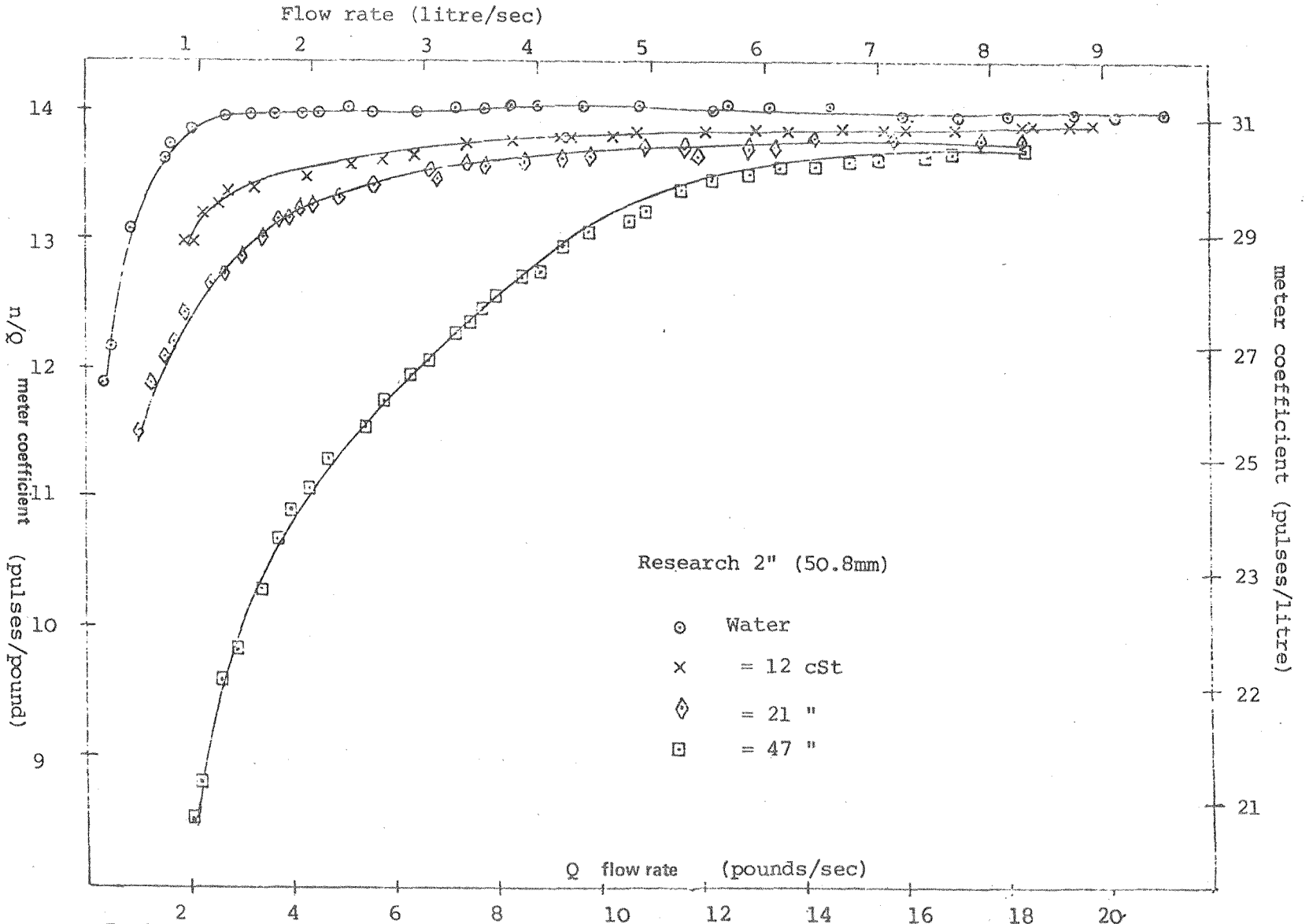

Fig. 16. The effect of viscosity on the research meter with a 3 bladed constant angle rotor. These are current experimental results and because of the opaqueness of the viscous test fluid some pulses could not be counted. The light beams were too weak to be picked up by photo cells (See Fig. 37)

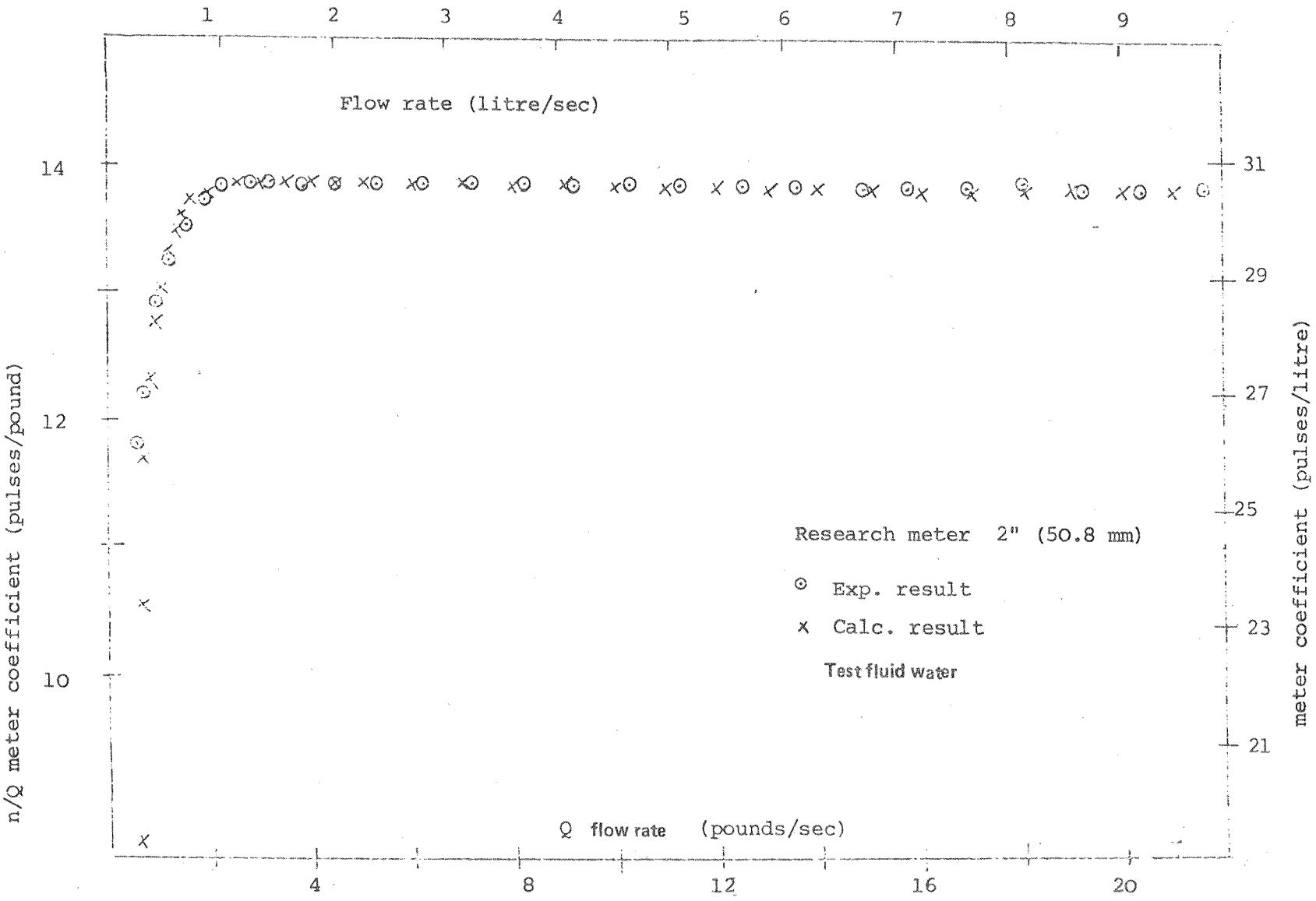

Fig. 17. The comparison between experimental and calculation results on a research turbine flow meter with 3 constant bladed angle rotor.

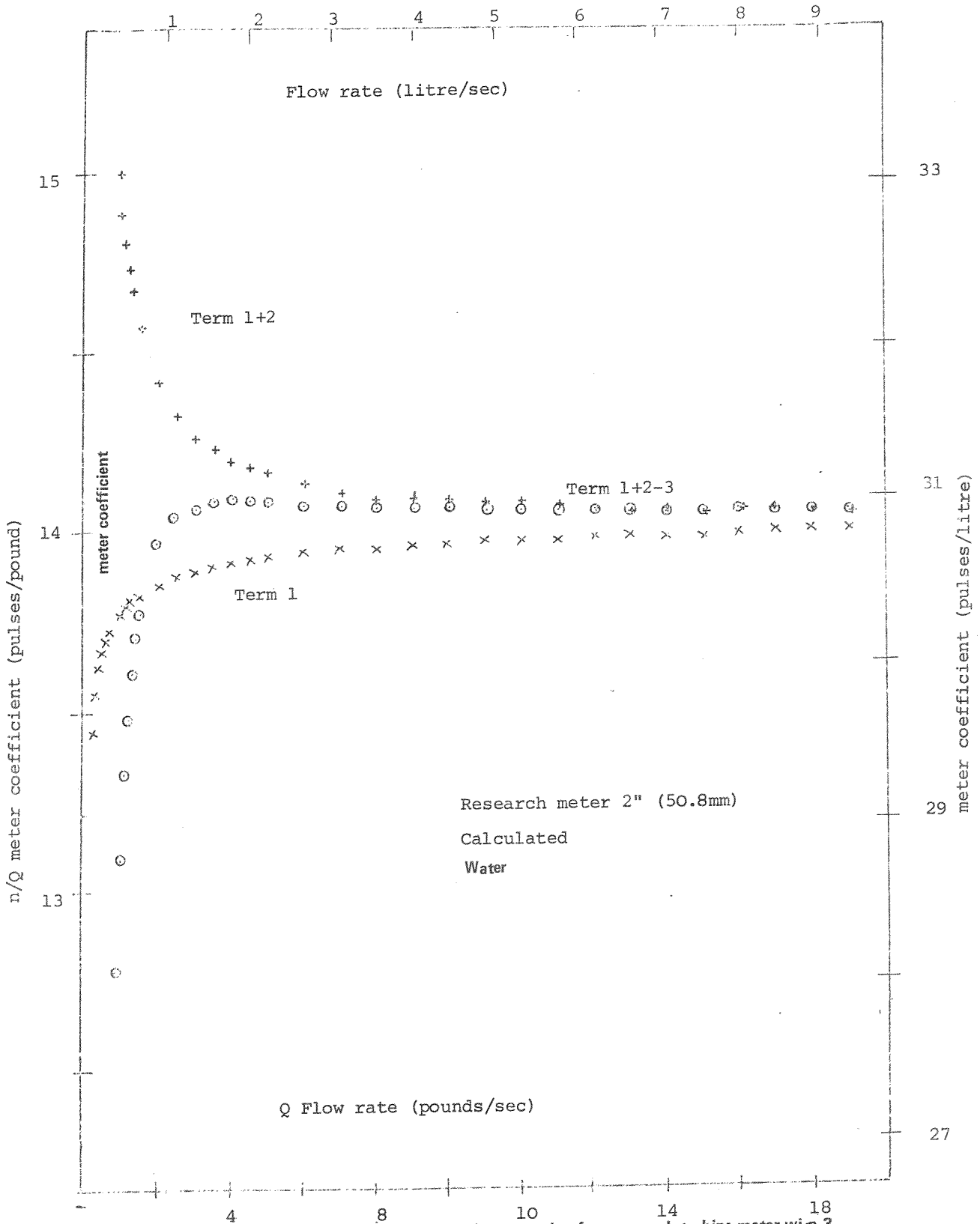

Fig. 18. The calculation of the 3 terms of the main turbine equation for a research turbine meter with 3 constant bladed angle rotor

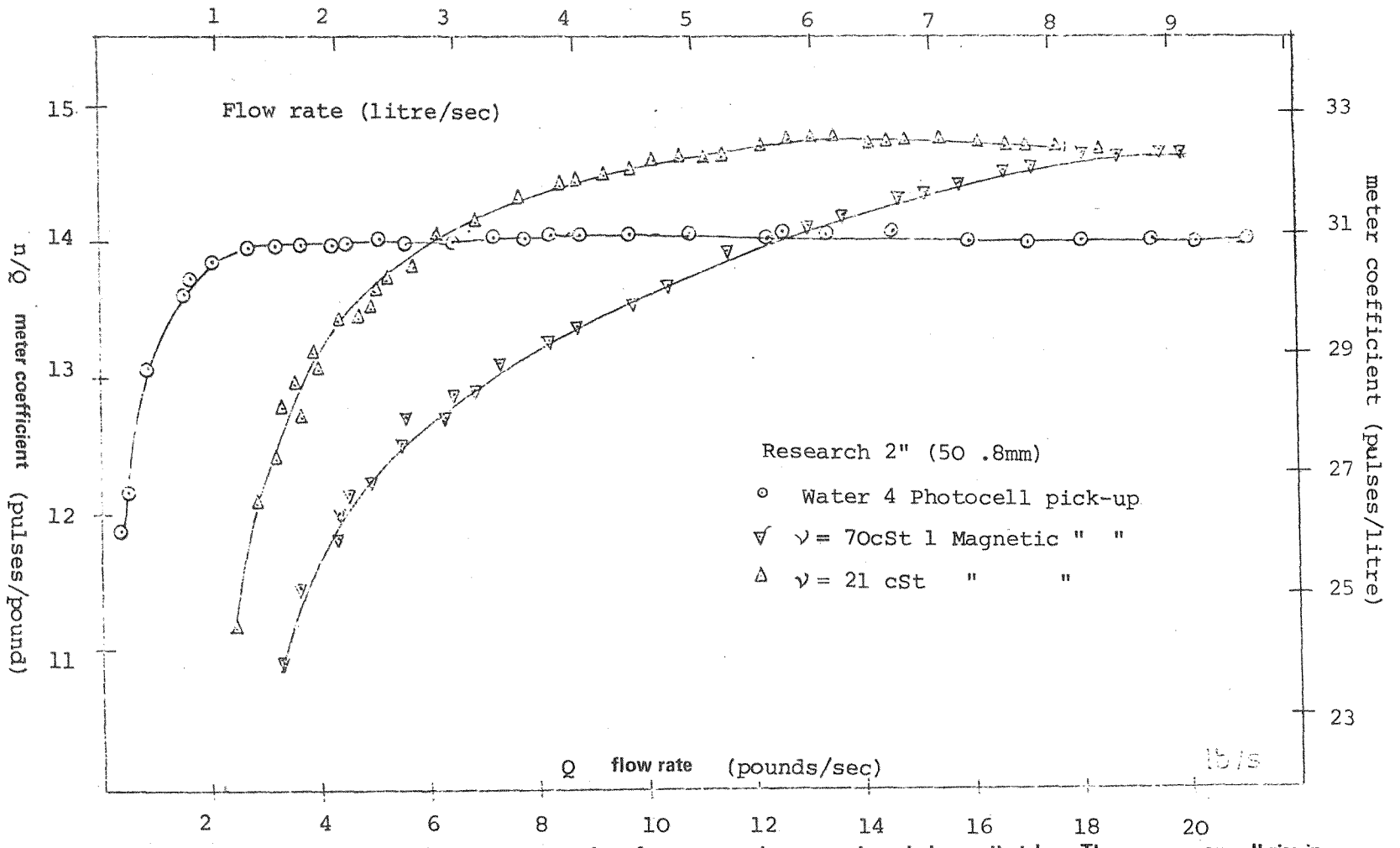

Fig. 19. The effect of viscosity on the research turbine flow meter using magnetic and photocell pickup. There was an overall rise in the calibration curve. (The magnetic pickup detected the lost pulses mentioned in Fig. 16, 20, 27, 37).

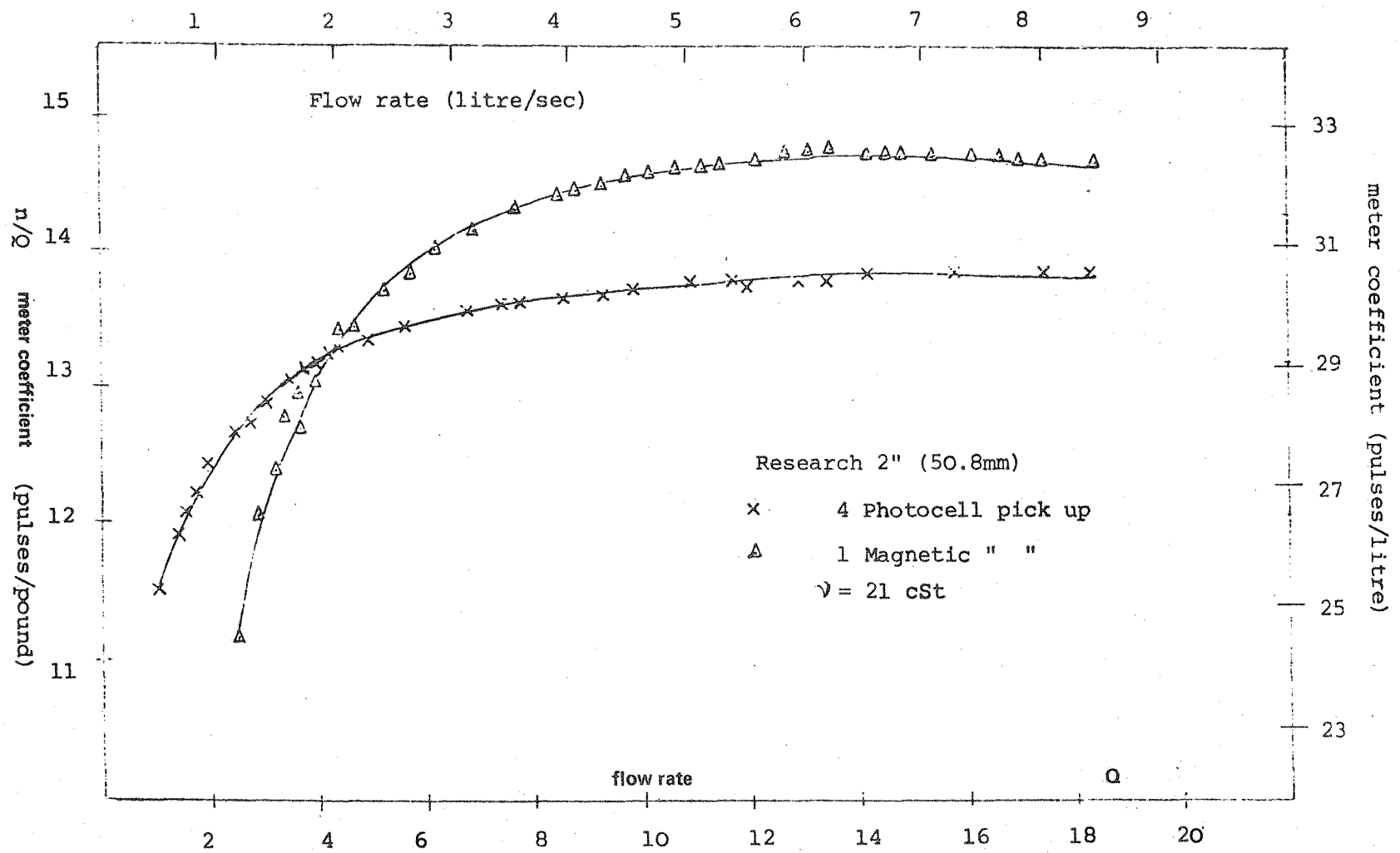

Fig. 20. The weak pulses reflected on the blade tip, which are lost due to the opaqueness of the viscous test fluid can be found by comparison between the number of pulses detected by magnetic pick up and photo cell pick up.

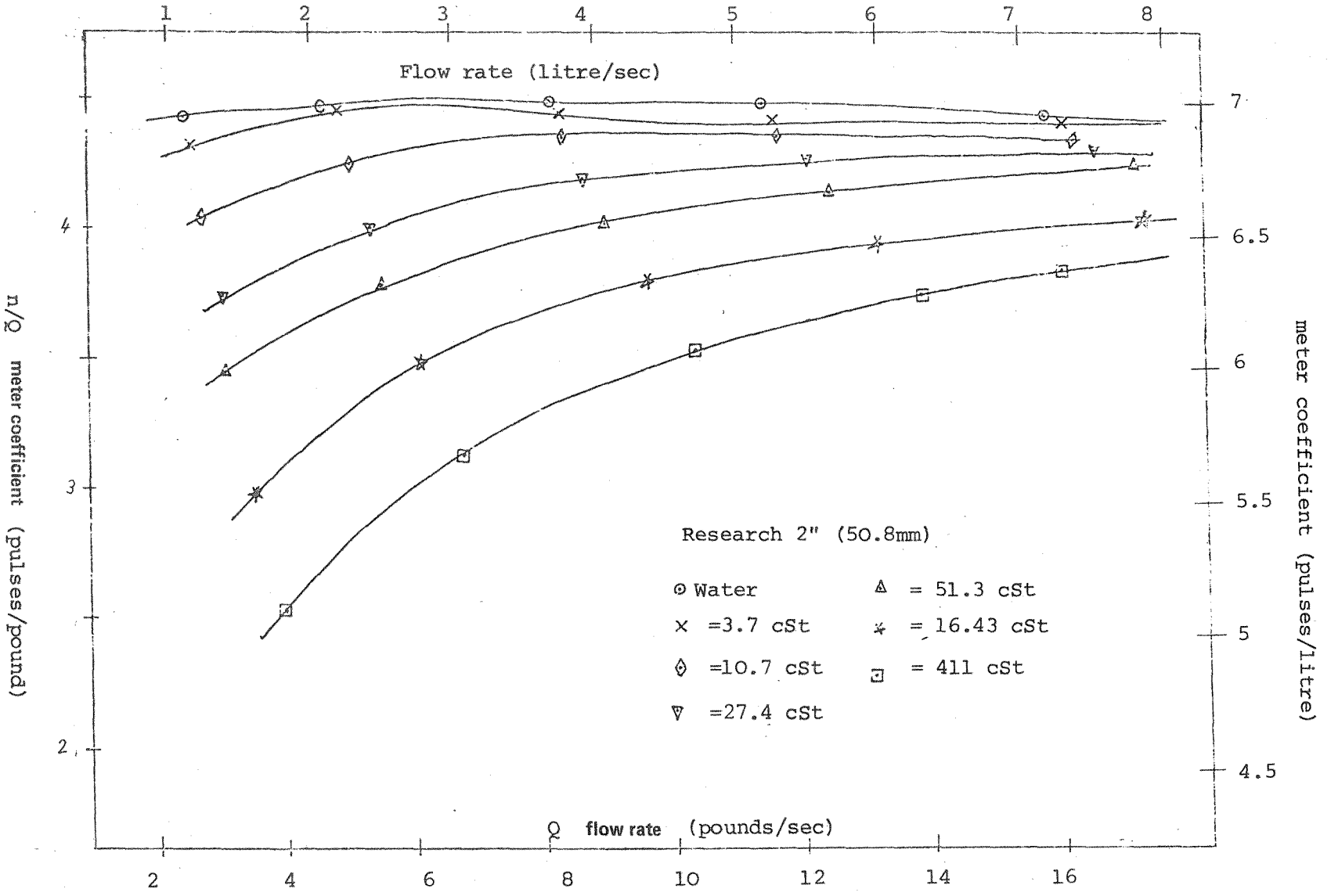

Fig. 21. The effect of viscosity on the research meter with a 3 bladed constant angle rotor. These were Salami's experimental results and because of the opaqueness of the viscous test fluid some pulses could not be counted. (The light beams were too weak to be picked up by the photo-cells). See Fig. 37

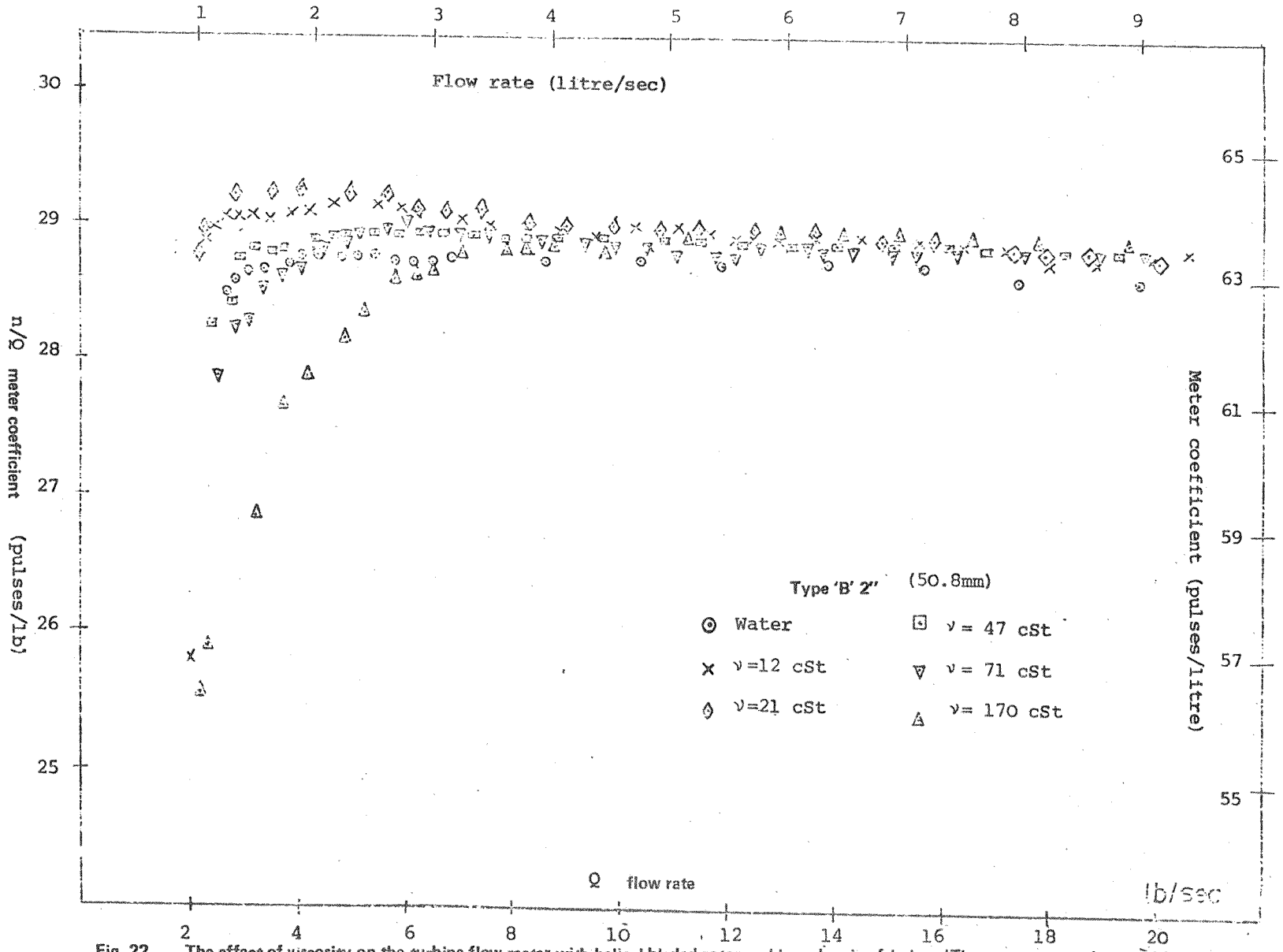

Fig. 22. The effect of viscosity on the turbine flow meter with helical bladed rotor and large bearing friction. (These meters were less sensitive to the change in fluid viscosity).

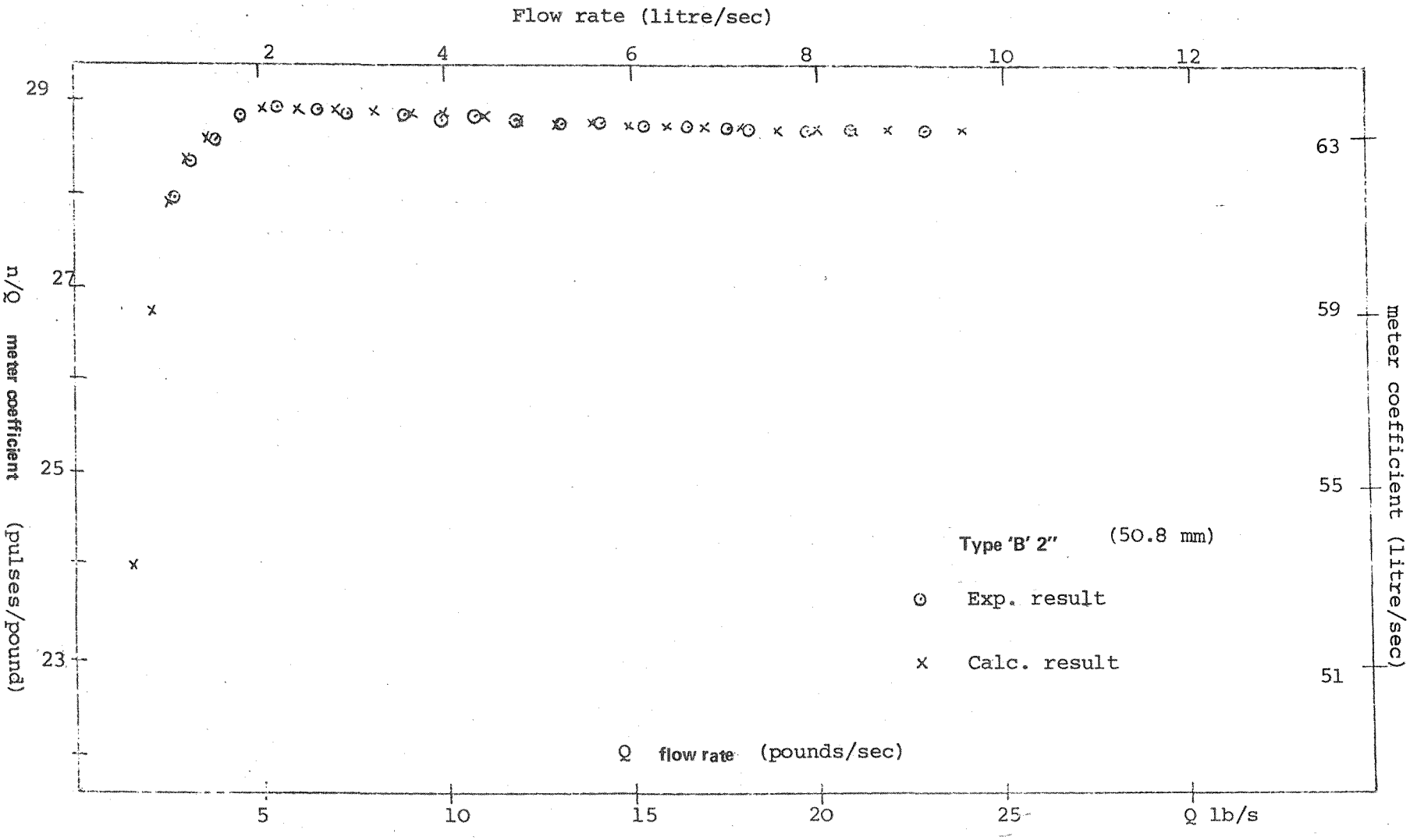

Fig. 23. The Comparison between experimental and calculated results for a commercial turbine flow meter with an 8 bladed helical rotor

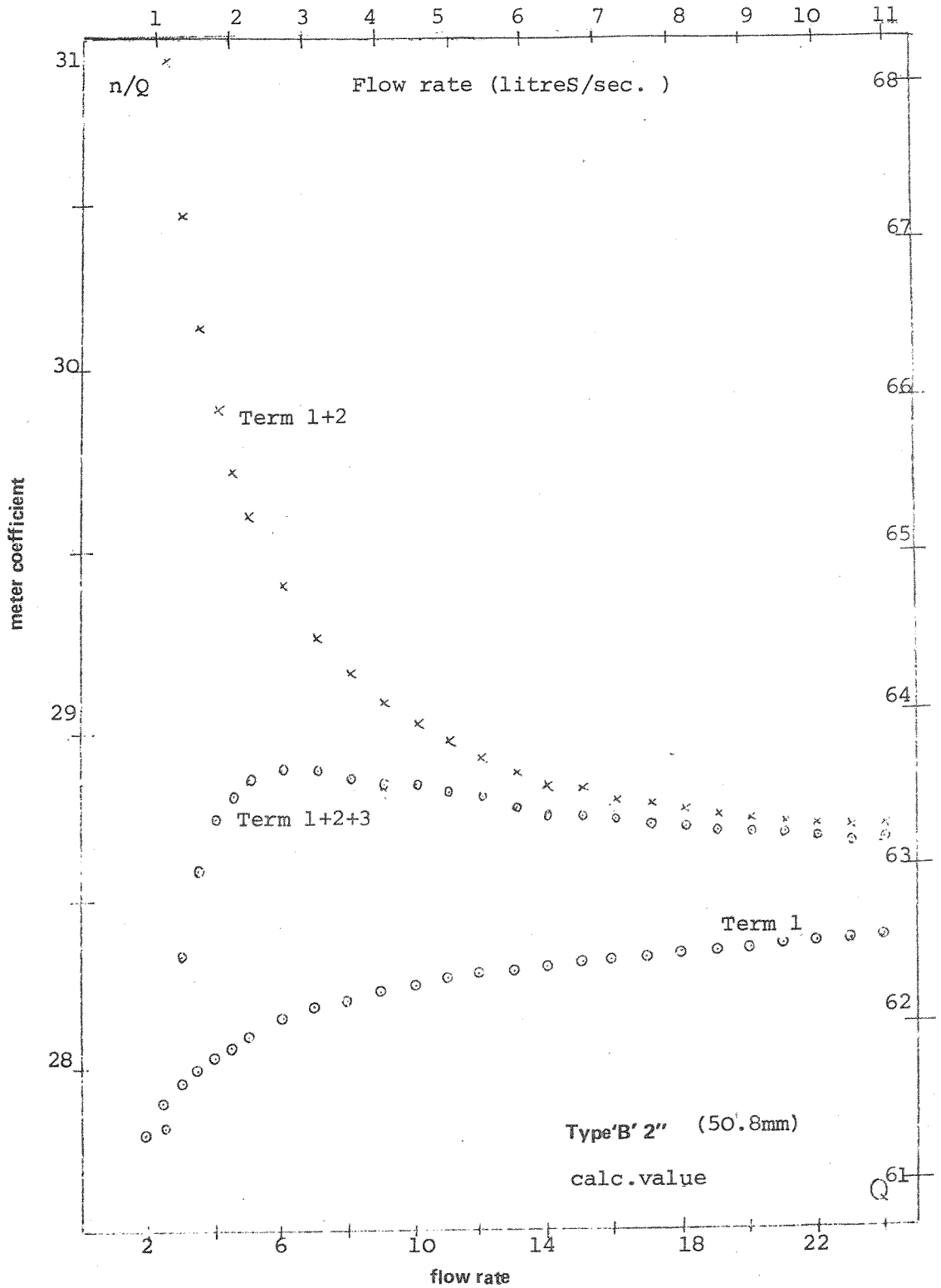

Fig. 24. Calculation of 3 terms of the main turbine equation for a commercial turbine meter with an 8 bladed helical rotor (water)

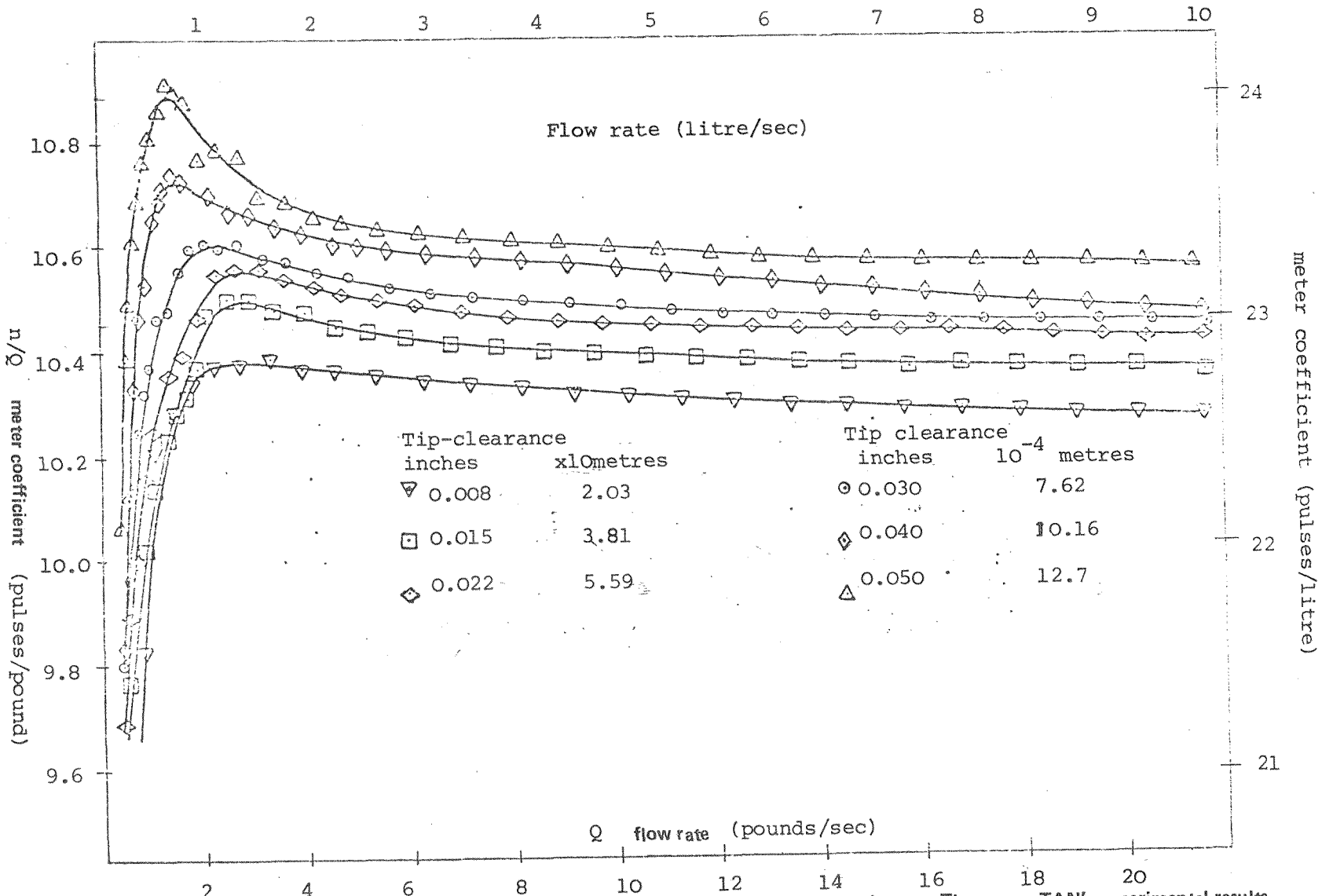

Fig. 25. The effect of tip clearance on the calibration curves of the helical blade research rotor. These were TAN's experimental results. He proved that an increase in tip clearance causes an overall rise in the calibration curve especially for low flow rates (caused the increase of the hump).

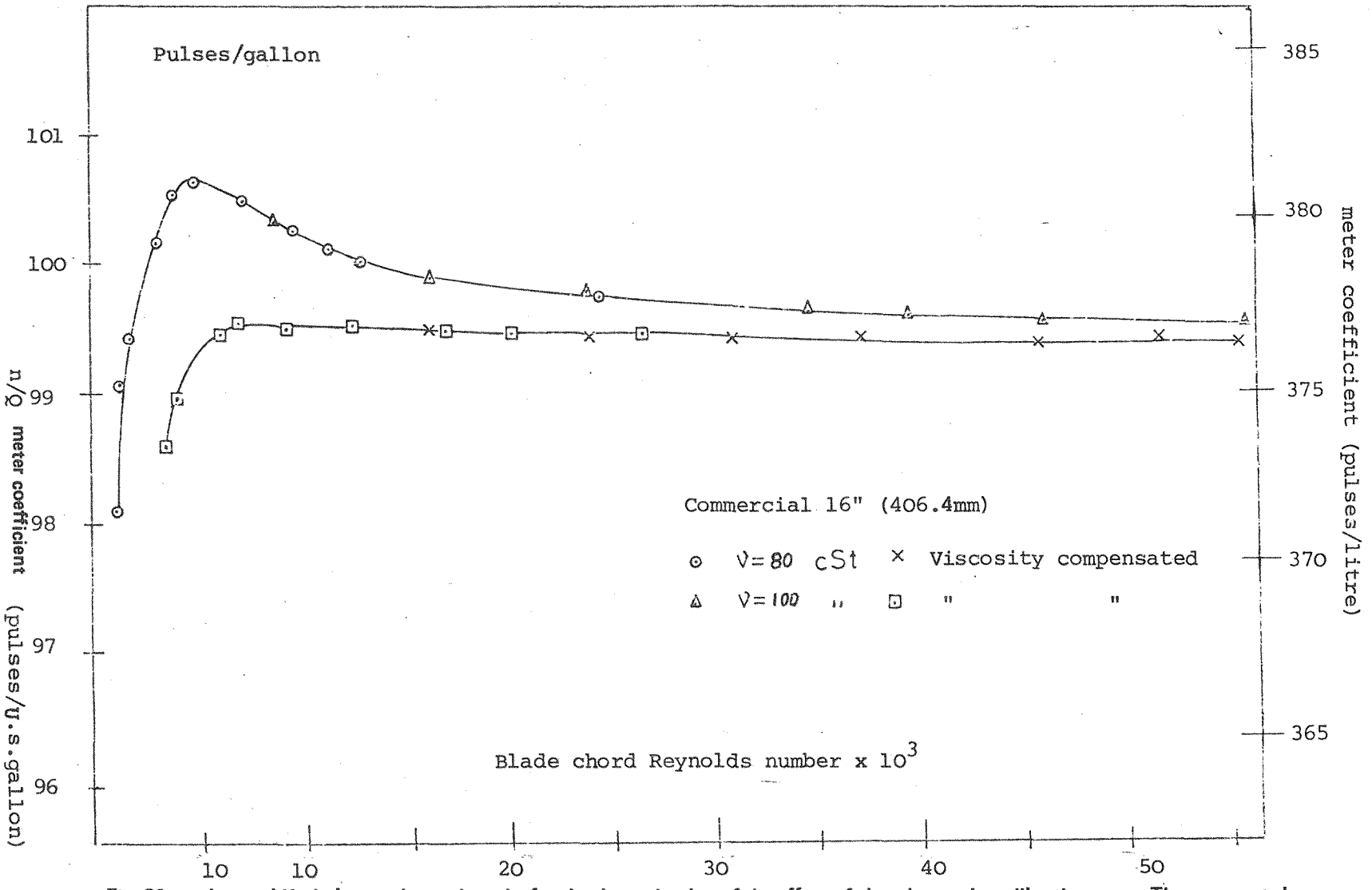

Fig. 26. Lee and Karby's experimental results for the determination of the effect of viscosity on the calibration curve. They connected the linear part and the non-linear part of the calibration curve of two different fluid viscosities. They compensated for the effect of viscosity with an external load, which increases term 3 of MTE and gives a balance between different terms of MTE. This causes the disappearance of the hump created on the calibration curve.

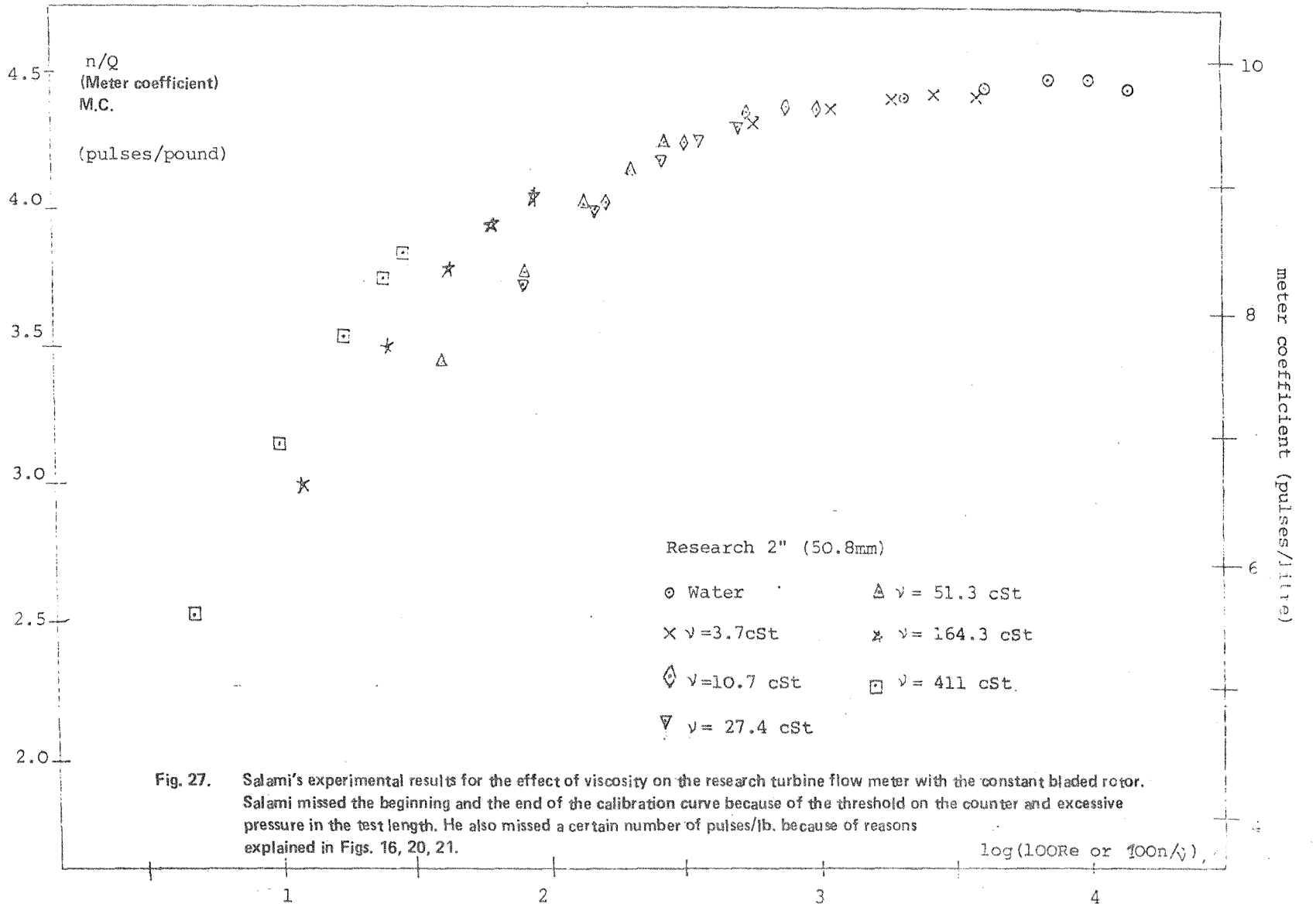

Fig. 27. Salami's experimental results for the effect of viscosity on the research turbine flow meter with the constant bladed rotor. Salami missed the beginning and the end of the calibration curve because of the threshold on the counter and excessive pressure in the test length. He also missed a certain number of pulses/lb. because of reasons explained in Figs. 16, 20, 21.

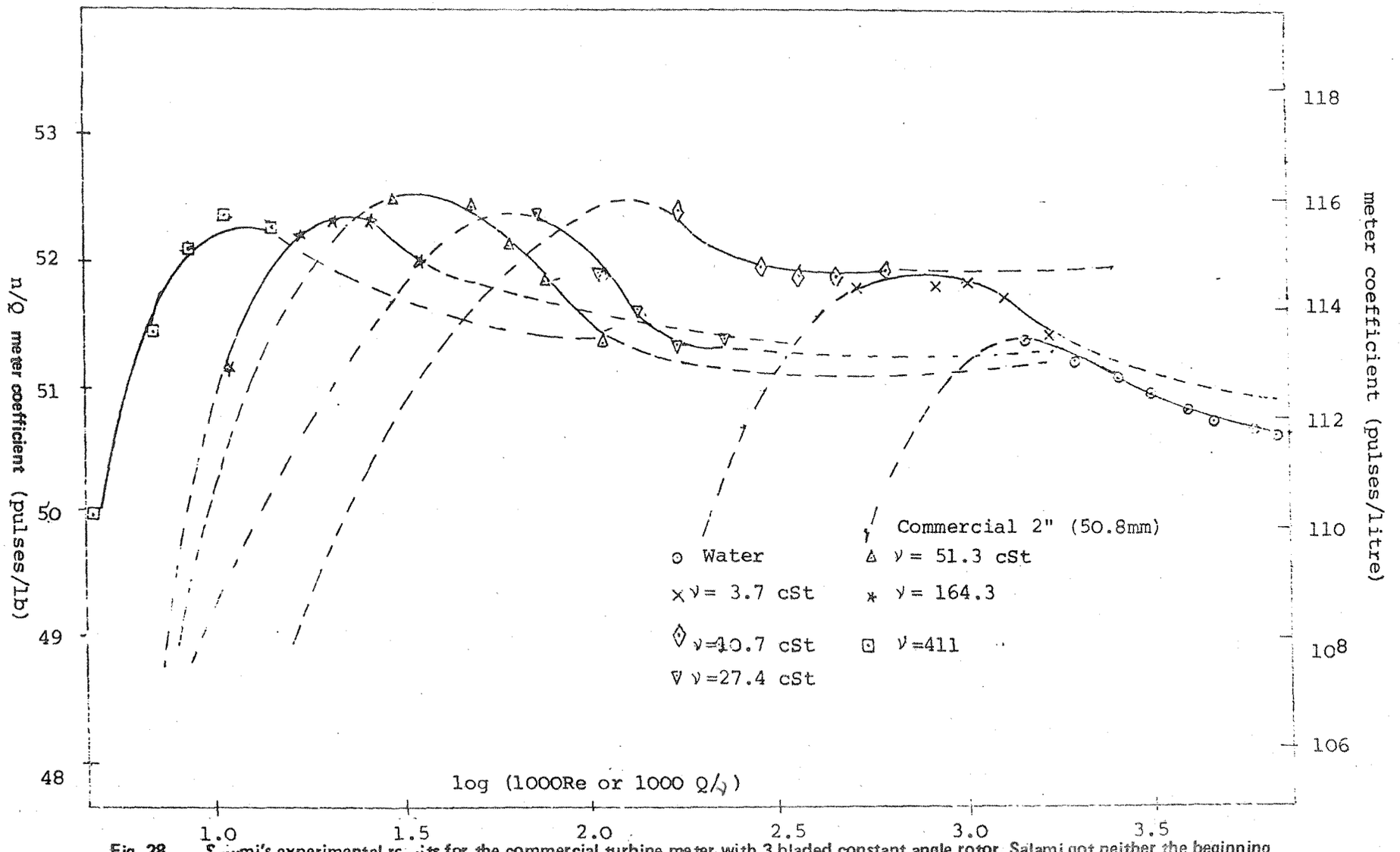

Fig. 28. Salami's experimental results for the commercial turbine meter with 3 bladed constant angle rotor. Salami got neither the beginning of the calibration curves (non linear part), because of the threshold of the counter, nor the end of it because of high pressure created in the test line due to an increase in viscosity (pump limit). Dashed lines indicate his expected results in these regions.

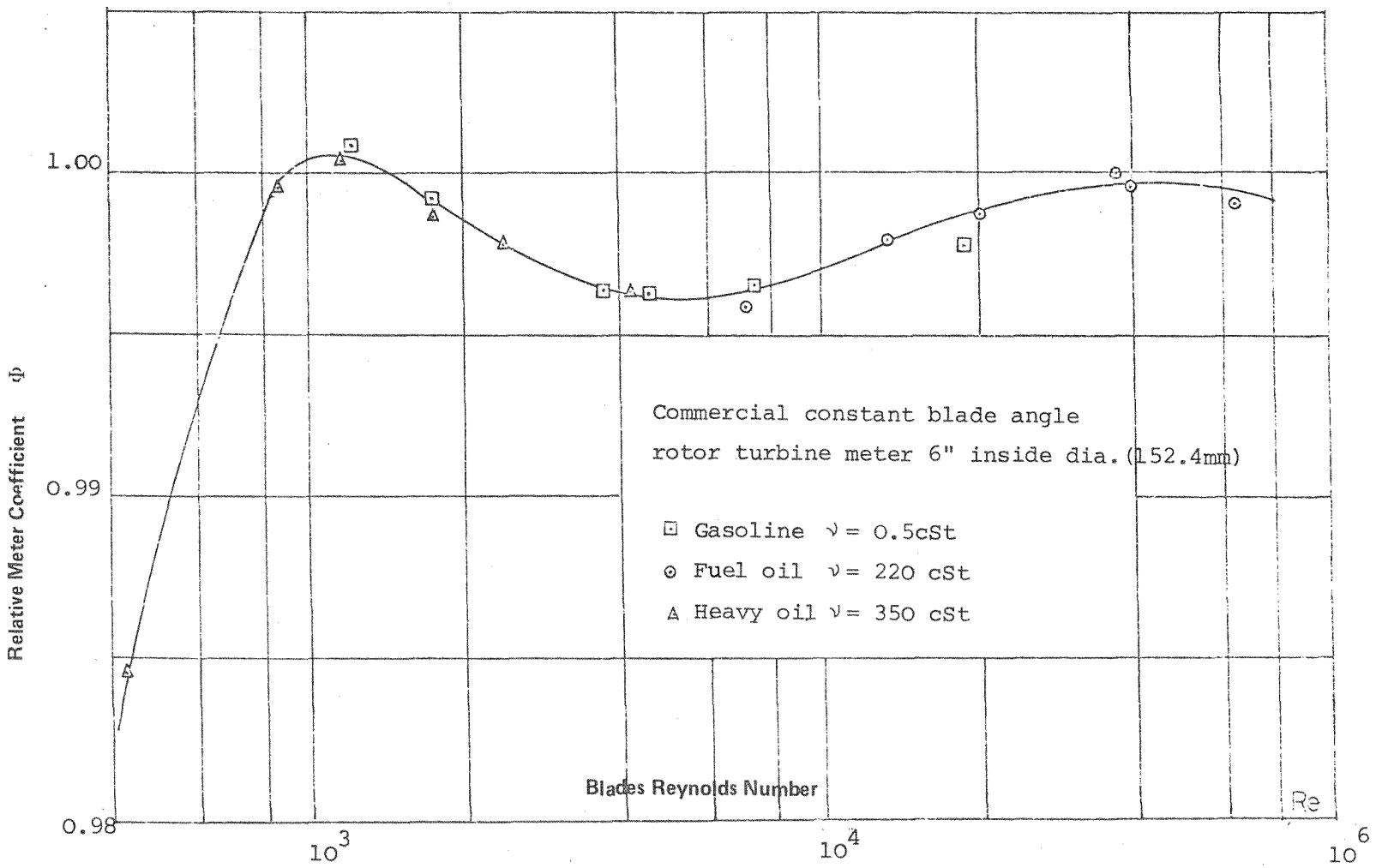

Fig. 29. The relationship between Φ and Re for a 6" commercial turbine meter with a 16 bladed helical angle rotor

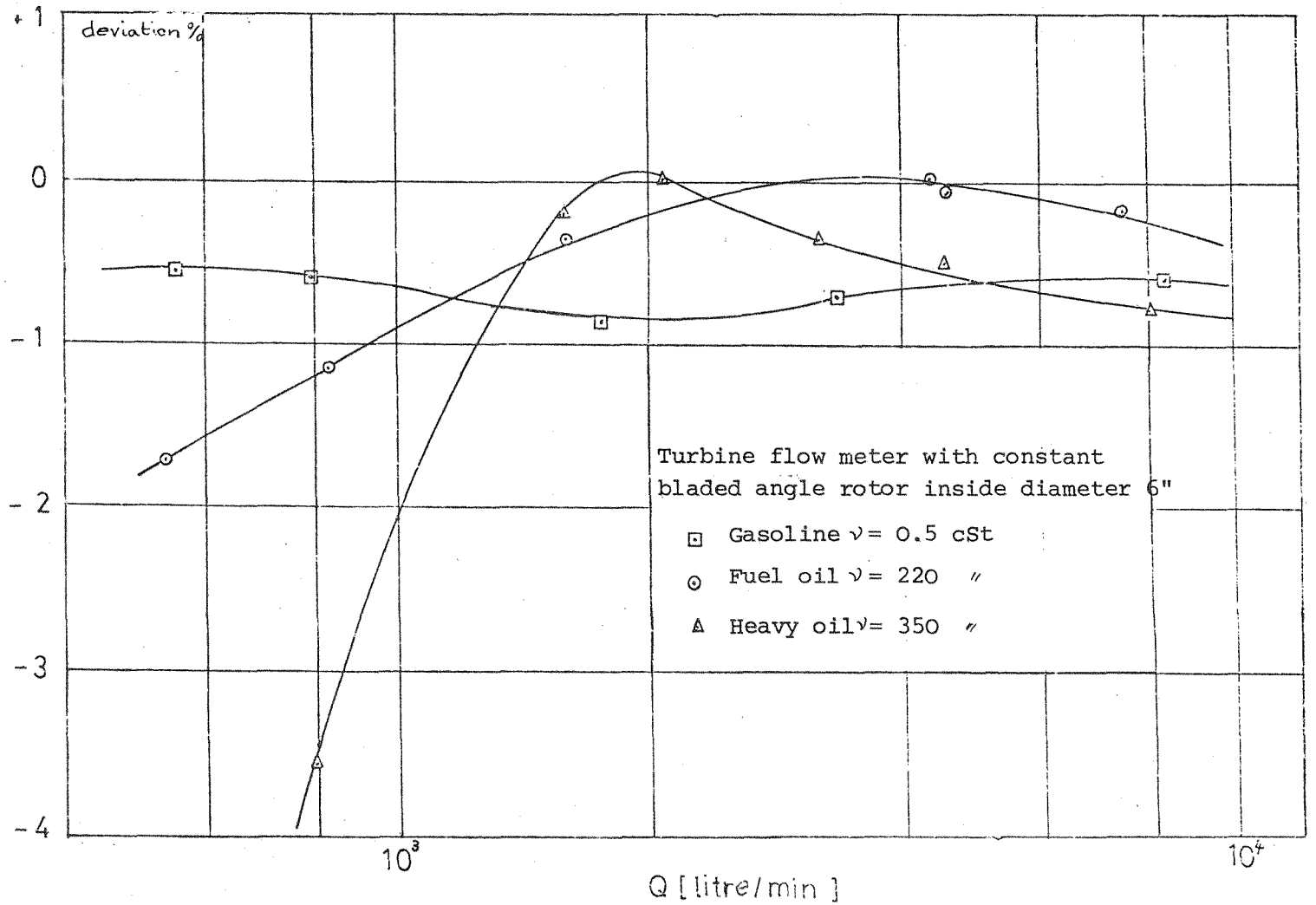

Fig. 30. The percentage error over the flow rate for the above meter with fluids of different viscosities.

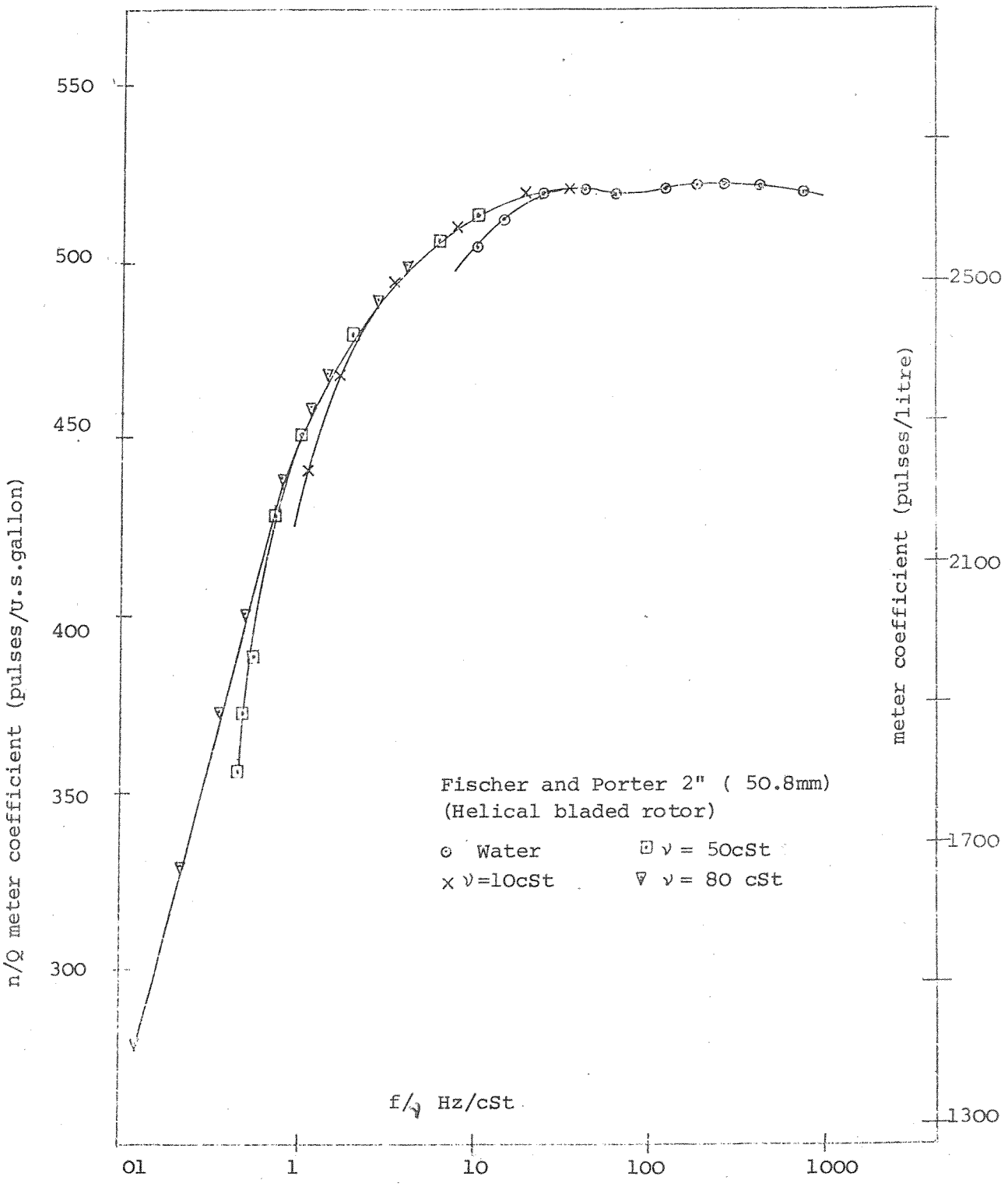

Fig. 31. The influence of fluid viscosity on the calibration curve for a commercial 2" turbine meter (linearity ±0.5% hel. blade)

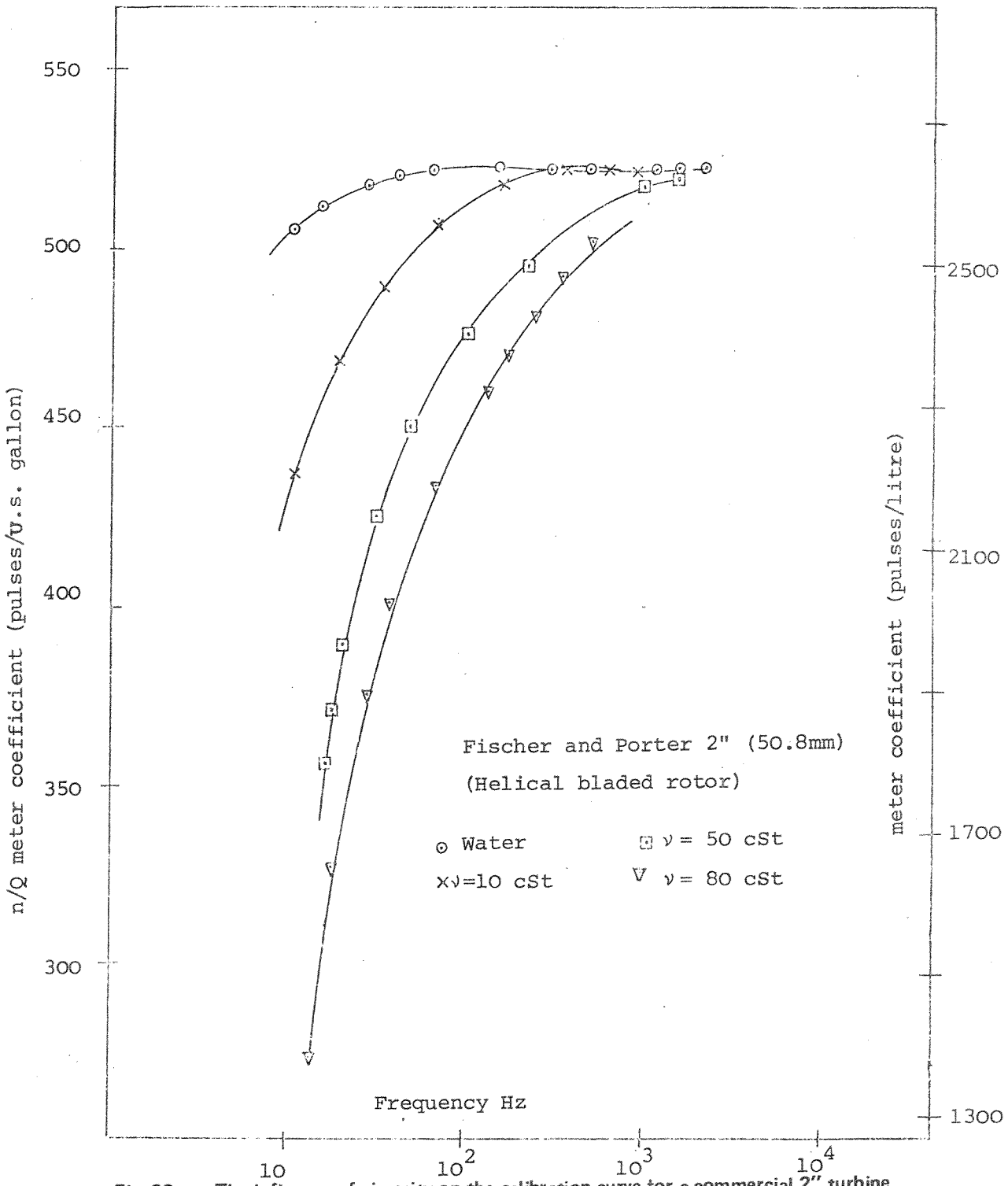

Fig. 32. The influence of viscosity on the calibration curve for a commercial 2" turbine meter in region of Low Re number

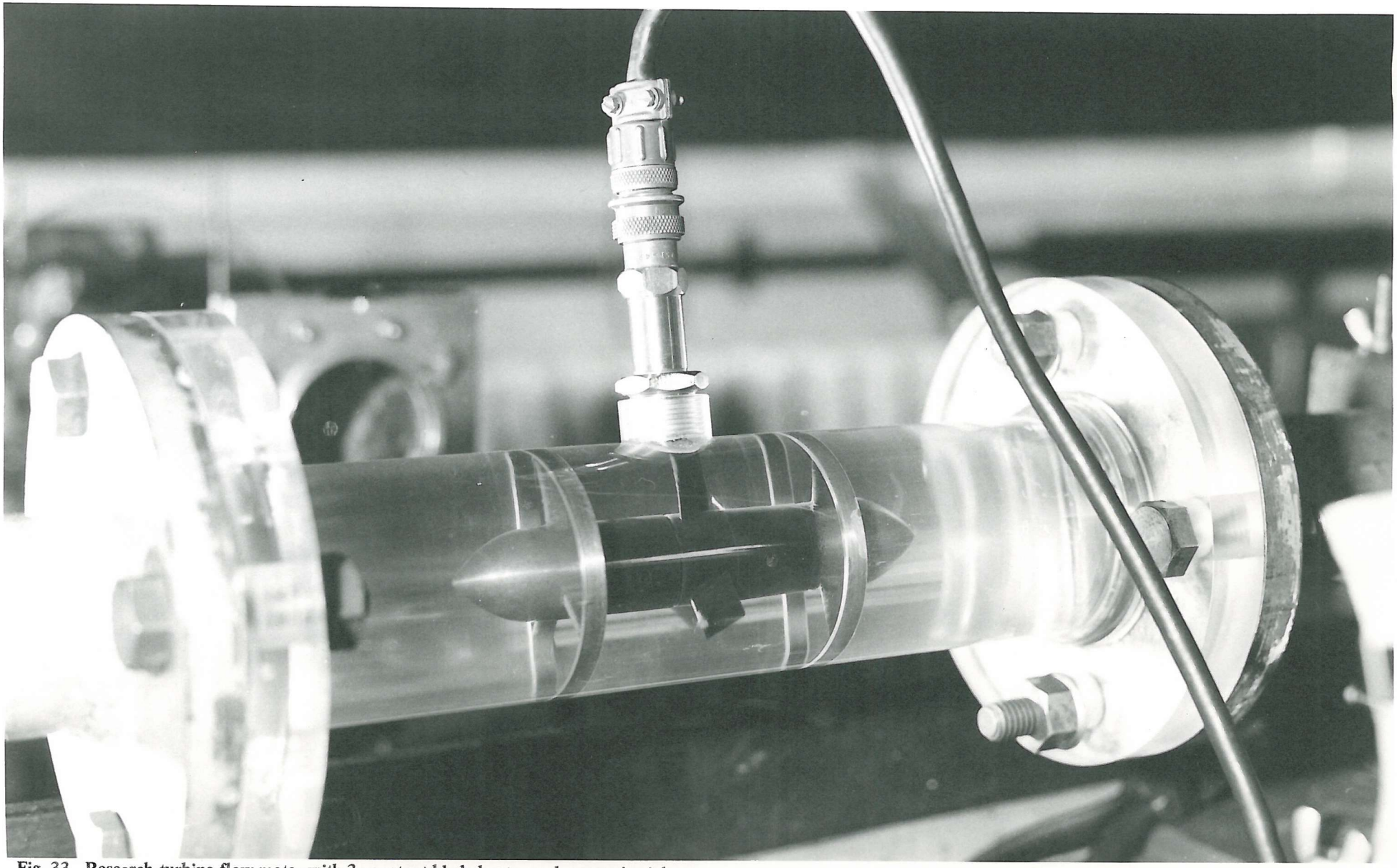

Fig. 33 Research turbine flow meter with 3 constant bladed rotor and magnetic pick-up

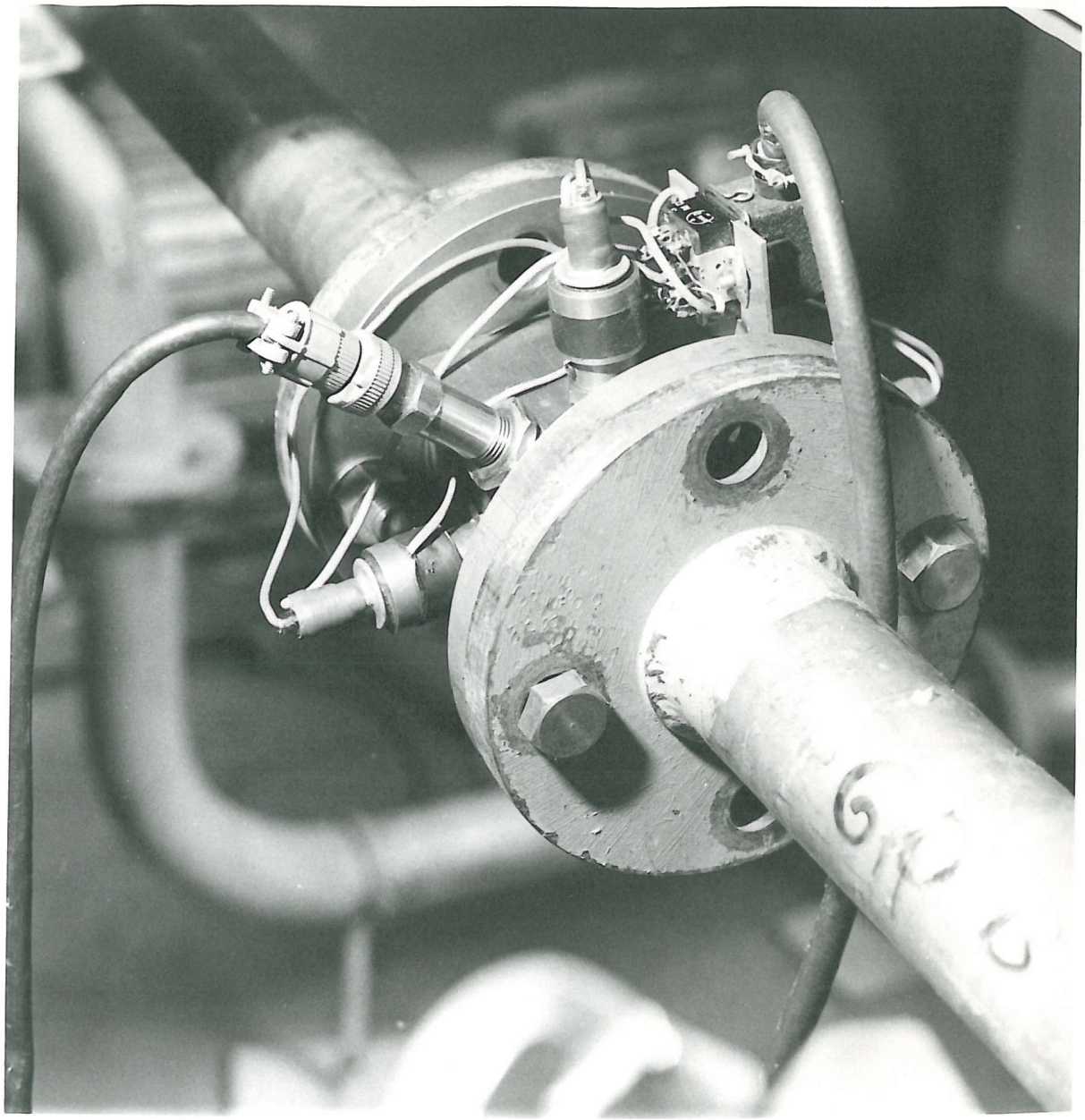

Fig. 34 Research turbine meter with 3 constant bladed rotor (4 photocell and 1 magnetic pick-up)

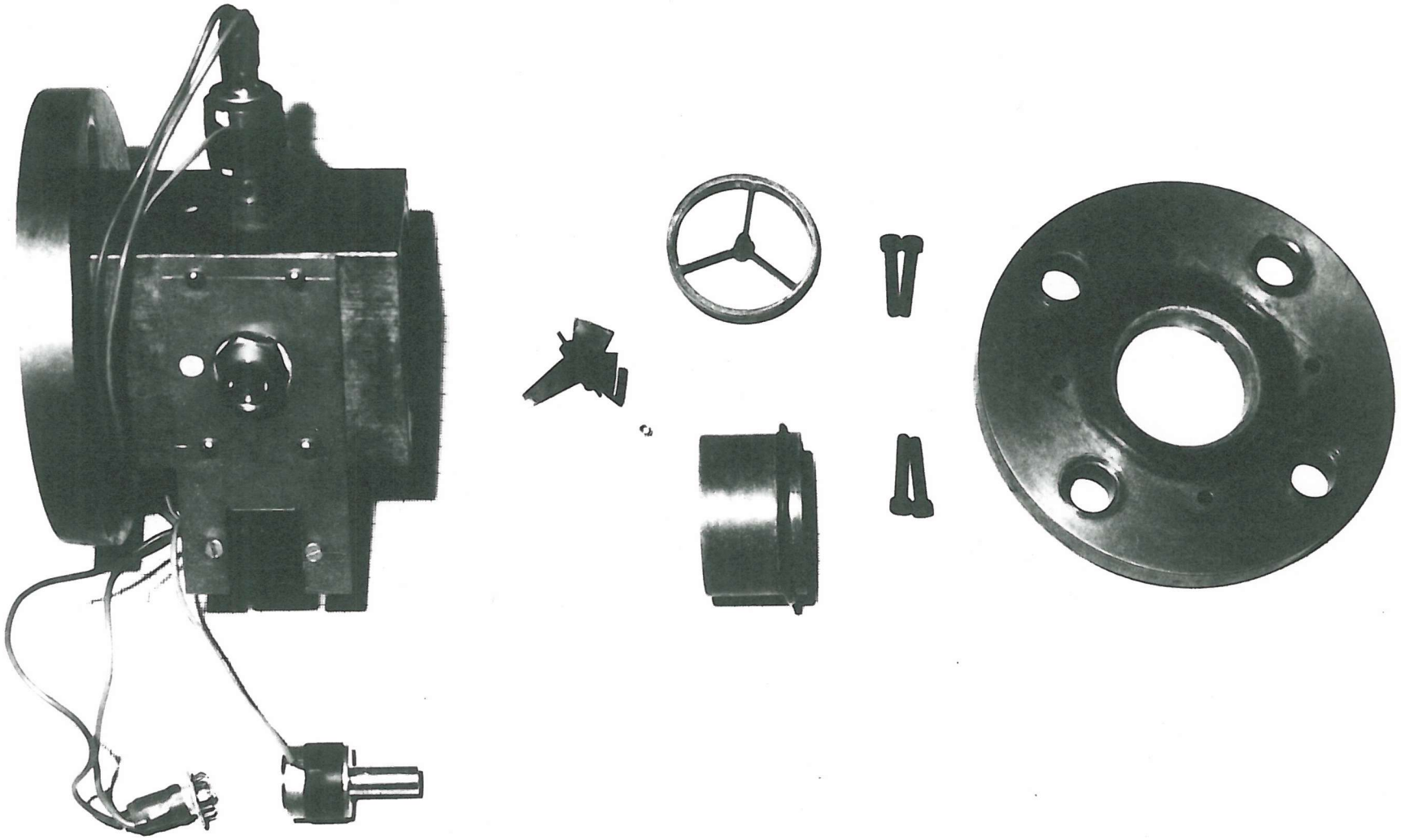

Figure 35. Partly dismantled view of research turbine flow meter with 4 photo cell pick-up

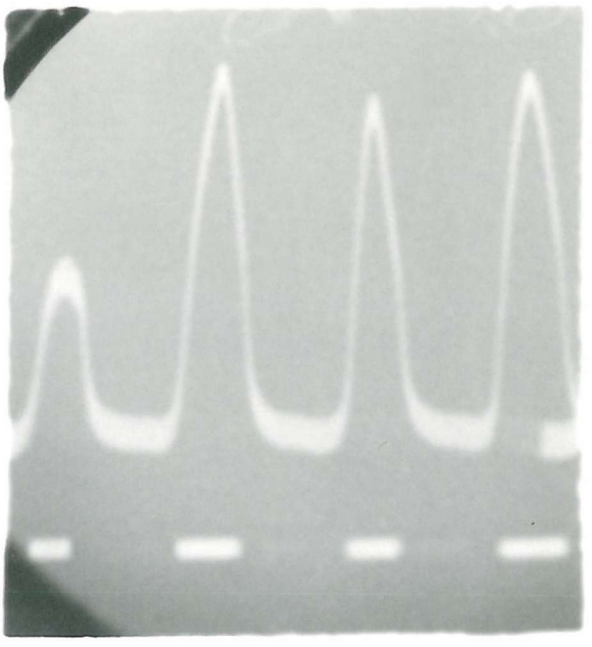

Fig. 36 Pulses produced from research meter with 4 photo cell pick-up corresponding schmidt-trigger signals (dots)

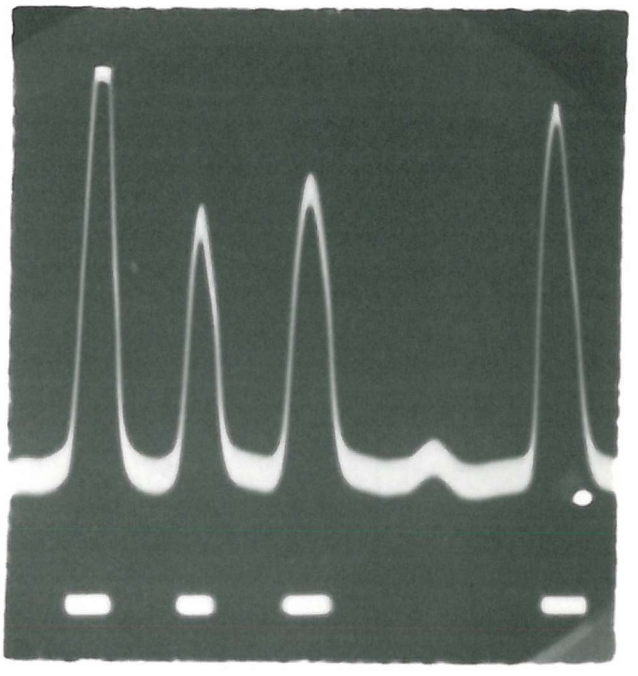

Fig. 37 Pulses from turbine flow meter with 4 photo cell pick-up and corresponding schmidt trigger signals. Pulse 4th from LHS insufficient to switch trigger

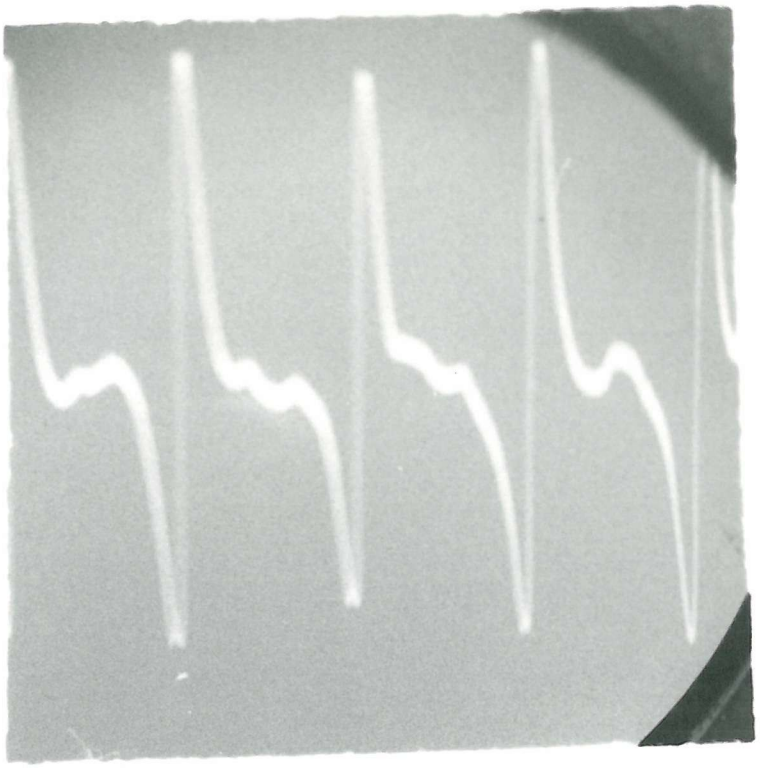

Fig. 38 Pulses from magnetic pick-up of research turbine meter

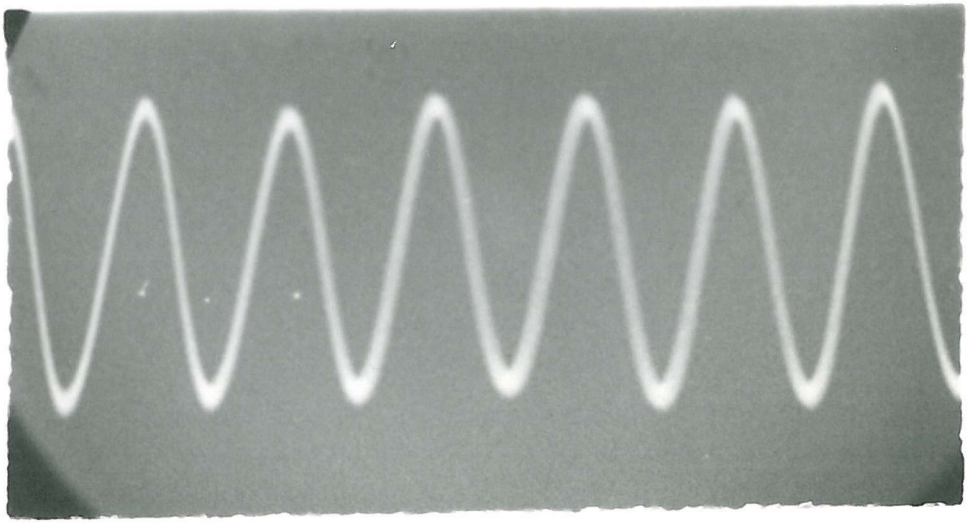

Fig. 39 Pulses from magnetic pick-up of a commercial turbine flow meter

Fig. 40 Control Panel of Calibration Rig

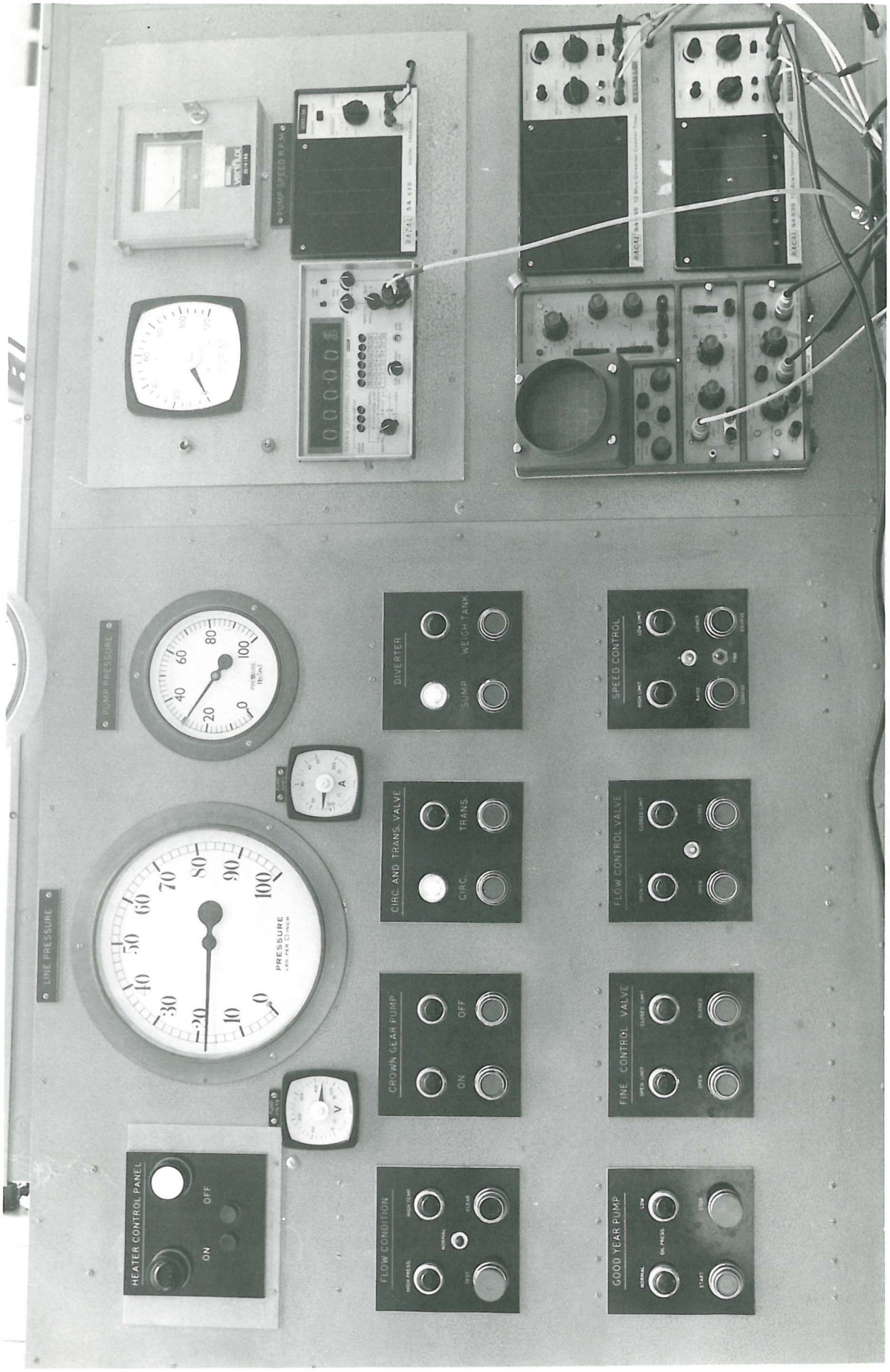

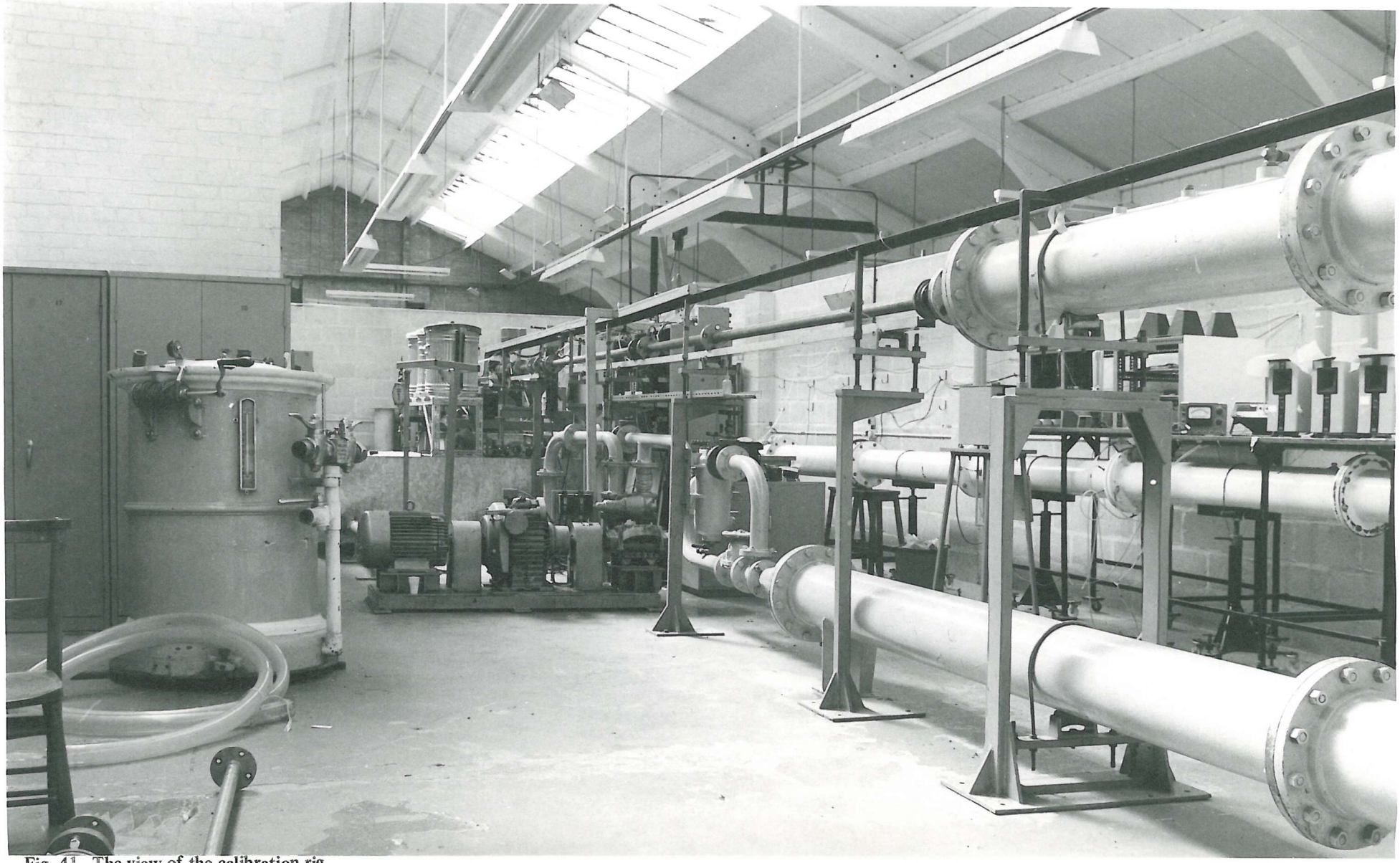

Fig. 41 The view of the calibration rig

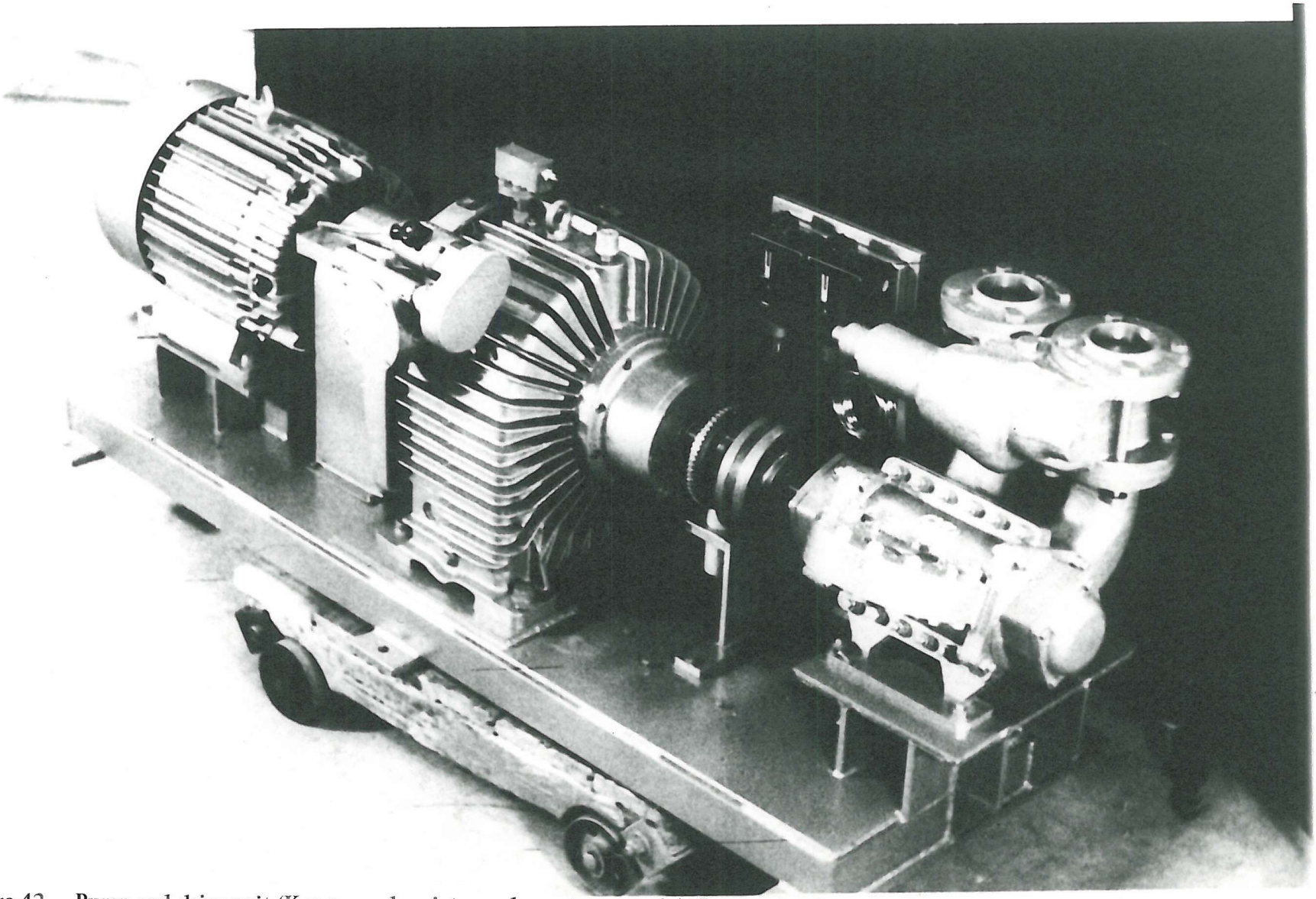

Figure 42. Pump and drive unit (Kopp speed variator and constant speed A.C. motor) prior to connection to the rig. Temperature and pressure protection switches are also shown

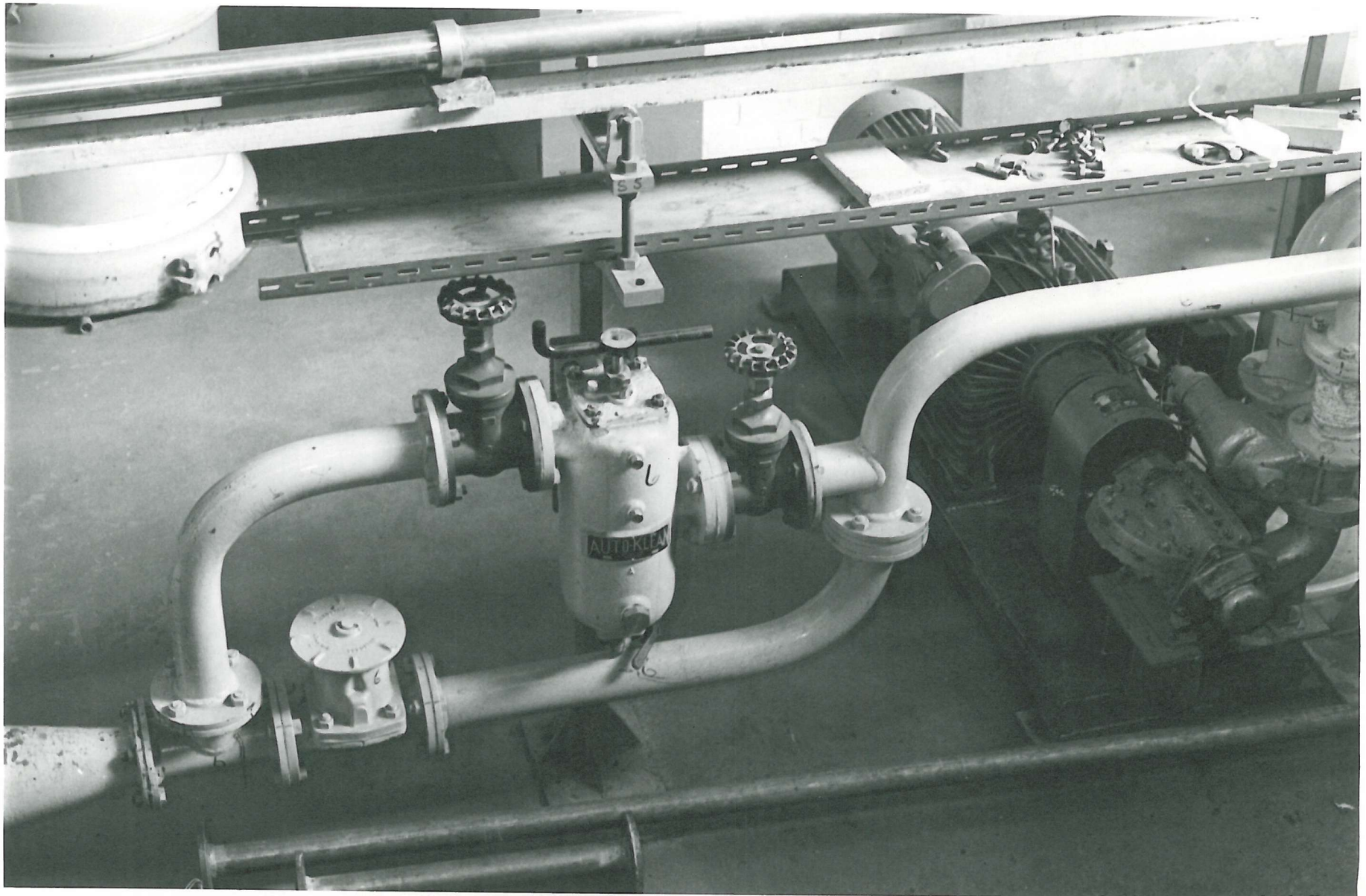

Figure 43. The filter system which includes a By-pass for diverting the flow from the filter when there is excessive line pressure (high flow rate)

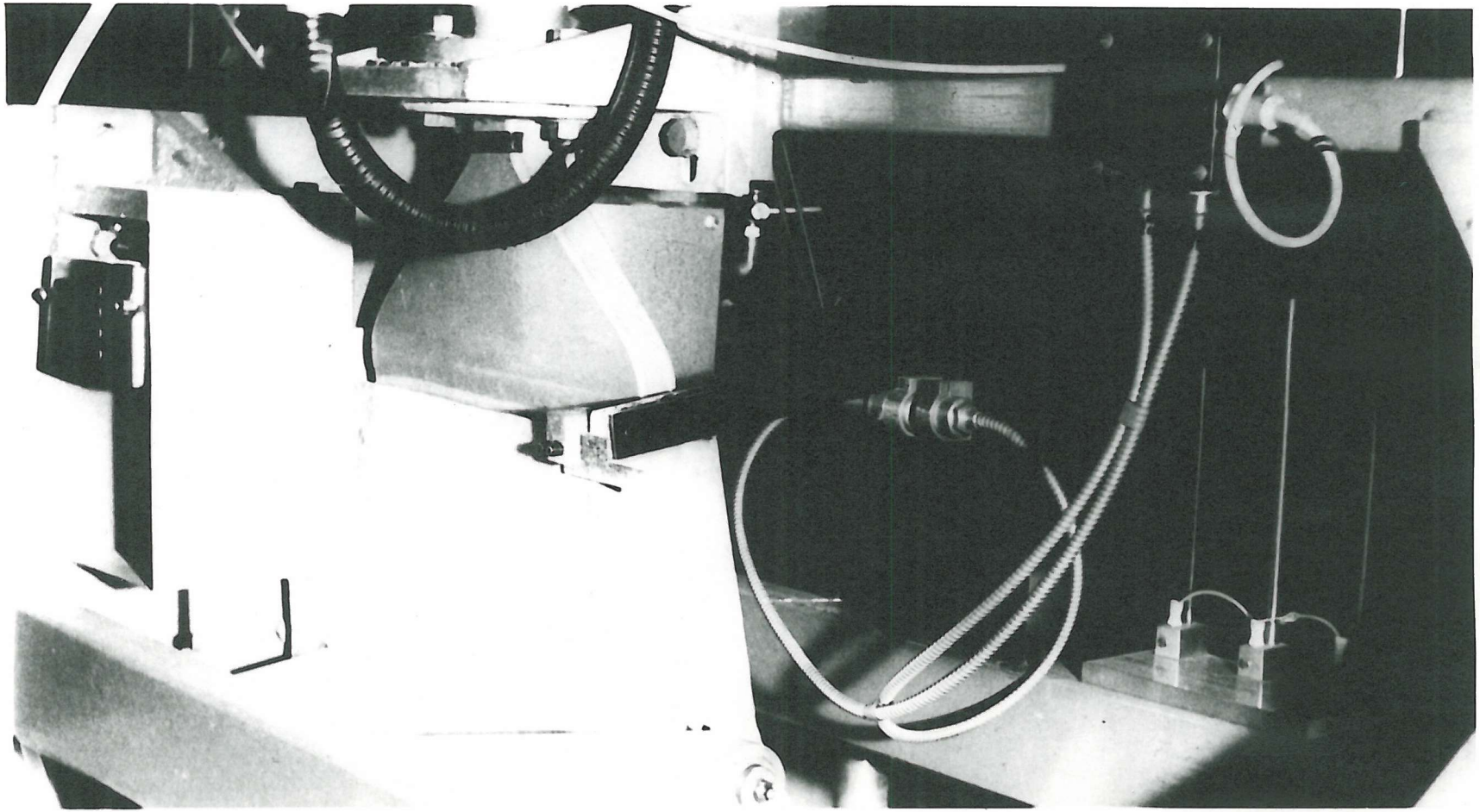

Figure 44. Close-up view of the flow diverting mechanism

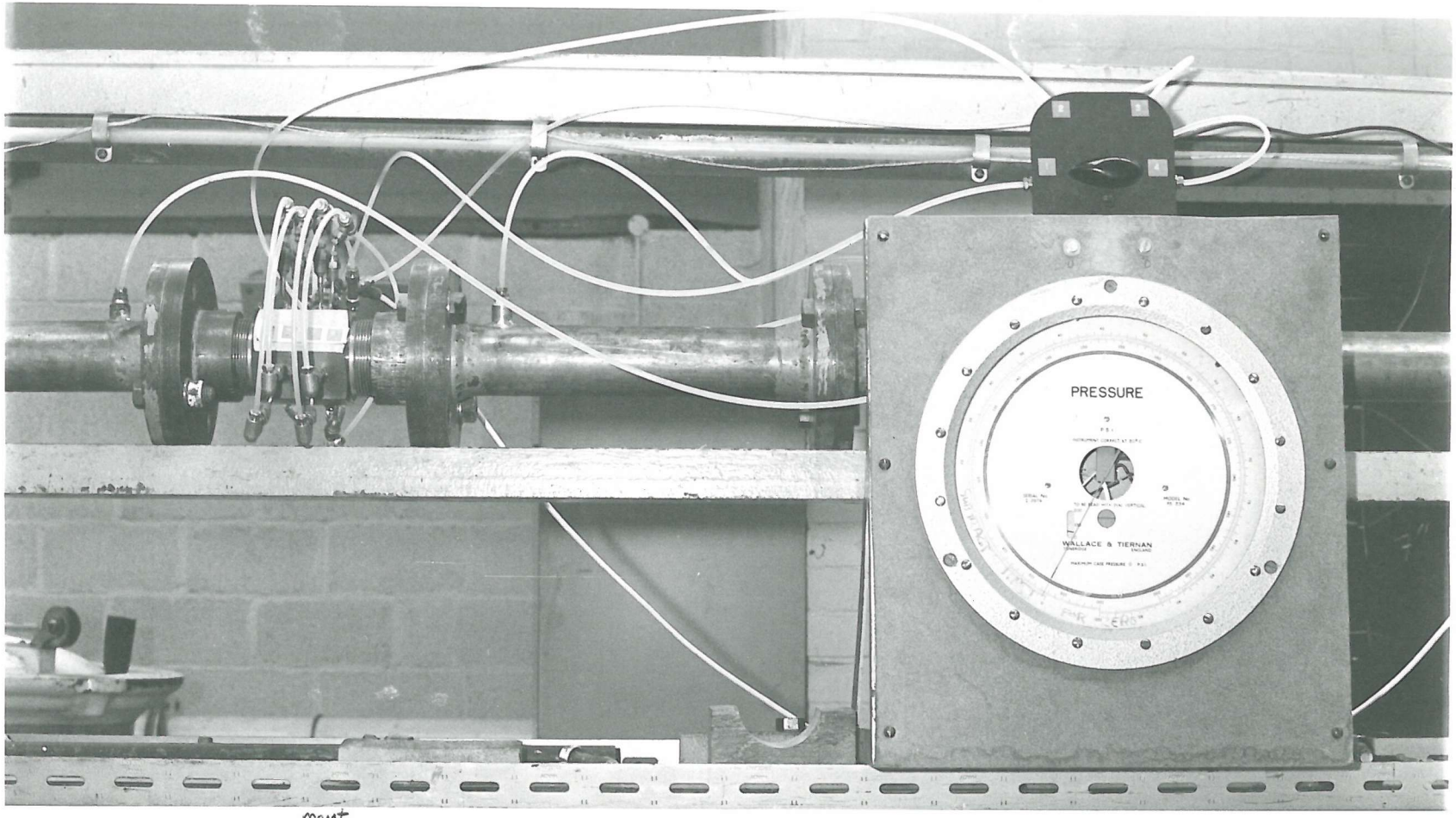

Fig. 45. Pressure measurement across the turbine blade and in upstream and downstream position of the rotor and far distance upstream and far distance downstream position

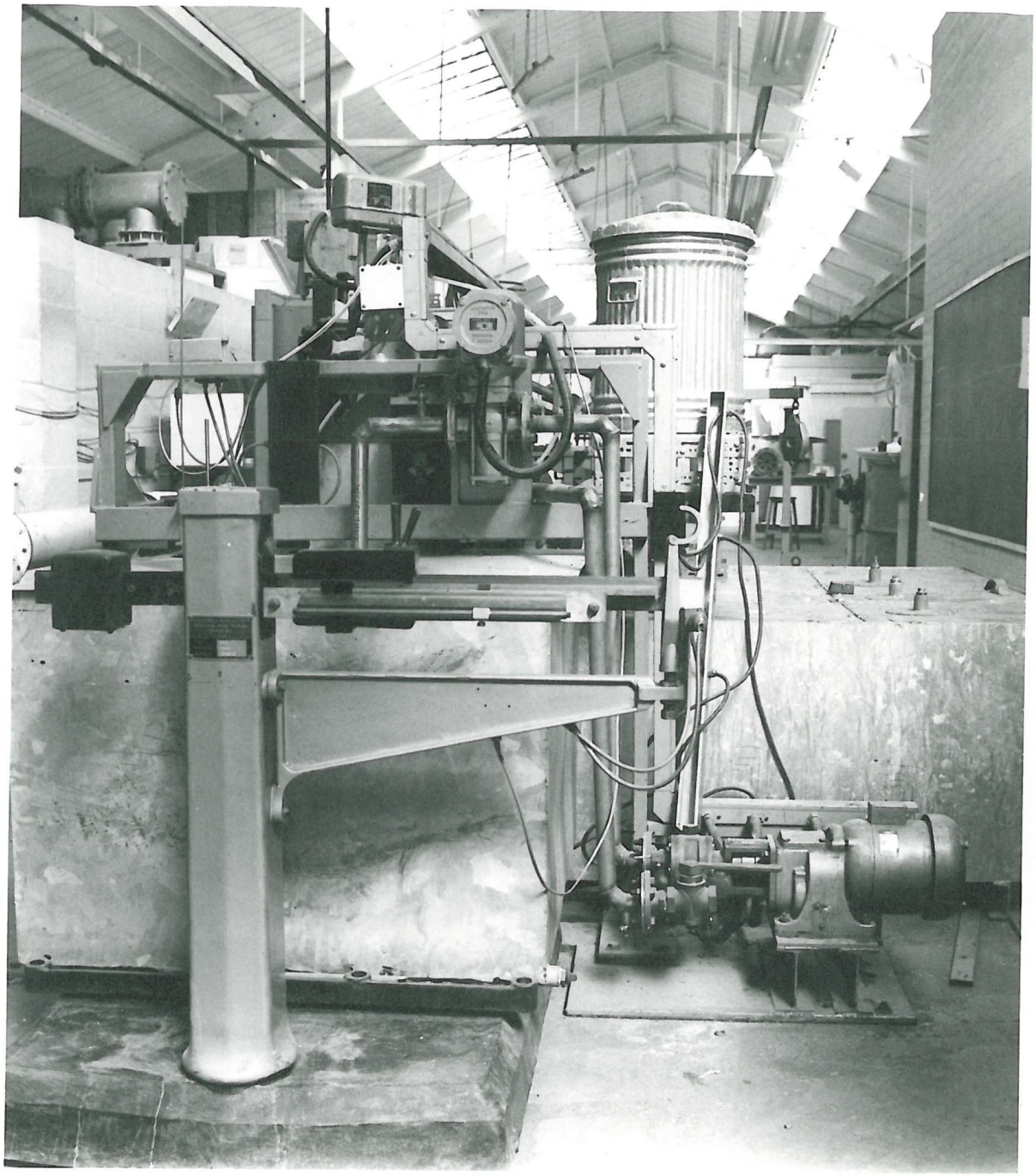

Figure 46. Weigh tank, weighing machine, fluid sump, transfer pump and viscosity container.

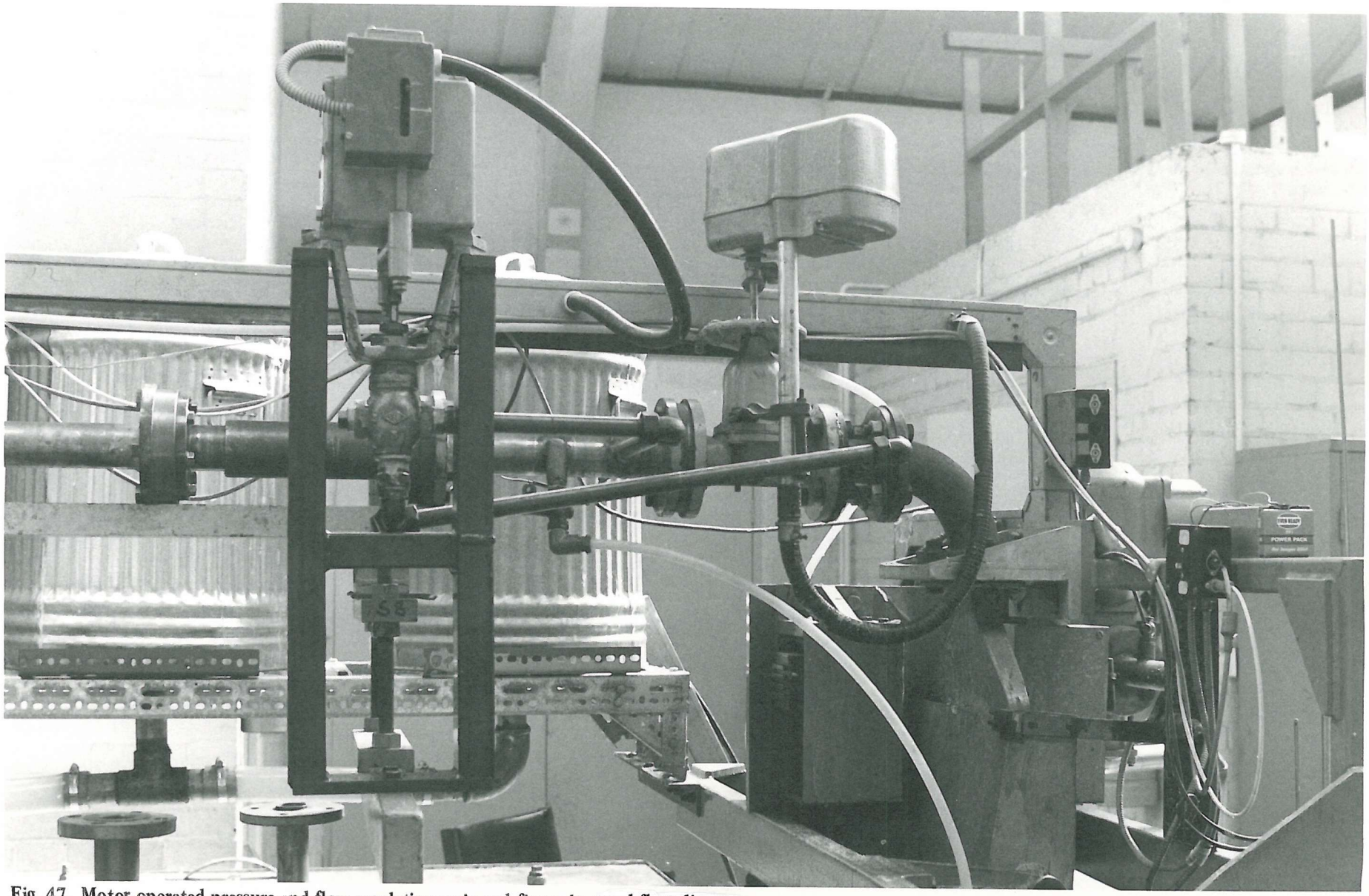

Fig. 47. Motor-operated pressure and flow regulating main and fine valves and flow diverter

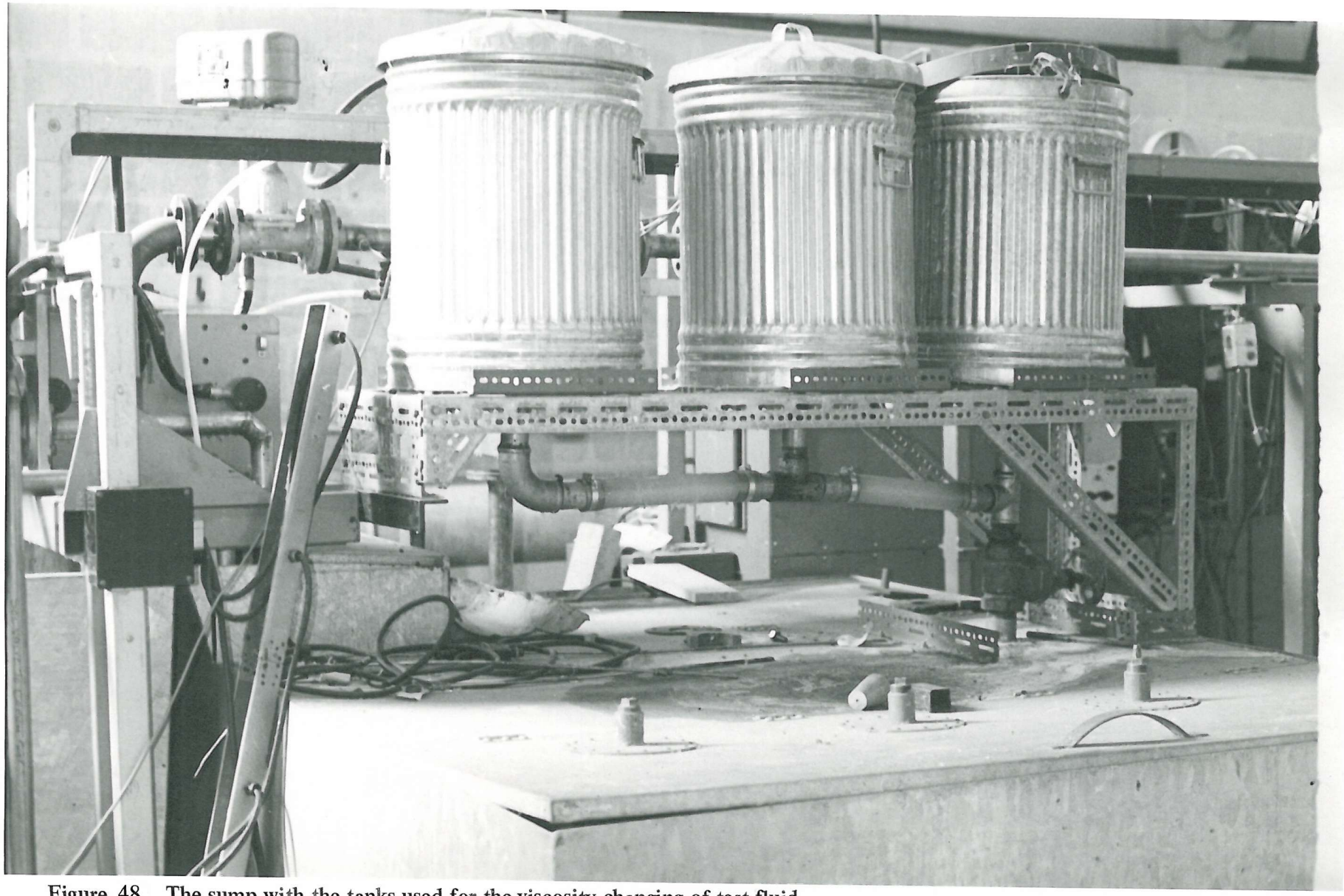

Figure 48 . The sump with the tanks used for the viscosity changing of test fluid

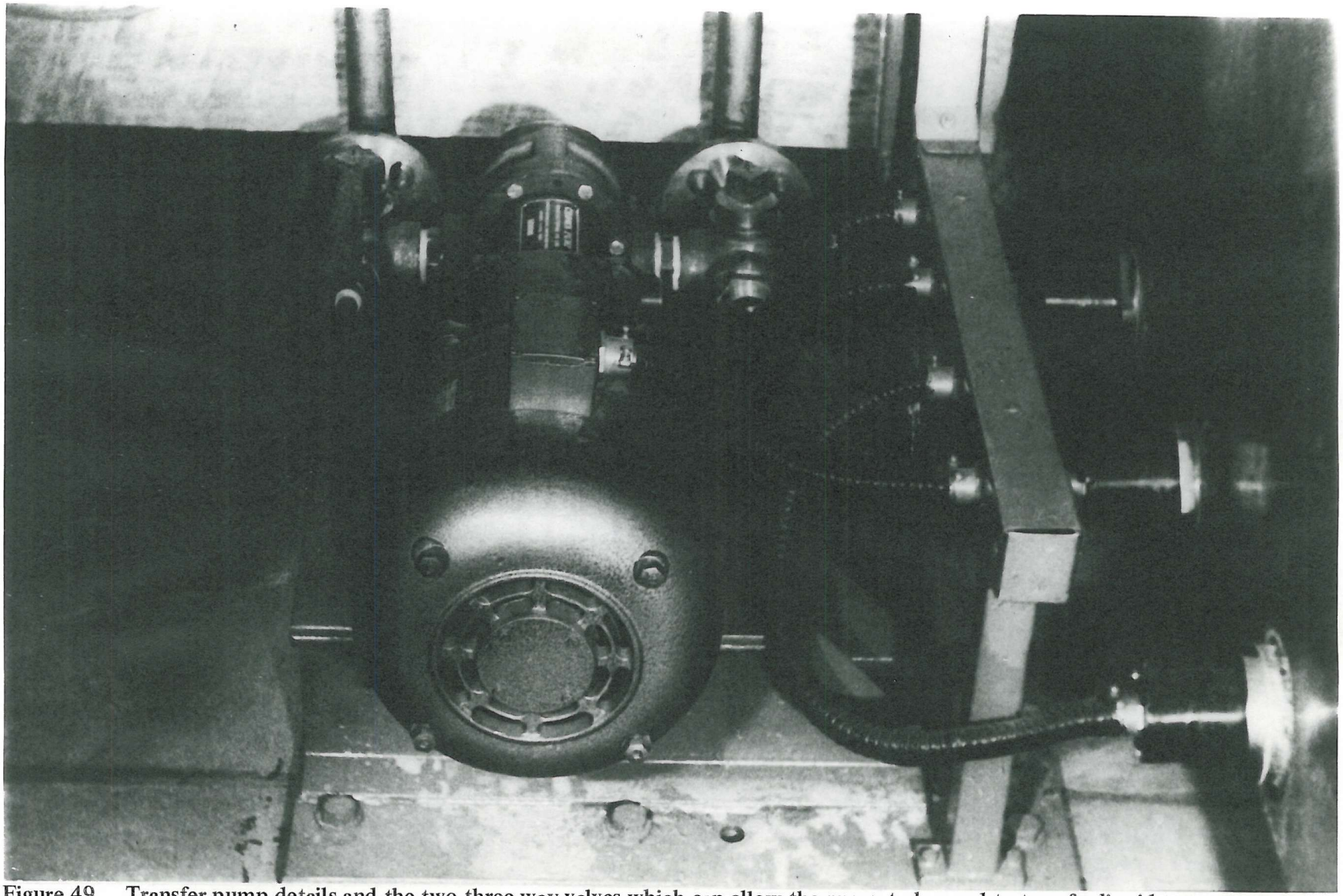

Figure 49. Transfer pump details and the two three-way valves which can allow the pump to be used to transfer liquid to or extract liquid from the rig.

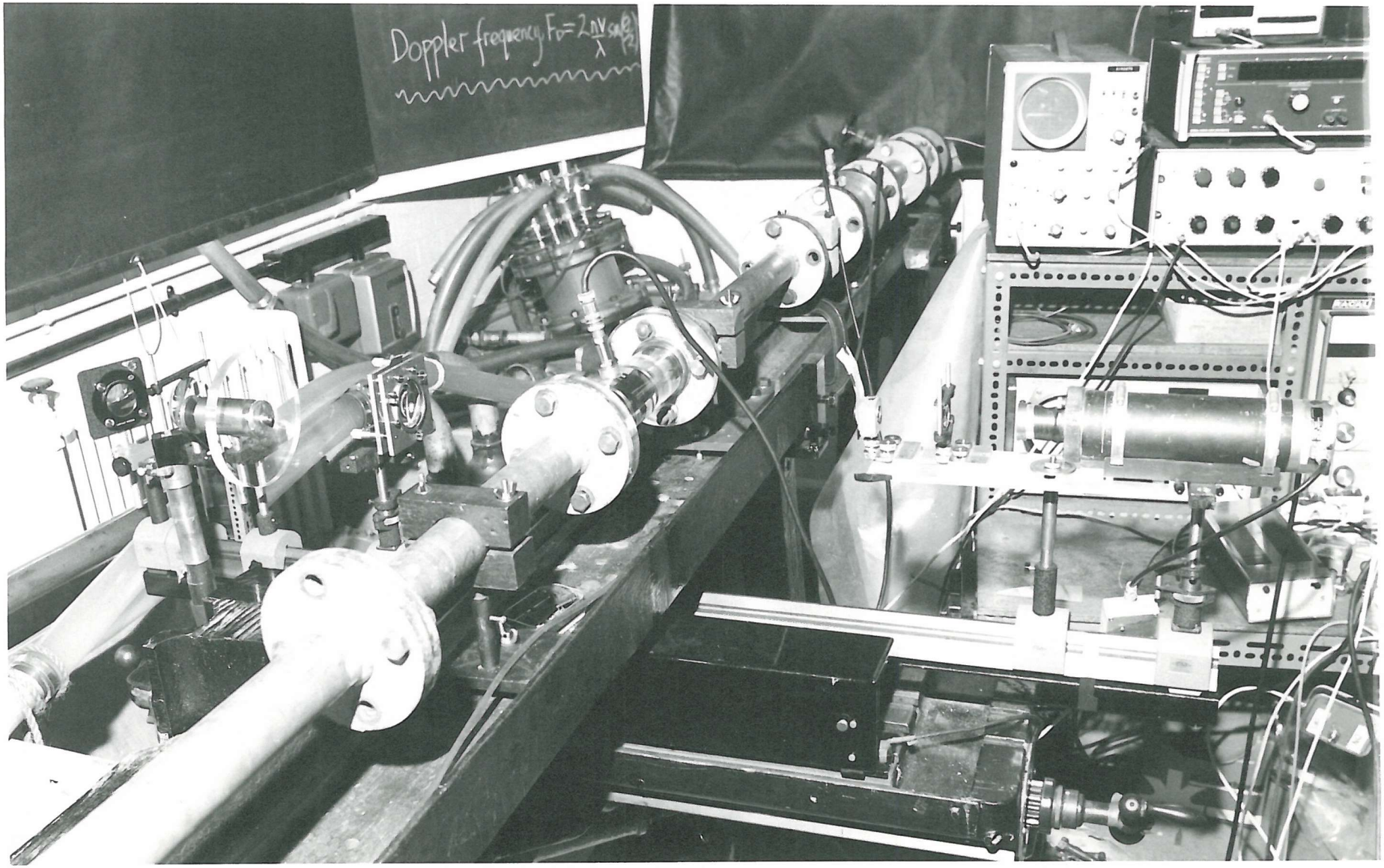

Fig. 50 Optical arrangement for velocity measurement through the research turbine meter

Fig. 51 Electronic signal processing for flow velocity measurement in upstream and downstream position of the turbine research flow meter with LDV

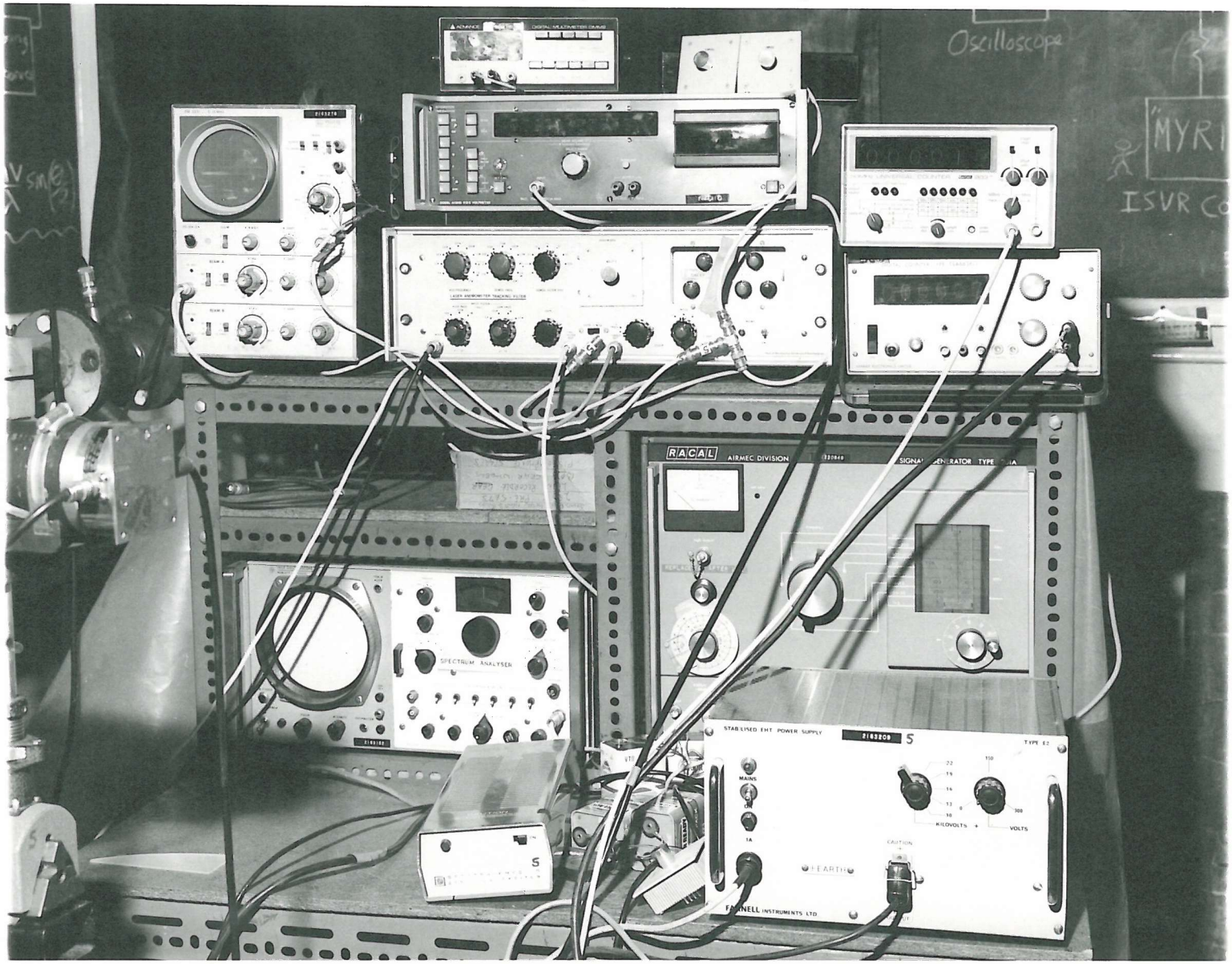

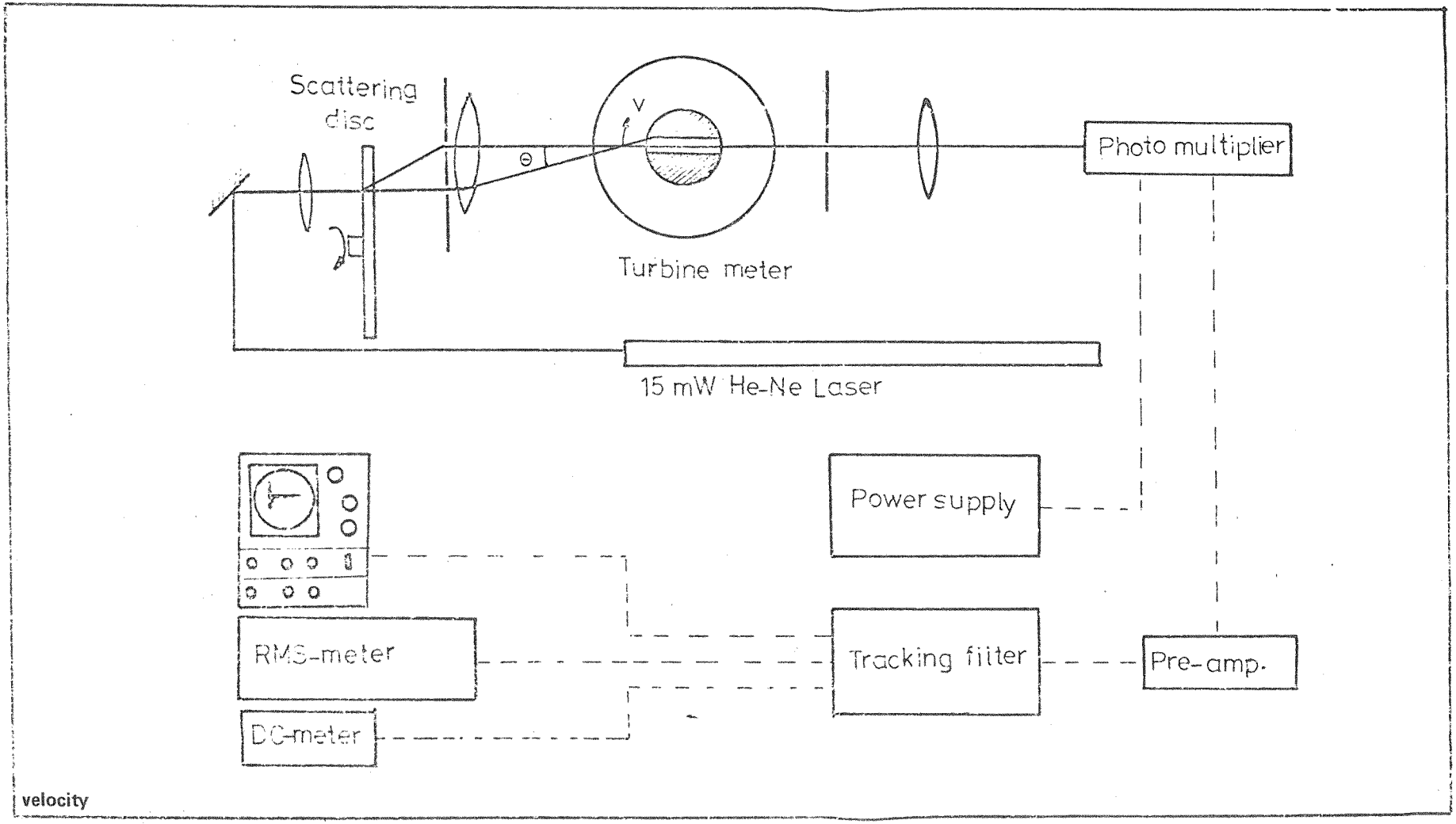

Fig. 52. Electronic signal processing for velocity measurement through the turbine flow meter with its optical arrangement

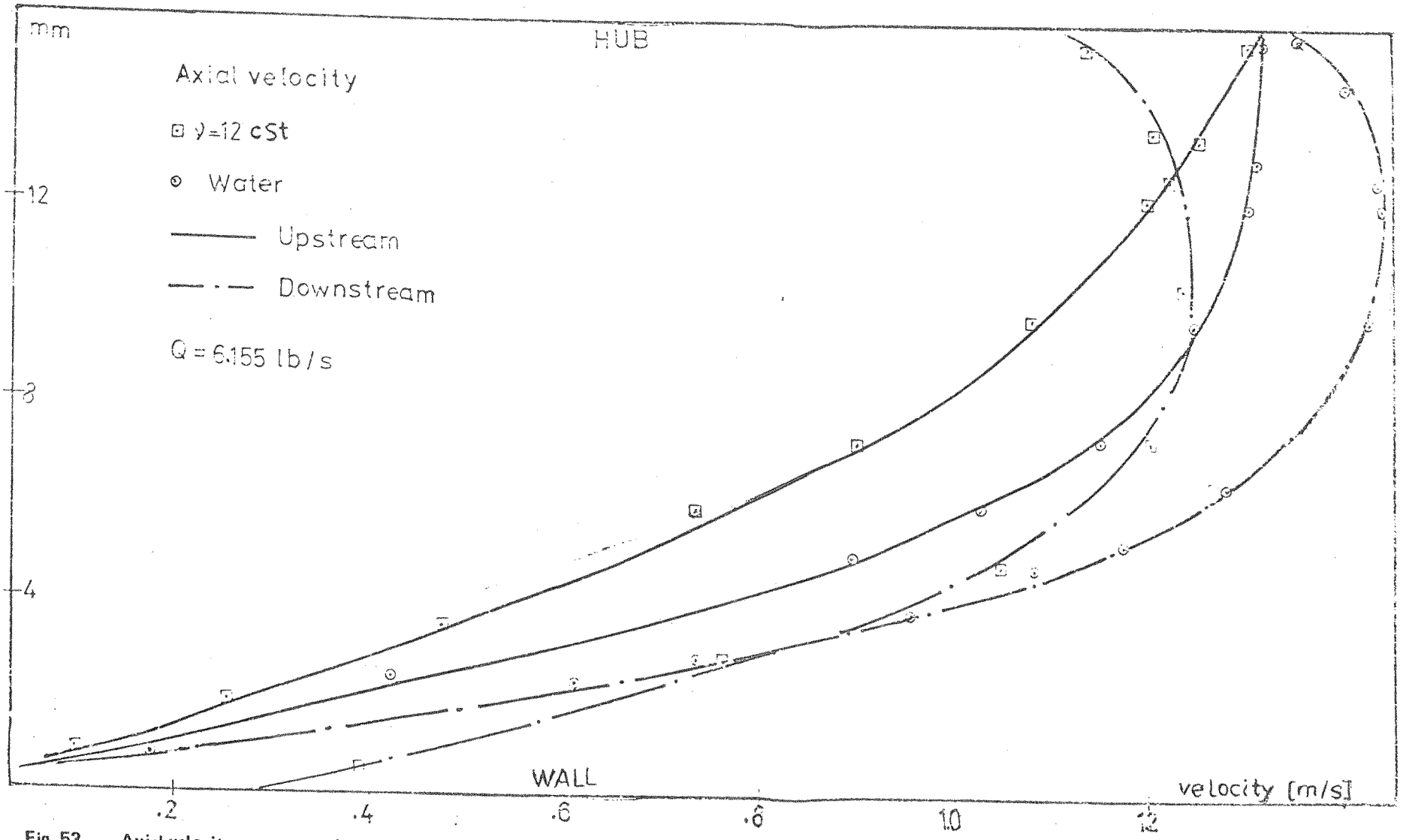

Fig. 53. Axial velocity component in research turbine flow meter in upstream and downstream position

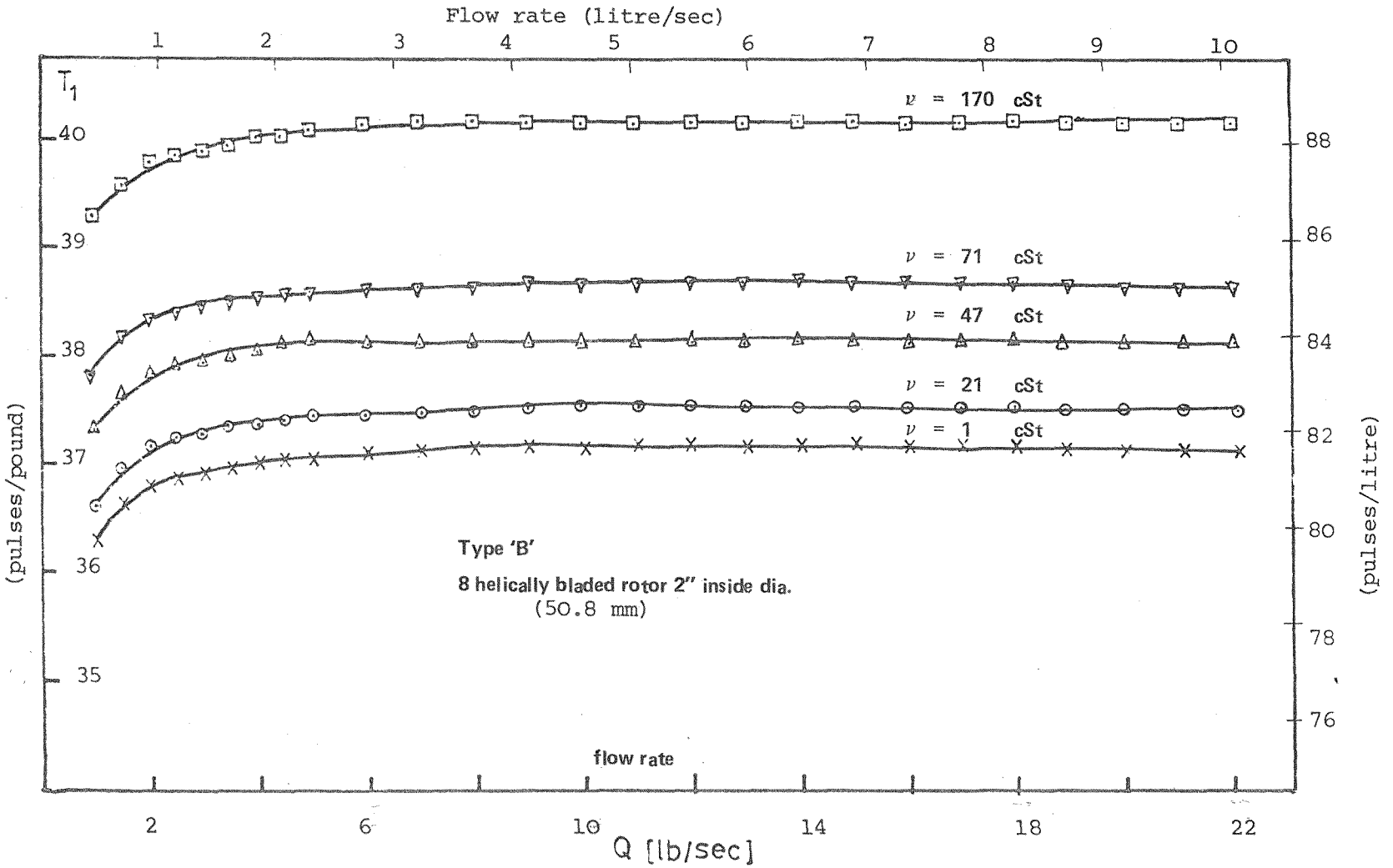

Fig. 54. The empirical calculation of $T_1 = f(Q)$ for a commercial turbine flow meter type 'B'. The value of T_1 has been calculated empirically by the least square method for different fluid viscosity

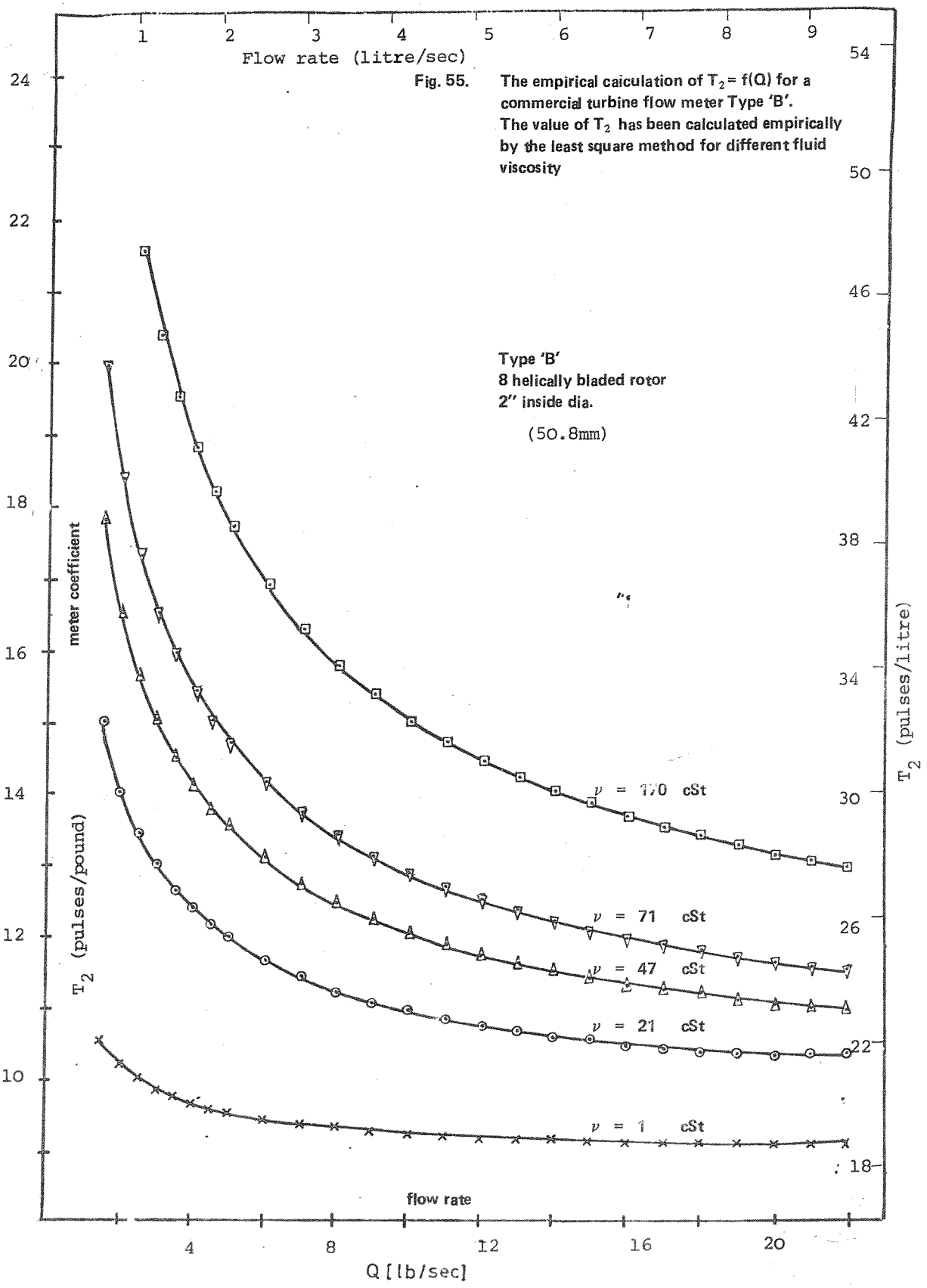

Fig. 55. The empirical caiculation of $T_2 = f(Q)$ for a commercial turbine flow meter Type 'B'. The value of T_2 has been calculated empirically by the least square method for different fluid viscosity

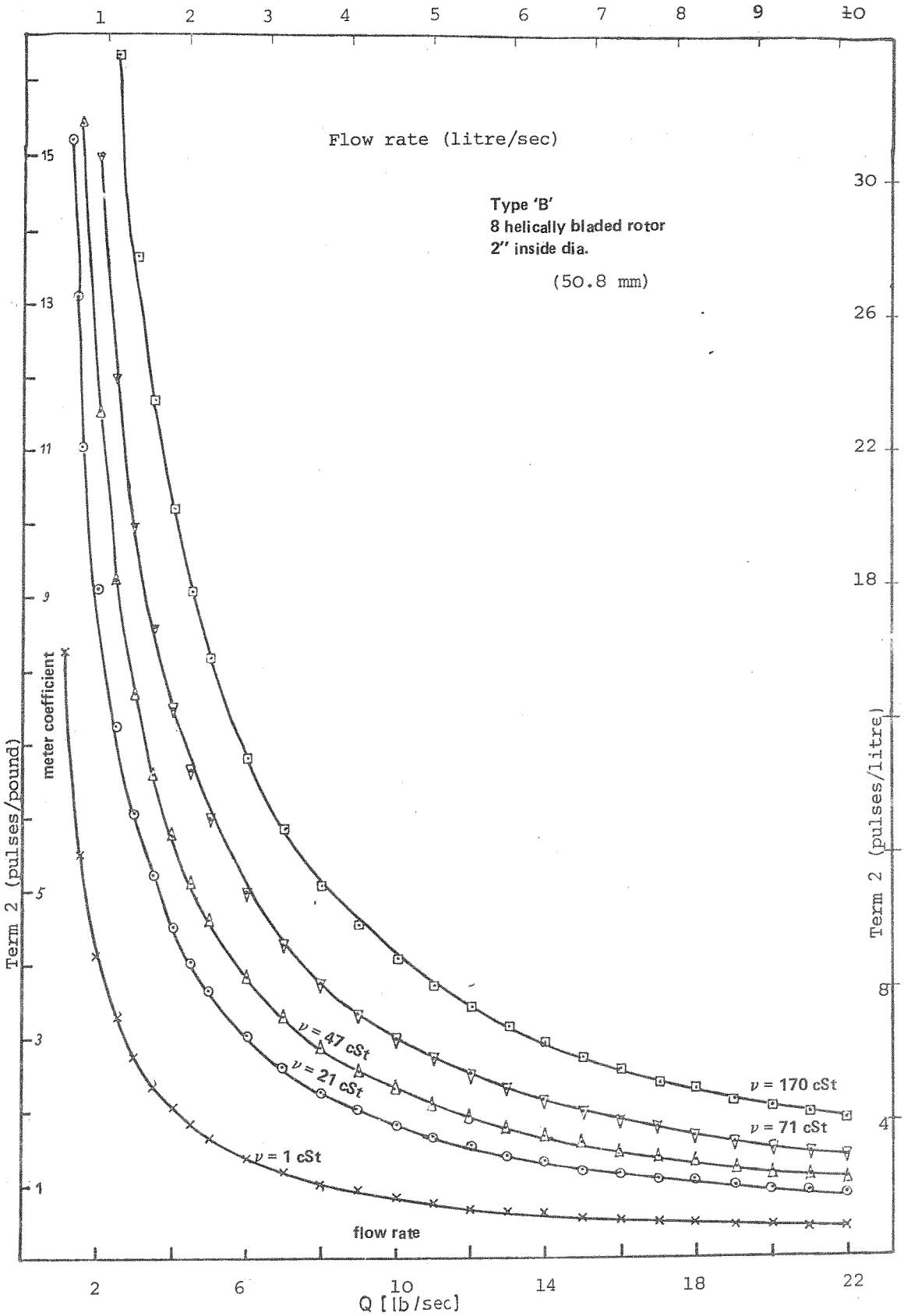

Fig. 56. The empirical calculation of term 2 of the main turbine equation for a commercial turbine flow meter type B. The value of term 2 has been plotted for various fluid viscosities

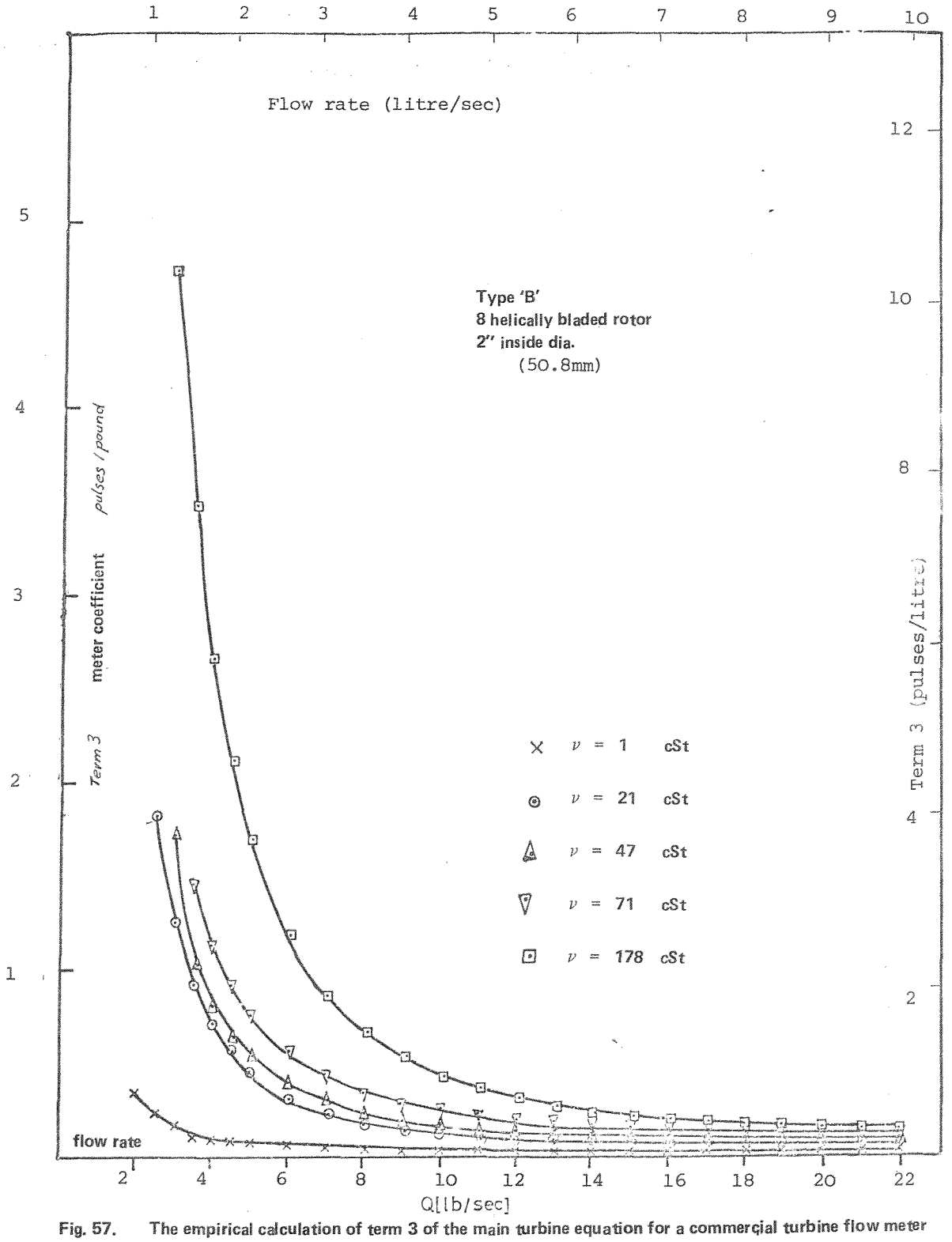

Fig. 57. The empirical calculation of term 3 of the main turbine equation for a commercial turbine flow meter type B. The value of term 3 has also been calculated for various fluid viscosities

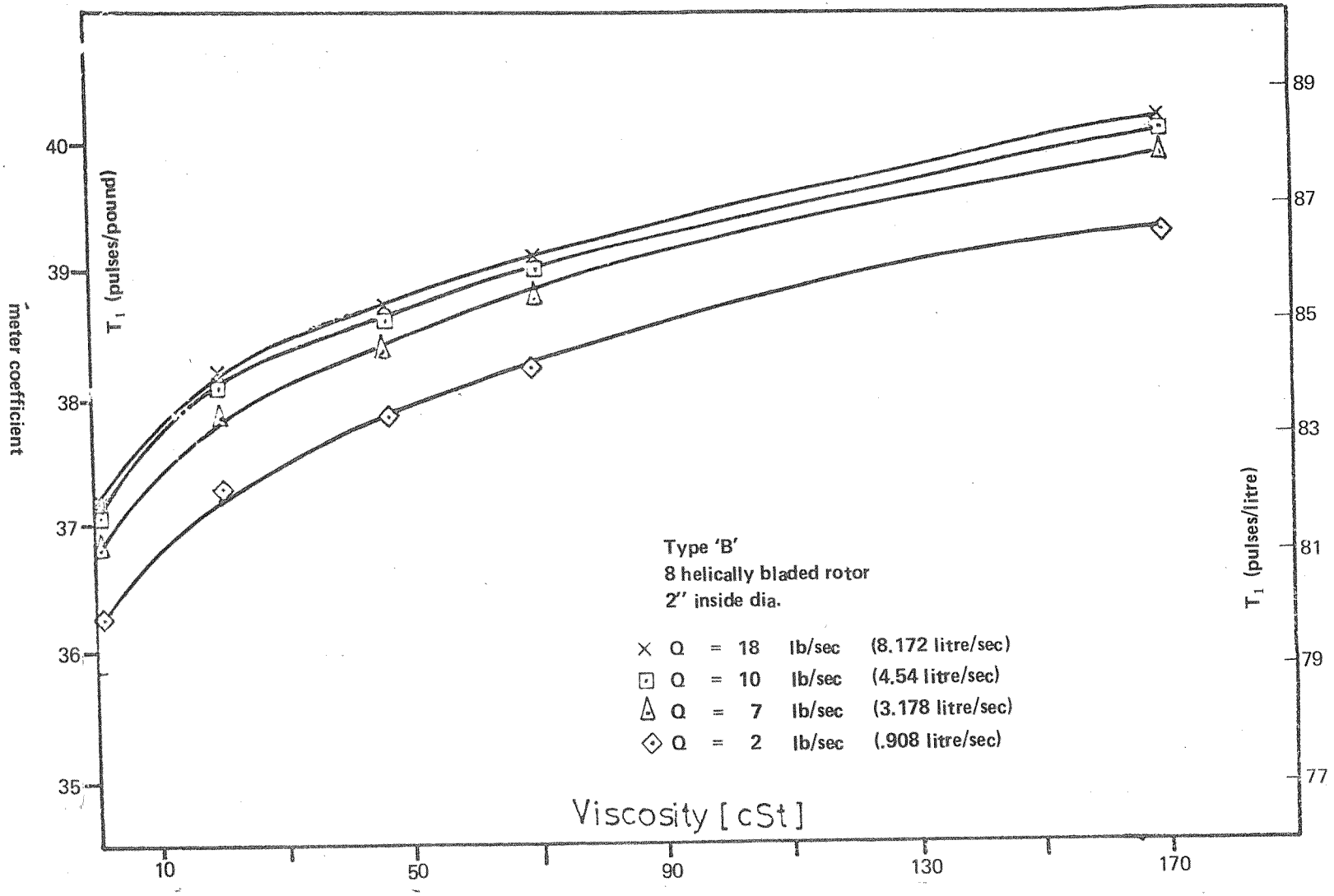

Fig. 58. The empirical calculation of T_1 with variation in the fluid viscosity for various flow rates.

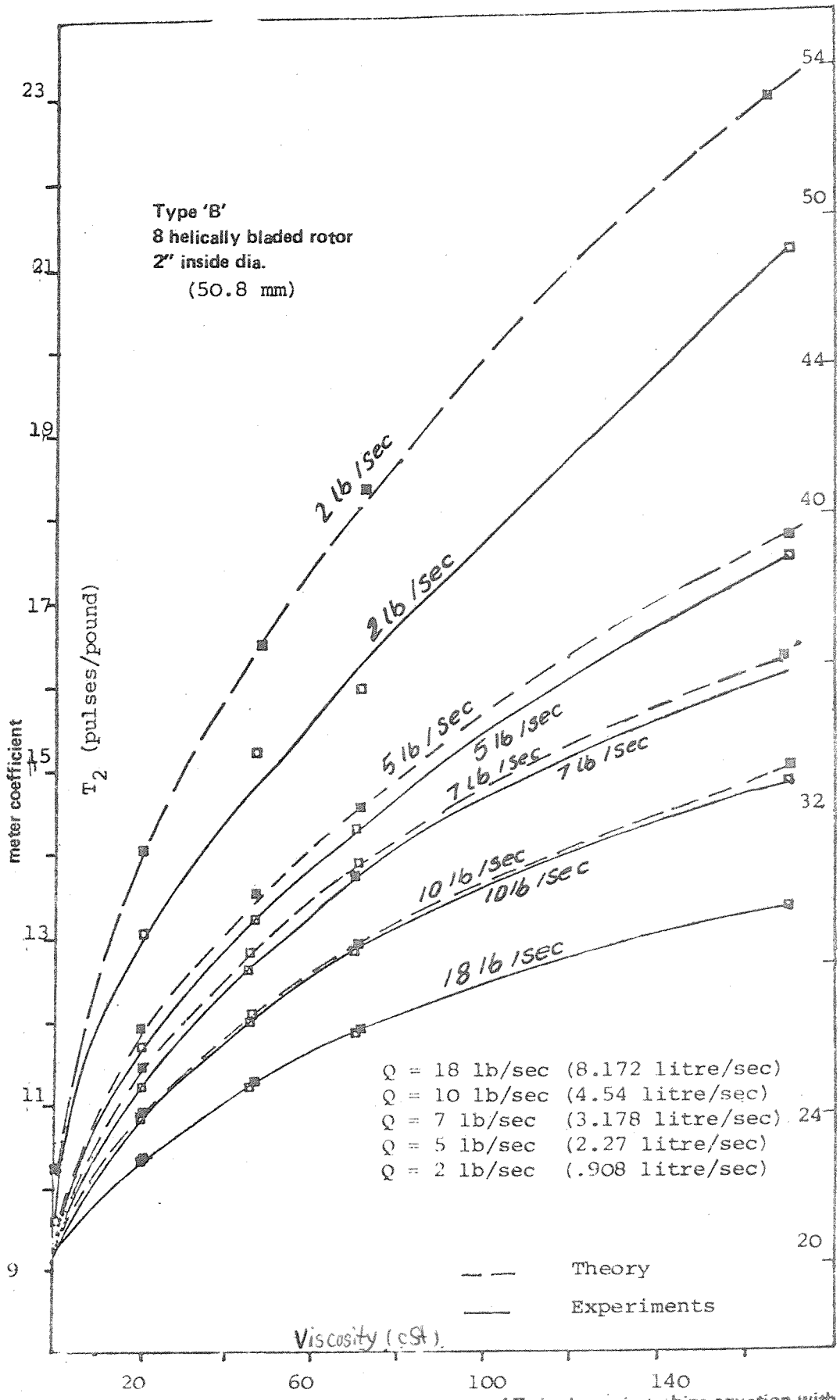

Fig. 59. The empirical and theoretical calculation of T_1 in the main turbine equation with variations in fluid viscosity and different flow rates.

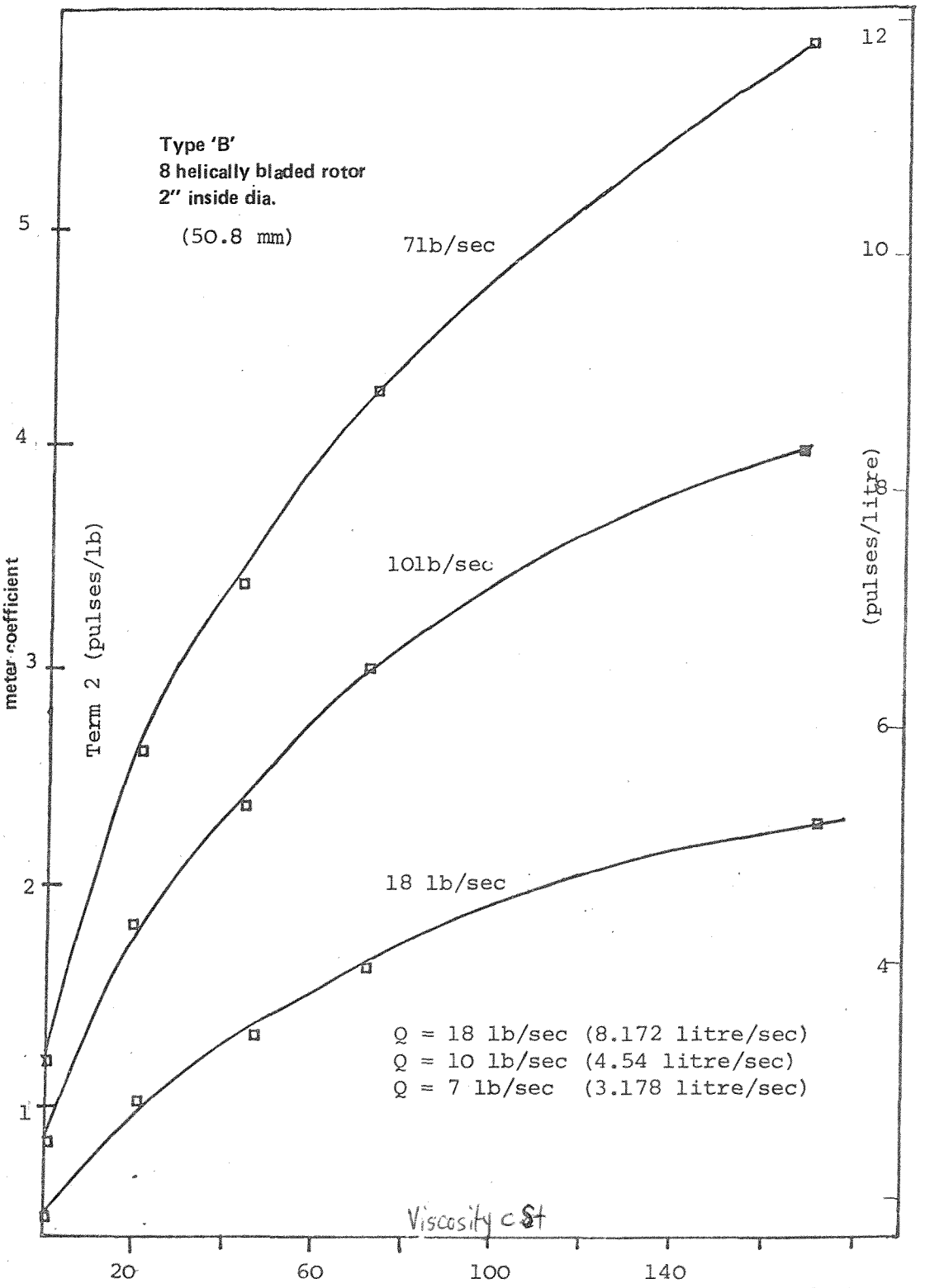

Fig. 60. The empirical calculation of term 2 of the main turbine equation for various fluid viscosities and flow rates.

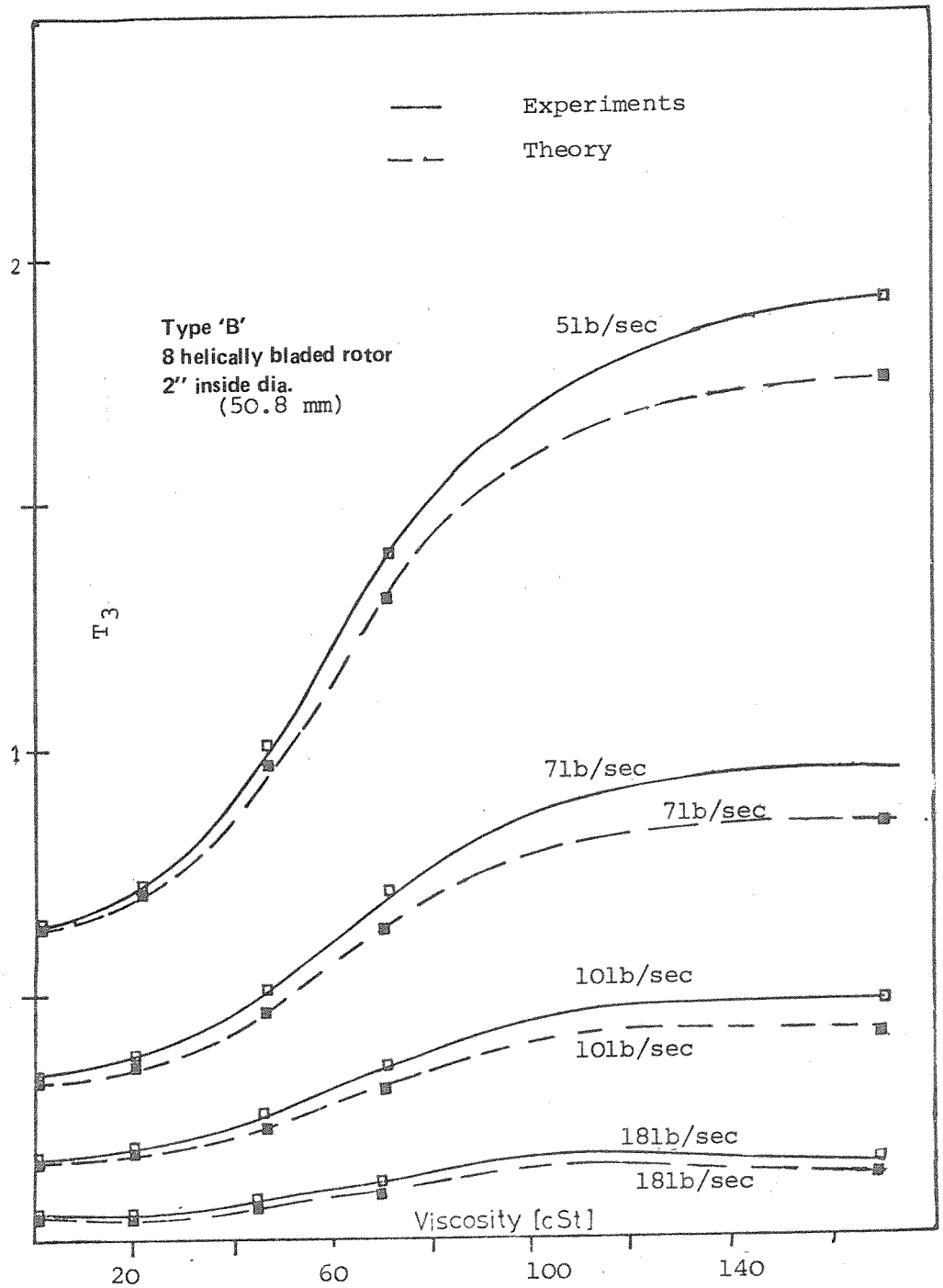

Fig. 61. The empirical and theoretical calculation of T_3 of the main turbine equation for various fluid viscosities and flow rates.

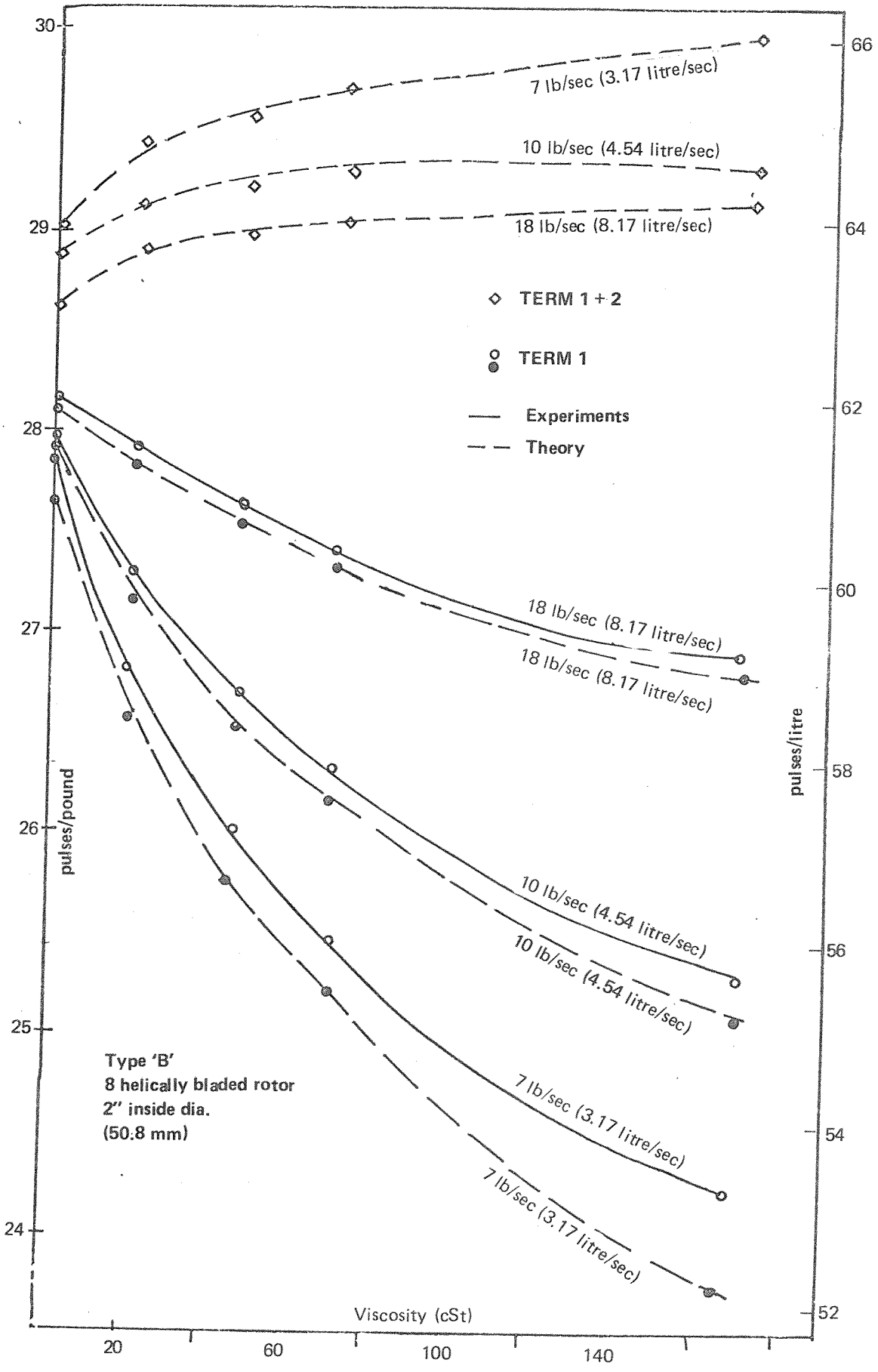

Fig. 62. The empirical and theoretical calculation of TERM 1 and empirical calculation of TERM 1 + 2 of the main turbine equation for various fluid viscosities and flow rates.

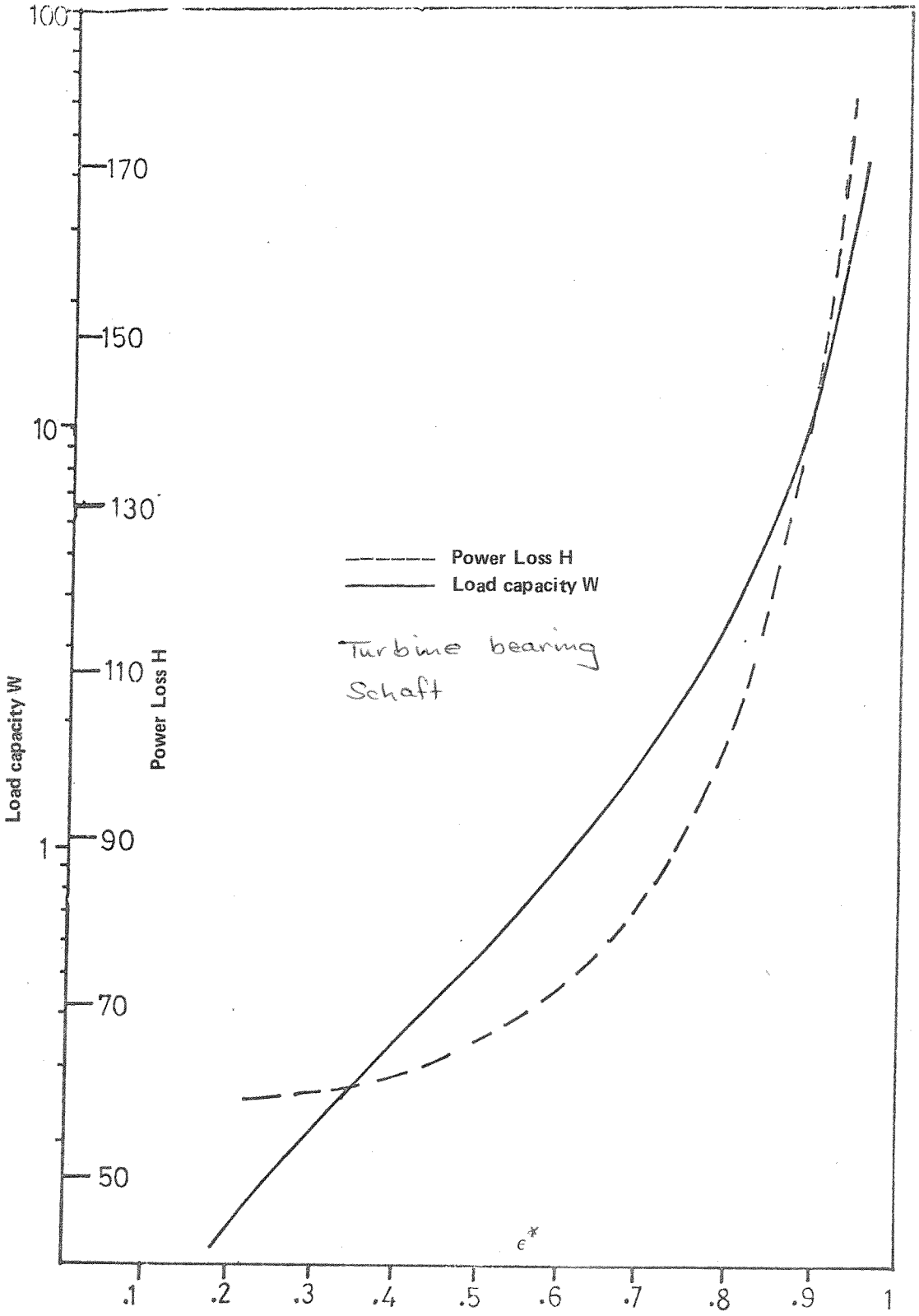

Fig. 63. Power loss H and load capacity w for a central circumferential groove and a single axial groove at the maximum film thickness

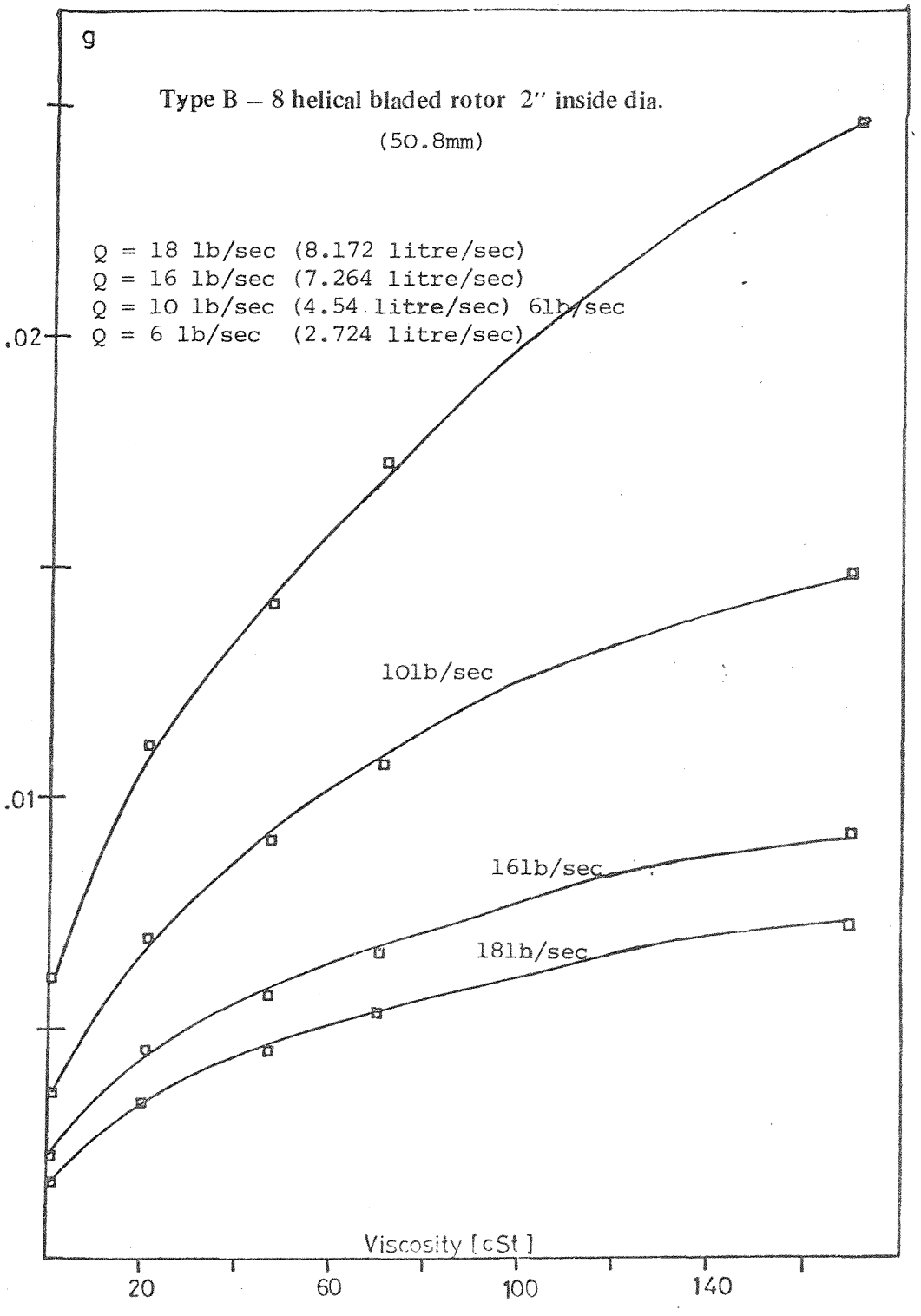

Fig. 64. The empirical calculation of leakage ratio g for various viscosities and flow rates.

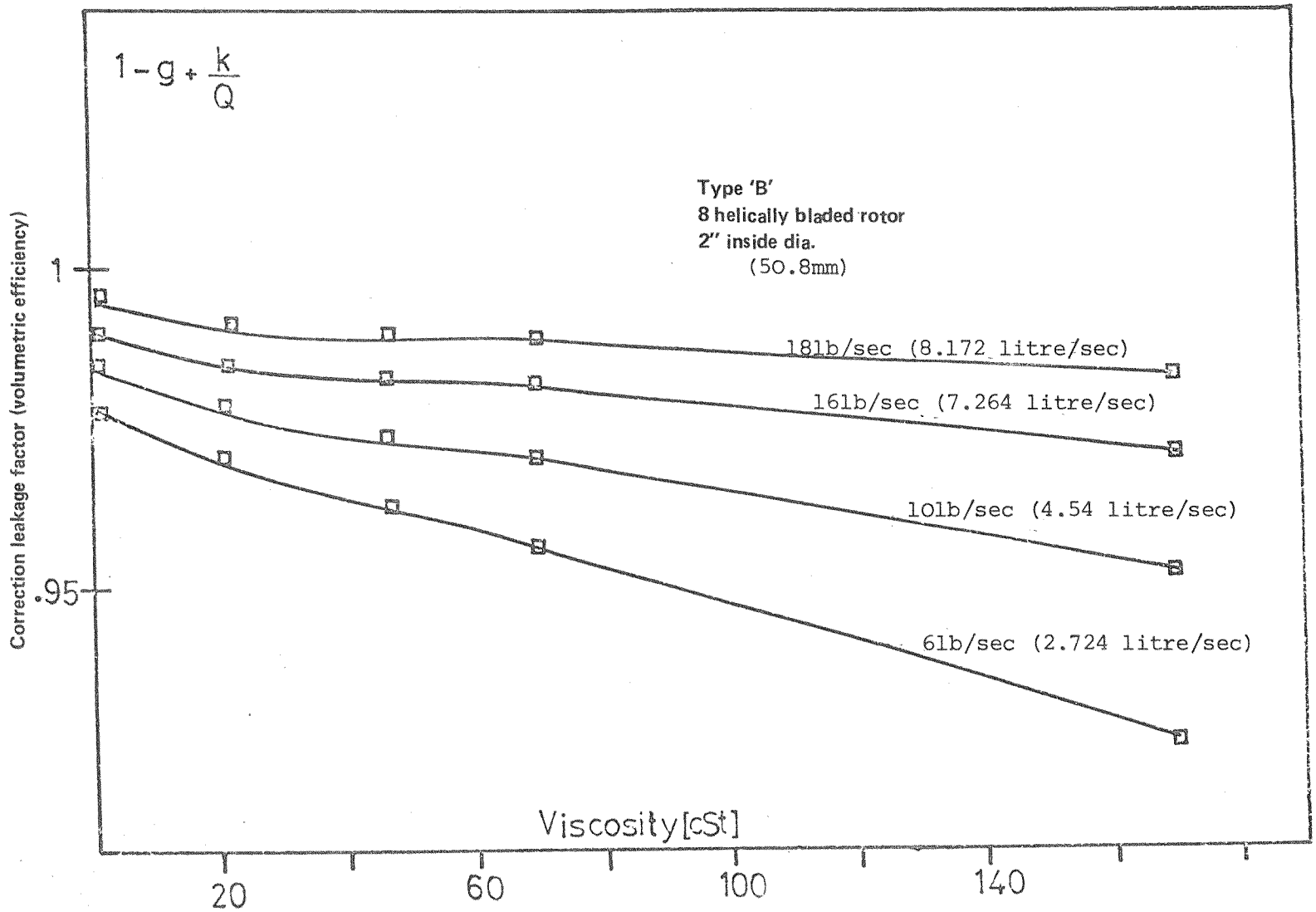

Fig. 65. The empirical calculation of turbine flow meter volumetric efficiency for various fluid viscosities and flow rates

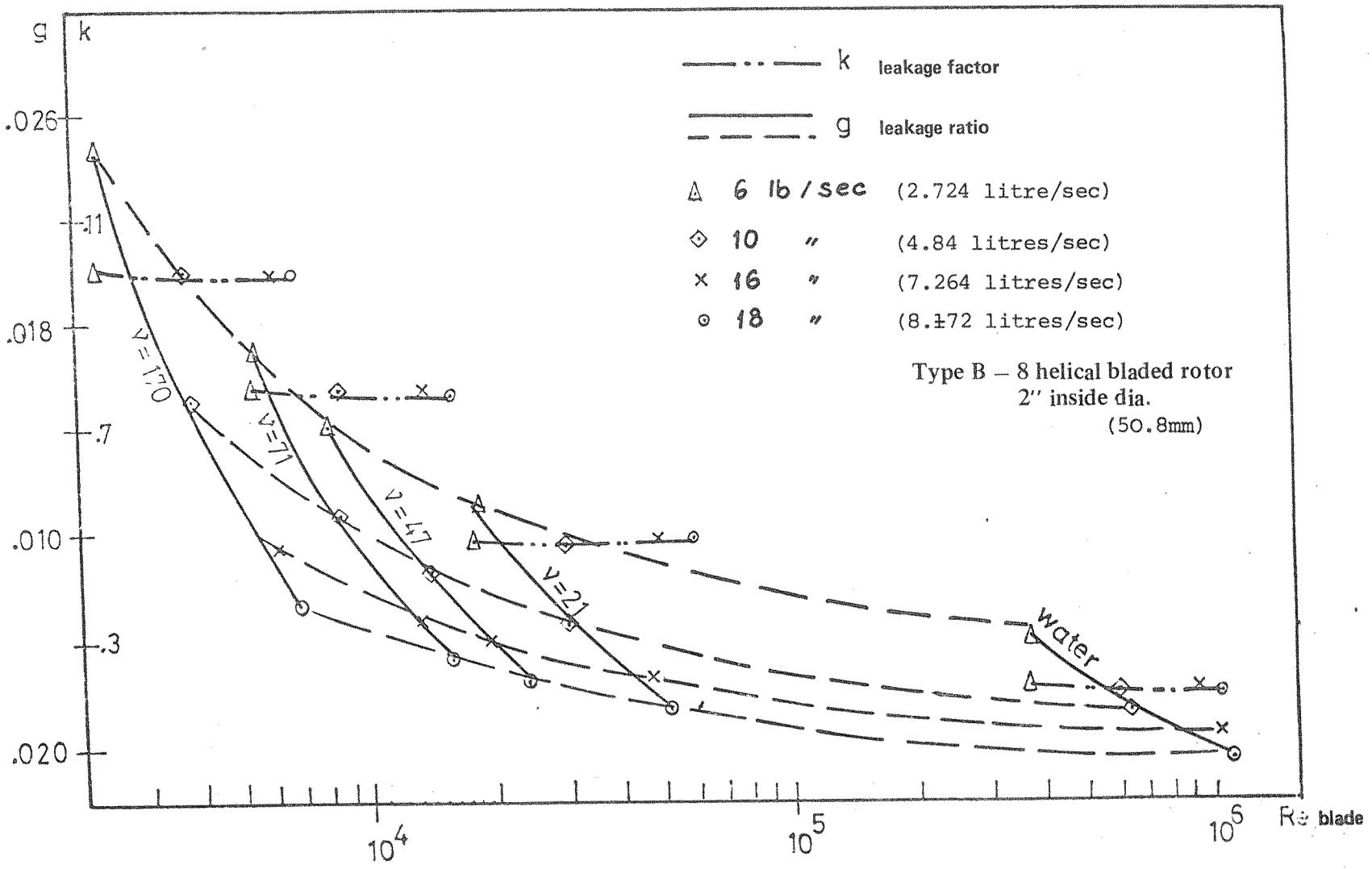

Fig. 66. The empirical calculation of leakage ratio and leakage factor for differing Reynolds number and various flow rates and fluid viscosities.

Fig. 67. The ratio of axial force to blade radius ($\frac{dA}{dr}$) against the local fluid velocity ratio (u/U)

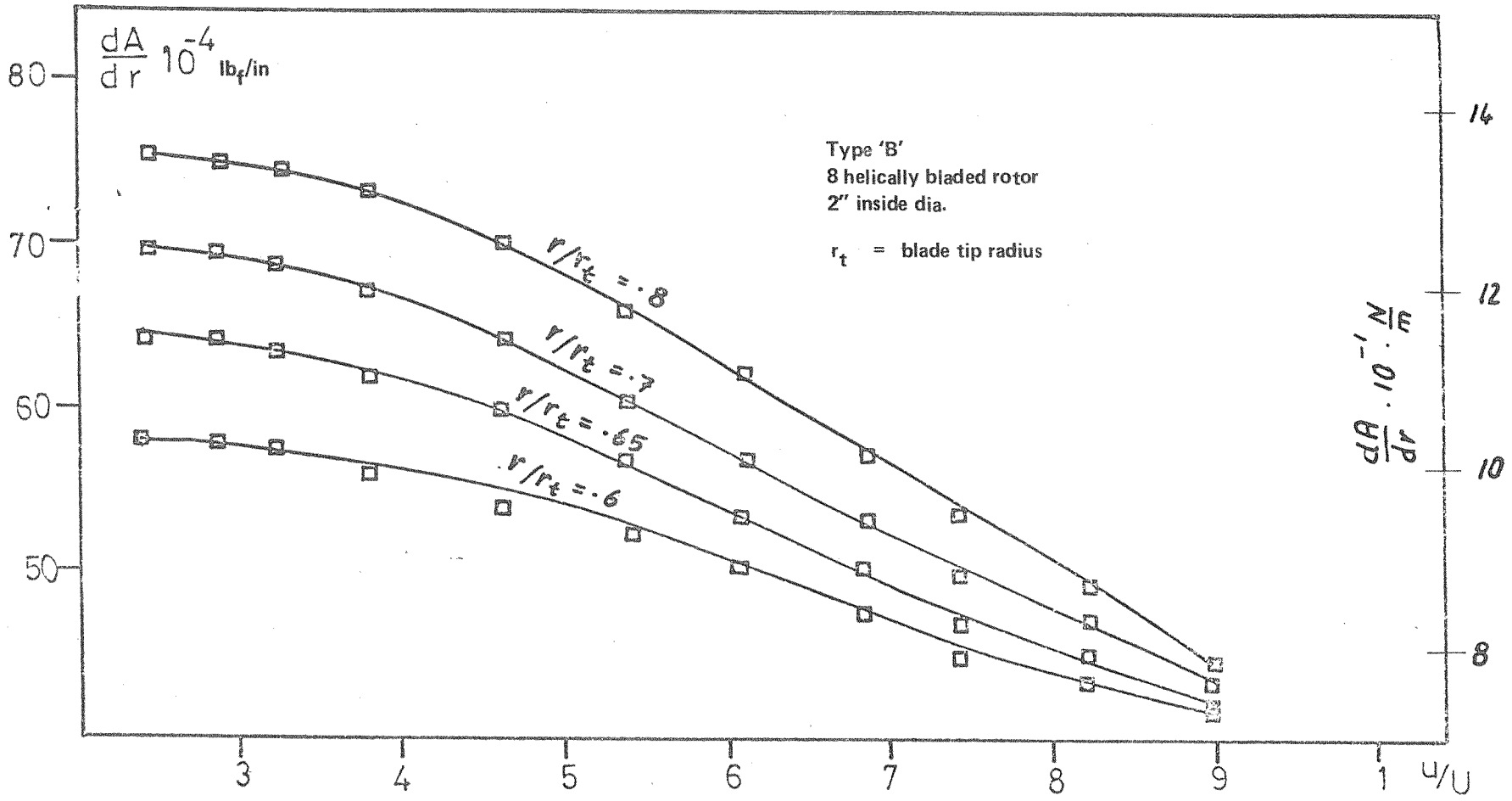

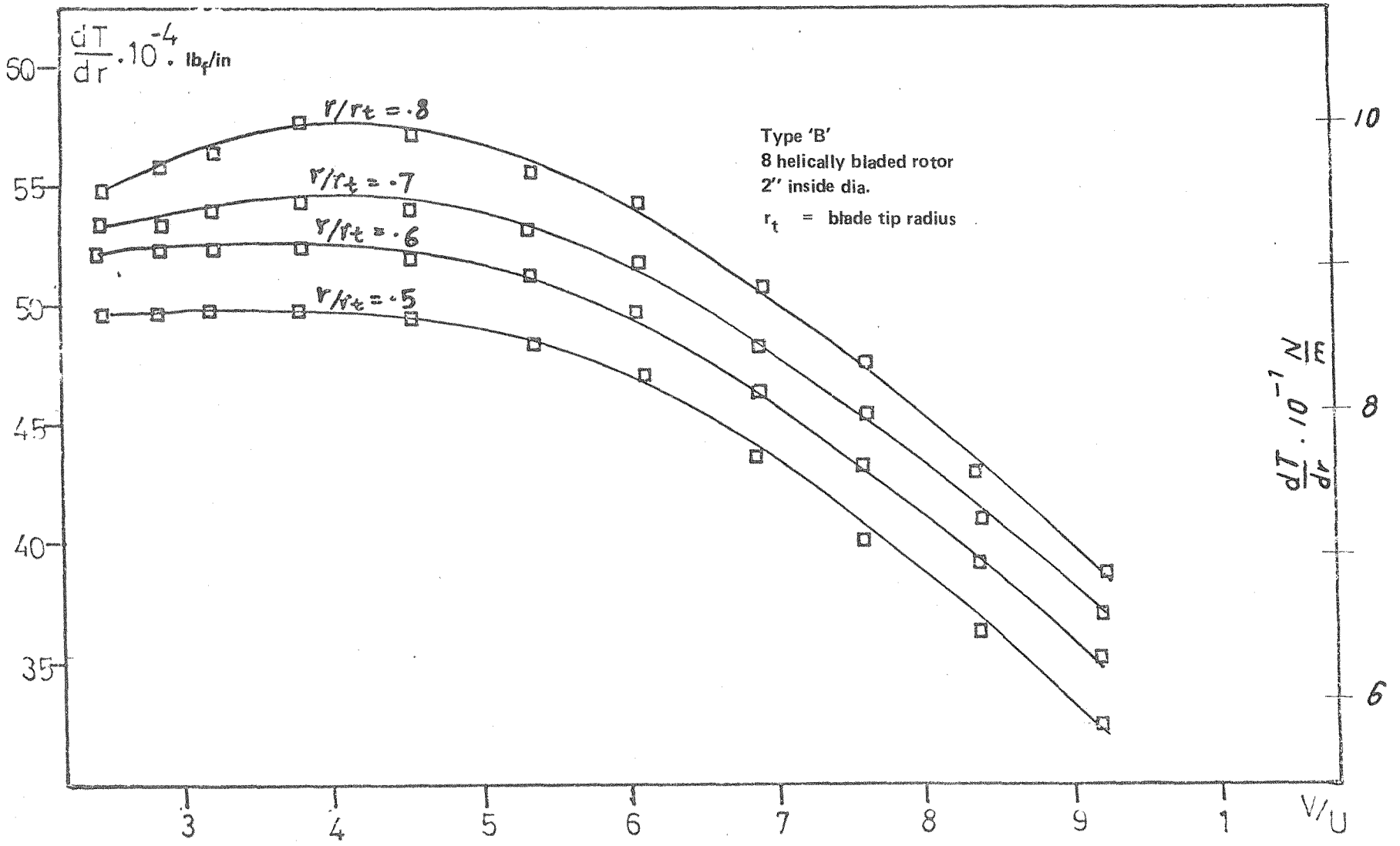

Fig. 68. The tangential force distribution against tangential fluid velocity ratio

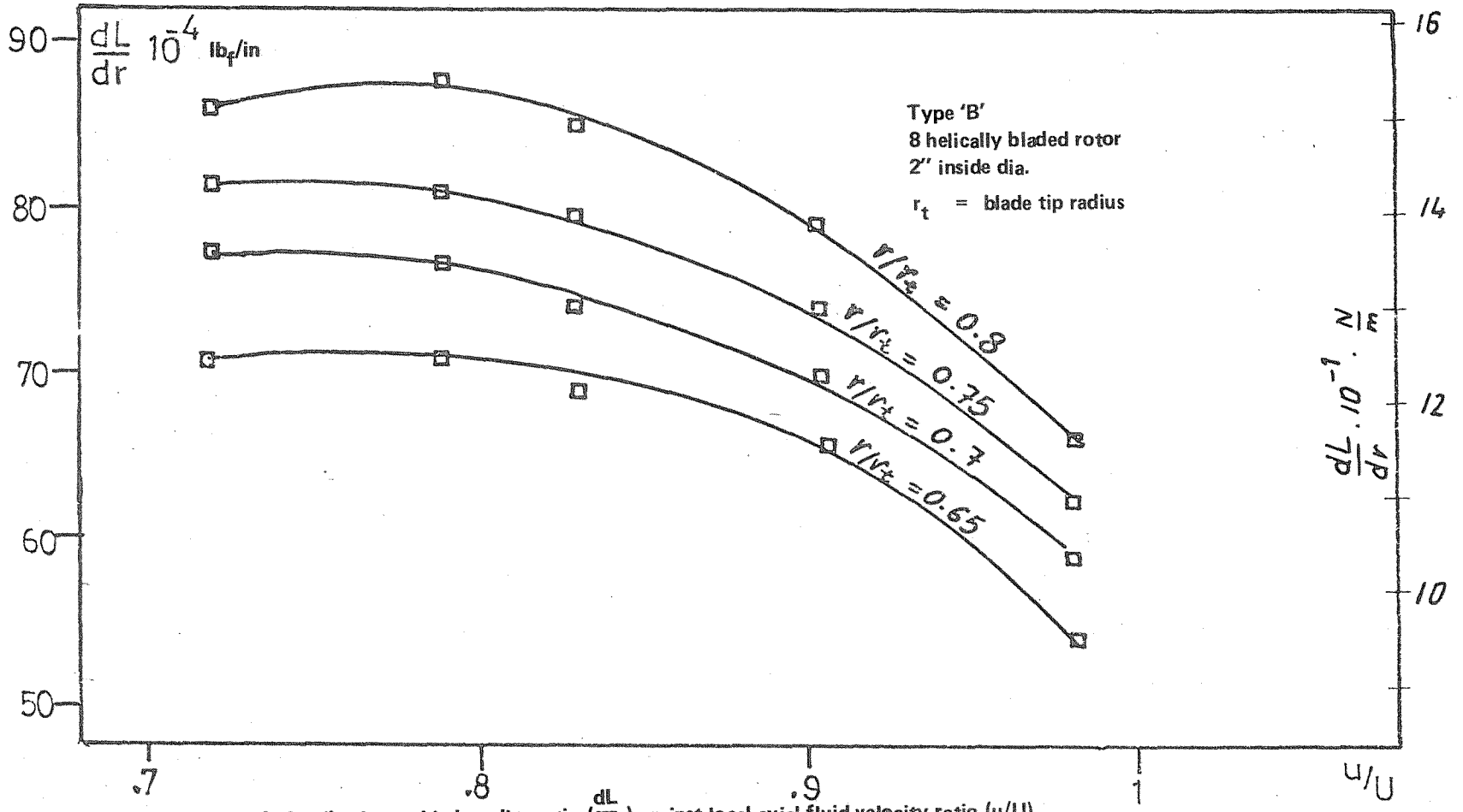

Fig. 69. The lift distribution to blade radius ratio ($\frac{dL}{dr}$) against local axial fluid velocity ratio (u/U)

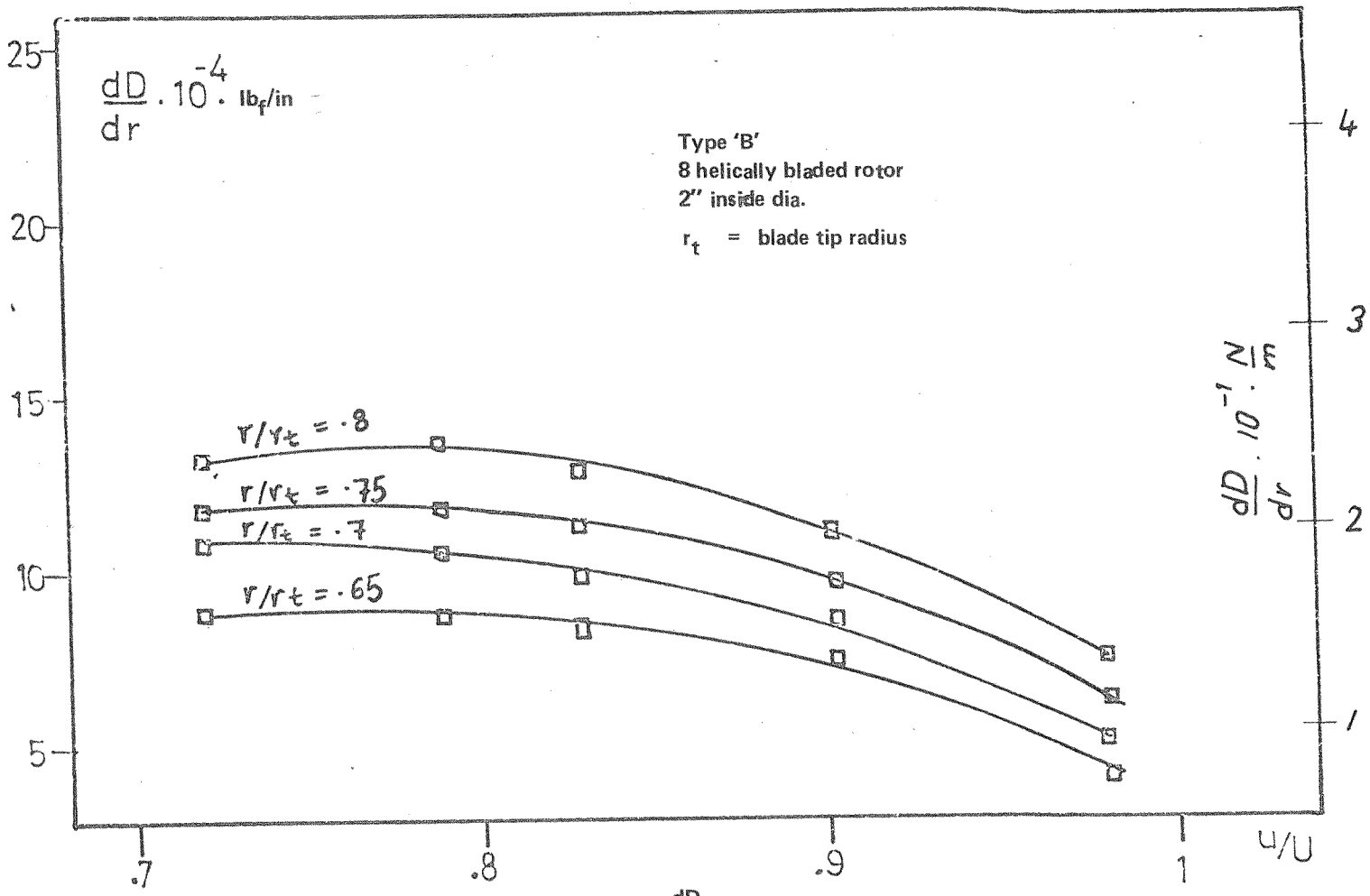

Fig. 70. The drag force distribution to blade radius ratio $(\frac{dD}{dr})$ against local axial fluid velocity ratio (u/U)

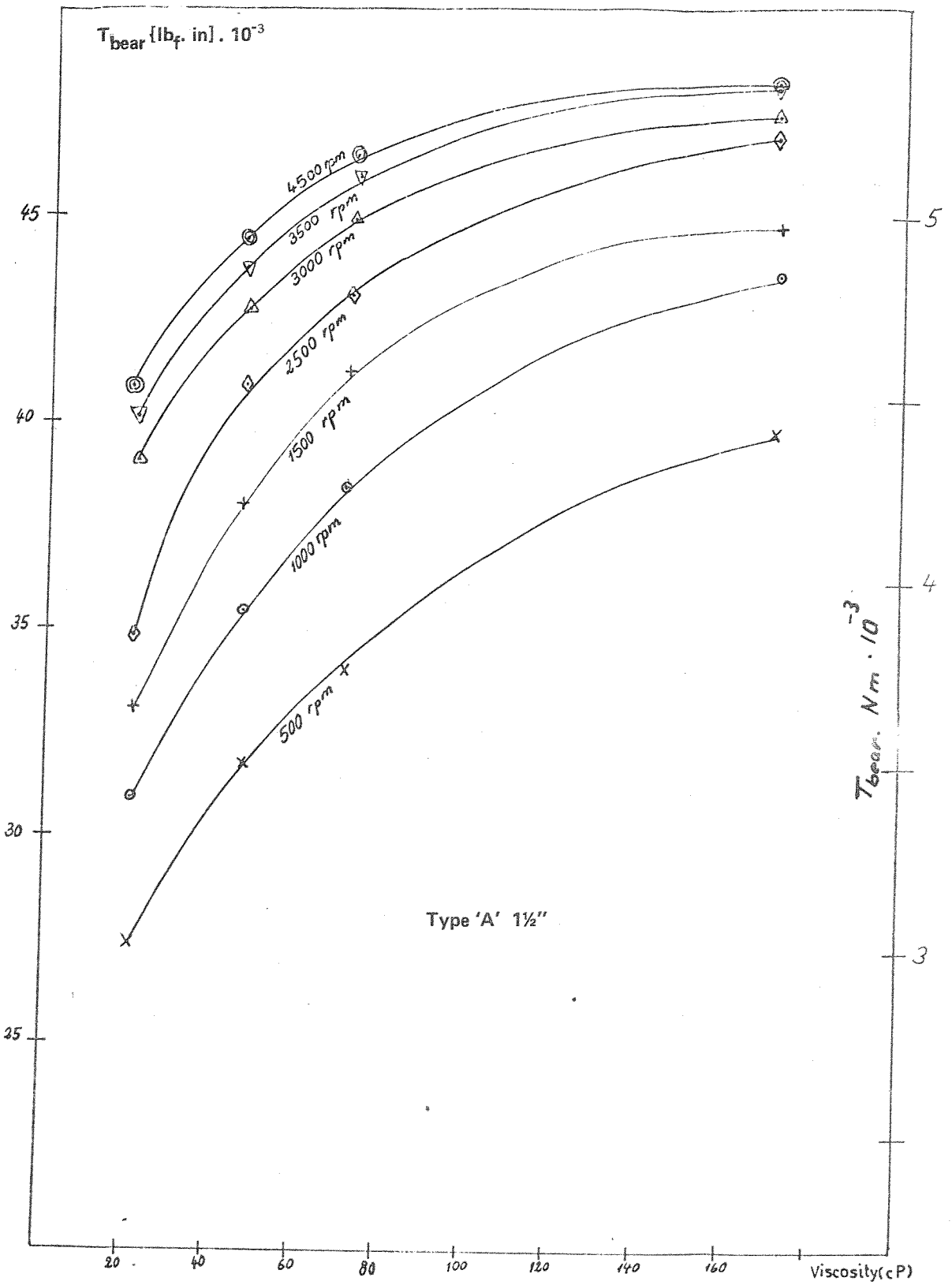

Fig. 71 The bearing friction torque against the fluid viscosity with Sommerfield's assumption for heavily loaded bearing friction force.

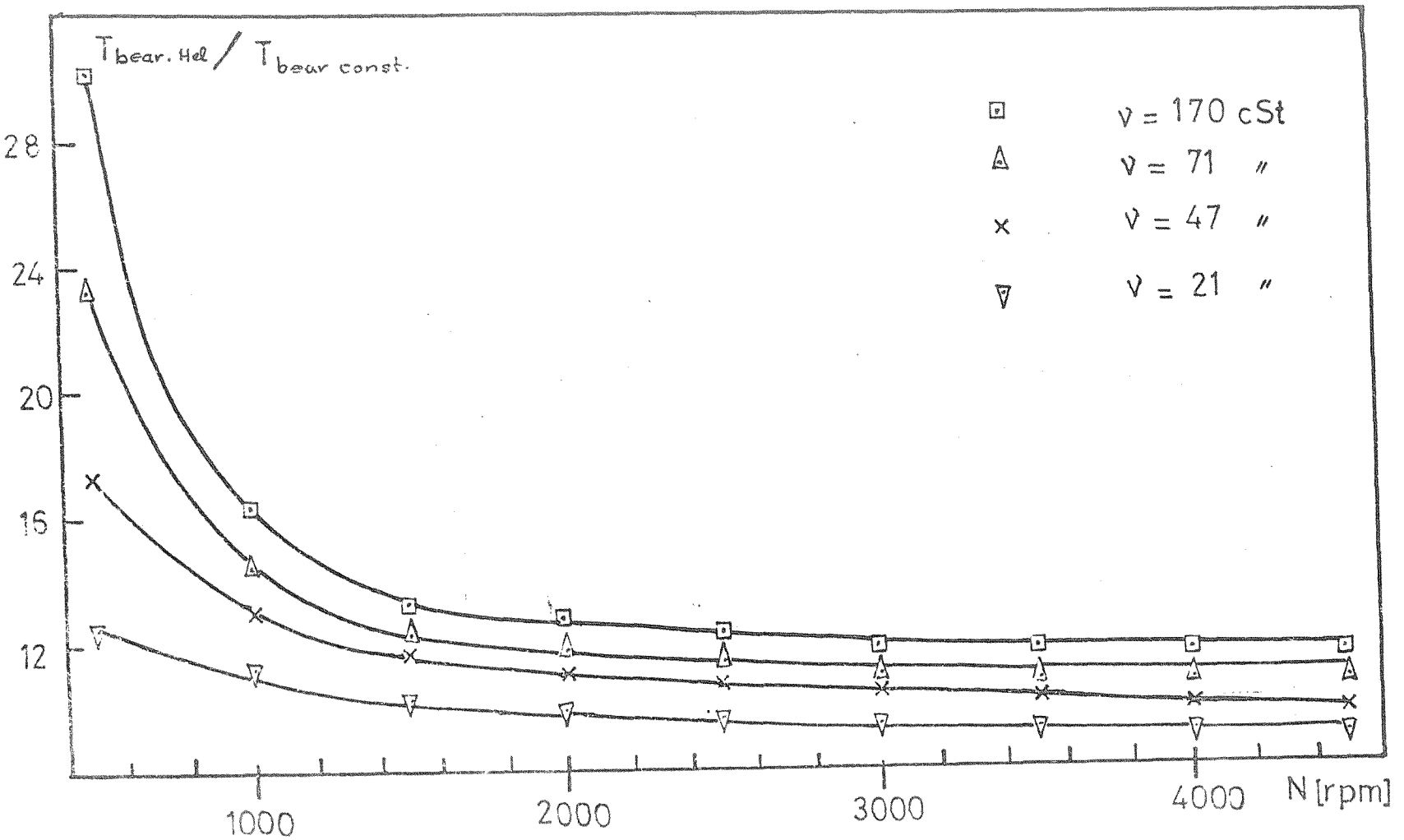

Fig. 72. The ratio between the bearing friction torque of a turbine flow meter Type 'A' and Type 'C' with heavily loaded (Sommerfield's assumption) and lightly loaded (Petrov's assumption) bearing friction force respectively

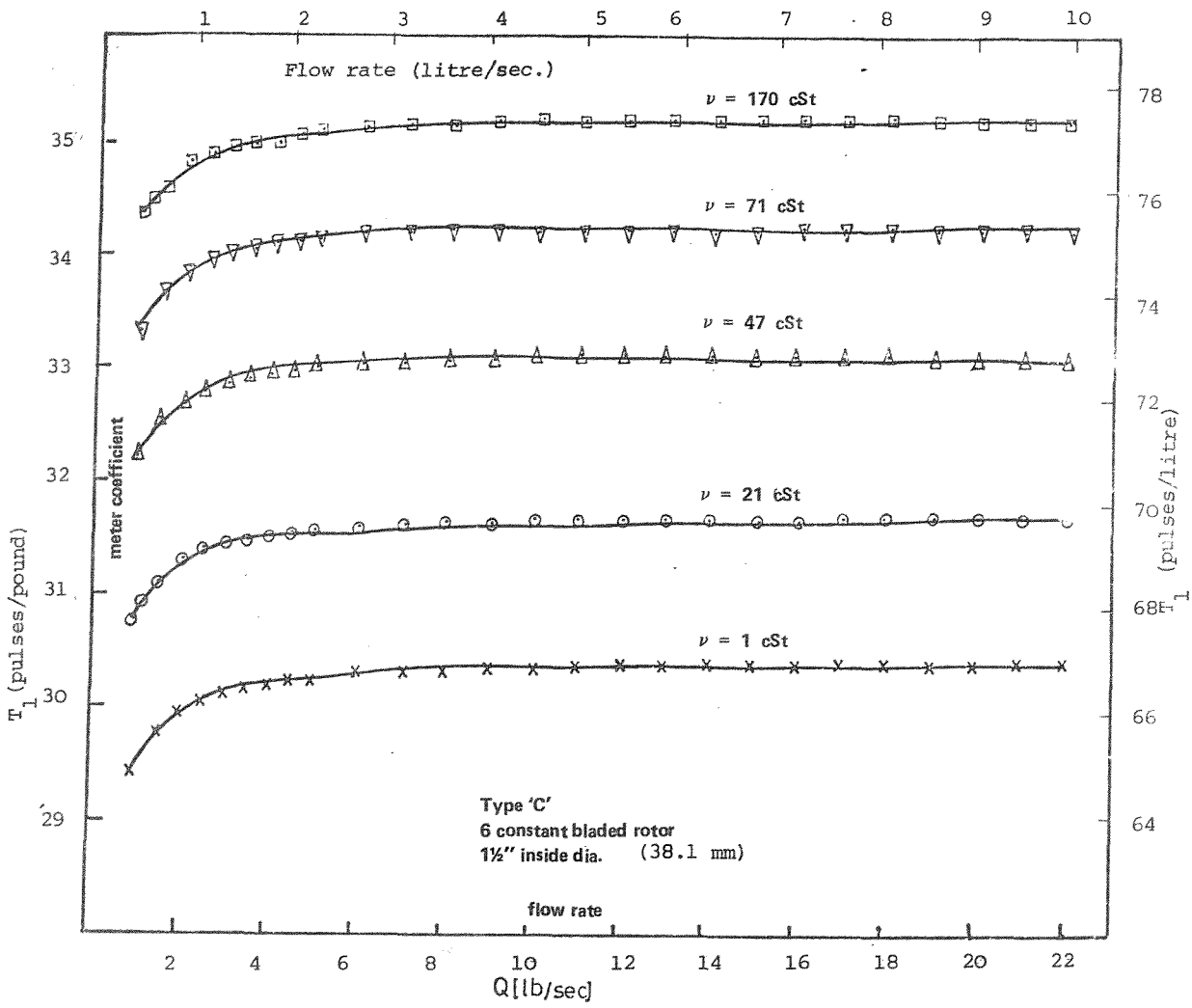

Fig. 73. The empirical calculation of T_1 of the main turbine equation for commercial turbine flow meter Type 'C'. The values of T_1 have also been calculated for different fluid viscosities.

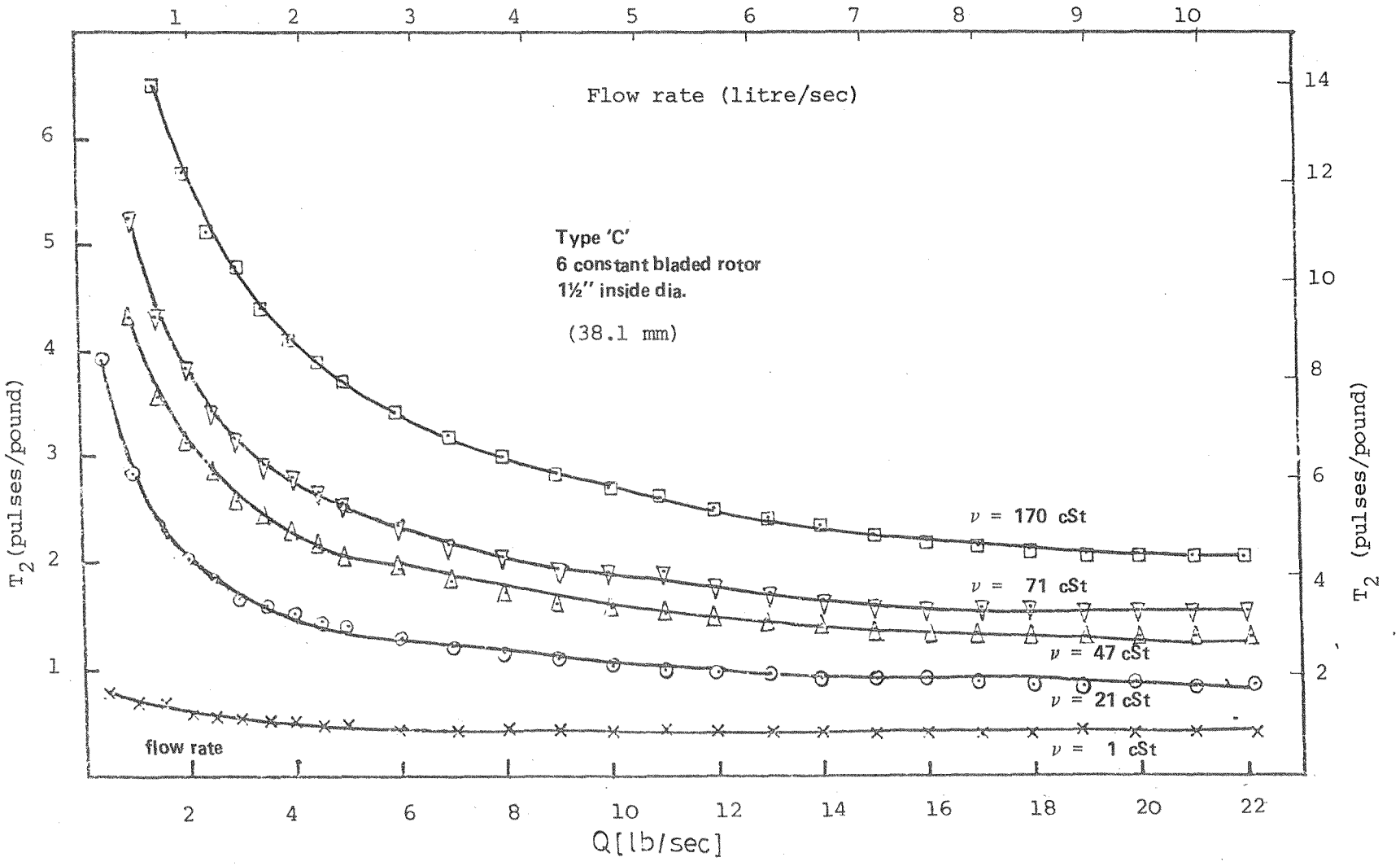

Fig. 74. The empirical calculation of term 2 of main turbine equation for commercial turbine flow meter Type 'C'. The values of term 3 have also been calculated for different fluid viscosities

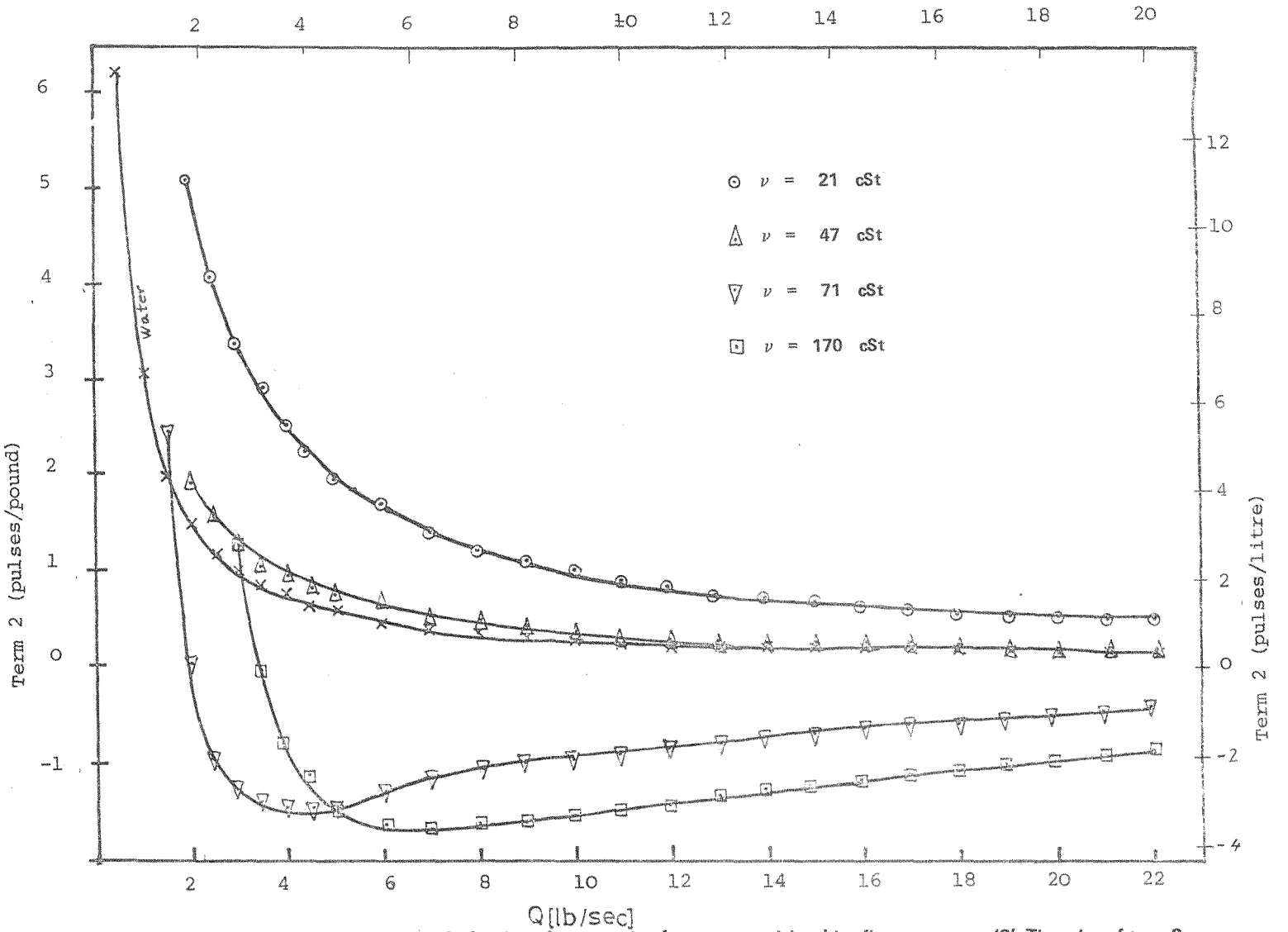

Fig. 75 The empirical calculation term 2 of main turbine equation for a commercial turbine flow meter type 'C'. The value of term 2 has also been calculated for different fluid viscosities

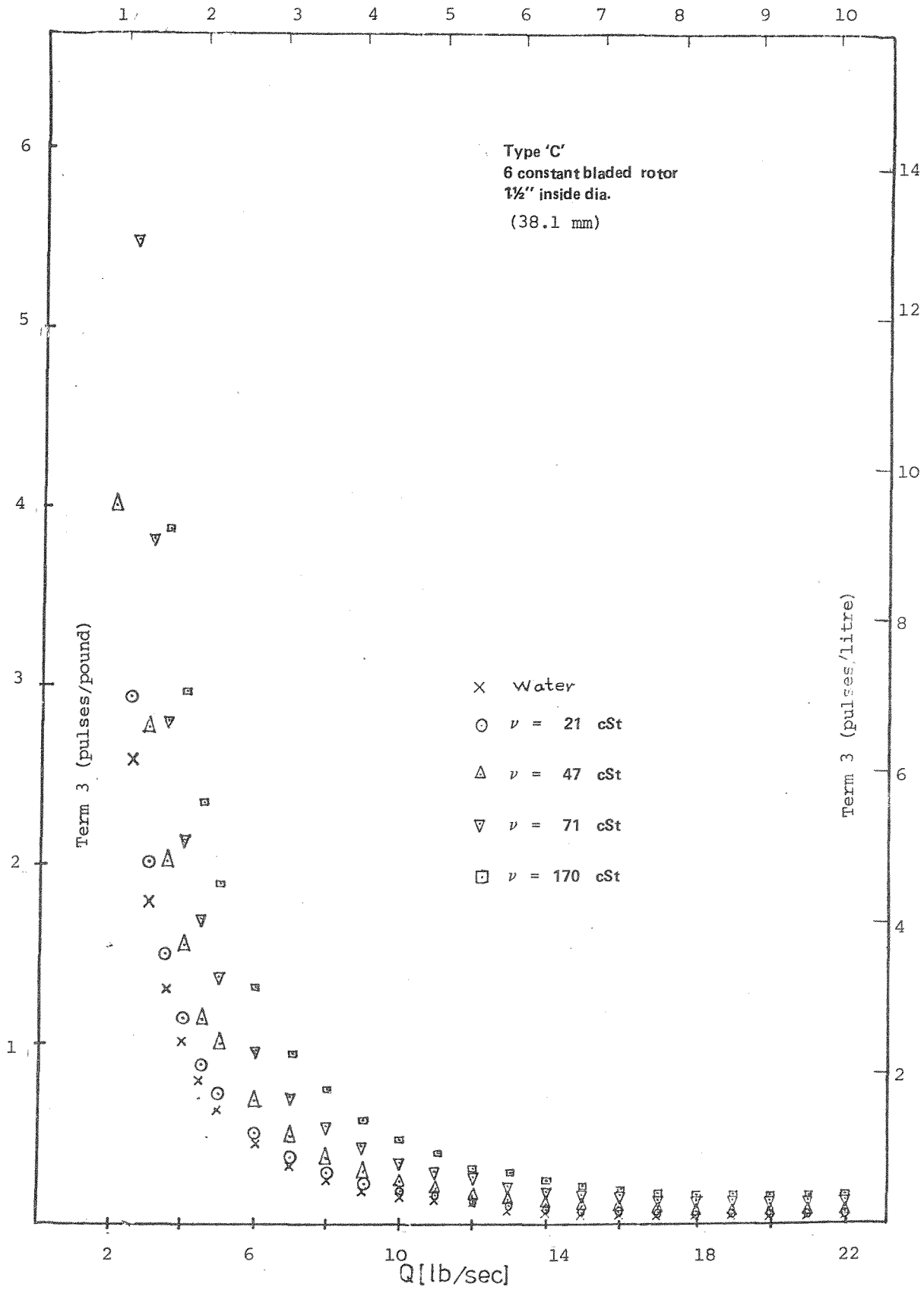

Fig. 76. The empirical calculation of term 3 of main turbine equation for a commercial turbine flow meter Type 'C'. The value of term 3 has also been calculated for different fluid viscosities

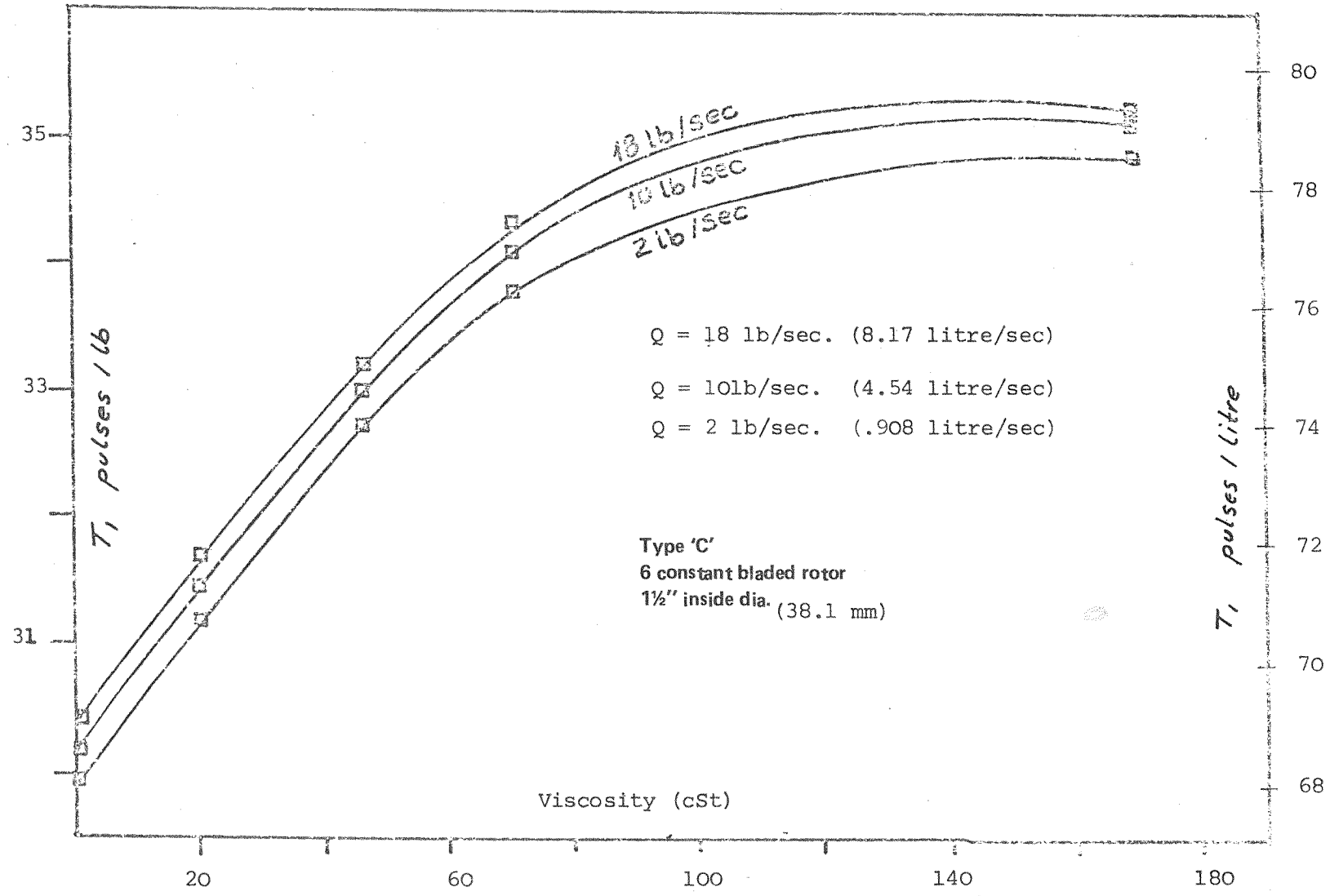

Fig. 77. The empirical calculation of T_1 of the main turbine equation for a commercial turbine flow meter type 'C' against fluid viscosity for various flow rates

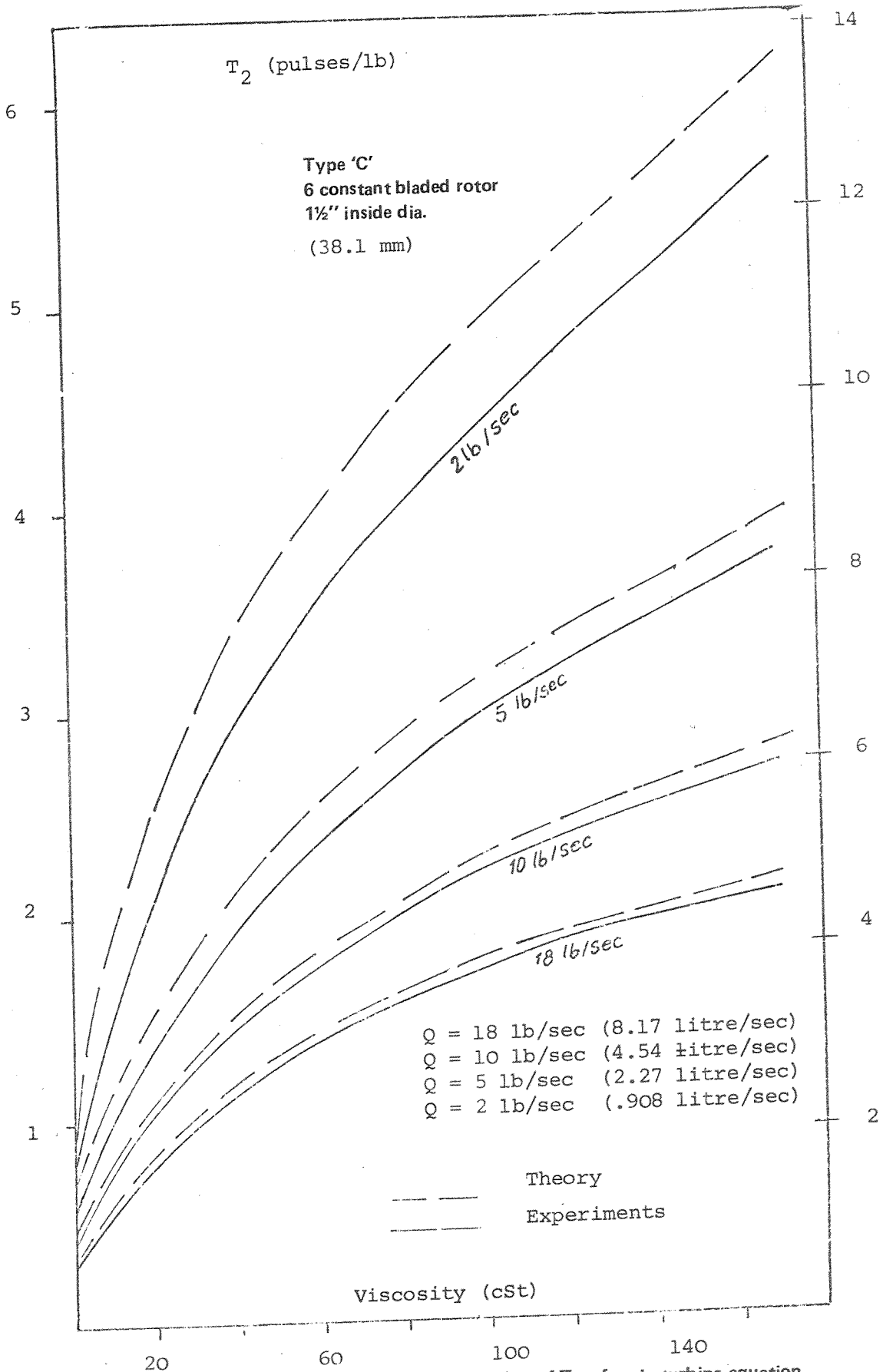

Fig. 78. The empirical and theoretical calculation of T_2 of main turbine equation for a commercial turbine flow meter type C against viscosity for different flow rates

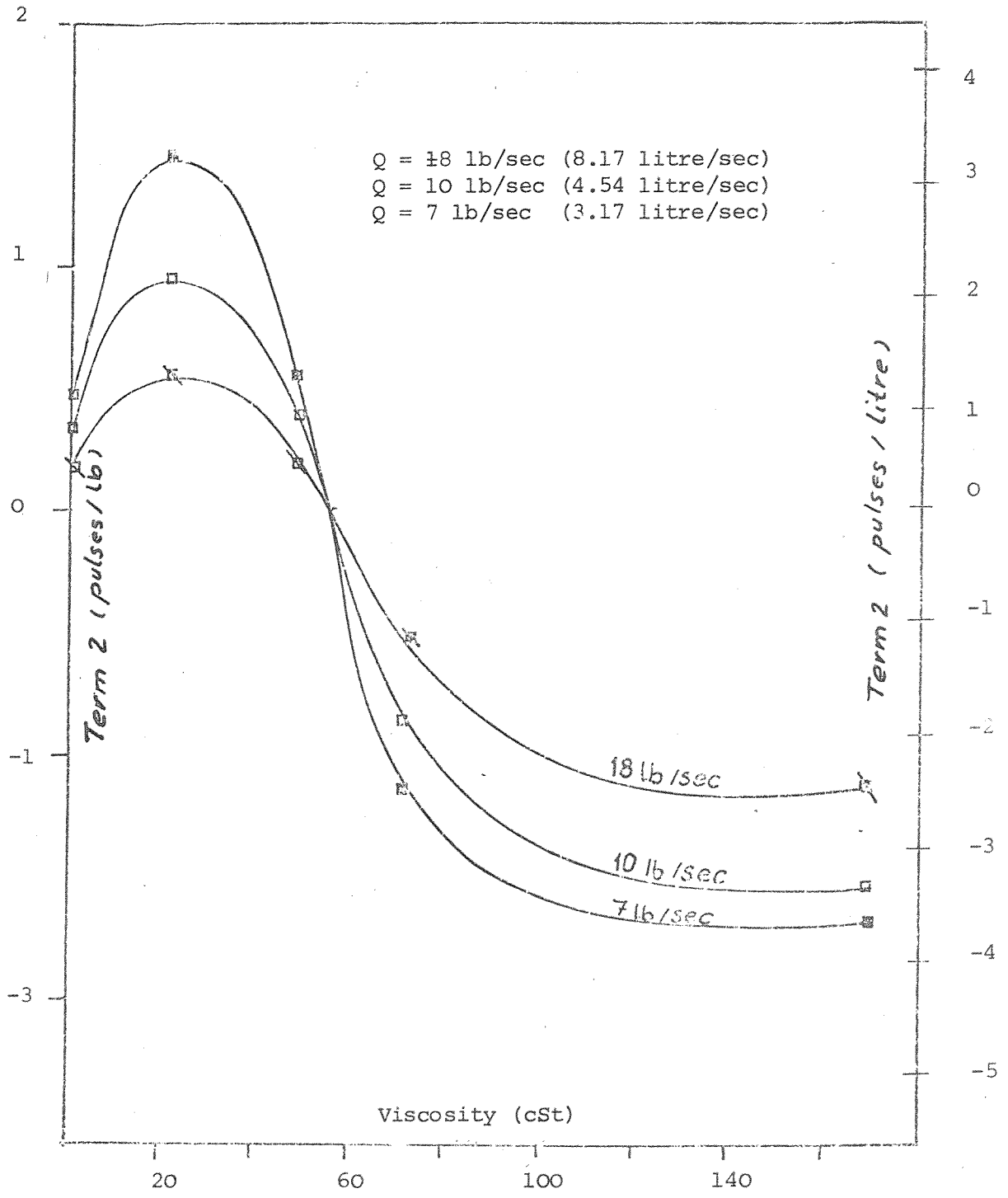

Fig. 79. The empirical calculation of term 2 of main turbine equation for a commercial turbine flow meter type 'C' against fluid viscosity for different flow rates

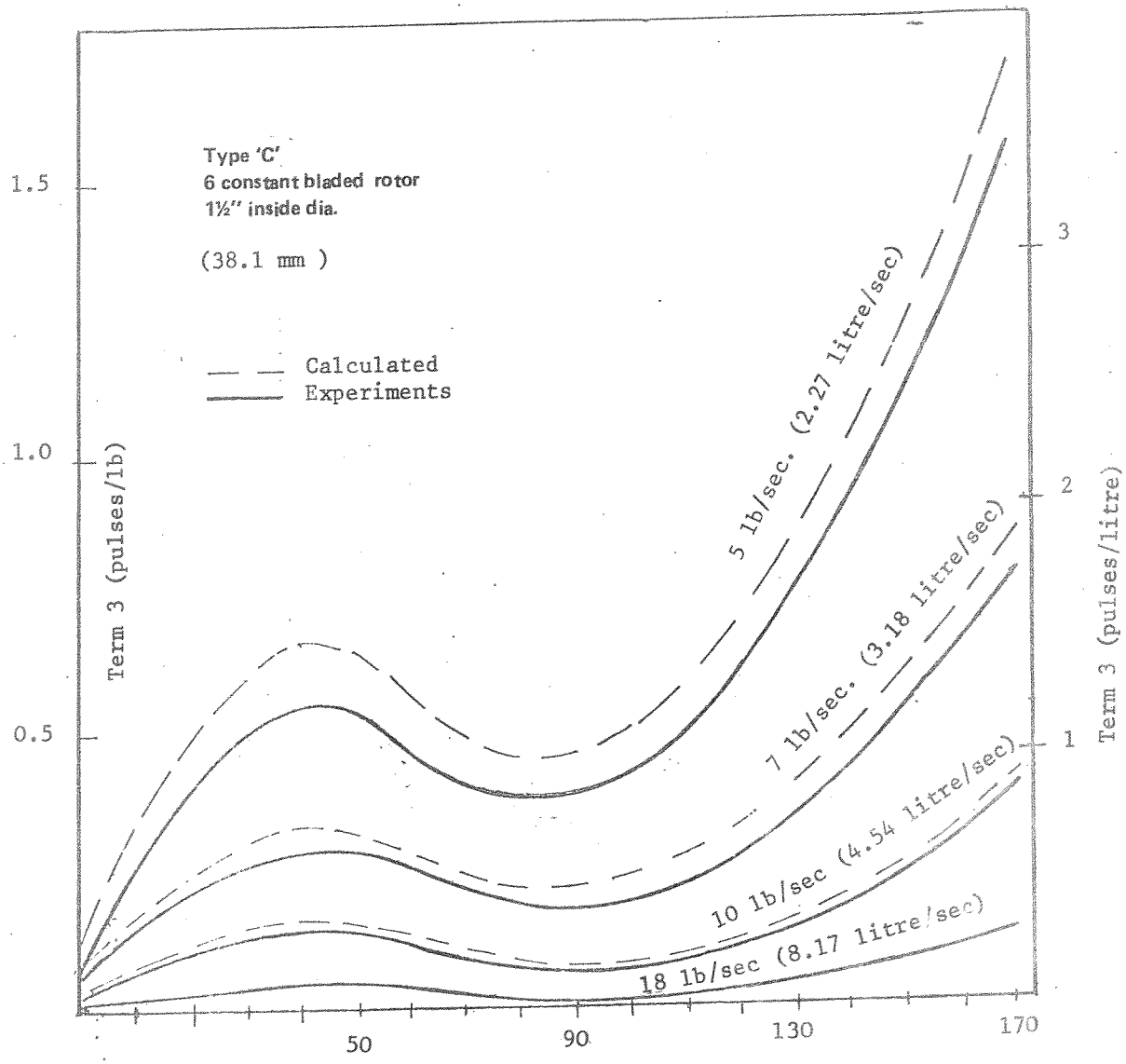

Fig. 80. The empirical and theoretical calculation of term 3 of the main turbine equation against fluid viscosity for different flow rates

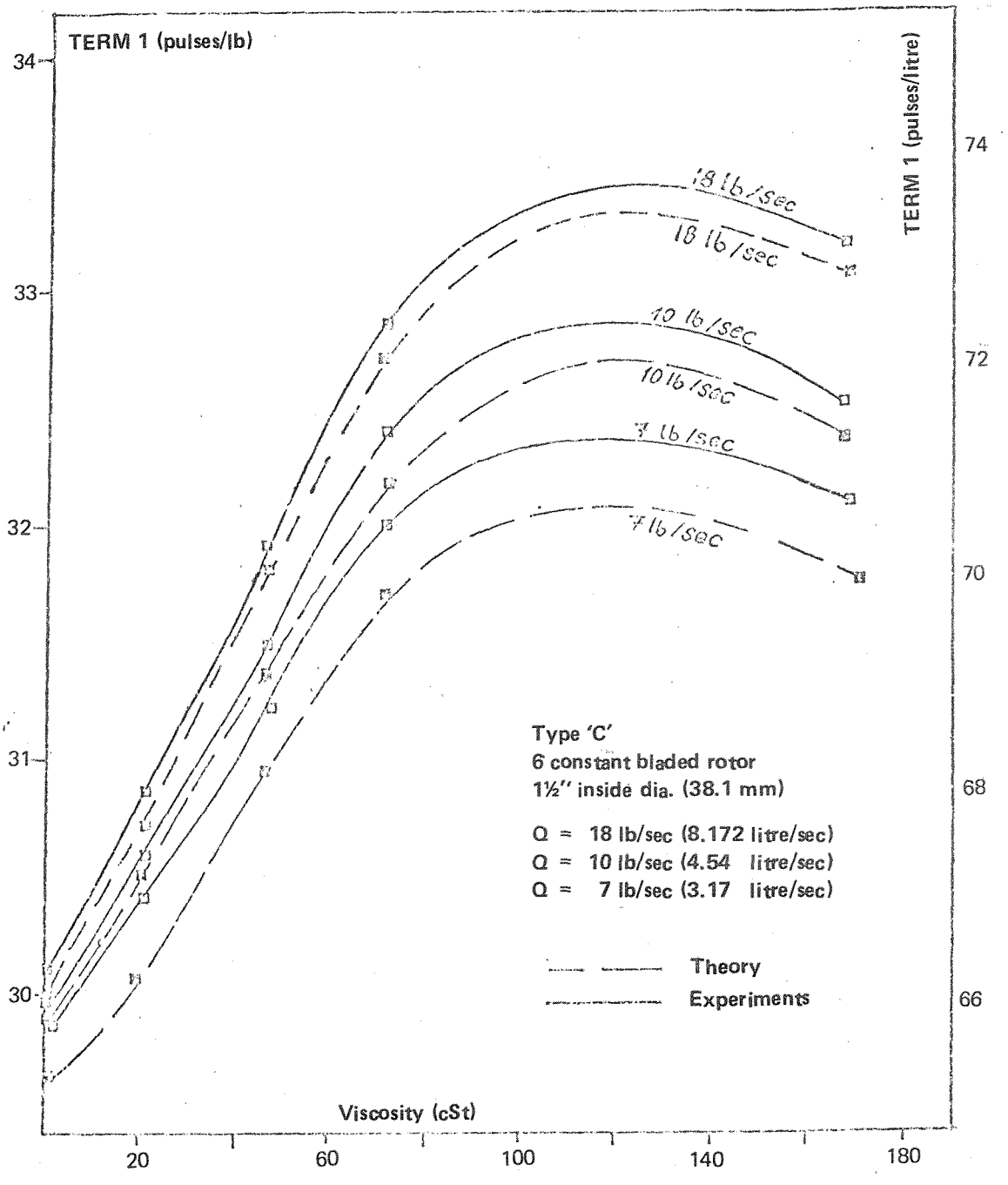

Fig. 81a The empirical and theoretical calculation of TERM 1 of main turbine equation against fluid viscosity for different flow rates

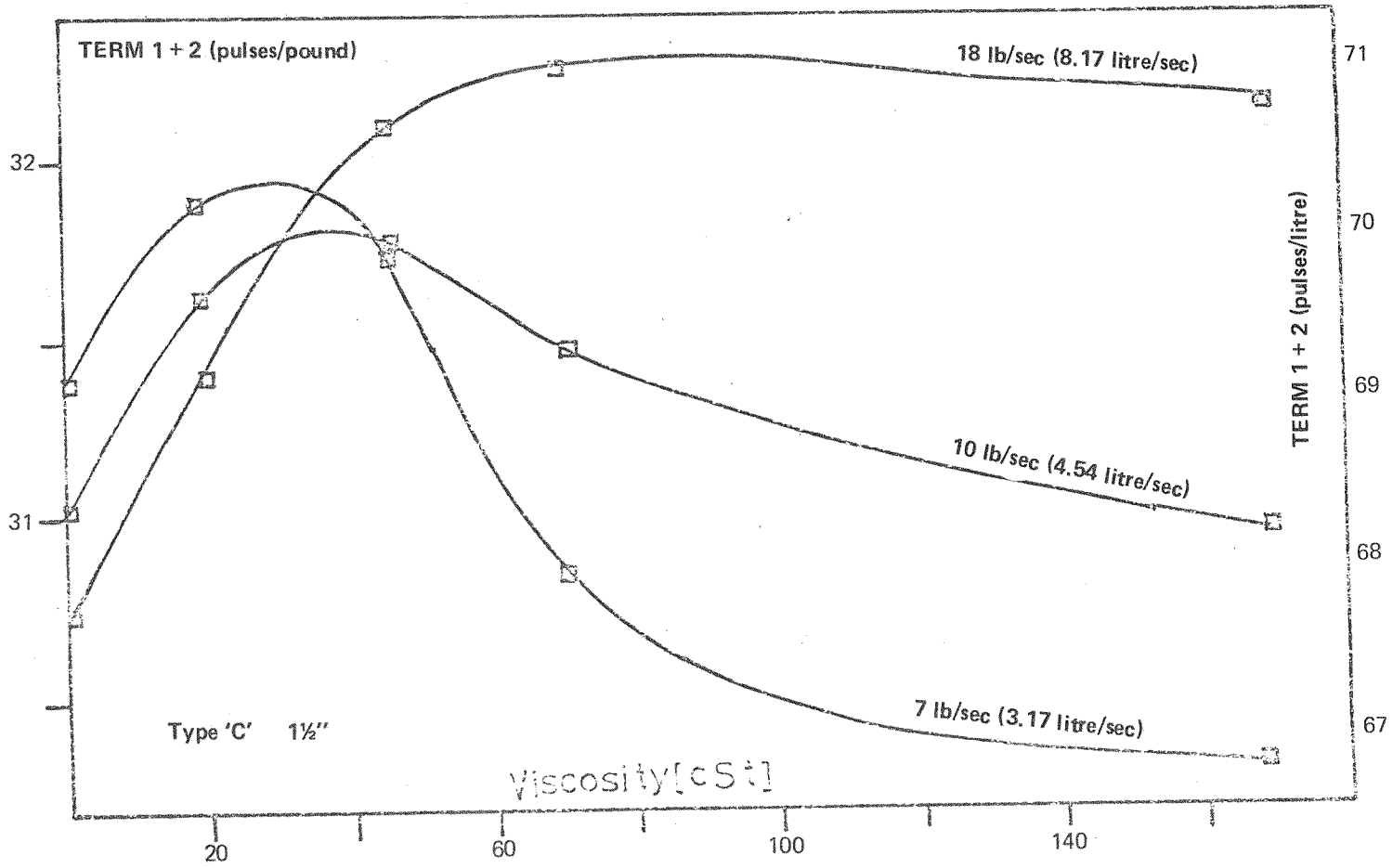

Fig. 81b. The empirical calculation of TERM 1 + 2 of the main turbine equation against fluid viscosity for different flow rates

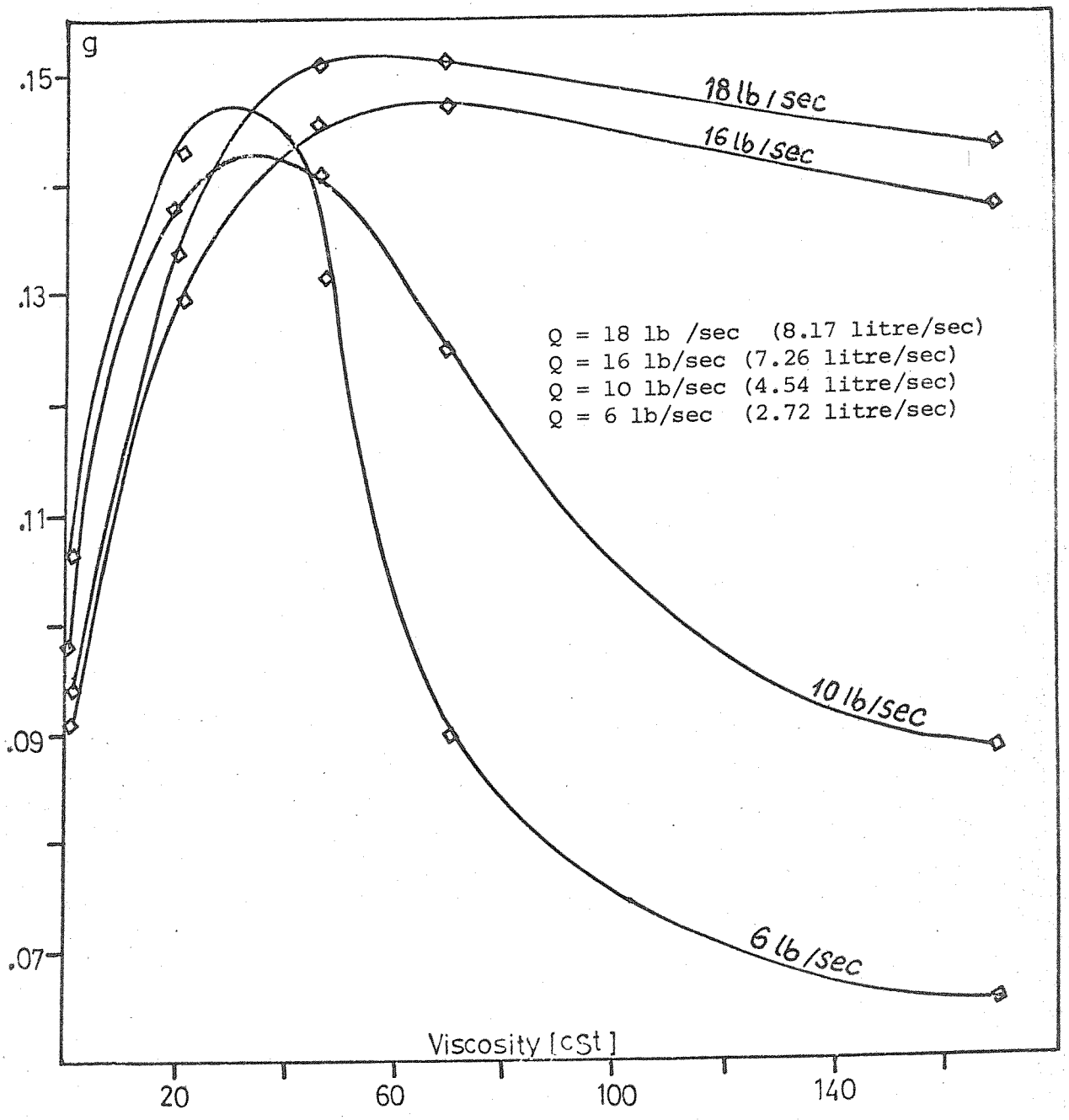

Fig. 82. **The empirical calculation of leakage ratio g against fluid viscosity for a commercial turbine flow meter Type 'C'**

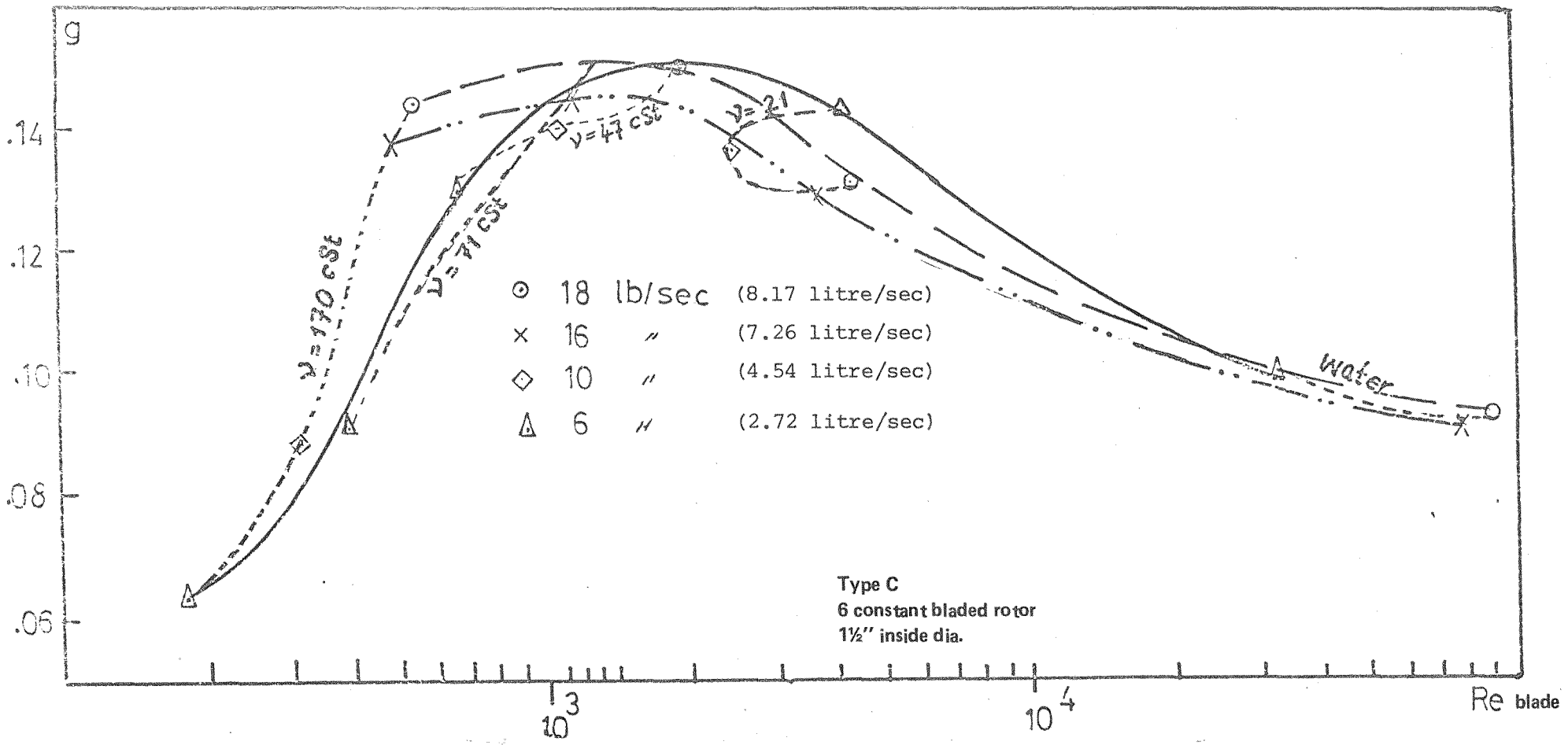

Fig. 83 The empirical calculation of leakage ratio, g, against the blades' Reynolds number for different fluid viscosities

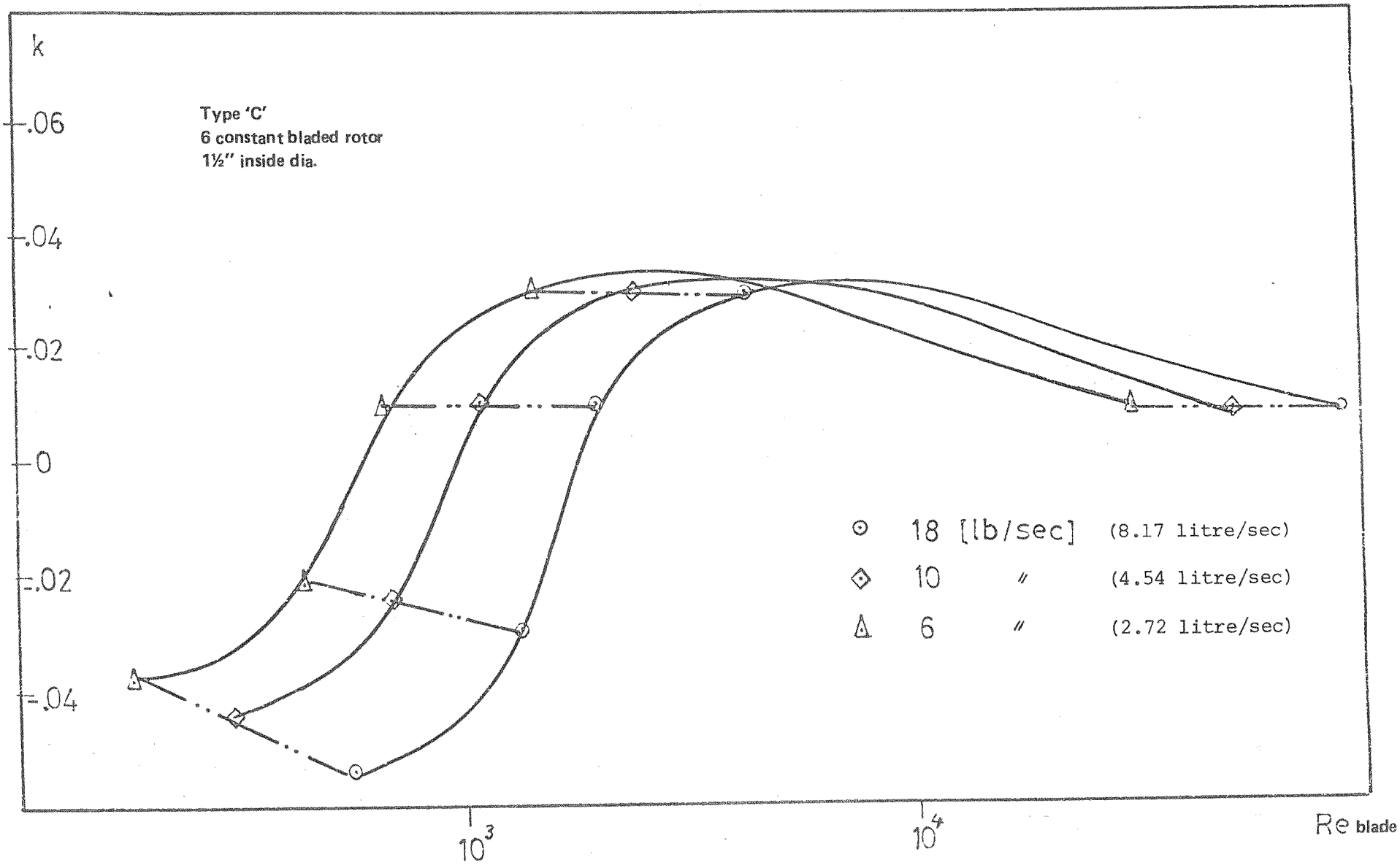

Fig. 84 The empirical calculation of leakage factor, k, against the blades' Reynolds number for different fluid viscosities

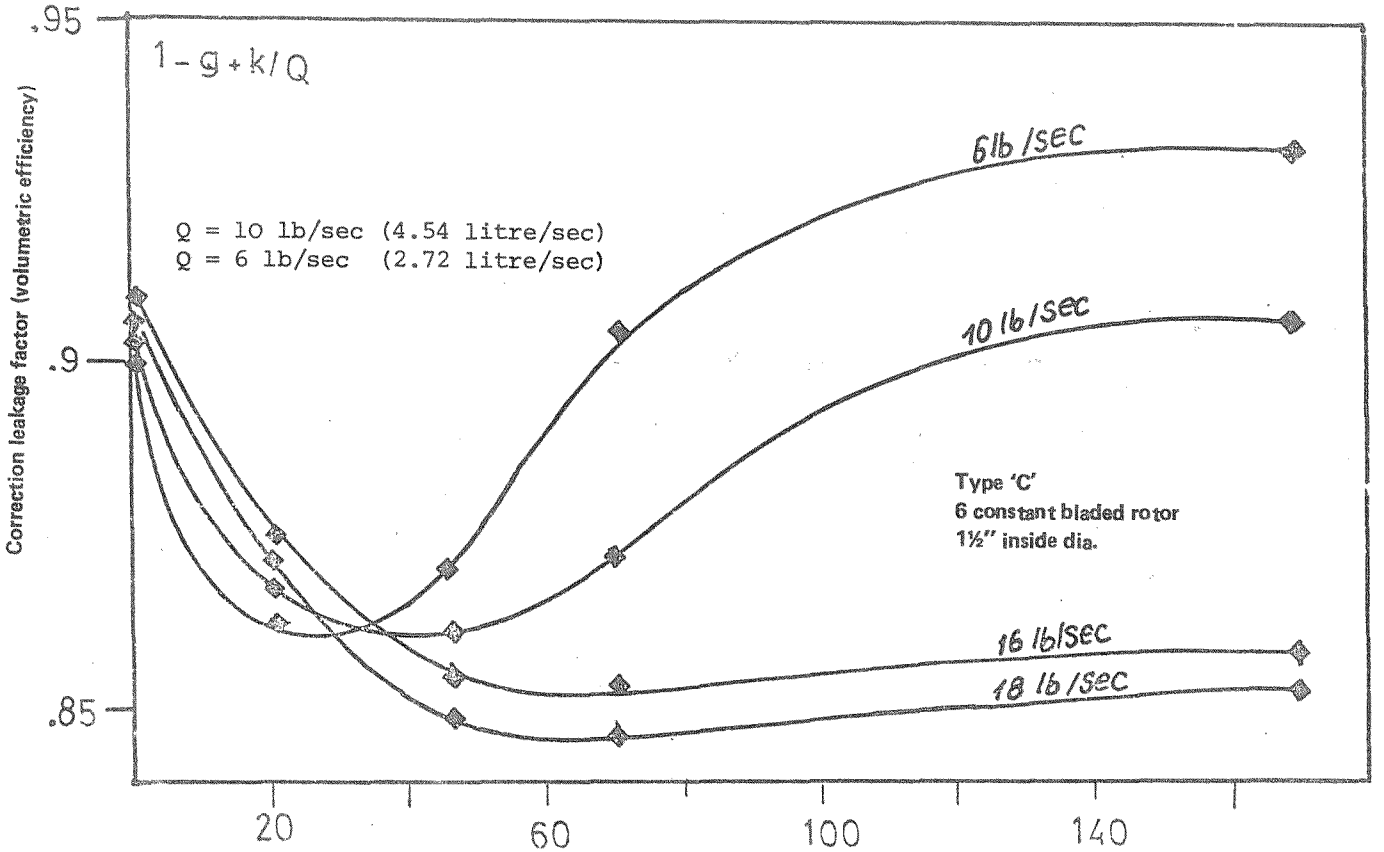

Fig. 85 The empirical calculation of volumetric efficiency of a commercial turbine flow meter type 'C' against fluid viscosity

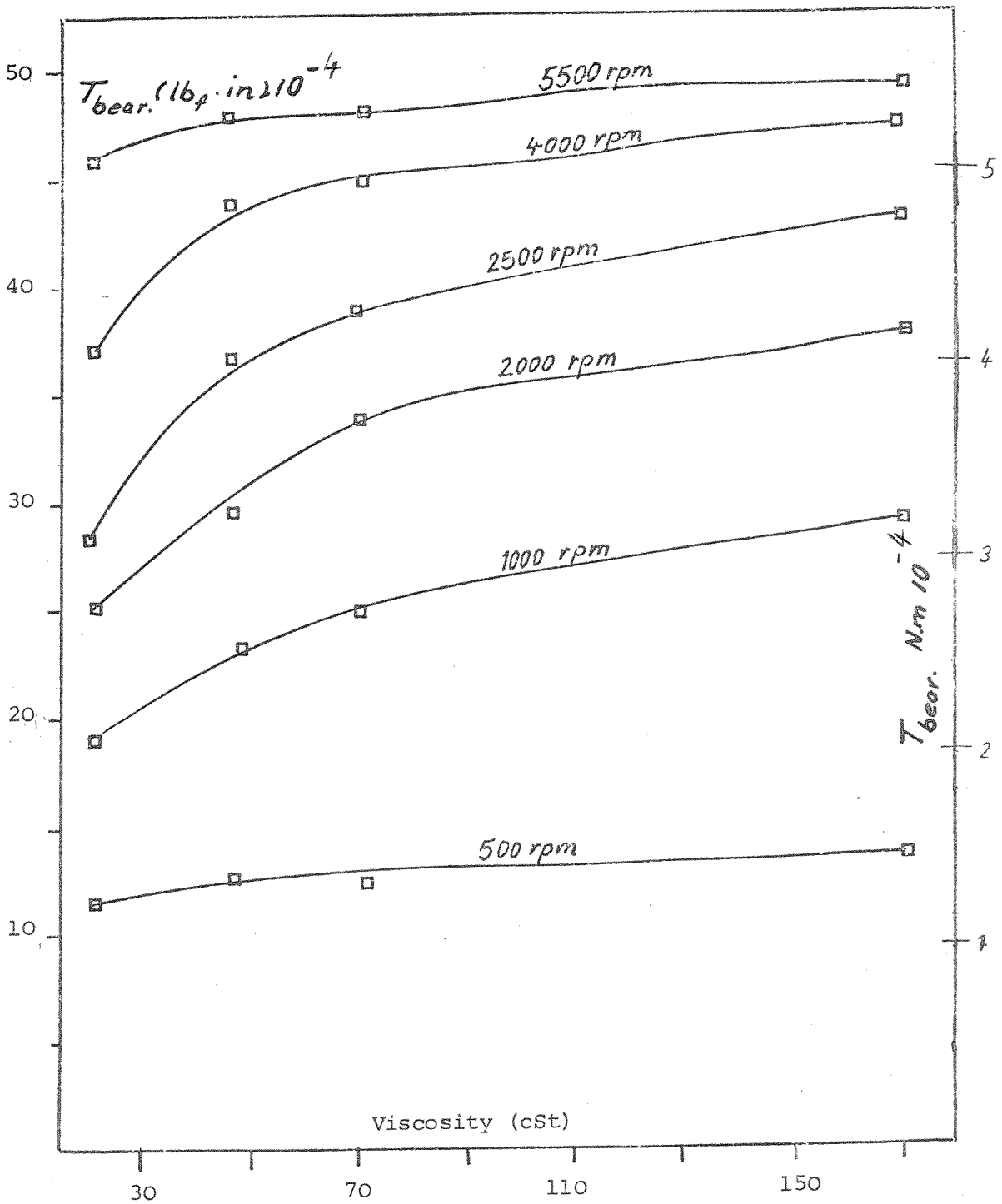

Fig. 86. The calculation of bearing friction torque for a lightly loaded turbine flow meter type 'C' with the Petrov assumption against fluid viscosity

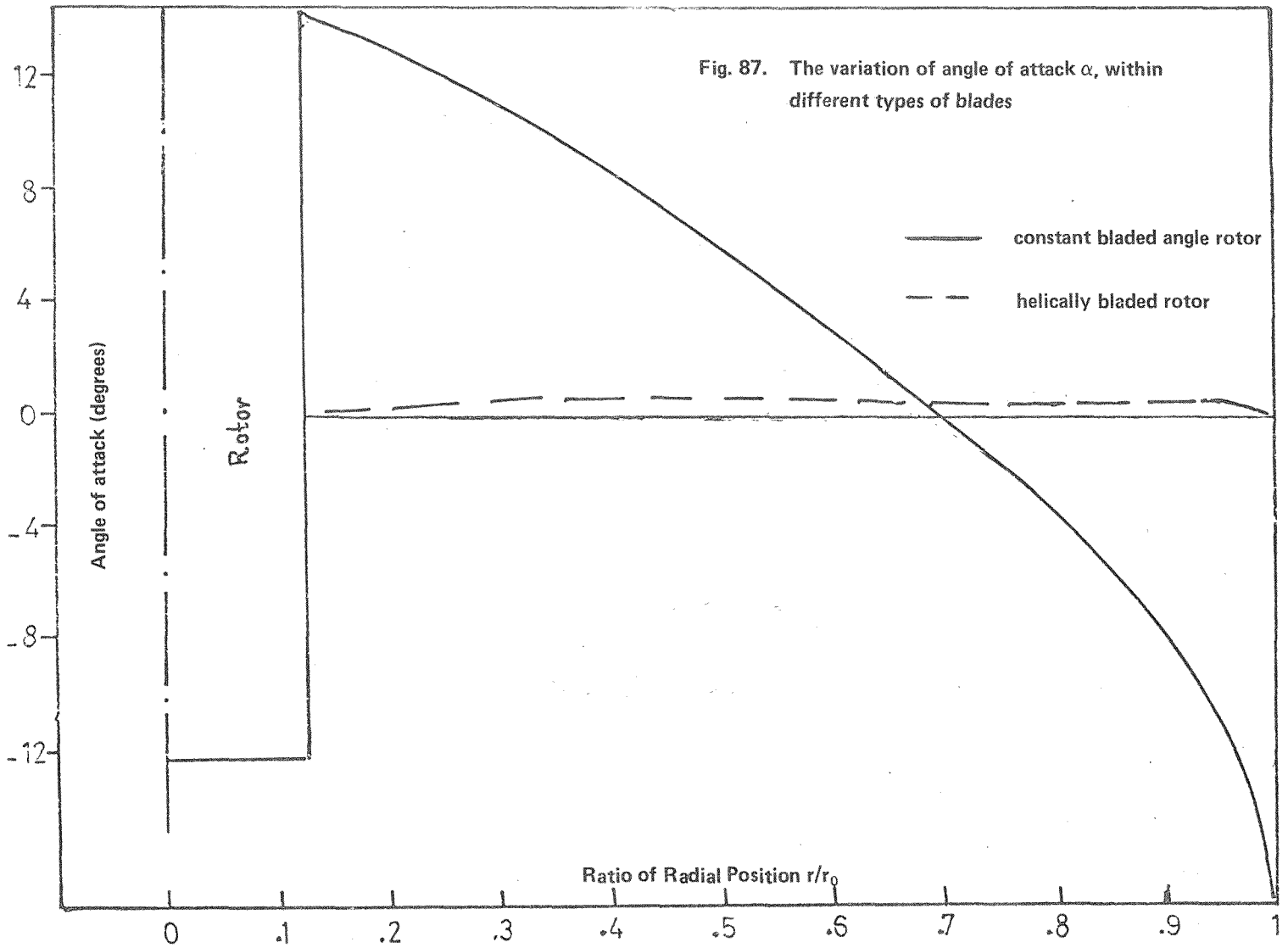

Fig. 87. The variation of angle of attack α, within different types of blades

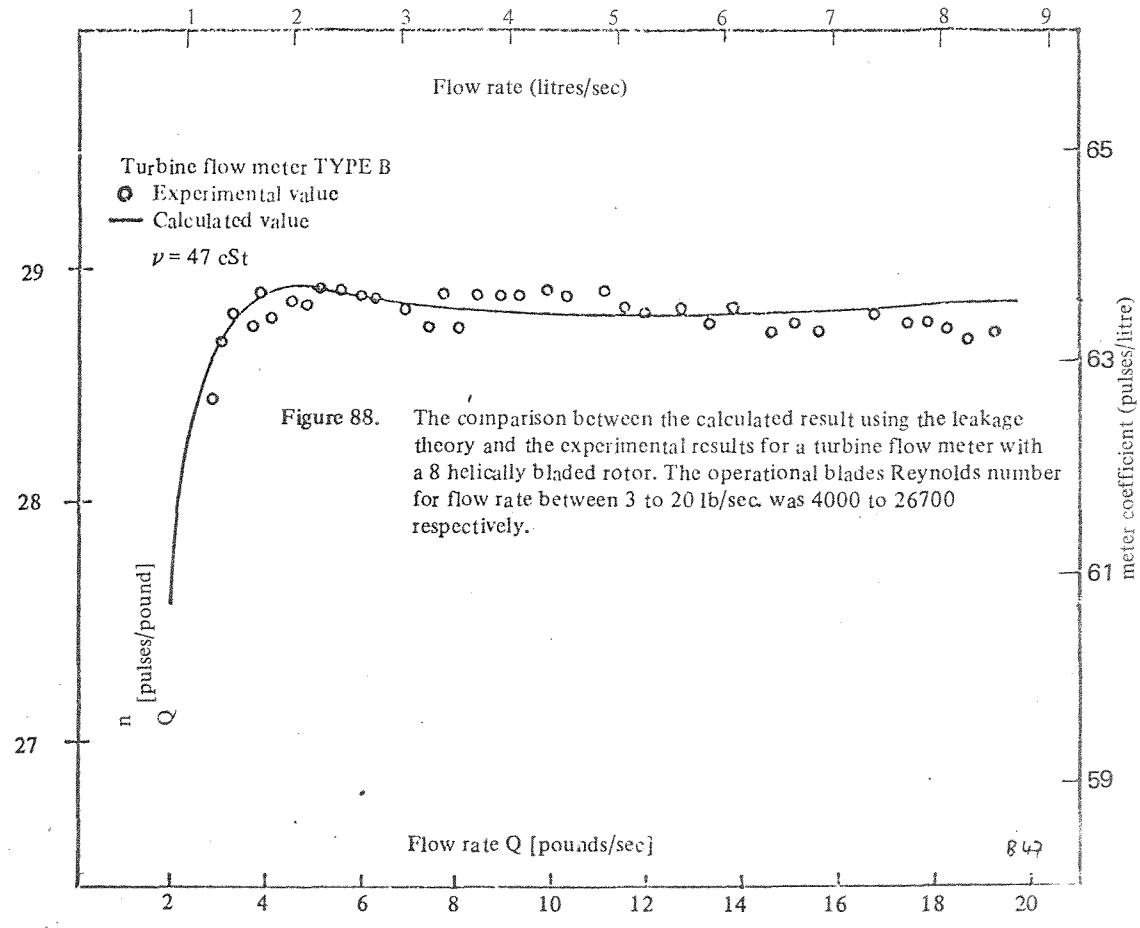

Figure 88. The comparison between the calculated result using the leakage theory and the experimental results for a turbine flow meter with a 8 helically bladed rotor. The operational blades Reynolds number for flow rate between 3 to 20 lb/sec. was 4000 to 26700 respectively.

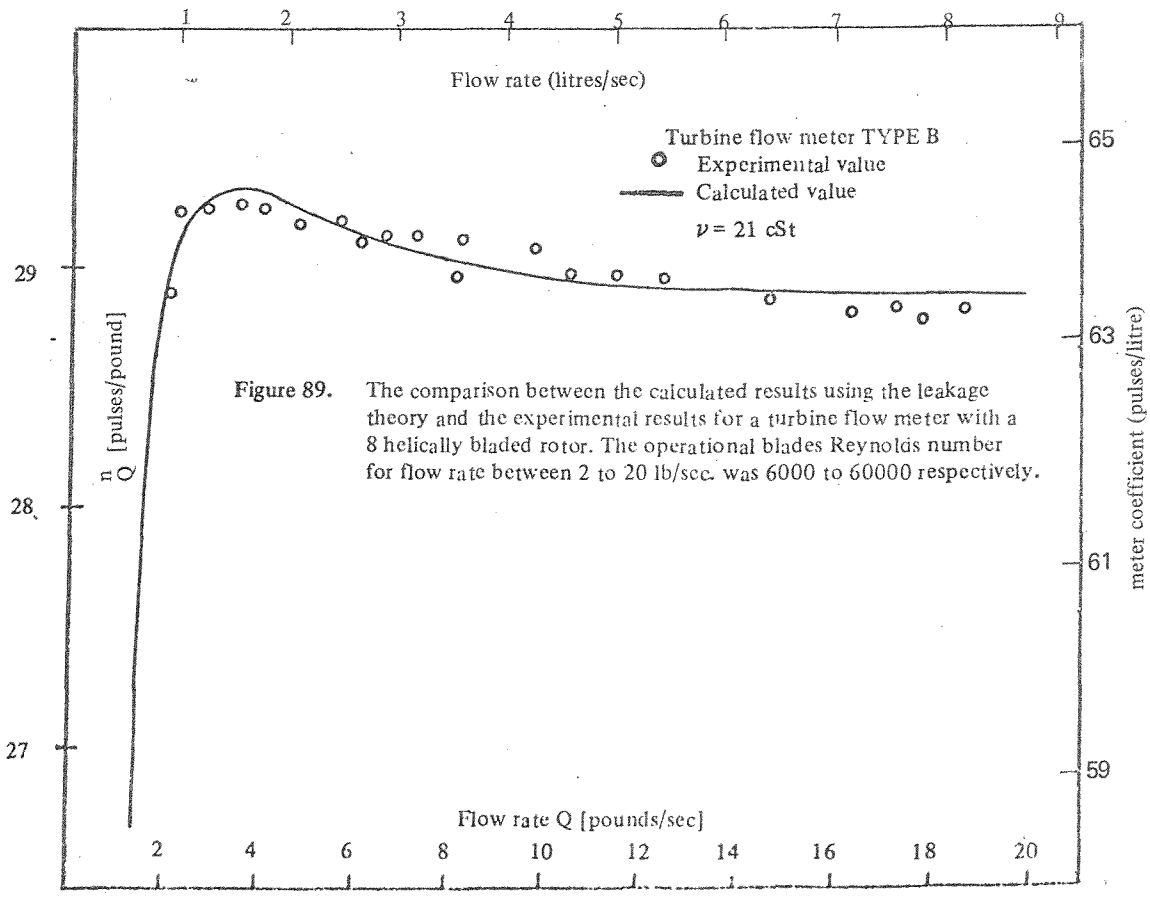

Figure 89. The comparison between the calculated results using the leakage theory and the experimental results for a turbine flow meter with a 8 helically bladed rotor. The operational blades Reynolds number for flow rate between 2 to 20 lb/sec. was 6000 to 60000 respectively.

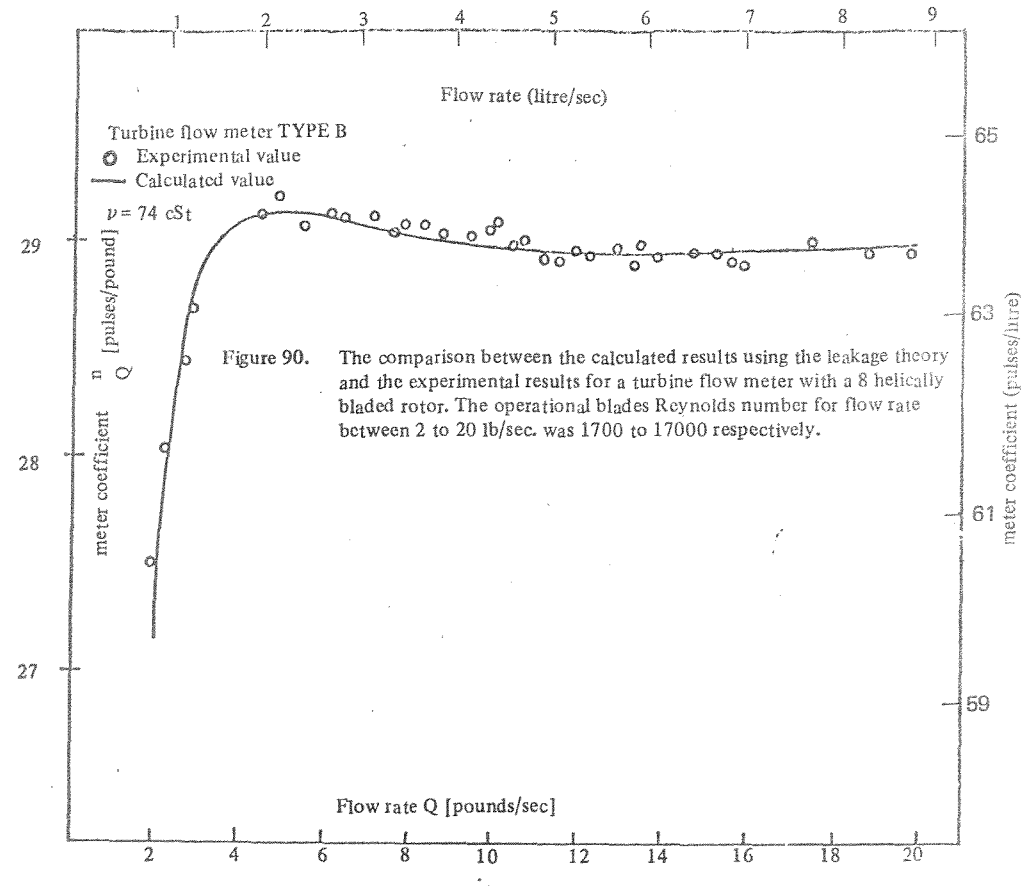

Figure 90. The comparison between the calculated results using the leakage theory and the experimental results for a turbine flow meter with a 8 helically bladed rotor. The operational blades Reynolds number for flow rate between 2 to 20 lb/sec. was 1700 to 17000 respectively.

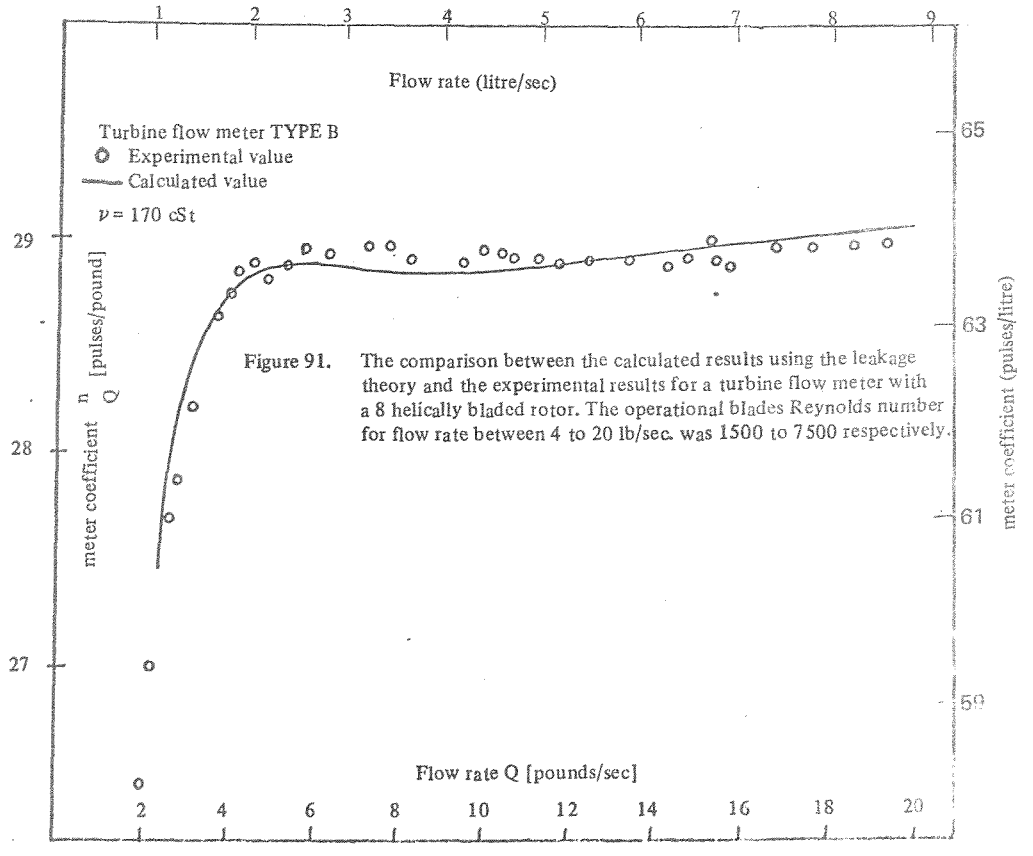

Figure 91. The comparison between the calculated results using the leakage theory and the experimental results for a turbine flow meter with a 8 helically bladed rotor. The operational blades Reynolds number for flow rate between 4 to 20 lb/sec. was 1500 to 7500 respectively.

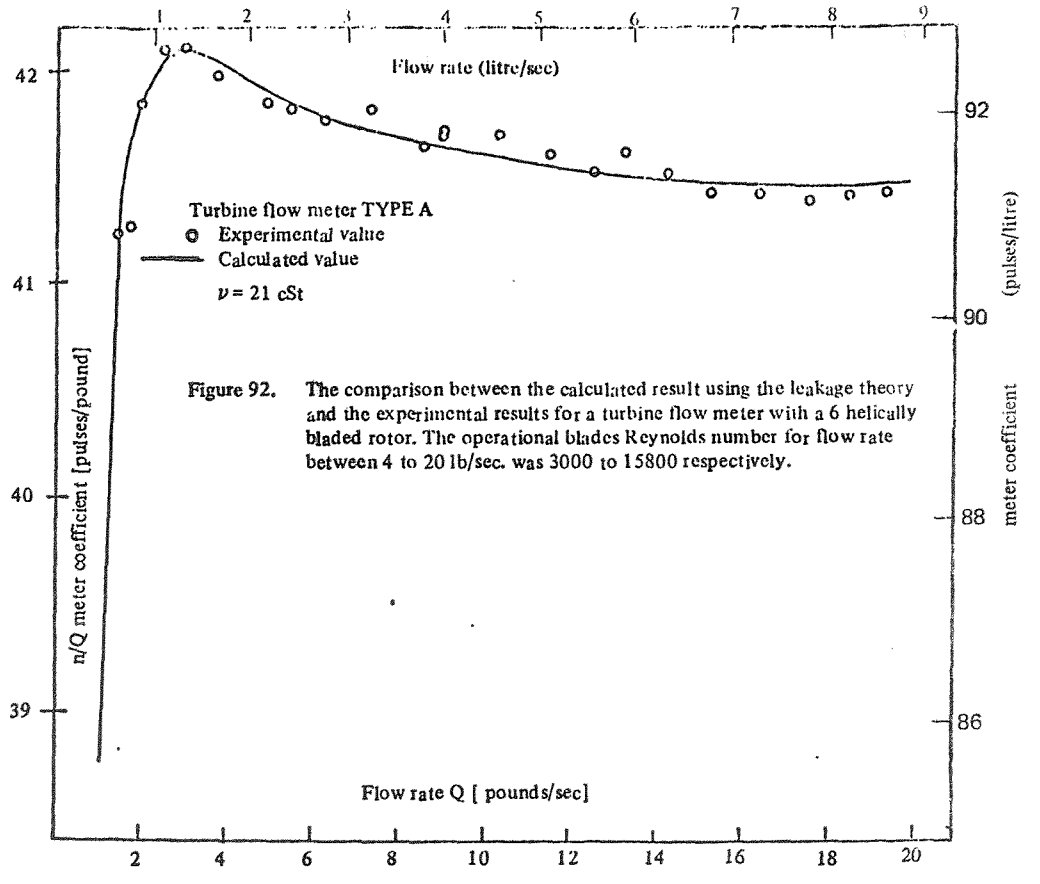

Figure 92. The comparison between the calculated result using the leakage theory and the experimental results for a turbine flow meter with a 6 helically bladed rotor. The operational blades Reynolds number for flow rate between 4 to 20 lb/sec. was 3000 to 15800 respectively.

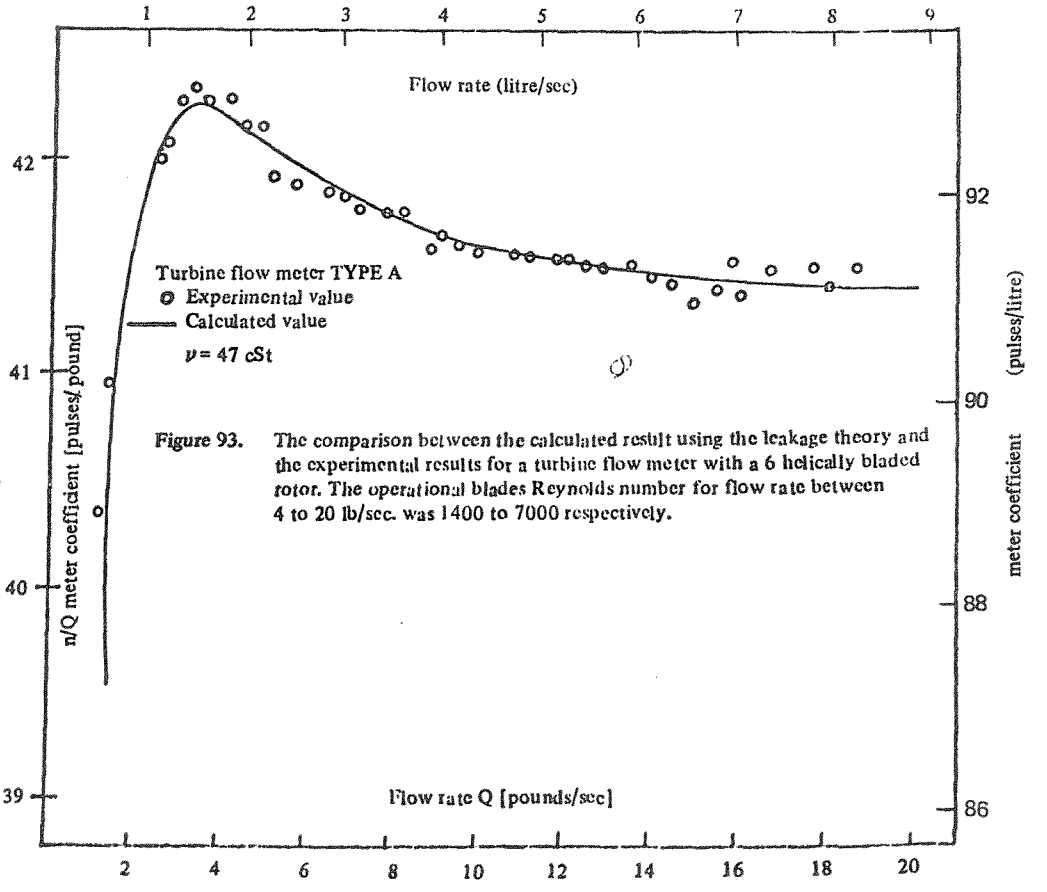

Figure 93. The comparison between the calculated result using the leakage theory and the experimental results for a turbine flow meter with a 6 helically bladed rotor. The operational blades Reynolds number for flow rate between 4 to 20 lb/sec. was 1400 to 7000 respectively.

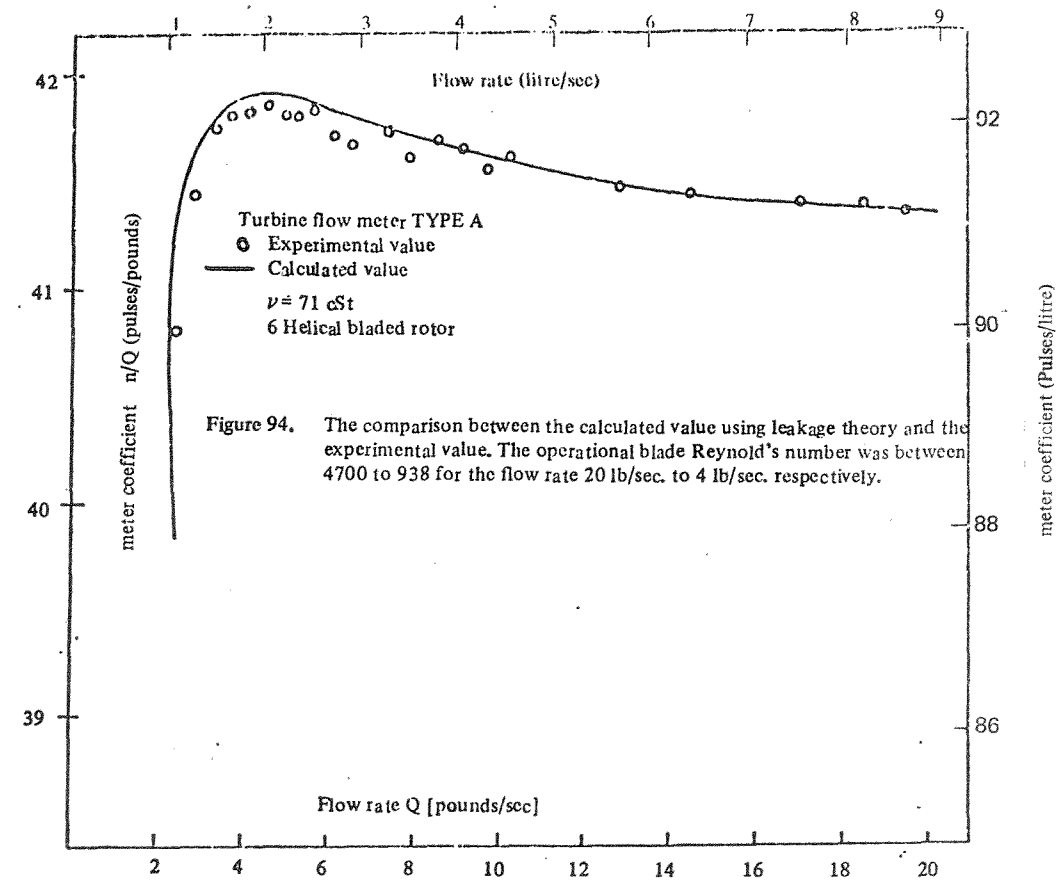

Figure 94. The comparison between the calculated value using leakage theory and the experimental value. The operational blade Reynold's number was between 4700 to 938 for the flow rate 20 lb/sec. to 4 lb/sec. respectively.

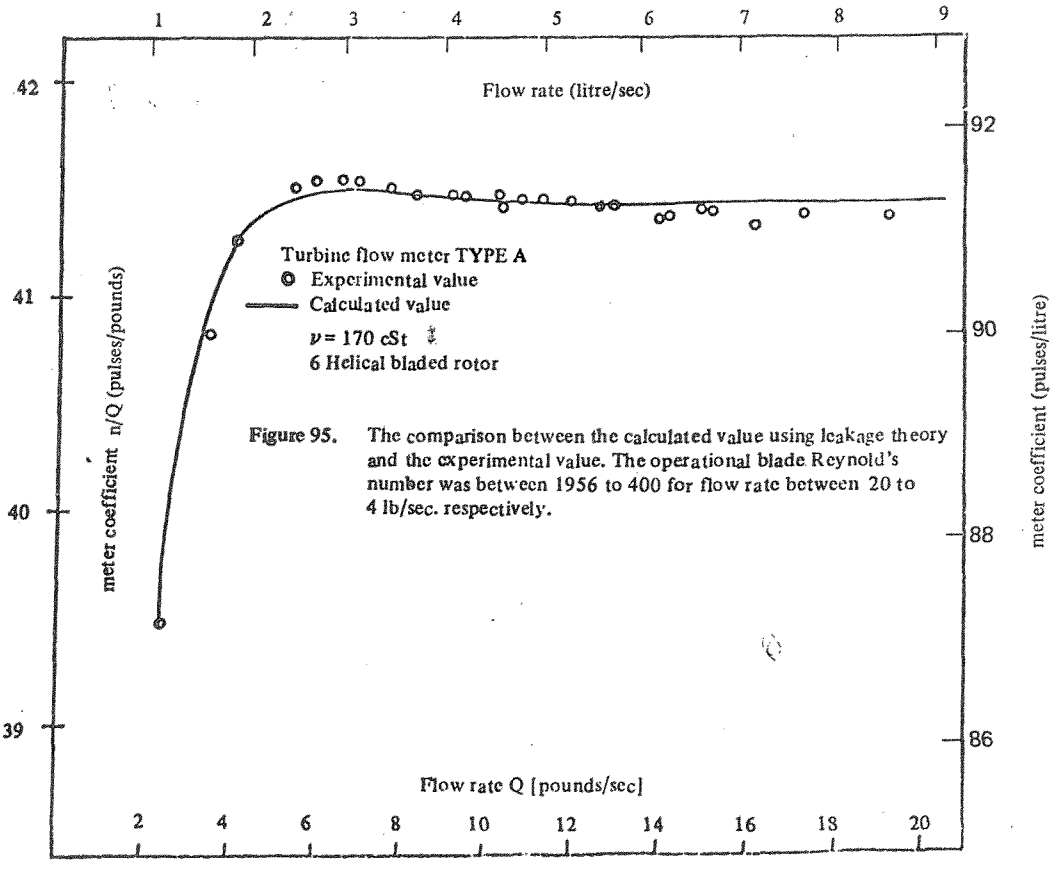

Figure 95. The comparison between the calculated value using leakage theory and the experimental value. The operational blade Reynold's number was between 1956 to 400 for flow rate between 20 to 4 lb/sec. respectively.

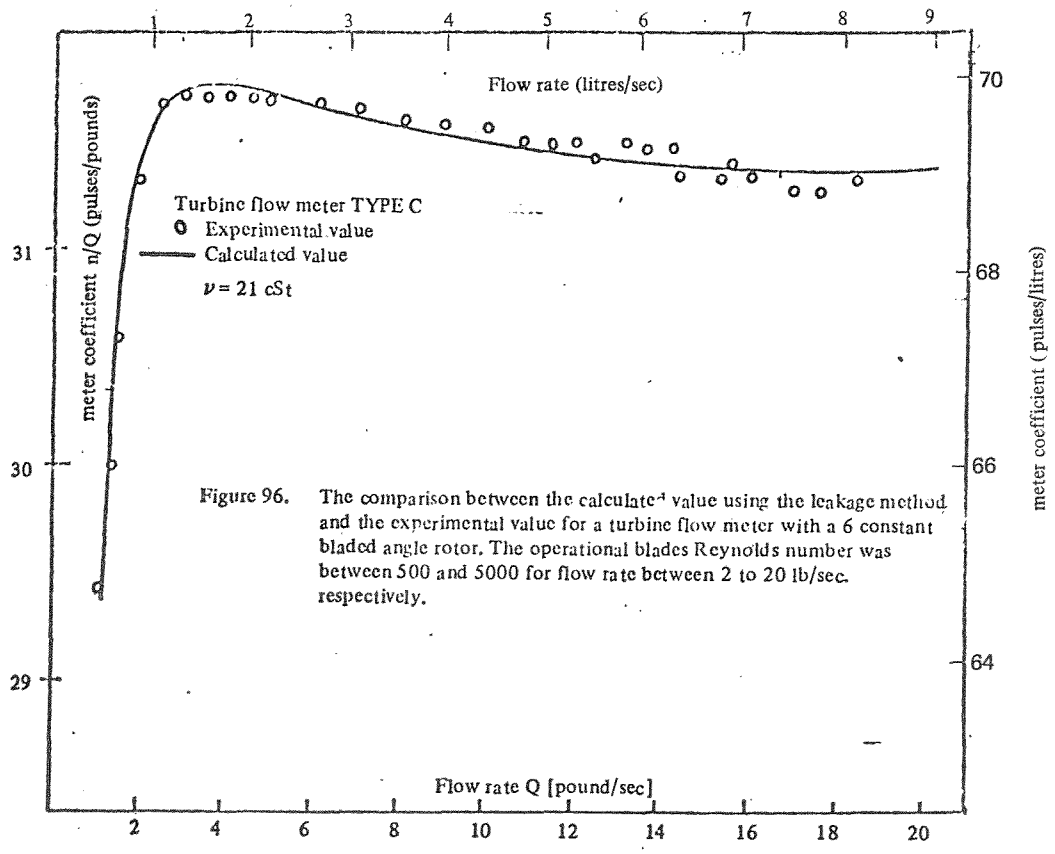

Figure 96. The comparison between the calculated value using the leakage method and the experimental value for a turbine flow meter with a 6 constant bladed angle rotor. The operational blades Reynolds number was between 500 and 5000 for flow rate between 2 to 20 lb/sec. respectively.

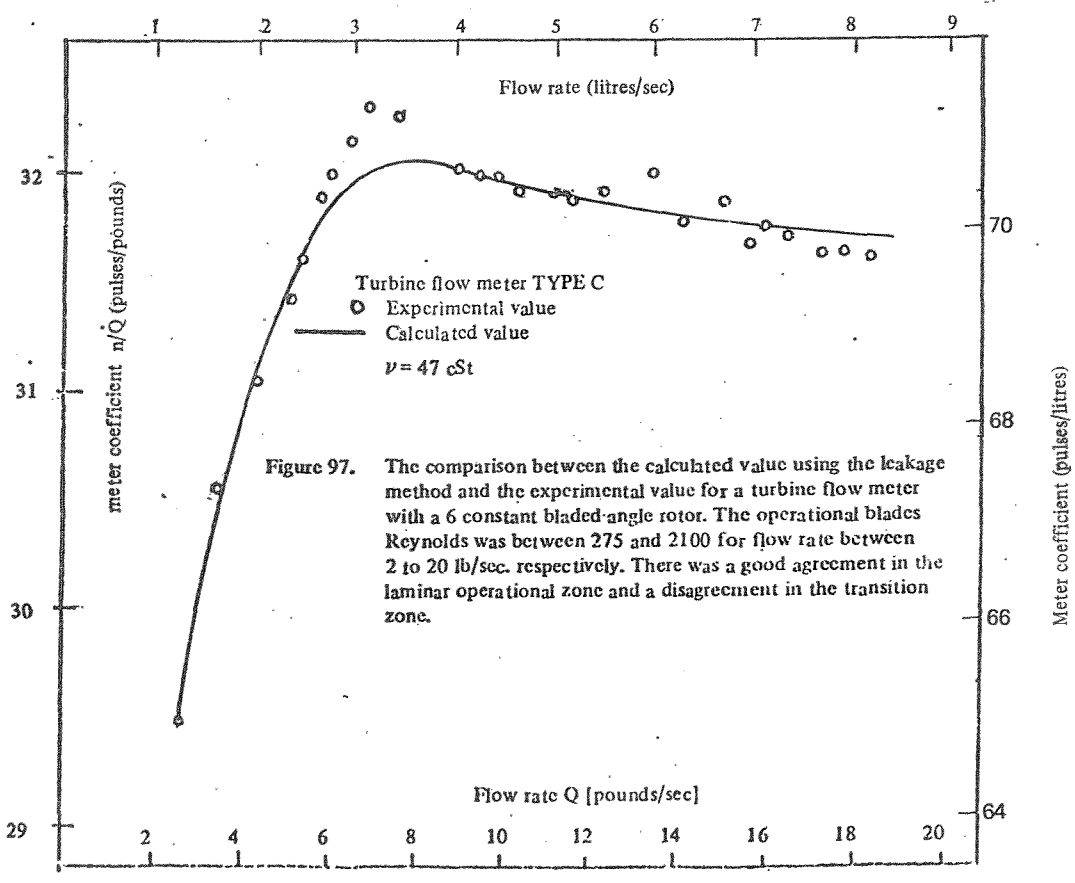

Figure 97. The comparison between the calculated value using the leakage method and the experimental value for a turbine flow meter with a 6 constant bladed-angle rotor. The operational blades Reynolds was between 275 and 2100 for flow rate between 2 to 20 lb/sec. respectively. There was a good agreement in the laminar operational zone and a disagreement in the transition zone.

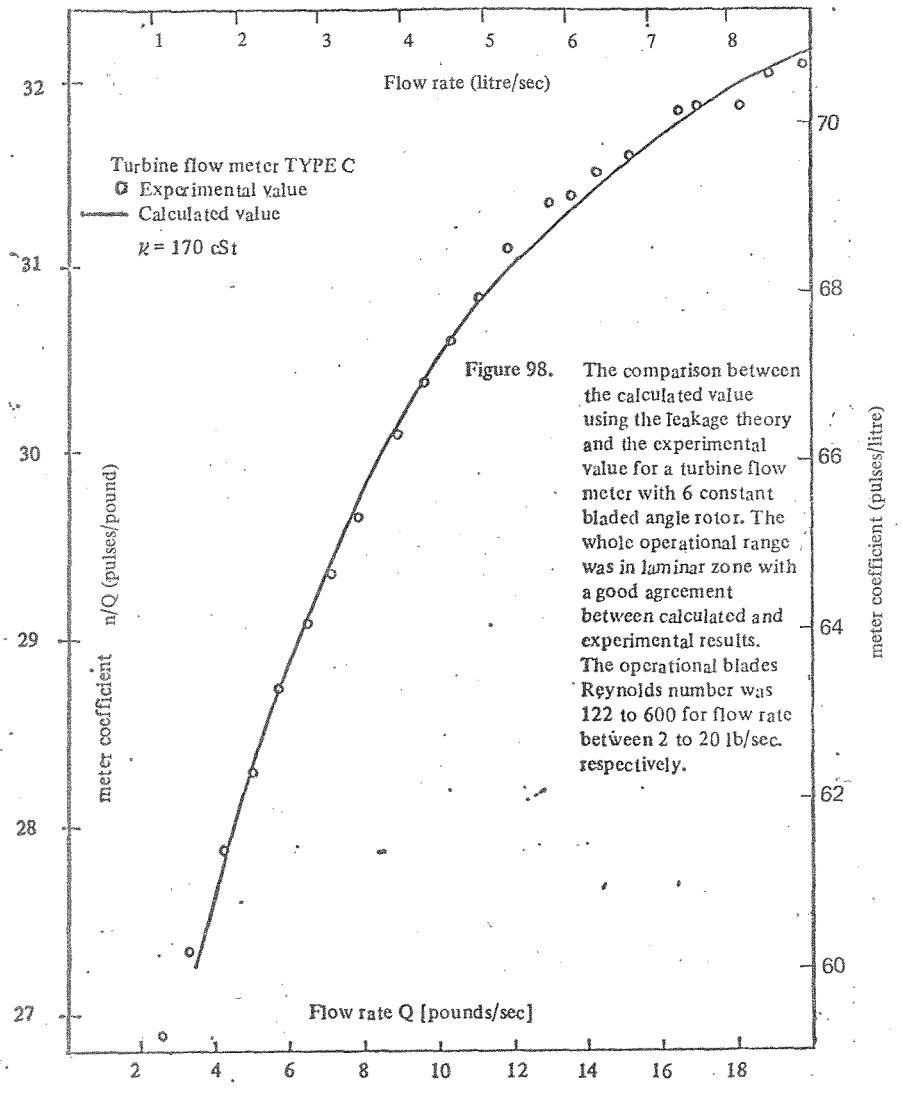

Figure 98. The comparison between the calculated value using the leakage theory and the experimental value for a turbine flow meter with 6 constant bladed angle rotor. The whole operational range was in laminar zone with a good agreement between calculated and experimental results. The operational blades Reynolds number was 122 to 600 for flow rate between 2 to 20 lb/sec. respectively.

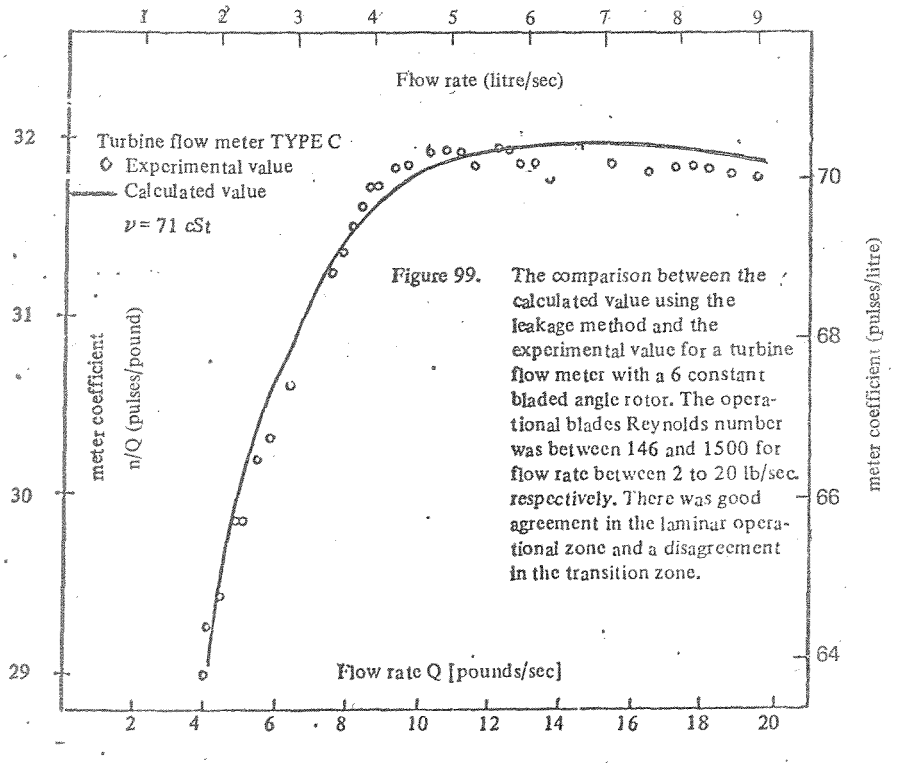

Figure 99. The comparison between the calculated value using the leakage method and the experimental value for a turbine flow meter with a 6 constant bladed angle rotor. The operational blades Reynolds number was between 146 and 1500 for flow rate between 2 to 20 lb/sec. respectively. There was good agreement in the laminar operational zone and a disagreement in the transition zone.